Catalyzed Hydrogen Release from BH- and BNH-based Hydrogen Storage Materials

Mehdi Mostajeran

Thesis submitted to the

Faculty of Graduate & Postdoctoral Studies

University of Ottawa

in partial fulfillment of the requirements for the

Ph.D. degree in the

Ottawa-Carleton Chemistry Institute

Thèse soumise à

Faculté des études supérieures et postdoctorales

Université d'Ottawa

en vue de l'obtention du Doctorat en philosophie à

L'Institut de chimie d'Ottawa-Carleton

uOttawa

Abstract

In order to reduce our ties to fossil-based energy and mitigate the undeniable impacts of climate change on the environment, remarkable efforts have been directed over the last 4 decades toward developing renewable energy sources such as solar, wind, geothermal, etc. For transportation applications biofuels, electricity and hydrogen all offer potential solutions although current usage is still largely linked to fossil fuels (bio-based ethanol-gasoline mixtures, power generation for battery recharging, and steam reforming for hydrogen production). While hydrogen offers the greatest potential in terms of energy density, its poor volumetric density (0.01 MJ/L at RT) requires costly compression and pressurized storage. When future technology finally allows for efficient hydrogen release from water splitting, we need to have optimal solutions in place for hydrogen storage. One promising solution is chemical hydrogen storage in which thermolysis of a chemical precursor affords a controlled hydrogen release that can then be reversed in an off-board regeneration step. With a focus on maximum gravimetric hydrogen storage, various BNH compounds have been shown to be promising chemical hydrogen storage precursors. In this *Thesis* we summarize the state of the art in B-N-H hydrogen storage compounds (**Chapter 1**) and then investigate several new chemical hydrogen storage solutions with a focus on portable power generation.

In the first project (**Chapter 2**) we sought to prepare a robust, base-metal borohydride hydrolysis catalyst for use in a custom hydrogen generator designed to use the reaction heat to help separate the borate spent fuel. Active 'reverse opal' layered double hydroxide (LDH) catalysts were prepared and tested. While the classical Ni-Mg-Al LDH released 3.4 equiv. of hydrogen at 50 °C in 150 minutes, the polystyrene templated Ni-Mg-Al catalyst released 4 equiv. of hydrogen with a higher initial rate under the same reaction conditions. The long-term objective of this project was to test these catalysts in fuel cells for underground mine forklifts with our industry collaborator (Kingston Process Metallurgy Inc.).

In the next three chapters, the synthesis and hydrogen release properties of ammine metal borohydrides [$M(BH_4)_m(NH_3)_n$, AMBs] were investigated. As promising hydrogen storage materials with high hydrogen content (10-15 wt%), AMBs can access lower hydrogen release temperatures resulting from the combination of protic ($N\text{-}H^{\delta+}$) and hydridic ($B\text{-}H^{\delta-}$) hydrogens. While AMBs also do not suffer from diborane formation that plagues thermolysis of metal borohydrides, hydrogen release is often accompanied by small concentrations of ammonia that deactivate the fuel cell catalyst. Our objective for this work was to identify

base metal catalysts that could suppress ammonia formation by further reducing the energy barrier to H_2 release.

In **Chapter 3** our studies of the solution synthesis of AMB materials (Y, La, Zn, etc.) in coordinating solvents such as tetrahydrofuran (thf) and diethyl ether revealed the unexpected formation of ammonia-borane (H_3NBH_3, AB). It was shown that while the amounts of produced AB correlate with the Zhang electronegativity for the *s*- and *p*-block metals, ionic radius is a stronger determining factor for the transition metals. It was also observed that reducible metals such as Ti and V produce large amounts of AB while Zn produced the least. This knowledge was then used in **Chapter 4** to prepare pure samples of the Y and La complexes, $M(BH_4)_3(NH_3)_4$ that were characterized by thermal analysis (TGA-MS), powder X-ray diffraction, FT-IR and ^{11}B and ^{1}H MAS NMR spectroscopy. Furthermore, a series of base-metal nanoparticle catalysts, prepared using a novel route from MCl_2 and liquid hexylamine-borane, was shown to suppress ammonia formation from these Y and La AMBs. Immobilizing 5 wt.% of Co NPs on $Y(BH_4)_3(NH_3)_4$ and 5 wt.% of Fe NPs on $La(BH_4)_3(NH_3)_4$ resulted in reduction of ammonia release by three- and fourfold, respectively. In **Chapter 5** the attempted solution synthesis of $Zn(BH_4)_2(NH_3)_2$ revealed complications due to preferred formation of $M^IZn(BH_4)_3$ [instead of $Zn(BH_4)_2$] from the reaction of $ZnCl_2$ and M^IBH_4 (M^I= Li, Na, K). As a result, the mixed-metal AMB, $KZn(BH_4)_3(NH_3)_n$ was prepared and characterized. Although the effects of both heterogeneous and homogeneous catalysts were not as pronounced as those for Y and La, using 5 wt.% FeNPs resulted in fourfold reduction in the amount of released ammonia which led to a purer hydrogen stream (98.9 mol%) compared to the uncatalyzed thermolysis (97.0 mol%).

Finally, in **Chapter 6** our results are considered vs. the current state of the art and suggestions are made for further investigations.

Acknowledgments

I could not have passed the way I have been through in the past 5 years without endless help and support of many people.

Prof. Baker: Since the first day, you have been a positive, enthusiastic, challenging and supportive friend/boss to me all the time. You showed me how to work hard and enjoy doing it at the same time. You always see the bright sides of the obstacles. You did not let me feel disappointed by getting bad results. You have always pushed me to go forward and have taught me how to be a better thinker. Words are not capable of describing how much I am grateful to experience my PhD studies with you. Finally, I will definitely miss those fun hours which we spent together, especially on Sundays, fixing papers and answering reviewer comments. Thanks for the opportunity and your tireless support.

Although my lab on the 5th floor was far from the other Baker's labs in the 4th floor, I was really fortunate to work with many smart people. I thank Kaitie, Uttam, Christian, Graham, Nick, Hassan, Ben and Steve for their friendship and assistant. I would like to thank Dr. Gang Ye for helping me step by step in solid state NMR experiments. He is extremely knowledgeable in NMR and always offered me some new solutions for complicated problems. I would like also to mention the undergraduate students whom I mentored: Thomas McFarland (UBC medicine), Michael Reynen (uToronto pharmacy) and Nishaan Brar (uToronto medicine). You guys were wonderful colleagues and I wish you all the best in your studies and future careers.

I appreciate the referees who kindly accepted to be the examiners for my thesis: Professors Abdel Sayari and Darrin Richeson (uOttawa), Sean Barry (uCarleton) and Tom Autrey (Pacific Northwest National Laboratory). Also, I appreciate the University of Ottawa, CCRI and chemistry department for providing the facilities and instrumentation.

I especially thank my brother and sister in law, Mohammad and Narges, and my friends Pedram and Sahar for their friendship, support and more importantly delicious burgers and BBQs we had. Mom and Dad, you supported me in every single decision I have made in my life. You have always believed in me and my capabilities. Meisam and Erfan, my brothers, thanks for being my crazy supportive buddies. And finally, one person needs an honorable mention. My wife, Zahra, thank you for all of your infinite

patience, love, support and optimism you unconditionally dedicated to me during my studies and writing this thesis.

Table of Contents

List of Abbreviations

etc	et cetera
Mt	Megatons
CO_2	Carbon dioxide
C_6H_6	Benzene
DC	Direct current
μ_{JT}	Joule-Thomson coefficient
CNAr	2,6-dimethylphenyl isocyanide
cod	1,5-cyclooctadiene
PEMFC	Proton exchange membrane fuel cell
NOx	Nitrogen oxide
ca.	*circa*, approximately
cf.	compare
US DOE	US Department of Energy
DCM	Dichloromethane
DEE	Diethyl ether
DMSO	Dimethyl sulfoxide
thf	Tetrahydrofuran
DFT	Density functional theory
kWh	Kilowatt-hour
CFRP	Carbon fiber reinforced plastic
LH_2	Liquid hydrogen
LNH_3	Liquid ammonia
Equiv.	Equivalents
MOF	Metal-organic frameworks
SBU	Secondary building units
h(rs)	Hour(s)
AB	Ammonia-borane
HxAB	n-hexyl ammonia-borane
BN	Boron nitride / Boron nitrogen
MAB	Metal amidoboranes
Hz	Hertz
i.e.	That is, in other words
MBH	Metal borohydride
AMB	Ammine metal borohydride
χp	Pauling electronegativity
Me	Methyl
GHSC	Gravimetric hydrogen storage capacity
T_{dec}	Decomposition temperature
MS	Mass spectrometry
NMR	Nuclear magnetic resonance
TGA	Thermogravimetric analysis
DSC	Differential scanning calorimetry
FT-IR	Fourier transform infrared spectroscopy
PXRD	Powder X-ray diffraction
MAS NMR	Magic angle spinning nuclear magnetic resonance
SBH	Sodium borohydride ($NaBH_4$)

LDH	Layered double hydroxide
LDO	Layered double oxide
3-DOM	three-dimensionally ordered macroporous
HT	Hydrotalcite
TEM	Transmission electron microscop
SEM	Scanning electron microscope
EDX	Energy dispersive X-ray
ICP	Inductively coupled plasma
in vacuo	In a vacuum
In situ	In the reaction mixture
MNP	Metal nanoParticle
SQ	Single quantum
DQ	Double quantum
IL	Ionic liquid
Tf	Triflamide
mp	Melting point
bp	Boiling point

List of Figures

List of Schemes

List of Tables

List of Contributions

Publication resulting from the chapters of this thesis

4) **Mostajeran M.**; Reynen MA.; Brar N.; Baker RT. Solution Synthesis and Dehydrogenation of Ammine Zinc-Potassium Borohydride, $KZn(BH_4)_3(NH_3)_3$ *Dalton Trans., **2017**, manuscript in preparation (Full length article).*

3) **Mostajeran M.**; Prévot V.; Mal SS.; Mattiussi E.; Davis BR.; Baker RT. Base-Metal catalysts based on porous layered double hydroxides for alkaline-free sodium borohydride hydrolysis *Int. J. Hydrogen Energy, **2017**,* 42, 20092-20102.

2) **Mostajeran M.**; Ye E.; Desgreniers S.; Baker RT. Base-metal nanoparticle-catalyzed hydrogen release from ammine yttrium and lanthanum borohydrides *Chem. Mater., **2017**, 29, 742-751 (Full length article).*

1) **Mostajeran M.**; Wolstenholme DJ.; Frazee C.; McGrady GS.; Baker RT. Solution-based routs to ammine metal borohydrides: formation of ammonia-borane *Chem. Commun., **2016**, 52, 2581-2584. (Communication).*

Conference Presentations:

11) Mostajeran M.; Baker RT. Wanted hydrogen storage materials: Solution synthesis and dehydrogenation of ammine potassium-zinc borohydride, $[KZn(BH_4)_3(NH_3)_3]$ (Poster presentation) – 100th Canadian Chemistry Conference and Exhibition, Toronto, May 28 – June 1, **2017**
10) Mostajeran M.; Baker RT. Catalysis for energy storage: Improved hydrogen release from ammine metal borohydrides (**Oral presentation**) – Boron in the Americas (BORAM XV), Queen's University, Kingston, June 25-28, **2016**.
9) Mostajeran M.; Baker RT. Catalysis for energy storage: Improved hydrogen release from ammine metal borohydrides (Poster presentation) – 24th Canadian Symposium on Catalysis, Ottawa, May 8-11, **2016**
8) Mostajeran M.; Baker RT. Size isn't everything: Impact of nanoparticles on portable power applications (Poster presentation) – 6th annual NanoOntario Conference, Ottawa, November 5-6, **2015**
7) Mostajeran M.; Baker RT. Cleaning the stream: Catalytic H_2 release from metal borohydride ammoniates (**Oral presentation**) – 98th Canadian Chemistry Conference and Exhibition, Ottawa, June 13-17, **2015**
6) Mostajeran M.; Baker RT. Clean H_2 from B-N-H materials for portable power applications (Poster presentation) – Ontario and Canada Research Chairs Symposium, Toronto, April 1-2, **2015**
5) Mostajeran M.; Baker RT. Hydrogen release from metal borohydride ammoniates: on-board power generation (Poster presentation) – 1000 Islands Energy Research Forum (TIERF), Ottawa, October 23-25, **2014**
4) Mostajeran M.; Baker RT. Transition metal catalyzed hydrogen release from metal borohydride ammoniates (Poster presentation) – 97th Canadian Society of Chemistry (CSC), Vancouver, June 1-5, **2014**

3) Mostajeran M.; Baker RT. Investigating catalyzed hydrogen release from ammine metal borohydride (AMB) complexes (Poster presentation) – 4th H_2CAN AGM and Annual conference, Mont-Tremblant, June 2-6, **2013**
2) Mostajeran M.; Baker RT. New materials for portable power generation: improving selectivity in hydrogen release from metal borohydride ammoniates (Poster presentation) – 45th Inorganic Discussion Weekend (IDW-2012), Ottawa, November 2-4, **2012**
1) Mostajeran M.; Baker RT. Porous base-metal catalysts for sodium borohydride hydrolysis (Poster presentation) – 3rd H_2CAN AGM & Annual conference, Niagara Falls, June 7-9, **2012**

Attended summer schools:

2) American Chemical Society Summer School on Green Chemistry and Sustainable Energy, Golden, Colorado, USA, July 22-29, **2013** (All expenses were paid by ACS.)

1) Canadian Synchrotron Summer School - Synchrotron Techniques in Materials Research, Canadian Light Source Facilities (CLS), Saskatchewan, July 16-24, **2012**

Chapter 1: Introduction

1.1. Renewable Energy Sources for Transportation

One of the most complex challenges of the 21st century is the ready availability of "energy" in the face of rapidly growing climate change resulting largely from fossil fuel combustion.[1] While power generation is well suited to a multisource solution based on solar, wind, geothermal, hydro, nuclear, etc., transportation fuel options are considerably more limited.[2] Utilization of gasoline and diesel fuel in internal combustion engines currently dominates global mobility. For Canada's increasing 732 megatonnes (Mt) of carbon dioxide emissions in 2014, the transportation sector accounted for 171 Mt CO_2 (23%, Figure 1.1).[3]

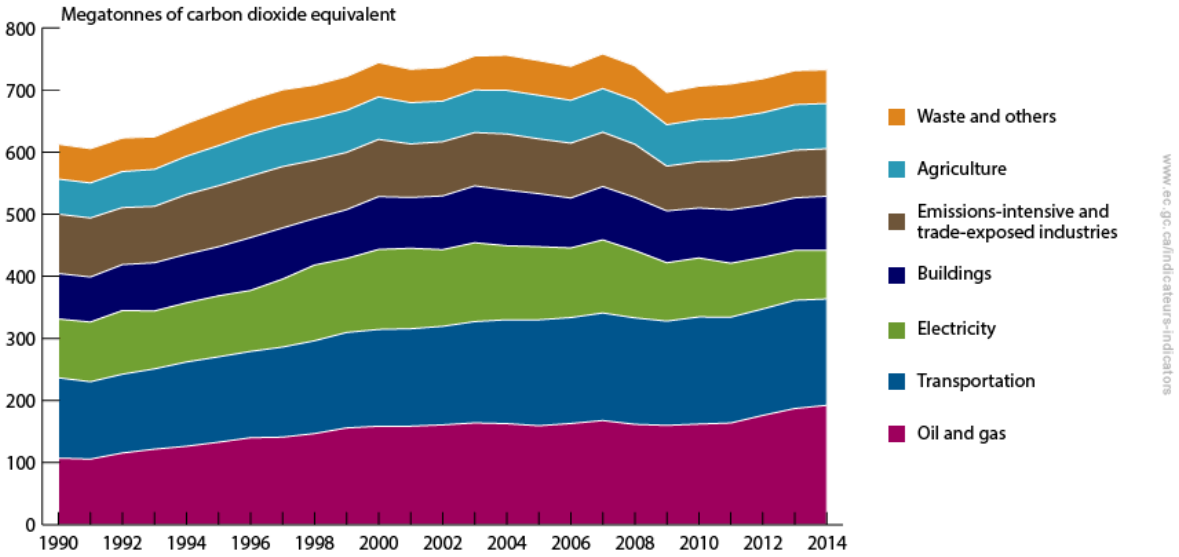

Figure 1.1. Greenhouse gas emissions, in megatonnes of carbon dioxide, in Canada from 1990 to 2014. Reprinted from Environment and Climate Change Canada.

As a result, the development of carbon neutral transportation options has recently attracted great attention in research and development with billions of dollars in investments. While much focus has been on improved water electrolysis and more efficient batteries to enable electric vehicles for local transportation,[4] steady efforts have also been progressing on generation of hydrogen from renewable sources for utilization in efficient fuel cells.[5]

1.2. Renewable Energy Source Metrics

As scientists and engineers strive to develop the next generation of renewable energy technologies, policy makers weigh the potential benefits of the various options.[6]
The following metrics need to be evaluated for a sustainable energy system:[7]

- **Quality**: The service quality of the new energy source has to be comparable to established systems.
- **Environmental sustainability**: Implementing and decommissioning of the energy system should have minimal impact on Nature's equilibria.
- **Economic cost**: Although the initial cost of the new service might be greater than the established systems, it soon has to be lower.
- **Long-term availability**: The energy system must be available for a reasonable period of time in the future.
- **Global distribution**: A uniform global distribution is expected with respect to geopolitical tensions among countries and territories.
- **Resilience to surprise**: The new energy system must be resilient to unpredicted and unforeseeable technological, economic and environmental circumstances.

1.3. Hydrogen Economy

Hydrogen, as an energy carrier, attracted considerable attention during the energy crisis in the 1970s and 1980s.[8] Harnessing renewable power sources to produce hydrogen from water and subsequent use of hydrogen in a fuel cell to generate power and regenerate the water appears at first as an ideal solution. About 71% of the Earth's surface is covered with water, more than 321 million cubic miles.[9] Moreover, hydrogen has the highest energy per mass compared to other fuels.[10] On the negative side however, hydrogen is a gas at ambient temperature and pressure, making its storage for transportation applications a challenging technical issue that is also associated with safety risks.[11]

1.3.1. Hydrogen Production

Hydrogen is currently produced on a large scale through the steam-methane reforming process shown in the equation below:[7]

$$CH_4 + 2H_2O + \text{energy} \longrightarrow 4H_2 + CO_2$$

In addition to the reaction itself, the fossil fuel burned in this process to provide the required energy emits large amounts of carbon dioxide. Hence, research efforts are underway to develop inexpensive and more environmentally friendly methods to produce hydrogen on a large scale for commercial applications.

The other method normally used to generate ultra-pure hydrogen is electrolysis of water in which pure oxygen is produced simultaneously with hydrogen.[12] Alternatively and economically more interesting, the Chloralkali process,[13] which proceeds through

electrolysis of sodium chloride (NaCl) solutions, is employed to produce H_2, chlorine and NaOH. This method requires large amounts of direct current (DC) electricity and so requires efficient conversion of renewable energy sources such as solar or wind which is currently under development. Nuclear energy could also be used to "co-produce"[7] hydrogen with electricity but both costs and waste management reduce the sustainability of this approach.[14]

1.3.2. Hydrogen Power

Similar to helium and neon, hydrogen warms up upon expansion so leaking hydrogen gas from storage containers could result in an explosion (self-ignition). This property of hydrogen is explained by its negative Joule-Thomson coefficient (μ_{JT}, change in the temperature of a real gas when its pressure varies under constant enthalpy conditions). However, the stored chemical energy in the covalent bond between hydrogen atoms in H_2 could be released easily via an internal combustion engine or a fuel cell. To implement hydrogen technology safe, cheap and viable storage techniques with high capacities are required to deliver the hydrogen fuel through a nationwide infrastructure. In the following sections in this chapter, a short overview of challenges in considering hydrogen as a fuel will be presented.

1.3.2.1. Internal Combustion Engines

Hydrogen internal combustion engines are relatively inexpensive to design and build, simple, easy to operate and maintain, user friendly and well established among most of the car manufacturers such as Toyota, BMW and General Motors. Combustion of hydrogen, similar to other fuels, releases a great amount of energy in the form of heat. Most internal combustion engines are incredibly inefficient in converting the released energy of the burned fuel into usable energy (*i.e.* low thermal efficiency). Even with the current high-tech engines, the highest thermal efficiency was reported to be 38% for the Toyota Prius.[15] Manufacturing hydrogen internal combustion engines costs ca. 1.5 times more than that of gasoline engines while producing only 20% more power.[16] While hydrogen burning engines seem at first to be clean and emission free, inclusion of nitrogen from the air still leads to NOx emissions which are actually higher than from gasoline due to hydrogen's higher combustion temperature.[17]

1.3.2.2. Proton Exchange Membrane Fuel Cell Systems

With the development of Proton Exchange Membrane Fuel Cells (PEMFC), converting hydrogen's chemical energy to locomotive power can be achieved with higher efficiency than internal combustion engines.[18] Moreover, its low temperature operation allows for emission–free power generation from hydrogen. The negative *anode* of the fuel cell conducts the electrons resulting from oxidation of hydrogen molecules to protons from an external circuit to the positive *cathode*. The cathode conducts electrons from the external circuit to the surface of the fuel cell catalyst where they recombine with the protons and oxygen to produce water. PEMFC membranes are usually made of highly proton-conductive sulfonated polymers, such as DuPont's Nafion,[19] and have to be hydrated to allow for passing protons while blocking the electrons.[20] As mentioned earlier, each PEMFC includes catalysts, for both the hydrogen oxidation and oxygen reduction steps, usually consisting of supported porous platinum nanoparticles.[21] Finally, the hydrogen feed for fuel cells has to be very pure to avoid detrimental effects on the catalyst activity and life-time. An overview of a PEMFC is shown in Scheme 1.1.

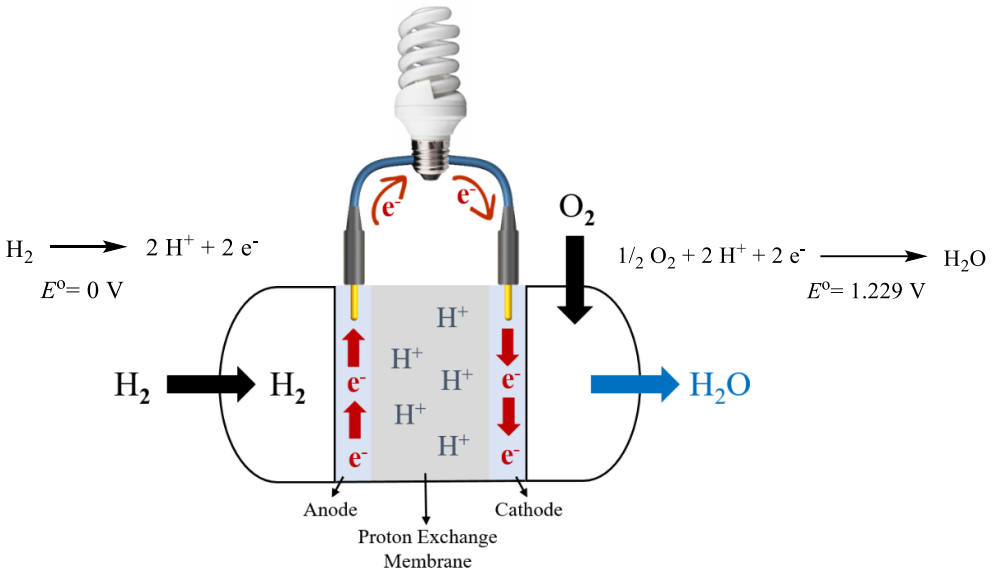

Scheme 1.1. Schematic overview of a proton exchange membrane fuel cell.

This type of fuel cell is also being developed for both portable and stationary power generation.[22] They require less maintenance than internal combustion engines as they have less moving parts and so should last longer. However, widespread adoption of PEMFCs by the transportation industry requires the use of safe storage alternatives of the hydrogen gas fuel.

In the following section a short review of H_2 storage techniques will be detailed.

1.4. Overview of Hydrogen Storage Techniques

Low volumetric energy density of hydrogen gas (energy content per unit volume, 0.01 MJ/L) requires safe and viable storage techniques. The US DOE targets for 2015 for onboard hydrogen storage systems include:[23]

- Gravimetric: 3.0 kWh/kg system (9.0 wt.% hydrogen)
- Volumetric: 2.7 kWh/L system (81 g H_2/L)
- Cost: \$67/kg H_2

The most common means of physical hydrogen storage methods are shortly described below.

1.4.1 Compressed gas

The most common method of hydrogen storage, especially for fuel cell vehicles, is compressed hydrogen in pressurized tanks. These tanks store hydrogen and operate at room temperature. While being light, they must be extremely robust in order to withstand high pressures. They are normally made of materials such as aluminum and carbon fiber reinforced plastic (CFRP). However, research continues on more advanced materials to improve mechanical and operational properties. For instance, a tank at 345 atm can store hydrogen equivalent to a gravimetric capacity of 5.5 wt.% (*cf.* DOE target is 9.0 wt.% hydrogen density).[24]

1.4.2 Liquefaction (LH_2)

Liquefying of hydrogen gas is employed to increase its volumetric energy. It needs to be performed at extremely low temperatures (20 K) and therefore, is sometimes called *cryogenic* storage.[25] As the result, lighter and smaller containers could be employed in practical applications. Preparing LH_2 is highly energy intensive; moreover, liquid hydrogen absorbs heat easily from its surroundings and evaporates fast. These limitations, in spite of recent remarkable technological improvements, make LH_2 still impractical especially for portable power applications.

1.4.3. Sorbent Materials

Hydrogen can be adsorbed in the pores and channels of porous materials such as metal-organic frameworks (MOFs). MOFs or porous coordination polymers (PCPs) are synthetic crystalline materials that consist of inorganic secondary building units (SBUs, metal complexes or clusters) and organic molecules as linkers which assemble into 3D networks with a porous lattice,[26] providing high surface area, tunable porosity and

structural diversity. High thermal stability and, more importantly, chemical tunability of MOFs have attracted an enormous amount of research intensity,[27] with applications ranging from gas storage[28] and air purification[29] to drug delivery,[30] chemical sensing[31] and catalysis.[32] In addition to variation of the SBUs and linkers, the size, geometry and composition of the MOF's interior walls can be tuned through synthetic and post-synthetic methods. Similar to a hydrogen sponge, several MOFs have been studied for hydrogen storage purposes[33] (Figure 1.2) including Zn[34] and Zr[35] based MOFs. While MOFs exhibit high uptake capacities at cryogenic temperatures (up to 99.5 mg/g, ~9 wt.%),[36] storage capacities are much lower at RT (around 1 wt.%) due to weak interactions between hydrogen and the MOF structure.[37]

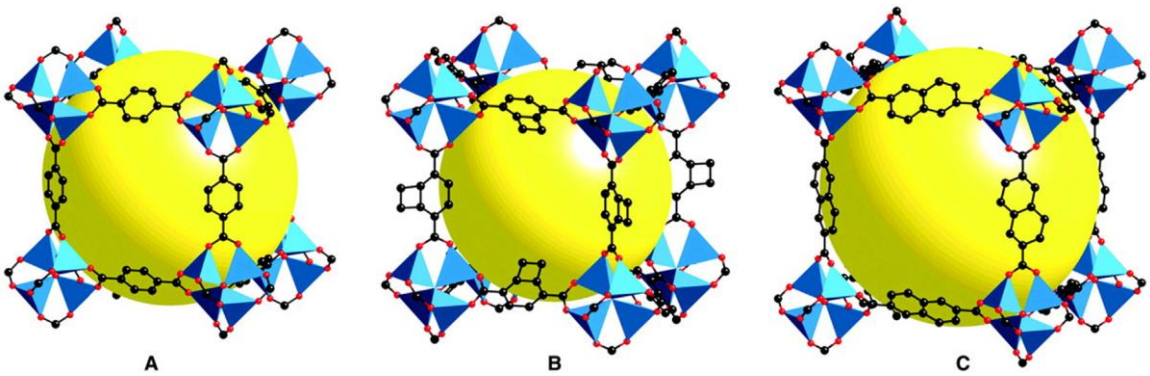

Figure 1.2. Single crystal X-ray structures of MOF-5 (A), IRMOF-6 (B) and IRMOF-8 (C). The cavities in their cubic structure are employed to hold hydrogen molecules through van der Waals interactions with the framework.[33]

Hydrogen density of the discussed physical hydrogen storage techniques are listed in the Table 1.1.[24b]

Table 1.1. Physical storage methods, properties and operation conditions

Storage media	H_2 capacity* (wt.%)	H_2 density (Kg/m^3)	Operating conditions
Compressed gas	13	< 40	RT, 800 atm
Liquid hydrogen	varies	71	Cryogenic temp. (-253 °C), 1 atm
Porous materials	2	150	-80 °C to RT, 1-100 atm

* Hydrogen storage density of the whole storage system.

In addition to physical storage, hydrogen can undergo chemisorption in metals.[38] Reversible H_2 storage can be achieved in metal hydrides at reasonably low temperatures and pressures, allowing for their use in commercial applications such as nickel hydride batteries and portable electronic device rechargers. For transportation applications,

however, most metal hydrides just add too much weight to the vehicle. As a result, focus has turned to complex metal hydrides containing the lightest metals (Li, Be, Mg, Al; see below) and even to so-called chemical hydrides that encompass other light elements such as nitrogen and boron.[39] These compounds contain large quantities of hydrogen, are lightweight and their hydrogen release can be promoted using additives/catalysts.

1.4.4. Chemical Hydrides

Chemical hydrides include binary metal hydrides such as AlH_3,[40] intermetallic hydrides including $NaAlH_4$,[41] azacycloalkanes[42] and ammonia-borane (NH_3BH_3).[55] Ammonia (NH_3),[43] hydrazine (N_2H_4)[44] and methanol (CH_3OH)[45] also belong to this category. These candidates commonly suffer from sluggish dehydrogenation kinetics and the hydrogen released from these compounds is often contaminated with volatile impurities that tend to deactivate the fuel cell catalyst.

Table 1.2. Chemical Hydrogen Storage Candidates – short summary

Chemical	H_2 capacity (wt.%)	Pros	Cons
NH_3[43]	17.6	Cat. release	High T, poison gas
$M(BH_4)_n$[46]	10-15	Stable and robust	Solid, high T, no chemical regen.
$M(BH_4)_n + H_2O$[47]	5	Liquid, cat. release	Ineff. chemical regen.
Azacycloalkanes[42]	7	Liquid, reversible, cat. release	High T, slow release
NH_3BH_3[48]	13-16	Cat. release, chemical regen	Solid, volatile borazine
$M(NH_2BH_3)_n$[49]	11-13	No borazine	Solid, MBH_4 by-product
$M(BH_4)_x(NH_3)_y$[50]	10-15	Low T hydrogen release	Solid, no chemical regen.
BNC heterocycles[51]	5-7	Liquid, cat. release	Complicated synthesis, ineff. chemical regen.
$N_2H_4BH_3$[52]	13		Solid product is shock-sensitive

1.5. Chemical Hydrogen Storage Materials

Storage of hydrogen in a chemical bond offers some important advantages, especially for transportation applications. Controlled hydrogen release through heating, chemical reaction, and/or catalysis offers a safe, high-capacity storage option. Identification of a

universally useful chemical hydrogen storage material has not yet been achieved (Table 1.2). Some leading contenders are discussed below.

1.5.1. Reversible Organic Storage Materials

Liquid organic compounds that can be easily dehydrogenated to liquid products offer the exciting possibility of a "drop-in" to our existing fuel distribution infrastructure with the dehydrogenated spent fuel being off-loaded at refueling stations. Early studies on liquid organic hydrogen carriers were focused on reversible dehydrogenation of cycloalkanes and hydrogenation of the corresponding aromatics.[53] Some cycloalkane candidates are shown in Table 1.3.[54] As these compounds suffer from large dehydrogenation enthalpies and high temperatures needed for catalyzed H_2 release hydrogen, researchers turned to azacycloalkanes.[42]

Table 1.3. Potential cycloalkane-based liquid chemical hydrides.

Storage compound	Hydrogenated form	Dehydrogenated form	H_2 wt.%	H_2 g/L
Cyclohexane[55]			7.2	56.0
Methylcyclohexane[56]	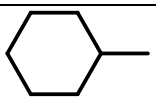	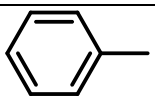	6.2	47.4
Decalin[57]	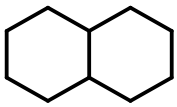	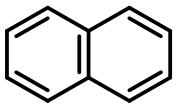	7.3	65.3
Bicyclohexyl[57]	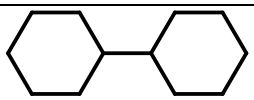	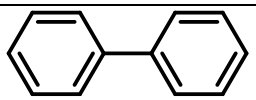	7.3	64.2

Hydrogen release from nitrogen containing heterocycles was introduced through a series of patents by Pez and co-workers at Air Products in 2006.[58] Further experimental studies revealed that partial substitution of carbon atoms by nitrogen in cycloalkanes results in lower dehydrogenation enthalpy for the materials making heterocycles more suitable liquid chemical storage materials (Table 1.4).[59] The high hydrogen contents of aza-cycloalkanes could be released reversibly albeit with slow kinetics and at high temperatures. For example while less than 1 wt.% hydrogen could be released from dodecahydrofluorene at 170 °C within 20 hrs over a 5 wt.% Pd/C catalyst (with 95% selectivity to the completely dehydrogenated product), dodecahydro-N-ethylcarbazole released its entire hydrogen content at the same temperature but within 94 min (Figure 1.3).[60]

Table 1.4. Aza-cycloalkane liquid chemical hydrides

Storage media	Hydrogenated form	Dehydrogenated form	H_2 wt.%	H_2 g/L
Dodecahydrocarbazole[60]	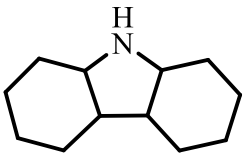	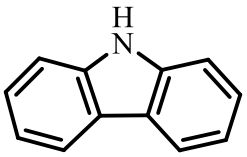	6.7	87
Dodecahydro-N-ethylcarbazole[60]	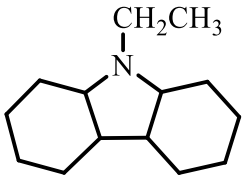	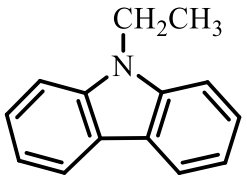	5.8	54
Indoline[59]	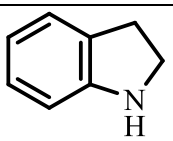	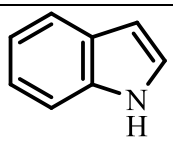	1.7	18.1
4-Aminopiperidine[61]	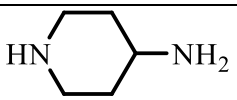	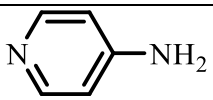	6.0	57
Perhydro-4,7-phenanthroline[62]	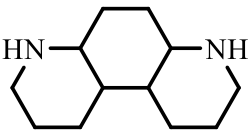	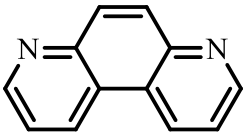	7.2	69

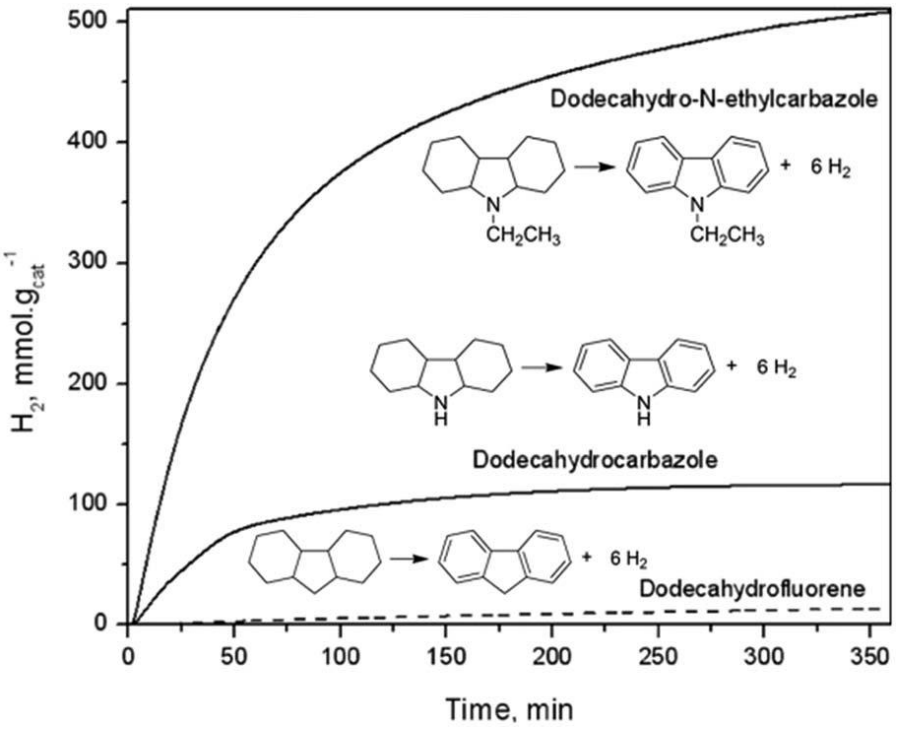

Figure 1.3. Catalytic dehydrogenation rate comparison of dodecahydrofluorene, dodecahydrocarbazole and dodecahydro-N-ethylcarbazole at 170 °C over a 5 wt.% Pd/C catalyst.[60]

Hydrogenation of azacycloalkanes is not always highly selective to exclusively give the completely hydrogenated product. In work by Smith,[63] hydrogenation of dodeca-N-ethylcarbazole to dodecahydro-N-ethylcarbazole gave rise to the production of octa- and tetrahydro-N-ethylcarbazole intermediates. Therefore, only 4.0 wt.% hydrogen could be recovered from dehydrogenation of dodecahydro-N-ethylcarbazole (rather than 5.8 wt.% theoretical capacity).

N-substituted heterocyles with high hydrogen densities, favorable kinetics and low release temperatures, fulfill many of the requirements for liquid hydrogen storage systems, showing great potential for future applications. However, there are some challenges that need to be considered. The fully dehydrogenated product of dodecahydro-N-ethylcarbazole, N-ethyl carbazole, has a melting point of 68 °C and all the efforts to overcome this issue, including partial dehydrogenation and blending, result in lowering the hydrogen content of this material.[64] Moreover, associated with high costs, highly reactive catalysts are necessary for both dehydrogenation and hydrogenation reactions not only to enhance the kinetics but also to improve the selectivity to yield only the completely hydrogenated products.

1.5.2. Ammonia and Hydrazine

With 17.8 wt.% density, hydrogen release from ammonia was first introduced by British chemist Arthur Titherley in 1897.[65] In his system hydrogen was released from decomposition of sodium amide ($NaNH_2$), which was itself made from the reaction of ammonia and sodium metal.

$$2\ Na + 2\ NH_3 \longrightarrow 2\ NaNH_2 + H_2$$

$$2\ NaNH_2 \longrightarrow 2\ Na + N_2 + 2\ H_2$$

$$2\ NH_3 \longrightarrow 3\ H_2 + N_2$$

Ammonia contains 30% more volumetric energy density than liquid hydrogen and its transportation, distribution and storage infrastructure is globally well-established.[66] Ammonia decomposes partially at temperatures as high as 690 °C[67] while catalytic systems, such as cesium promoted graphite-supported ruthenium,[68] still require temperatures higher than 300 °C.[66] Ammonia starts to decompose at 377 °C with

completion at 607 °C over Ni/Al_2O_3 fixed bed catalyst while maintaining the high activity for 5 consecutive cycles.[69] Decomposition of ammonia is endothermic (ΔH_r= +46 KJ/mol) and the equilibrium shifts more towards ammonia with decreasing temperature therefore, constant removal of hydrogen from the decomposition equilibrium helps to achieve higher conversions. Solid ammonia storage materials such as $Mg(NH_3)_6Cl_2$ with 9.2 wt.% hydrogen capacity[70], have been introduced to address safety issues on storing and carrying liquid ammonia for portable applications.

Although recent improvements make its storage safer, ammonia is still overlooked as a potential fuel alternative especially because of its high toxicity. Release of ammonia gas, as the result of a car crash for example, would be devastating for human lives. Moreover, ammonia is a strong σ-donor ligand and a poison for the fuel cell catalysts' active sites, reducing the efficiency of the fuel system.

Anhydrous hydrazine is liquid at room temperature with 12.5 wt.% hydrogen density and based on the type of catalyst[71] and the reaction conditions it can decompose via two different pathways:[72]

$$N_2H_4 \longrightarrow N_2 + 2\ H_2 \qquad \Delta H = -95.4\ KJ/mol$$

$$3\ N_2H_4 \longrightarrow 4\ NH_3 + N_2 \qquad \Delta H = -157\ KJ/mol$$

With respect to the lower N-N bond energy (60 kJ/mol) in comparison to N-H (84 kJ/mol), decomposition of hydrazine is thermodynamically more favored to proceed through the second alternative in which NH_3 and N_2 are the products. Therefore, development of active and selective catalysts is of great importance for obtaining pure hydrogen from hydrazine.[42]

Anhydrous hydrazine is an explosive compound; thus, its use imposes severe safety concerns for practical applications. Hydrous hydrazine such as hydrazine monohydrate, $N_2H_4{\cdot}H_2O$ with 8.0 wt.% hydrogen density, is also liquid at room temperature and safer to handle. It has been reported to release 3 equivalents of pure hydrogen (proved by ^{15}N NMR) at room temperature with a Rh_4Ni alloy nanocatalyst.[73] Other catalytic systems which produced pure hydrogen from hydrazine are listed in Table 1.5. In this table the TOF values were measured based on the number of available catalytic sites on surface of the catalysts. Hydrazine and its derivatives are toxic materials and in spite of high hydrogen densities and mild dehydrogenation behaviors, technical issues such as foaming in hydrazine-boranes during their heat treatment have hampered practical applications. Also, regeneration of these materials is still challenging.

Table 1.5. Kinetic statistics of selective catalysts in hydrogen release from hydrous hydrazine.

Catalyst	Temp. (°C)	TOF (h^{-1})	Catalyst	Temp. (°C)	TOF (h^{-1})
$Ni_{0.93}Pt_{0.07}$[74]	25	2.8	$Pt_{0.8}Ni_{0.2}$@ZIF-8[75]	50	69
$Ni_{0.95}Ir_{0.05}$[76]	25	2.2	$Ni_{88}Pt_{12}$@MIL-101[77]	50	350
$Pt_{12}Ni_{48}$@G4-OH[78]	70	240	NiFe[79]	70	4.2
$Ni_{60}Pt_{40}$-SF[80]	25	120	NiFe/Cu[81]	70	35
$Rh_{4.4}Ni$/graphene[82]	25	14	Ni_3Fe/C[83]	20	556
$Ni_{0.9}Pt_{0.1}/Ce_2O_3$[84]	25	28	NiMoB-La(OH)$_3$[85]	50	13.3

1.5.3. BNH Compounds

BNH compounds are among the most promising materials for hydrogen storage.[86] In addition to being light elements, they form a number of compounds, many of which contain both protic N-H and hydridic B-H bonds, combination of which is often facile at low temperatures. Ammonia-borane (H_3NBH_3, AB) is the most well-studied metal-free hydrogen storage material with 19.6 wt.% hydrogen density.[87] It can be prepared in high yields from reaction of $NaBH_4$ with $(NH_4)_2SO_4$ or NH_4Cl.[88] AB is a stable solid at room temperature, typically insoluble in non-polar organic solvents due to its extensive inter- and dihydrogen bonding (*i.e.* N-H$^{\delta+}\cdots^{\delta-}$H-B). However, it is somewhat soluble in ether solvents and has been used as a green reducing agent for many organic transformations.[89]

Complete catalytic thermolysis of AB proceeds through a three-step process at around 100, 150 and >500 °C producing ~6.5 wt.% hydrogen in each step.[90] In spite of favorable kinetics of catalyzed hydrogen release from AB (Scheme 1.2), presence of the volatile BN benzene analog, borazine (boiling point= 51 °C), hinders application of AB for portable power applications.[91] Borazine mixes with the H_2 stream and is detrimental to the fuel cell catalyst.

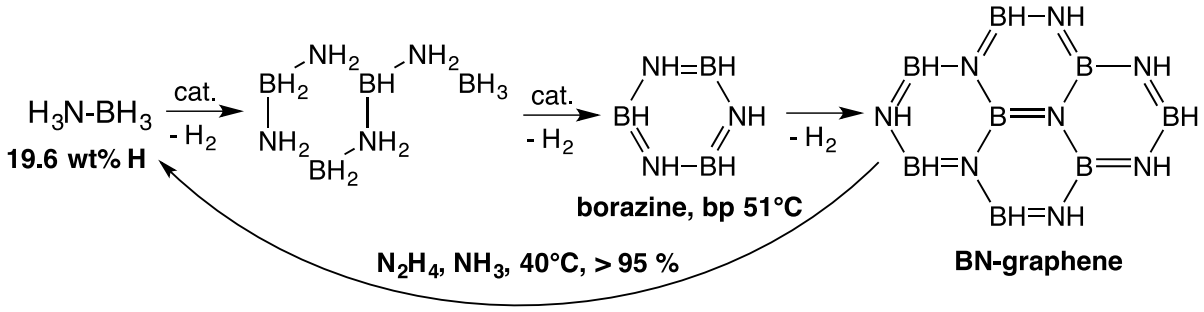

Scheme 1.2. An overview of stepwise catalytic hydrogen release from ammonia-borane (AB) in addition to regeneration.

Several strategies have been developed to improve the dehydrogenation properties of AB (*i.e.* increase rate, decrease thermolysis temperature and reduce borazine formation) including hydrolysis,[92] nano-confinment,[90b,93] dispersion in organic solvents,[90c,94] dispersion in ionic liquid[95] and catalysis.[96] Although the last decade has seen impressive advances in liquid AB formulations and base metal catalysts, borazine contamination remains problematic and the exothermic nature of its H_2 release requires a chemical regeneration step (currently using hydrazine-ammonia mixtures).

Another strategy to reduce the thermolysis temperature of AB is to synthesize derivatives in which one N-H bond is replaced with a metal cation such as alkali- or alkaline earth metal, producing metal amidoboranes [MABs, $M(NH_2BH_3)_n$].[97] Chen et al. showed that $LiNH_2BH_3$ and $NaNH_2BH_3$ release 2 equiv. of hydrogen, corresponding to 10.9 and 7.5 wt.%, at 92 °C and 89 °C respectively.[98] A summary of the reported MABs is represented in Table 1.6. Synthesis and hydrogen release properties of several other metal amidoboranes were also patented by Los Alamos National Laboratory researchers.[99]

Table 1.6. Hydrogen density and decomposition temperatures onset (T_{dec}) of selected MABs.

Storage medium	H_2 wt.%	T_{dec} (°C)	Storage medium	H_2 wt.%	T_{dec} (°C)
$LiNH_2BH_3$[98]	10.9	92	$Mg(NH_2BH_3)_2$[100]	10.0	104
$LiNH_2BH_3{\cdot}NH_3BH_3$[101]	14.0	80	$Mg(NH_2BH_3){\cdot}2NH_3$[102]	11.4	50
$NaNH_2BH_3$[98]	7.5	89	$Ca(NH_2BH_3)_2$[103]	7.2	120
KNH_2BH_3[104]	6.5	80	$Sr(NH_2BH_3)_2$[105]	6.8*	60

* Released hydrogen stream is contaminated with NH_3 and B_2H_6 starting at 65 °C.

Hydrazine-borane ($N_2H_4{\cdot}BH_3$, 15.4 wt.% hydrogen capacity) and hydrazine bis(borane) ($N_2H_4{\cdot}2BH_3$, 16.9 wt.% hydrogen capacity), with more hydrogen density than hydrazine, could release 6.5 wt.% and 10 wt.% hydrogen at 140 °C and 150 °C respectively under un-catalyzed conditions.[106] Hydrogen release from hydrazine-borane can be significantly enhanced using an equimolar amount of LiH.[106a] This mixture with 14.8 wt.% hydrogen density could release more than 11 wt.% hydrogen at 150 °C within 1 hour. Hydrazine-borane derivatives such as $LiN_2H_4BH_3$ and $NaNH_2BH_3$ are reported to exhibit enhanced kinetics compared to pristine hydrazine-borane producing more hydrogen with higher purity.[107] Several researchers have been quick to note, however, that dehydrogenation products derived from hydrazine-borane and its derivatives can be shock-sensitive.[52]

From the ammonia-borane family, 1,2-BN-heterocycles were recognized recently for hydrogen storage owing to their liquid state and fast release of hydrogen (Table 1.7). Presence of both hydridic and protic hydrogen atoms, similar to AB, facilitates hydrogen release under mild conditions.

Table 1.7. 1,2-BN-heterocycle hydrogen storage materials.

Storage compound	Hydrogenated form	Dehydrogenated form	H_2 wt.%	H_2 g/L
1,2-BN-cyclohexane[108]	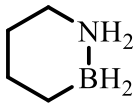	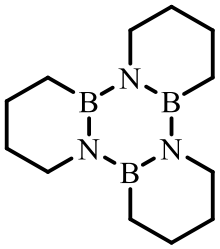	4.7	48
3-Methyl-1,2-BN-cyclopentane[109]	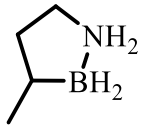	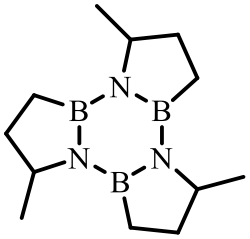	4.7	42

1,2-BN-cyclohexane with a melting point of 63 °C is an air/moisture stable molecule and thermal hydrogen release from this compound at 150 °C in toluene is reported to produce 3 equiv. of hydrogen through formation of a well-defined trimer (Figure 1.4).[108]

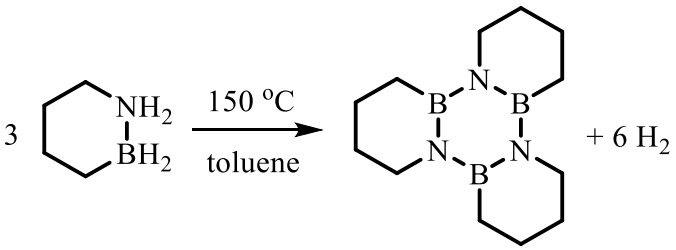

Figure 1.4. Dehydrogenative trimerization of 1,2-BN-cyclohexane.[108]

3-Methyl-1,2-BN-cyclopentane on the other hand, has a melting point of -18 °C which indicates a liquid phase for this compound at room temperature. Catalytic dehydrogenation over $FeCl_2$ or $NiCl_2$ at 80 °C follows the same path as 1,2-BN-cyclohexane producing 6 equiv. of hydrogen and a cyclohexane shaped trimer over 20 min (Figure 1.5).[109]

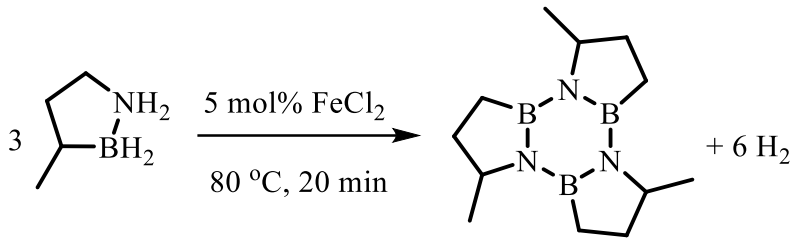

Figure 1.5. Catalytic hydrogen release from 3-methyl-1,2-BN-cyclopentane under mild conditions.[109]

In contrast to 1,2-BN-cyclohexane, the dehydrogenation product of 3-methyl-1,2-BN-cyclopentane is also liquid at room temperature. Although these compounds are currently difficult to prepare, desirable kinetics and thermodynamics, especially for 3-methyl-1,2-BN-cyclopentane, in addition to low cost metal halide catalysts make these liquid hydrogen storage materials viable candidates for portable power applications. Although their hydrogen content falls short of the US DOE target, their moderate hydrogen density could be doubled (greater than 9 wt.%) by further catalyzed dehydrogenation of the C-H bonds.

Two other important and well-studied chemical storage compounds are metal borohydrides (MBHs) and ammine metal borohydrides (AMBs) which are covered in the following sections.

1.6. Metal Borohydrides

Metal borohydrides ($M(BH_4)_n$, MBHs)[110] are stable compounds with high gravimetric hydrogen densities and adequate dehydrogenation temperatures and rates.[46] Thermodynamic stability of MBHs is due to charge transfer from the metal cation to the borohydride anions.[111] Owing to their favorable hydrogen storage properties they were initially studied for military purposes in the 1950s and lately for portable power applications.[39] MBH materials are generally synthesized by two techniques: 1) Mechano-chemical synthesis (ball-milling), a dry approach for physical mixing of the metal halide precursor and the borohydride source to yield the product via a simple metathesis reaction. In this method the metal halide salt by-product remains in the synthesis mixture. This is a convenient method from which some MBHs such as $LiZn_2(BH_4)_5$ can be prepared exclusively.[112] 2) Wet chemistry synthesis (solvent mediated synthesis) which often facilitates the preparation of pure materials. In this technique an organic solvent such as $S(CH_3)_2$ or toluene is utilized to dissolve the MBH product.[113] The consequent filtration step allows for separation of the metal halide by-product and evaporation of the solvent at reduced pressures affords the high purity metal borohydride product.

MBHs that have been synthesized and tested in the literature are listed in Figure 1.6.

1	2											13	14
Li 18.5	Be 20.8												
Na 10.7	Mg 14.9	3	4	5	6	7	8	9	10	11	12	[Al] 16.9	
K 7.5	Ca 11.6	Sc 13.5	Ti III 13.1 IV 15.0	V 12.7	Cr 9.9	[Mn] 9.5	[Fe] 9.4	[Co] 9.1	[Ni] 9.1	[Cu]* 5.1	Zn 4.4	[Ga] 10.6	Ge 12.2
Rb 4.0	Sr 6.9	Y 9.1	Zr 10.7	Nb 8.8						[Ag]* 3.3	[Cd] 2.9	[In] 7.6	[Sn] 9.1
Cs 2.7	Ba 4.8	Ln	Hf 6.8							[Au] 1.9	Hg 1.8	Tl 4.9	
		Ac											

Ln	La 6.6	Ce 6.6		Nd 6.4		Sm 6.2	Eu 6.2	Gd 6.0	Tb 5.9	Dy 5.8	Ho 5.8	Er 5.7	Tm 5.7	Yb 5.6	Lu 5.5
Ac		Th 5.5	Pa 5.6	U III 4.3 IV 5.4	Np 5.4	Pu 5.4									

Figure 1.6. Elements of the periodic table that have been used to prepare metal borohydrides with high gravimetric energy densities.[46] Metals in brackets are reported to form MBHs that are unstable at room temperature.

In MBHs hydrogen is bonded between the metal centre and the boron atom, forming three-center two electron bonds.[114] Making hydrogen from MBHs thus requires breaking these bonds and oxidation of the hydrides. Metal redox reactions are thus expected to occur during the thermolysis process which explains why volatile diborane impurities are normally observed. As for the chemical hydrides, the hydrogen content of MBHs can be released either by thermolysis or hydrolysis.

1.6.1. Hydrogen Release by Thermolysis

Isolated and characterized in 1940 by H. C. Brown,[115] $LiBH_4$ could release 13.5 wt.% hydrogen over the range of 200-453 °C with a SiO_2 catalyst while producing LiH and B by-products.[116] Regeneration of the by-product mixture (LiH + B) is reported to succeed at 345 atm of H_2 at 600 °C within 12 hrs.[117] Similar to $LiBH_4$, liberation of boron containing species at high temperatures is a common problem with most MBHs. Liberation of these B_xH_y species during the thermolysis reactions is not only toxic for the PEM fuel cell membrane and catalyst but also makes regeneration of the borohydride fuels nearly impossible. With the metal and boron atoms remaining in the dehydrogenated mixtures, there is a hope that they can re-adsorb hydrogen at elevated temperatures and pressures to regenerate the pristine metal borohydride. As mentioned earlier, thermolysis

of MBHs suffers from sluggish kinetics and numerous efforts have been made to improve the thermodynamics and kinetics of their hydrogen release.

Regarding thermodynamic effects, changes in Gibbs free energy are determined by two factors: enthalpy and entropy, which give rise to the equation: $\Delta G = \Delta H - T\Delta S$. Assuming that entropy comes only from hydrogen gas formation ($S^0 = 130$ J/Kmol), the enthalpy change is the only thermodynamic factor determining whether a reaction is spontaneous or not (*i.e.* $\Delta G \leq 0$). For MBHs two approaches are followed to tailor the thermodynamic stabilities: a) destabilization of MBHs starting materials; and b) stabilization of dehydrogenation products (Figure 1.7).

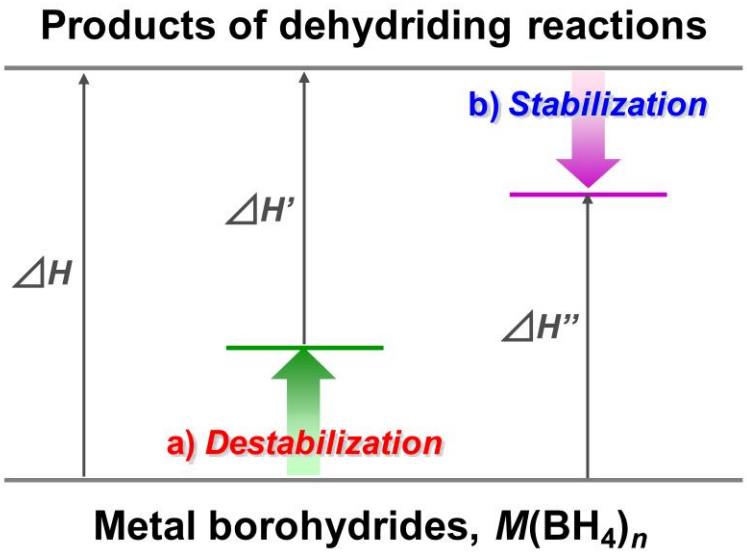

Figure 1.7. Two main approaches for tailoring the thermodynamic stability of MBHs: a) destabilization of MBHs reagents; b) stabilization of dehydrogenated products.[46]

It has been concluded that the Pauling electronegativity (χp) of metals is one thermodynamic factor controlling the thermal stability of MBHs,[118] as metals with $\chi p > 1.5$ form MBHs that are too thermally unstable to be used as hydrogen storage materials.[119] These findings indicate that T_{dec} can be estimated and tuned by the right choice of metal with acceptable thermal stability and favorable χp. Double-cation borohydrides,[120] $M^nM'^m(BH_4)_{n+m}$, in which M and M' are two metals with different stabilities, is one approach that is suggested to increase the stability of some MBHs.[46] For instance, ball milling of a 1:1 mixture of as prepared $Y(BH_4)_3$ (containing 48 wt.% LiCl) and $RbBH_4$ gave rise to $Rb[Y(BH_4)_4]$ as the only crystalline phase observed by powder XRD (in addition to LiCl). However, the same reaction with $CsBH_4$ yielded $Cs[Y(BH_4)_4]$ and another phase denoted as $Cs_2Li[Y(BH_4)_{6-x}Cl_x]$.[121] A total of 3.7 and 3.5 wt.%

hydrogen could be released from $RbY(BH_4)_4/3LiCl$ and a mixture of $CsY(BH_4)_4$ and $CsY(BH_4)_4/3LiCl$ below 400 °C respectively (Figure 1.8).

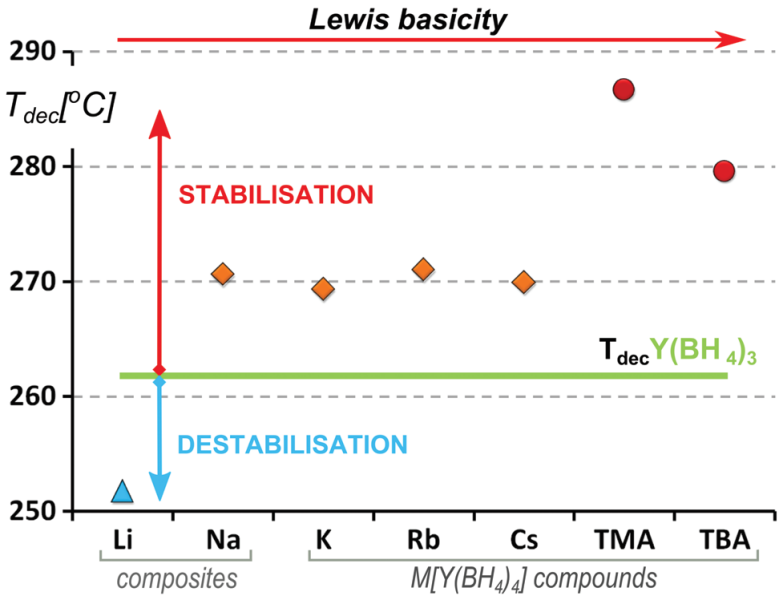

Figure 1.8. Thermal stability of a series of $Y(BH_4)_3/MBH_4$ composites.[121] M= Li, Na, K, Rb, Cs, $(CH_3)_4N$ (TMA) and $(n\text{-}C_4H_9)_4N$ (TBA).

Compared to pure $Y(BH_4)_3$ prepared by solution metathesis in dimethyl sulfide,[113] from which TGA-MS results indicated release of 6.7 wt.% hydrogen with a small amount of diborane, thermolysis of $Rb[Y(BH_4)_4]$ and $NaY(BH_4)_2Cl_2$ afforded no diborane.[122] Similarly, thermolysis of bimetallic lanthanum borohydrides, $NaLa(BH_4)_4$ and $K_3La(BH_4)_6$, in the range of RT to 400 °C showed 5.9 and 2.8% weight loss with no detectable diborane.[123]

Another approach for facilitating the dehydrogenation thermodynamics of MBHs is stabilization of the dehydrogenation products which is achieved through combination with other elements, metal hydrides and some other techniques.[46] Al-doped $LiBH_4$ performs as a reversible hydrogen storage and its thermolysis produces LiH and AlB_2 along with hydrogen.[124] Thermal decomposition of $2LiBH_4$-Al occurs through a three-step process:[125] 1) *280-375 °C* in which minor hydrogen release accompanies the concurrent formation of B and AlB_2. 2) *375-500 °C* in which hydrogen release is the major event through two simultaneous reactions: $2\ LiBH_4 + AlB_2 \rightarrow 2\ LiH + Al + 4\ B + 3\ H_2$ and $2\ LiBH_4 + Al \rightarrow 2\ LiH + AlB_2 + 3\ H_2$. 3) *500-550 °C* during which $LiBH_4$ and AlB_2 fully decompose while LiAl could be formed through the reaction of Al and LiH ($LiH + 2Al \rightarrow 2LiAl + H_2$). $LiBH_4$ was also reported to release 13.8 wt.% hydrogen efficiently at T_{dec}= 410 °C, producing LiH and B by-products.[126] Addition of MgH_2 by decreasing T_{dec} to 168 °C, produced LiH and MgB_2 instead.[127] It has also been reported

that addition of some transition metal halides such as $TiCl_3$, TiF_3 and ZnF_2 are capable of destabilizing $LiBH_4$ and reducing the dehydrogenation temperature through a cation exchange process and *in situ* formation of unstable transition metal borohydrides.[128] $Mg(BH_4)_2$ with 14.9 wt.% hydrogen density is among the MBHs with the highest gravimetric hydrogen storage capacities. It releases 13.7 wt.% hydrogen without borane impurities between 262-527 °C. The initial dehydrogenation temperature of $Mg(BH_4)_2$ was reduced significantly to 88 °C by addition of $TiCl_3$ perhaps due to formation of less stable $MgTi_x(BH_4)_{(2+nx)}$ (n = number of participating Ti atoms).[129]

Dehydrogenation of metal borohydrides is typically a step-wise process consisting of several intermediates. Each step of this process faces an activation energy and here is where a catalyst can play a kinetic role. Two approaches have been investigated for this purpose: 1) addition of catalysts and additives, 2) nanoconfinement in the pores and channels of porous materials.

The entire 8.4 wt.% hydrogen capacity of $Zn(BH_4)_2$, prepared from ball milling 1:2 ratio of $ZnCl_2$ and $NaBH_4$, could be released between 100-115 °C. Doping with 1.5 mol% of a commercial nanoNi catalyst decreased both the melting and the dehydrogenation onset temperatures, from 93 and 100 °C to 90 and 70 °C respectively. Moreover, the amount of released diborane decreased by a factor of 20 compared to the uncatalyzed sample.[130] Zinc borohydride, $Zn(BH_4)_2$, was first synthesized by Schlesinger et al. in 1951 through the reaction of pure ZnH_2 and diborane (B_2H_6) in diethyl ether and described as a colorless solid which slowly decomposes in air above 50 °C and reacts violently with water.[131] Although the elemental analysis of the solid obtained after solvent evaporation indicated a ratio of 1:2 for Zn:B, no structural evidence was obtained. Prior to being considered as a hydrogen storage candidate, zinc borohydride in ether or tetrahydrofuran (thf) was widely used as a potent *in-situ* chemo, regio and streoselective reducing agent for a variety of organic transformations due to its ease of preparation and strong reducing ability.[132]

Incorporation of chemical hydrogen storage compounds into nanoporous materials is reported to enhance their hydrogen release process through decreasing the onset release temperature and/or increasing the selectivity of the released gas to hydrogen.[46] This concept was first demonstrated for AB which resulted in a notable reduction in the dehydrogenation temperature as well as borazine formation.[133] Dehydrogenation of $LiBH_4$ was observed to occur 50 times faster when confined in a nanoporous carbon scaffold with nanopores of 13 nm.[134] Recently, other strategies such as mixing with

reduced graphene oxide[135] and ionic liquids[136] also were employed to improve the kinetics of hydrogen release from a variety of metal borohydrides.

1.6.2. Hydrogen Release by Hydrolysis

As thermolysis of metal borohydrides suffers from high hydrogen release temperatures, sluggish kinetics and diborane contamination of the hydrogen stream, researchers have also pursued the hydrolysis route. Providing protic hydrogens from water enables an easier combination of $H^{\delta-}$ and $H^{\delta+}$ atoms, resulting in lower hydrogen release temperature and a cleaner H_2 stream. Water is also a green and non-toxic solvent so its use does not impose environmental problems.

From the MBHs to date $LiBH_4$ (18.5 wt.% H_2), $NaBH_4$ (10.8 wt.% H_2) and KBH_4 (7.5 wt.% H_2) have been considered for hydrolysis according to the following reaction:

$$MBH_4 + 4H_2O \longrightarrow MBO_2 + 4\ H_2 \qquad (M= Li, Na \text{ and } K)$$

In practical applications it is necessary to keep the metal borate by-product soluble, so excess water has to be utilized to produce the hydrated metal borate. Obviously, handling excess water significantly reduces the efficiency of the MBH fuel (gram of H_2 per gram of the fuel). Gravimetric hydrogen storage capacity (GHSC) of $NaBH_4$-H_2O when 4 mol of water are required per each mol of $NaBH_4$ for the hydrolysis reaction is reduced from a theoretical value of 10.8 to 7.3 wt.% while the best systems to date report a GHSC between 6 and 7 wt.%.[137]

$$MBH_4 + 4H_2O \xrightarrow{H_2O} MBO_2{\cdot}2H_2O + 4\ H_2 \qquad (M= Li, Na \text{ and } K)$$

The majority of MBH hydrolysis reports have focused on $NaBH_4$, due to higher stability and ease of handling, as the Li and K salts are hygroscopic and release hydrogen spontaneously. To minimize auto hydrolysis of the MBHs under ambient conditions the solutions containing them are kept basic.[138] However, they suffer from sluggish hydrolysis kinetics, clogging due to formation of borate by-products and low net gravimetric hydrogen storage capacities.[139] Hydrolysis of $LiBH_4$ gives rise to multiple products depending on the hydrolysis conditions (such as temperature) including $LiBO_2$, $LiBO_2{\cdot}H_2O$ and $LiBO_2{\cdot}2H_2O$ ($Li[B(OH)_4]$).[140] Uncatalyzed hydrolysis of KBH_4 proceeds with the slowest rate among these MBHs.[138b] To improve the efficiency, CO_2-promoted hydrolysis of KBH_4 was reported recently.[141]

The first catalyzed hydrolysis of $NaBH_4$ was reported by Schlesinger in 1953.[142] A series of acidic accelerators including oxalic acid, succinic acid, phosphorous (V) oxide, aluminum chloride and boric oxides were used and catalytic accelerators included Raney Ni and MCl_2, where M = Fe, Co, Ni and Cu. It was observed that $NaBH_4$ pellets containing 5 wt.% $CoCl_2$ catalyst released hydrogen 10 times faster than pellets containing 50% boric acid by weight. Elemental analysis of the black material obtained from addition of solid $CoCl_2$ to a $NaBH_4$ solution indicated a cobalt to boron ratio of 1.99:1 representing cobalt boride, Co_2B, which was believed to be the catalytically active species. Catalyzed hydrogen release through hydrolysis of $NaBH_4$ has been at the center of attention for the last two decades as its thermolysis occurs at temperatures over 450 °C.[143] Several homogeneous and heterogeneous catalysts have been explored for this reaction, improving every aspect of reactivity in the hydrolysis system. [47,144] A more recent review by Demirci looked at global statistics of the research dedicated to this reaction from 2003-2013, summarizing the scientific and technical issues.[145]

Hydrolysis reactions of MBHs are highly exothermic due to replacing the weak B-H bonds in the borohydride fuel with much stronger B-O bonds in the borate by-products. This makes the fuel regeneration energy intensive. Nonetheless, catalyzed hydrolysis of $NaBH_4$ was scaled up for use in a fuel cell and in an actual vehicle prototype by Millennium Cell Inc. in New Jersey, USA in the late 1990s. In the first sodium borohydride fueled car, ***Genesis*** (Figure 1.9), hydrogen was released "on demand" by passing a saturated alkaline solution of $NaBH_4$ in water over a supported Ru catalyst and then converted to electricity using two stacks of PEMFCs under the hood of the car. The amount of hydrogen was enough to power the 5-passenger car over 400 miles without refueling while the only emission product was *pure water*! In spite of a number of refinements, the water-driven $NaBH_4$ system could not meet the expected DOE performance targets for 2010 and a "***no-go***" recommendation was made for $NaBH_4$ hydrolysis in vehicles based on the following criteria:[137]

1) Need for an alkaline solution to minimize $NaBH_4$ auto hydrolysis;
2) Need to carry excess water to solubilize sodium borate ($NaBO_2$) by-product which reduces the gravimetric storage capacity;
3) Large heat of reaction makes fuel regeneration energy intensive.

Figure 1.9. First sodium borohydride fueled car designed by Millennium Cell, NJ.

1.7. Ammine Metal Borohydrides

Metal borohydride complexes with coordinated ammonia molecules, denoted as ammine metal borohydrides (AMBs, $M(BH_4)_m(NH_3)_n$), normally contain 10-15 wt.% hydrogen capacity and are very promising hydrogen generators if the metal is Lewis acidic enough to discourage dissociation of the ammonia ligand. The number of BH_4 ligands is limited to the oxidation state of the metal centre whereas, the number of ammonia molecules can vary (from 1 to 8) based on the metal reaction conditions.[39] The dihydrogen bonding[50] between the hydridic B-H and protic N-H bonds renders the AMBs insoluble and lowers the energy barrier to H_2 release. As a result, lower hydrogen release temperatures are expected for AMBs *vs.* MBHs. For instance, T_{dec} for $LiBH_4$ was decreased from 380 to 135 °C in Co-catalyzed thermolysis of $Li(NH_3)_{4/3}BH_4$.[146]

Coordination of ammonia to unstable MBHs such as $Zn(BH_4)_2$ and $Al(BH_4)_3$, affords more stable solid AMBs ($Zn(BH_4)_2(NH_3)_n$ and $Al(BH_4)_3(NH_3)_n$) with even higher hydrogen contents. For instance $Al(BH_4)_3$ with 16.9 wt.% hydrogen is a volatile liquid (bp = 44 °C), whereas $Al(BH_4)_3(NH_3)_6$ (17.4 wt.% hydrogen) is a solid crystalline compound at room temperature that releases 11.8 wt.% H at 168 °C.[147] Decomposition temperatures of AMBs are correlated with the electronegativity of the metal center;[50] that is metals with higher χp exhibit lower decomposition temperatures. This correlation, shown in Figure 1.10, demonstrates a destabilizing effect for those stable MBHs with low electronegativity (χp < 1.6) upon coordination to ammonia (*i.e.* lower T_{dec}). On the other hand, metals with high electronegativity (χp > 1.6) in unstable MBHs tend to be stabilized upon coordination of ammonia (*i.e.* higher T_{dec}). This information may be used to design the right AMB for portable power applications.

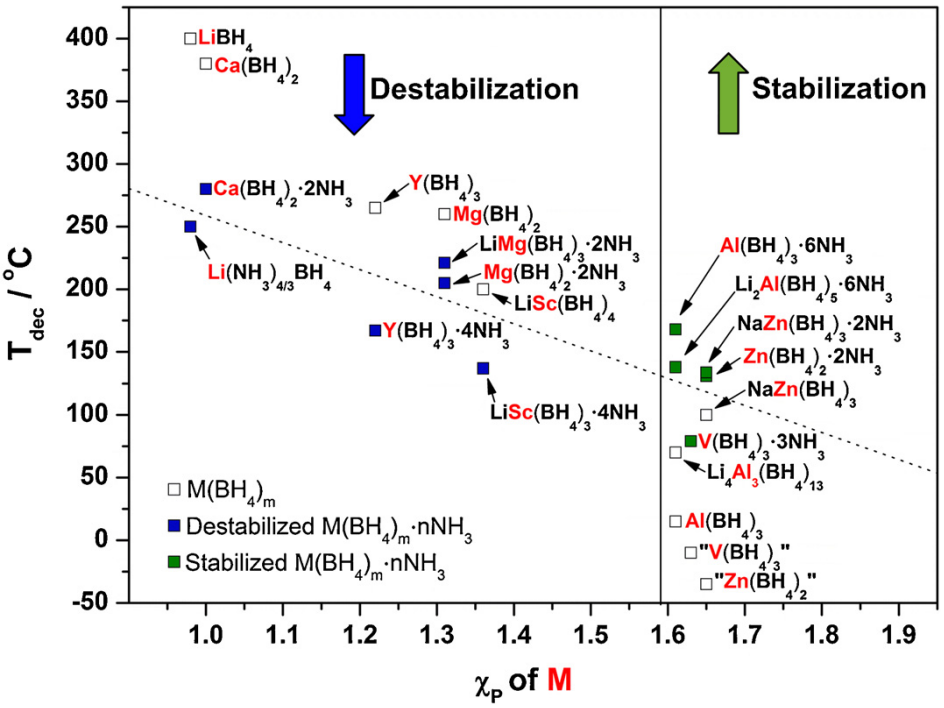

Figure 1.10. Experimental correlation of T_{dec} as a function of Pauling electronegativity (χp) of the metal center for comparison of selected MBHs and AMBs.[50] Ammonia coordination destabilizes MBHs having metals with low electronegativity, and stabilizes MBHs having metals with high electronegativity.

Ammonia contamination in the released hydrogen from AMBs is an important factor in which the composition of the released gas is largely governed by the ratio of NH/BH bonds, that is, systems having more protic hydrogens tend to release ammonia as an impurity.[148] For example, while hydrogen release is predominant in $Mg(BH_4)_2(NH_3)_2$,[149] large amounts of ammonia were observed from $Mg(BH_4)_2(NH_3)_6$.[150]

Most AMBs are synthesized through mechano-chemical (ball-milling) approaches, similar to MBHs. While being convenient and straightforward, this method allows for tailoring the amount of coordinated ammonia ligands to achieve high purity of hydrogen streams. A series of $Ca(BH_4)_2(NH_3)_n$[151] (n=1, 2, 4, 6) and $Y(BH_4)_3(NH_3)_n$[152] (n= 1, 2, 3, 4, 5, 6, 7) AMBs were obtained through sequential heat treatment of the complex with the highest number of coordinated ammonia molecules. Some AMBs such as $Ti(BH_4)_3(NH_3)_n$[153] (n= 3, 5) were prepared by ball-milling the corresponding $TiCl_3$ ammoniate ($TiCl_3 \cdot nNH_3$, n=3, 5) with stoichiometric amounts of $LiBH_4$. The number of coordinated ammonias in the chloride precursor was modified through heating procedures under vacuum in the belief that this stoichiometry will be maintained during the ball milling process. So, in one report $Zn(BH_4)_2(NH_3)_2$ was synthesized from mechano-chemical synthesis while the solvent-mediated route gave an ammonia:Zn ratio

of 4.[154] The main disadvantage of ball-milling approaches however, is retention of large quantities of alkali metal halide by-product in the reaction mixture. While initially being considered as "dead mass", later worked showed that such impurities not only reduce the gravimetric hydrogen capacity of the AMB system, but also can initiate side reactions decreasing the selectivity of the evolved gas.[155] A short review of the reported AMBs in each group of the periodic table is presented below.

1.7.1 Group 1: Lithium

Among the alkali metals, ammine Li borohydride has been utilized extensively for hydrogen storage applications. A series of $LiBH_4 \cdot nNH_3$ AMBs (n=1-4) was synthesized by dissolving $LiBH_4$ in liquid ammonia in the 1950s.[156] Heat treatment of $LiBH_4 \cdot NH_3$ until 300 °C under dynamic flow of Ar showed 40.6% weight loss and the released gas consisted of mainly NH_3 (*cf.* $LiBH_4$ starts to decompose at ~280 °C and theoretical NH_3 content is *ca.* 44 wt.%).[157] Addition of some metal chlorides such as $MgCl_2$, $ZnCl_2$ and $AlCl_3$, which readily coordinate to ammonia to form stable ammine metal complexes,[158] results in more ionic character of the M-N bonds, suppressing ammonia release and promoting combination of the more positively charged N-H with the BH_4 hydrides.[157] $LiBH_4(NH_3)_{4/3}$ containing equal number of protic and hydridic hydrogens, could release 17.8 wt.% hydrogen in a closed vessel with 320 ppm ammonia impurity in the temperature range of 135-250 °C using a nanosized Co catalyst.[146] Other strategies to enhance the hydrogen release from ammine lithium borohydride included immobilization on carbon nanotubes,[159] modification with AB,[160] confinement by Al_2O_3 nanoscaffolds[161] and doping with Mg and Al.[162]

1.7.2 Group 2: Magnesium and Calcium

The diammoniate complex of magnesium borohydride, ($Mg(BH_4)_2(NH_3)_2$), which was prepared from thermal decomposition of the hexaammine complex, with 16.0 wt.% hydrogen is a promising storage material for hydrogen.[149] With a melting point of 90 °C, hydrogen (13.1 wt.%) was released from 137 to 400 °C. While thermal decomposition of $Mg(BH_4)_2(NH_3)_2$ is endothermic, which makes the dehydrogenation more readily reversible, a minor (unmeasured) amount of ammonia was suggested to be released during the heating process. Improved hydrogen release properties of $Mg(BH_4)_2(NH_3)_2$ have been reported through multiple strategies including mixing with additives such as $NaAlH_4$[163] and AB[164] and synthesis of double-cation AMBs such as $LiMg(BH_4)_3(NH_3)_2$.[165] Mechanochemical reaction of $Mg(BH_4)_2$ and 6 atm of NH_3 at

room temperature yields $Mg(BH_4)_2(NH_3)_6$.[150] Heat treatment of hexammine magnesium borohydride from 85-600 °C proceeds via 6 stages with 7 equiv. of H_2 and 4 equiv. of NH_3 being released over the same temperature range. Incorporation into the activated carbon micropores (Scheme 1.3) reportedly lowered the H_2 release temperature to 40 °C which is 85 °C lower than that of bulk $Mg(BH_4)_2(NH_3)_6$.[166]

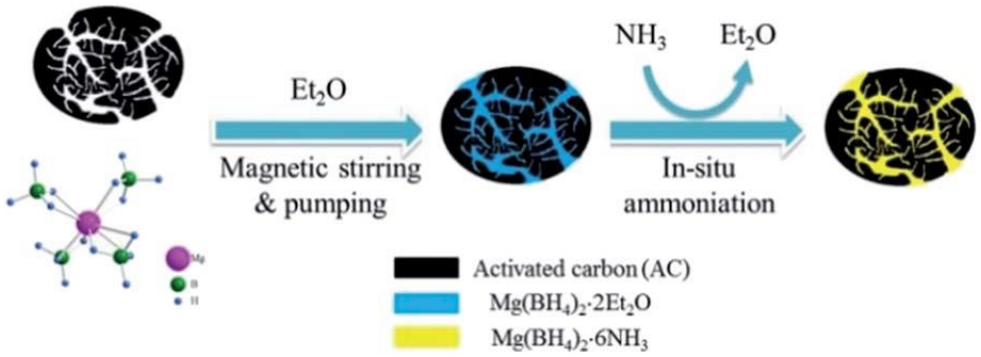

Scheme 1.3. Schematic synthesis of nanoconfined $Mg(BH_4)_2(NH_3)_6$ in microporous activated carbon.[166]

Ca-AMBs, $Ca(BH_4)_2(NH_3)_n$ (n=1, 2, 4, 6), were reported in 1989 by Kravchenko et al.[167] who found that decomposition up to 230 °C under a dynamic flow of argon yielded only ammonia (Scheme 1.4).[167]

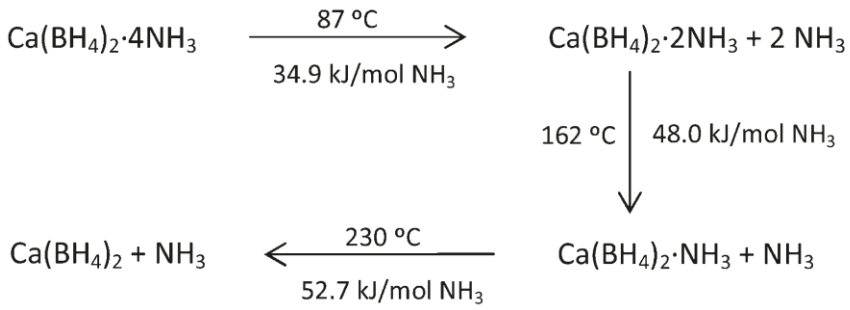

Scheme 1.4. Thermal decomposition pathway of $Ca(BH_4)_2(NH_3)_4$ under a dynamic flow of argon.[167]

In contrast, thermolysis of $Ca(BH_4)_2(NH_3)_2$ in a closed vessel released 11.3 wt.% H with only traces of ammonia contamination between 250-500 °C. Addition of one equiv. of $LiBH_4$ tremendously improved the hydrogen release properties of $Ca(BH_4)_2{\cdot}NH_3$[151] with the onset temperature decreased to 80 °C and, release of 12.3 wt.% highly pure hydrogen up to 350 °C. Similarly, high purity hydrogen streams (>99 %) were also reported from thermolysis of $Ca(BH_4)_2(NH_3)_4/2Mg(BH_4)_2$, $Ca(BH_4)_2(NH_3)_2/Mg(BH_4)_2$ and $Ca(BH_4)_2{\cdot}NH_3/Mg(BH_4)_2$ below 300 °C due to the introduction of further BH groups.[168]

1.7.3 Group 3: Scandium, Yttrium, Lanthanum

The mixed-cation scandium borohydride ammoniate, $LiSc(BH_4)_4(NH_3)_4$ (15.7 wt.% H), prepared by ball-milling $ScCl_3{\cdot}4NH_3$ and 3 equiv. of $LiBH_4$, possesses an orthorhombic structure (Figure 1.11).[169] The authors claimed that 16 wt.% of 99% pure hydrogen (measured by MS) (9.5 wt.% from the sample containing 3 equiv. LiCl) was released up to 300 °C. While the lack of B_2H_6 formation suggests that the released hydrogen is due to the combination of N-H and B-H bonds, this would yield a maximum of 13.4 wt.%.

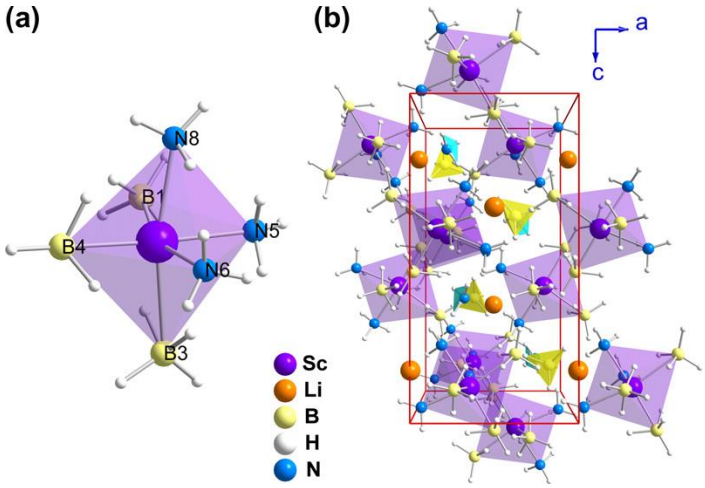

Figure 1.11. (a) Coordination of NH_3 and BH_4 units to Sc and (b) Crystal structure of $LiSc(BH_4)_4(NH_3)_4$.[169]

Further attempts to improve the dehydrogenation properties from $ScCl_3.xNH_3/mLiBH_4$ (x= 3, 4, 5; m= 3, 4, 5) mixtures indicated that the H_2 purity is higher with samples containing more B-H bonds and the highest with a balanced ratio of N-H/B-H bonds.

Ammine yttrium borohydride, $Y(BH_4)_3(NH_3)_4$, with 11.9 wt.% hydrogen density and an equal number of hydrides and protons was synthesized by ball-milling $YCl_3{\cdot}4NH_3$ and 3 equiv. of $LiBH_4$.[170] Compared to $Y(BH_4)_3$ which releases 7.8 wt.% H upon heating to 500 °C,[171] dehydrogenation of Y-AMB proceeds in three steps with major hydrogen releases at 86, 179 and 279 °C. Overall, a total of 9.3 wt.% hydrogen (90.5 mol% pure) was released by heat treatment of Y-AMB from 60-300 °C in a closed system. Under a dynamic flow of nitrogen gas $Y(BH_4)_3(NH_3)_4$ showed 22.8% weight loss indicating liberation of a large amount of NH_3. Two resonances were observed in the ^{11}B MAS NMR of the as synthesized $Y(BH_4)_3(NH_3)_4$ at -28.6 and -39 ppm (ratio of 1:2) which were used in combination with powder XRD data to propose an orthorhombic crystal structure with distorted octahedral geometry and the formula of $[Y(BH_4)_2(NH_3)_4](BH_4)$. In this structural model there are two kinds of BH_4^- units: two coordinated to Y and one in its outer coordination sphere which is held through dihydrogen bonds to the

coordinated NH_3 ligands (Figure 1.12a). This structural model was re-visited by Jensen et al.[152] who showed that all the BH_4^- and NH_3 ligands are coordinated to Y and that the previous work analyzed a mixture of tetra- and hepta-ammoniates (Figure 1.12b).

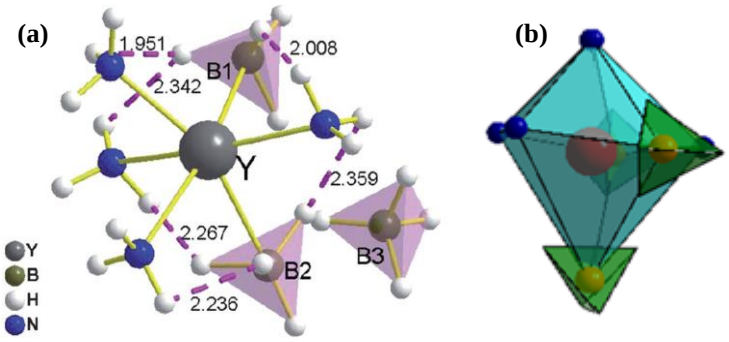

Figure 1.12. Y-AMB crystal structures proposed by (a) Xuebin Yu for $[Y(BH_4)_2(NH_3)_4]BH_4$[170] and (b) Torben Jensen for $Y(BH_4)_3(NH_3)_4$.[152]

1.7.4. Group 4: Titanium, Zirconium

Three titanium-AMBs have been introduced: $Ti(BH_4)_3{\cdot}3NH_3$, $Ti(BH_4)_3{\cdot}5NH_3$, and $Li_2Ti(BH_4)_5{\cdot}5NH_3$.[153] $Ti(BH_4)_3$ is a volatile and unstable MBH at RT;[172] however, coordination of ammonia ligands to Ti stabilizes the compounds resulting in more favorable dehydrogenation properties. The $Ti(BH_4)_3(NH_3)_n$ (n=3, 5) complexes were synthesized through mechano-chemical mixing of $TiCl_3(NH_3)_n$ with $LiBH_4$. Consequently, $LiBH_4$ adducts of Ti-AMB, $Li_mTi(BH_4)_{3+m}(NH_3)_n$, were prepared from the reaction of $Ti(BH_4)_3(NH_3)_n$ and $LiBH_4$. The authors claimed release of 14 wt.% pure hydrogen (indicated by MS results) from $Ti(BH_4)_3(NH_3)_3$ over the range of 60-300 °C in a two-step process centered at 109 and 152 °C (Table 1.8). In contrast, $Ti(BH_4)_3(NH_3)_5$ released ~13.4 wt.% hydrogen with minor ammonia contamination, in a single step process, from thermolysis to 300 °C. Furthermore, 15.8 wt.% pure hydrogen could be obtained from thermolysis of $Li_2Ti(BH_4)_5(NH_3)_5$ (16.5 wt.% H) in the temperature range of 75-300 °C (cf. 14% could be derived from combination of N-H and B-H bonds).

Table 1.8. Dehydrogenation properties of ammine titanium borohydrides.

Storage compound	TG (wt.%)	Released gas contents		
		H_2 (wt.%)	NH_3 (wt.%)	H_2 purity (mol%)
$Ti(BH_4)_3(NH_3)_3$	14	14	0	100
$Ti(BH_4)_3(NH_3)_5$[1]	22.0	13.4	7.3	96
$Ti(BH_4)_3(NH_3)_5 + LiBH_4$[1]	18.0	15.0	2	98.5
$Li_2Ti(BH_4)_5(NH_3)_5$	15.8	15.8	0	100

$Zr(BH_4)_4$ is a volatile MBH (mp = 32 °C) that releases both hydrogen and diborane at 157 °C.[173] On the other hand, ammine zirconium borohydride, $Zr(BH_4)_4(NH_3)_8$, with 14.0 wt.% H and the highest number of coordinated ammonia ligands among all AMBs, exhibits a unique crystal structure (side-bicapped trigonal prism) compared to other AMBs.[174] Due to the volatility of $Zr(BH_4)_4$, Zr-AMB was prepared from the low temperature reaction of ammonia gas with sublimed $Zr(BH_4)_4$, derived from ball-milling $ZrCl_4$ and $LiBH_4$. A total of 22.8% weight loss was observed up to 300 °C over a single stage process with a peak at 130 °C. While no diborane could be detected, concurrent formation of ammonia decreased the hydrogen purity to 83.7 mol%. Additives such as AB and MBHs were explored to improve the Zr-AMB dehydrogenation kinetics. As a result, H_2 purity was increased to 96.1 mol%, although with lower extent of release (7 wt.%), using $Zr(BH_4)_4(NH_3)_8$-4AB with a peak temperature at 85 °C.[175] Ball-milling of $Zr(BH_4)_4(NH_3)_8$ with 2 equiv. of $MgBH_4$ afforded a material that gave 99.8 mol% pure hydrogen with a peak at 106 °C.[176] The lower dehydrogenation temperature was attributed to ammonia transfer to $Mg(BH_4)_2$ which resulted in a more balanced number of BH_4 and NH_3 ligands on Zr.

1.7.5. Group 5: Vanadium, Niobium

$V(BH_4)_3(NH_3)_3$ with a cubic structure was synthesized from ball-milling $VCl_3{\cdot}3NH_3$ and 3 equiv. of $LiBH_4$.[169] Thermolysis released 16.1 wt.% hydrogen (two steps with peaks at 79 °C and 125 °C), until 300 °C along with a small amount of ammonia contamination. The penta-ammoniate $V(BH_4)_3(NH_3)_5$ yielded 11.5 wt.% hydrogen but with a purity of only 85 mol%.[177] The dehydrogenation behavior of this AMB was improved through mixing with some additives such as LiH and $Mg(BH_4)_2$ (Table 1.9).

Table 1.9. Thermal dehydrogenation of $V(BH_4)_3(NH_3)_5$ and its composites.

Storage Media	H_2 wt.%	NH_3 wt.%	H_2 purity (mol%)
$V(BH_4)_3(NH_3)_5$	11.5	17.1	85
$V(BH_4)_3(NH_3)_5$ + 6 LiH	10.3	10.7	89
$V(BH_4)_3(NH_3)_5$ + 2 $LiBH_4$	13.5	11.7	91
$VMg(BH_4)_5(NH_3)_5$	12.7	4.5	96
$V(BH_4)_3(NH_3)_5$ + 2 $Mg(BH_4)_2$	12.4	0	100

Ammine niobium borohydride complexes were prepared mechano-chemically from $NbCl_5{\cdot}5NH_3$ and 5 equiv. of $Li(Na)BH_4$.[178] The authors claimed that a total of 8.1 wt.% pure hydrogen was released in the temperature range of 50-250 °C from

$NbCl_5 \cdot 5NH_3/5LiBH_4$. In contrast, 11.2 wt.% pure hydrogen was obtained from $NbCl_5 \cdot 5NH_3/5NaBH_4$ during heating between 65-250 °C. It was concluded that in addition to favorable N-H···H-B dihydrogen bonding interactions, B-H···H-B and N-H···H-N homo-polar interactions also take part in hydrogen formation, explaining the high purity of the released hydrogen from the Nb-based AMBs.

1.7.6. Group 6: Chromium

Hexamminechromium(III) borohydride was first synthesized in 1958 from the reaction of dry $[Cr(NH_3)_6]F_3$ and $NaBH_4$ in liquid ammonia (LNH_3) between -45 °C to -65 °C.[179] Similar to the ball-milling method, the NaF by-product was included in the reaction mixture. This AMB undergoes decomposition irreversibly to ammonia and hydrogen (not measured) starting at 60 °C under reduced pressure. Ball-milling of $CrCl_3 \cdot nNH_3$ (n= 3, 4, 5) with 3 equiv. $LiBH_4$ yielded a series of chromium-based AMBs.[180] The highest hydrogen purity of 91.8 mol% was observed with $CrCl_3 \cdot 3NH_3/3LiBH_4$ with 15.6% weight loss. Addition of 0.5 mol $ZnCl_2$ decreased weight loss to 8.1% but released a purer hydrogen stream (98.8 mol%). Salt metathesis of $CrCl_2$ and 2 equiv. of $LiBH_4$ in dimethyl sulfide, SMe_2, at low temperatures produced a mixture of multiple crystalline unknown phases.[181] In this approach LiCl, the metathesis by-product, is insoluble in SMe_2 and can be separated by filtration. The isolated Cr-AMB solid, after solvent evaporation, was unstable at RT and concurrent release of ammonia and hydrogen during heat treatment between 25-300 °C resulted in ~35% weight loss, suggesting the evolution of large amounts of ammonia.

1.7.7 Group 7: Manganese

Salt-free octahedral $[Mn(NH_3)_6](BH_4)_2$ was prepared from the solid-gas reaction of $Mn(BH_4)_2$ and dry ammonia gas.[182] $Mn(BH_4)_2$ itself was simply synthesized through salt metathesis of $MnCl_2$ and 2 equiv. of $LiBH_4$ in diethyl ether followed by extraction into SMe_2. Decomposition of $[Mn(NH_3)_6](BH_4)_2$ (with 44.5% weight loss) proceeds without melting from RT to 400 °C during which ammonia release is dominant.

A series of Mn-AMBs (with < 6 coordinated ammonia ligands) was also synthesized through mechanochemical treatment of $Mn(BH_4)_2 \cdot 6NH_3/nMn(BH_4)_2$ (n=1, 2, 3).[182] In contrast to hexaammine manganese borohydride, $Mn(BH_4)_2 \cdot NH_3$ (10.9 wt.% H) releases mainly hydrogen with a peak temperature at 130 °C (33% total weight loss) from RT to 160 °C.

1.7.8. Group 8: Iron

Fe-AMBs were synthesized through two methods. In the first method, $Fe(BH_4)_2$ was prepared from the low temperature (-50 °C) stirring of $FeCl_2$ and 2 equiv. of $LiBH_4$ in SMe_2. Addition of ammonia gas to the solution, after a filtration step to separate LiCl, resulted in the immediate precipitation of a mixture of solids that included ($[Fe(NH_3)_6](BH_4)_2$, 73 wt.% of identified crystalline solids). In a second approach, ammonia was condensed (LNH_3) onto the mixture of $FeCl_2$ and 2 equiv. of $LiBH_4$ and stirred together. Analysis of the solid obtained after removing excess NH_3 under vacuum also indicated a mixture of products that included ($[Fe(NH_3)_6](BH_4)_2$, 59 wt.% of identified crystalline solids).[181] No attempts were made to purify the Fe AMB product. Heat treatment of the Fe-AMB mixtures prepared in LNH_3 exhibited ~34% weight loss from 25-300 °C while the composition of the released gas consisted of more ammonia than hydrogen.

1.7.9. Group 9: Cobalt

The first synthesis of ammine cobalt borohydride complexes was reported in the 1950s when hexamminecobalt(III) borohydride was prepared from the stoichiometric reaction of $[Co(NH_3)_6]F_3$ and $NaBH_4$ in LNH_3.[179] This product decomposed to hydrogen and ammonia at RT under vacuum. Using cheaper cobalt starting materials such as $CoCl_2$ was not successful in preparing the Co-AMB as $CoCl_2$ is easily reduced to metallic cobalt in contact with $LiBH_4$ in $S(CH_3)_2$ even at low temperatures.[181] Addition of ammonia gas to this suspension resulted in formation of AB and not the Co-AMB. However, salt metathesis of $CoCl_2$ and $LiBH_4$ in LNH_3 forms $[Co(NH_3)_6](BH_4)_2$ (cubic structure, 40% yield) and a solid solution, $[Co(NH_3)_6](BH_4)_{2-x}Cl_x$ (16% yield, x= 0.96(2)). Thermolysis of this mixture from 25-300 °C revealed ~27% weight loss with an onset of 60 °C for both ammonia and hydrogen and formation of more ammonia at higher temperatures. New Co-AMBs with lower amounts of coordinated ammonia were prepared by ball-milling $CoCl_n{\cdot}3NH_3$ (n = 2, 3) and $LiBH_4$.[183] TGA-MS results for trivalent $LiCo(BH_4)_4(NH_3)_3$ (14.3 wt.%) from 25-300 °C indicated 15.1 wt% release (with respect to pure materials) of 99 mol% hydrogen. Corresponding results for divalent $LiCo(BH_4)_3(NH_3)_3$ (13.1 wt% H) yielded 11.5% hydrogen with only 93% purity. In isothermal studies their purported $Co(BH_4)_3(NH_3)_3$ complex released 5.2 wt% (2.9 wt% including LiCl) of pure hydrogen within 40 min at 80°C.

1.7.10 Group 12: Zinc

Zn^{2+}, with an electronic configuration of $3d^{10}$, resembles alkaline earth metal ions such as Mg^{2+} and Ca^{2+}. Therefore, structural and dehydrogenation properties of $Zn(BH_4)_2(NH_3)_2$ are often compared with the Mg and Ca complexes of the same formula.[154] The M-H bonds in this Zn-AMB are proposed to be shorter than those of the Mg and Ca analogues, leading to more ionic character for the hydride. Therefore, more favorable dehydrogenation properties are observed with Zn; recall that while almost no hydrogen was released from $Ca(BH_4)_2(NH_3)_2$ under dynamic N_2 flow,[167] 13.1 wt.% hydrogen was released from $Mg(BH_4)_2(NH_3)_2$ below 400 °C.[149] $Zn(BH_4)_2(NH_3)_2$ was synthesized mechano-chemically from $ZnCl_2{\cdot}2NH_3$ and 2 equiv. of $LiBH_4$ as the only crystalline product (Figure 1.13a), showing a monoclinic crystal structure.[154] With a hydrogen desorption onset of 90 °C $Zn(BH_4)_2(NH_3)_2$/2LiCl released 5.4 wt.% pure hydrogen (confirmed by MS results) up to 150 °C which is equal to 8.9 wt.% hydrogen with respect to pure material.

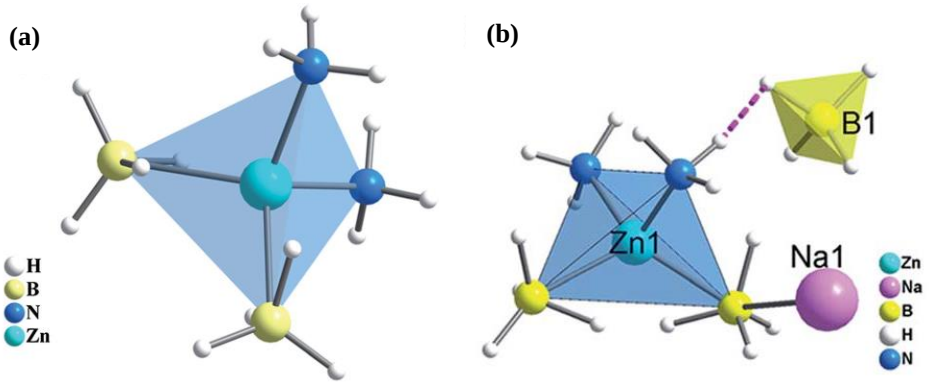

Figure 1.13. Crystal structure of (a) $Zn(BH_4)_2(NH_3)_2$[154] and (b) $NaZn(BH_4)_3(NH_3)_2$.[184]

The mixed-cation AMB, $NaZn(BH_4)_3(NH_3)_2$ (Figure 1.13b) was isolated as a solid after bubbling $NH_{3(g)}$ through a thf solution obtained from ball-milled $ZnCl_2$ and 3 equiv. of $NaBH_4$ followed by filtration.[184] With an orthorhombic crystal structure and 10.9 wt.% H, thermolysis of this AMB from 100-140 °C showed a 13.5% weight loss of H_2 and NH_3 (83.6 mol% hydrogen purity). A series of AB adducts of $NaZn(BH_4)_3(NH_3)_2$ was recently prepared by the ball-milling method. $NaZn(BH_4)_3(NH_3)_2$-nNH_3BH_3 (n= 1-5) displayed enhanced dehydrogenation properties compared to the pristine material.[185] Heating $NaZn(BH_4)_3(NH_3)_2$-$4NH_3BH_3$ to 250 °C released 11.6 wt.% hydrogen with 99.1 mol% purity and a peak temperature of 85 °C.

1.7.11. Group 13: Aluminum

Ammine aluminum borohydride is the only AMB from group 13 which has been considered for hydrogen storage applications so far due to its satisfactory dehydrogenation properties. Volatile and unstable $Al(BH_4)_3$[186] turns into more stable $Al(BH_4)_3(NH_3)_6$ upon coordination of ammonia with a theoretical hydrogen density of 17.4 wt.%.[187] A total of 11.8 wt.% hydrogen at 94.6 mol% purity was released from 60-300 °C which was improved slightly by $AlCl_3/LiBH_4$ additives. Immobilization of $Al(BH_4)_3(NH_3)_6$ on poly(styrene-co-divinylbenzene) resin remarkably boosted the kinetics of the dehydrogenation process and increased the purity of the evolved hydrogen (> 99 mol%).[188] $Al(BH_4)_3(NH_3)_3$ and $Al(BH_4)_3(NH_3)_4$ were reported to release 13.7 and 15.5 wt.% highly pure hydrogen during heating to 300 °C.[147] $Li_2Al(BH_4)_5(NH_3)_6$ was the first double-cation AMB, representing an ordered arrangement of cationic $Al(NH_3)_6^{3+}$ and anionic $Li_2(BH_4)_5^{3-}$ units.[148] TGA results from this solid indicated 23.2% weight loss by 300 °C and more than 10 wt.% pure hydrogen (>99 %) was released below 120 °C (in a closed vessel). The kinetics of dehydrogenation from $Li_2Al(BH_4)_5(NH_3)_6$ were improved significantly through addition of 0.5 equiv. of $Mg(BH_4)_2$. Over 10 wt.% pure hydrogen desorbed from $0.5Mg(BH_4)_2/Li_2Al(BH_4)_5(NH_3)_6$ below 120 °C within only 30 min.[189] A short review of aluminum complexes of BN- based hydrides has been published by Filinchuk.[190]

1.8. Thesis Summary

The concepts described in this chapter will come into context in the ensuing chapters of this *Thesis*. The work described in **Chapter 2** was initiated as a project funded by NSERC's national hydrogen research network, H_2CAN. Boyd Davis, President of Kingston Process Metallurgy and an adjunct professor of mining engineering at Queen's University in Kingston had been investigating catalyzed SBH hydrolysis in methanol solvent and needed a more robust catalyst. His long-term objective was to develop a base-free continuous hydrogen generator for portable power applications, including underground mine forklifts. After preliminary studies on supported base-metal catalysts by a Baker group undergrad, Emily Mattiussi, we had a visiting professor from France, Vanessa Prevot, who suggested that we try hierarchical metal-doped layered double hydroxides (LDHs). The preparation, characterization and catalytic performance of polystyrene-templated 'inverse opal' LDH catalysts are detailed in **Chapter 2**.

When Boyd Davis' company turned to other priorities, we teamed with Ged McLean from the BIC corporation in Vancouver who was interested in advanced solid hydrogen storage materials. We identified ammine metal borohydrides (AMBs) as promising materials based largely on the work by Xuebin Yu from Fudan University in Shanghai, China. Dissatisfied with the metal chloride 'dead mass' typically accompanying mechano-chemical synthesis methods, we set out to develop useful solution syntheses of AMBs. In **Chapter 3** it will be shown that solution synthesis of most AMBs in thf (and other organic solvents) is accompanied by unexpected formation of ammonia-borane. The determining factors responsible for formation of ammonia-borane were investigated for both main group and transition metals.

Hydrogen released from AMBs is usually contaminated by ammonia so we sought catalysts that would lower the activation barrier to dehydrogenative B-N bond formation. In **Chapter 4** solution routes to pure Y and La AMBs are developed and a series of base-metal nanoparticle catalysts, prepared using a novel route from MCl_2 (M= Fe, Co, Cu) and liquid hexylamine-borane, are then tested to assess their effects on thermolysis of these AMBs.

Our studies in Chapter 3 indicated that Zn AMBs were uniquely stable with respect to AB formation. In **Chapter 5** a series of mixed-cation AMBs, $M^{I}Zn(BH_4)_3(NH_3)n$ are prepared by solution methods and their dehydrogenation is investigated using powder X-ray diffraction, multinuclear MAS NMR, and thermal analysis. The effects of base metal nanoparticle catalysts are also discussed.

Finally, in **Chapter 6** the results from this thesis research are placed in the context of the current state of the art and some proposals for future studies are detailed.

1.9. References

(1) Gustavsson, L.; Haus, S.; Lundblad, M.; Lundström, A.; Ortiz, C. A.; Sathre, R.; Truong, N. L.; Wikberg, P.-E. *Renew. Sustain. Energy Rev.* **2017**, *67*, 612-624.
(2) Jiang, Z.; Xiao, T.; Kuznetsov, V. L.; Edwards, P. P. *Philosoph. Trans. Royal Soc. A Math., Phys. Eng. Sci.* **2010**, *368*, 3343-3364.
(3) Environment and Climate Change Canada.
(4) Farmann, A.; Sauer, D. U. *J. Power Sources* **2016**, *329*, 123-137.
(5) Alazemi, J.; Andrews, J. *Renew. Sustain. Energy Rev.* **2015**, *48*, 483-499.
(6) Lenz, V.; Ortwein, A. *Chem. Eng. Technol.* **2017**, *40*, 313-322.
(7) Scott, D. S. In *Smelling Land: The Hydrogen Defense Against Climate Catastrophe;* Canadian Hydrogen Association, **2008**.
(8) Mazloomi, K.; Gomes, C. *Renew. Sustain. Energy Rev.* **2012**, *16*, 3024-3033.
(9) Bleamaster, L. F.; Crown, D. A. *U.S. Geological Survey Geologic Investigations* **2010**, *3096*, 80225.

(10) Sarma, S. J.; Brar, S. K.; Le Bihan, Y.; Buelna, G. *Bioproc. Biosys. Eng.* **2015**, *38*, 1097-1102.
(11) Zhang, Z.; Hu, C. *Int. J. Hydrogen Energy* **2014**, *39*, 12973-12979.
(12) Wang, M.; Wang, Z.; Gong, X.; Guo, Z. *Renew. Sustain. Energy Rev.* **2014**, *29*, 573-588.
(13) Burney, H. S. In *Modern Aspects of Electrochem.*; White, R. E., Conway, B. E., Bockris, J. O. M., Eds.; Springer US: Boston, MA, 1993, p 393-438.
(14) Armaroli, N.; Balzani, V. *Chem. Sus. Chem.* **2011**, *4*, 21-36.
(15) http://www.greencarreports.com/news/1091436_toyota-gasoline-engine-achieves-thermal-efficiency-of-38-percent.
(16) http://www.autoblog.com/2009/08/20/greenlings-why-choose-a-fuel-cell-or-an-internal-combustion-eng
(17) Saravanan, N.; Nagarajan, G. *Int. J. Hydrogen Energy* **2009**, *34*, 9019-9032.
(18) Rezaei Niya, S. M.; Hoorfar, M. *J. Power Sources***2013**, *240*, 281-293.
(19) Mauritz, K. A.; Moore, R. B. *Chem. Rev.* **2004**, *104*, 4535-4586.
(20) Liu, Y.-L. *Polym. Chem.* **2012**, *3*, 1373-1383.
(21) Saha, M. S.; Neburchilov, V.; Ghosh, D.; Zhang, J. *Wiley Interdisciplin. Rev.: Energy and Environ.* **2013**, *2*, 31-51.
(22) Wang, Y.; Chen, K. S.; Mishler, J.; Cho, S. C.; Adroher, X. C. *Appl. Energy* **2011**, *88*, 981-1007.
(23)https://energy.gov/sites/prod/files/2014/03/f11/executive_summaries_h2_storage_coes.pdf.
(24) a) Hua, T. Q.; Ahluwalia, R. K.; Peng, J. K.; Kromer, M.; Lasher, S.; McKenney, K.; Law, K.; Sinha, J. *Int. J. Hydrogen Energy* **2011**, *36*, 3037-3049. b) Züttel A. *Mater. Today* **2003**, 6, 24-33.
(25) Doyoyo, M.; Faure, N. *J. Press.Vessel Technol.* **2008**, *130*, 031210-031210.
(26) Gascon, J.; Corma, A.; Kapteijn, F.; Llabrés i Xamena, F. X. *ACS Catal.* **2014**, *4*, 361-378.
(27) Abedi, S.; Azhdari Tehrani, A.; Ghasempour, H.; Morsali, A. *New J. Chem.* **2016**, 40, 6970-6976.
(28) Liu, J.; Thallapally, P. K.; McGrail, B. P.; Brown, D. R.; Liu, J. *Chem. Soc. Rev.* **2012**, *41*, 2308-2322.
(29) DeCoste, J. B.; Peterson, G. W. *Chem. Rev.* **2014**, *114*, 5695-5727.
(30) Keskin, S.; Kızılel, S. *Indust. Eng. Chem. Res.* **2011**, *50*, 1799-1812.
(31) Kreno, L. E.; Leong, K.; Farha, O. K.; Allendorf, M.; Van Duyne, R. P.; Hupp, J. T. *Chem. Rev.* **2012**, *112*, 1105-1125.
(32) Ranocchiari, M.; Bokhoven, J. A. v. *Phys. Chem. Chem. Phys.* **2011**, *13*, 6388-6396.
(33) Langmi, H. W.; Ren, J.; North, B.; Mathe, M.; Bessarabov, D. *Electrochim. Acta* **2014**, *128*, 368-392.
(34) Alesaadi, S. J.; Sabzi, F. *Int. J. Hydrogen Energy* **2015**, *40*, 1651-1656.
(35) Ren, J.; Langmi, H. W.; North, B. C.; Mathe, M.; Bessarabov, D. *Int. J. Hydrogen Energy* **2014**, *39*, 890-895.
(36) Farha, O. K.; Özgür Yazaydın, A.; Eryazici, I.; Malliakas, C. D.; Hauser, B. G.; Kanatzidis, M. G.; Nguyen, S. T.; Snurr, R. Q.; Hupp, J. T. *Nat. Chem.* **2010**, *2*, 944-948.
(37) Tan, C.; Yang, S.; Champness, N. R.; Lin, X.; Blake, A. J.; Lewis, W.; Schroder, M. *Chem. Commun.* **2011**, *47*, 4487-4489.
(38) Wu, H. *Chem. Phys. Chem.* **2008**, *9*, 2157-2162.
(39) Paskevicius, M.; Jepsen, L. H.; Schouwink, P.; Cerny, R.; Ravnsbaek, D. B.; Filinchuk, Y.; Dornheim, M.; Besenbacher, F.; Jensen, T. R. *Chem. Soc. Rev.* **2017**, *46*, 1565-1634.

(40) Gandhi, K.; Kumar Dixit, D.; Kumar Dixit, B. *Physica B: Condensed Matter* **2010**, *405*, 3075-3081.
(41) Xueping, Z.; Xin, F.; Shenglin, L. *J. Alloys Compd.* **2011**, *509*, 5873-5876.
(42) Zhu, Q.-L.; Xu, Q. *Energy Environ. Sci.* **2015**, *8*, 478-512.
(43) Klerke, A.; Christensen, C. H.; Norskov, J. K.; Vegge, T. *J. Mater. Chem.* **2008**, *18*, 2304-2310.
(44) Chen, J.; Lu, Z.-H.; Huang, W.; Kang, Z.; Chen, X. *J. Alloys Compd.* **2017**, *695*, 3036-3043.
(45) van de Watering, F. F.; Lutz, M.; Dzik, W. I.; de Bruin, B.; Reek, J. N. H. *Chem. Cat. Chem.* **2016**, *8*, 2752-2756.
(46) Li, H.-W.; Yan, Y.; Orimo, S.-i.; Züttel, A.; Jensen, C. M. *Energies* **2011**, *4*, 185.
(47) Demirci, U. B.; Miele, P. *Phys. Chem. Chem. Phys.* **2014**, *16*, 6872-6885.
(48) Rossin, A.; Peruzzini, M. *Chem. Rev.* **2016**, *116*, 8848-8872.
(49) Stennett, T. E.; Harder, S. *Chem. Soc. Rev.* **2016**, *45*, 1112-1128.
(50) Jepsen, L. H.; Ley, M. B.; Lee, Y.-S.; Cho, Y. W.; Dornheim, M.; Jensen, J. O.; Filinchuk, Y.; Jørgensen, J. E.; Besenbacher, F.; Jensen, T. R. *Mater. Today* **2014**, *17*, 129-135.
(51) Chen, G.; Zakharov, L. N.; Bowden, M. E.; Karkamkar, A. J.; Whittemore, S. M.; Garner, E. B.; Mikulas, T. C.; Dixon, D. A.; Autrey, T.; Liu, S.-Y. *J. Am. Chem. Soc.* **2015**, *137*, 134-137.
(52) Moury, R.; Demirci, U. *Energies* **2015**, *8*, 3118.
(53) Shukla, A.; Karmakar, S.; Biniwale, R. B. *Int. J. Hydrogen Energy* **2012**, *37*, 3719-3726.
(54) Alhumaidan, F.; Cresswell, D.; Garforth, A. *Energy Fuels* **2011**, *25*, 4217-4234.
(55) Kariya, N.; Fukuoka, A.; Utagawa, T.; Sakuramoto, M.; Goto, Y.; Ichikawa, M. *Appl. Catal. A Gen.* **2003**, *247*, 247-259.
(56) Shukla, A. A.; Gosavi, P. V.; Pande, J. V.; Kumar, V. P.; Chary, K. V. R.; Biniwale, R. B. *Int. J. Hydrogen Energy* **2010**, *35*, 4020-4026.
(57) Kustov, L. M.; Tarasov, A. L.; Tarasov, B. P. *Int. J. Hydrogen Energy* **2013**, *38*, 5713-5716.
(58) a) Pez, G. P.; Scott, A. R.; Cooper, A. C.; Cheng, H.; US Patent 7101530: **2006**; b) Pez, G. P.; Scott, A. R.; Cooper, A. C.; Cheng, H.; Wilhelm, F. C.; Abdourazak, A. H.; US Patent 7351395: **2008**.
(59) Moores, A.; Poyatos, M.; Luo, Y.; Crabtree, R. H. *New J. Chem.* **2006**, *30*, 1675-1678.
(60) Sotoodeh, F.; Huber, B. J. M.; Smith, K. J. *Appl. Catal. A Gen.* **2012**, *419–420*, 67-72.
(61) Cui, Y.; Kwok, S.; Bucholtz, A.; Davis, B.; Whitney, R. A.; Jessop, P. G. *N. J. Chem.* **2008**, *32*, 1027-1037.
(62) https://www.hydrogen.energy.gov/pdfs/progress06/iv_b_3_cooper.pdf.
(63) a) Sotoodeh, F.; Zhao, L.; Smith, K. J. *Appl. Catal. A Gen.* **2009**, *362*, 155-162; b) Sotoodeh, F.; Smith, K. J. *J. Phys. Chem. C* **2013**, *117*, 194-204.
(64) Teichmann, D.; Arlt, W.; Wasserscheid, P.; Freymann, R. *Energy Environ. Sci.* **2011**, *4*, 2767-2773.
(65) Titherley, A. W. *J. Chem. Soc. Trans.* **1897**, *71*, 469-471.
(66) Wang, W.; Herreros, J. M.; Tsolakis, A.; York, A. P. E. *Int. J. Hydrogen Energy* **2013**, *38*, 9907-9917.
(67) White, A. H.; Melville, W. *J. Am. Chem. Soc.* **1905**, *27*, 373-386.

(68) a) Raróg-Pilecka, W.; Szmigiel, D.; Kowalczyk, Z.; Jodzis, S.; Zielinski, J. *J. Catal.* **2003**, *218*, 465-469; b) Yin, S. F.; Xu, B. Q.; Zhou, X. P.; Au, C. T. *Appl. Catal. A Gen.* **2004**, *277*, 1-9.
(69) Plana, C.; Armenise, S.; Monzón, A.; García-Bordejé, E. *J. Catal.* **2010**, *275*, 228-235.
(70) Christensen, C. H.; Sorensen, R. Z.; Johannessen, T.; Quaade, U. J.; Honkala, K.; Elmoe, T. D.; Kohler, R.; Norskov, J. K. *J. Mater. Chem.* **2005**, *15*, 4106-4108.
(71) a) Zheng, M.; Cheng, R.; Chen, X.; Li, N.; Li, L.; Wang, X.; Zhang, T. *Int. J. Hydrogen Energy* **2005**, *30*, 1081-1089; b) Zheng, M.; Chen, X.; Cheng, R.; Li, N.; Sun, J.; Wang, X.; Zhang, T. *Catal. Commun.* **2006**, *7*, 187-191; c) Chen, X.; Zhang, T.; Ying, P.; Zheng, M.; Wu, W.; Xia, L.; Li, T.; Wang, X.; Li, C. *Chem. Commun.* **2002**, 288-289.
(72) a) Gu, H.; Ran, R.; Zhou, W.; Shao, Z.; Jin, W.; Xu, N.; Ahn, J. *J. Power Sources* **2008**, *177*, 323-329; b) Santos, J. B. O.; Valença, G. P.; Rodrigues, J. A. J. *J. Catal.* **2002**, *210*, 1-6.
(73) Singh, S. K.; Xu, Q. *J. Am. Chem. Soc.* **2009**, *131*, 18032-18033.
(74) Singh, S. K.; Xu, Q. *Inorg. Chem.* **2010**, *49*, 6148-6152.
(75) Singh, A. K.; Xu, Q. *Chem. Cat. Chem.* **2013**, *5*, 3000-3004.
(76) Singh, S. K.; Xu, Q. *Chem. Commun.* **2010**, *46*, 6545-6547.
(77) Cao, N.; Su, J.; Luo, W.; Cheng, G. *Int. J. Hydrogen Energy* **2014**, *39*, 9726-9734.
(78) Aranishi, K.; Singh, A. K.; Xu, Q. *Chem. Cat. Chem.* **2013**, *5*, 2248-2252.
(79) Singh, S. K.; Singh, A. K.; Aranishi, K.; Xu, Q. *J. Am. Chem. Soc.* **2011**, *133*, 19638-19641.
(80) Singh, A. K.; Xu, Q. *Int. J. Hydrogen Energy* **2014**, *39*, 9128-9134.
(81) Manukyan, K. V.; Cross, A.; Rouvimov, S.; Miller, J.; Mukasyan, A. S.; Wolf, E. E. *Appl. Catal. A Gen.* **2014**, *476*, 47-53.
(82) Wang, J.; Zhang, X.-B.; Wang, Z.-L.; Wang, L.-M.; Zhang, Y. *Energy Environ. Sci.* **2012**, *5*, 6885-6888.
(83) Tong, D. G.; Tang, D. M.; Chu, W.; Gu, G. F.; Wu, P. *J. Mater. Chem. A* **2013**, *1*, 6425-6432.
(84) Wang, H.-L.; Yan, J.-M.; Wang, Z.-L.; O, S.-I.; Jiang, Q. *J. Mater. Chem. A* **2013**, *1*, 14957-14962.
(85) Zhang, J.; Kang, Q.; Yang, Z.; Dai, H.; Zhuang, D.; Wang, P. *J. Mater. Chem. A* **2013**, *1*, 11623-11628.
(86) Huang, Z.; Autrey, T. *Energy Environ. Sci.* **2012**, *5*, 9257-9268.
(87) Stephens, F. H.; Pons, V.; Tom Baker, R. *Dalton Trans.* **2007**, 2613-2626.
(88) Sanyal, U.; Demirci, U. B.; Jagirdar, B. R.; Miele, P. *Chem. Sus. Chem* **2011**, *4*, 1731-1739.
(89) a) Shi, L.; Liu, Y.; Liu, Q.; Wei, B.; Zhang, G. *Green Chem.* **2012**, *14*, 1372-1375; b) Pham, V. H.; Hur, S. H.; Kim, E. J.; Kim, B. S.; Chung, J. S. *Chem. Commun.* **2013**, *49*, 6665-6667.
(90) a) Hamilton, C. W.; Baker, R. T.; Staubitz, A.; Manners, I. *Chem. Soc. Rev.* **2009**, *38*, 279-293; b) Tang, Z.; Chen, X.; Chen, H.; Wu, L.; Yu, X. *Angew. Chem. Int. Ed.* **2013**, *52*, 5832-5835; c) Bluhm, M. E.; Bradley, M. G.; Butterick, R.; Kusari, U.; Sneddon, L. G. *J. Am. Chem. Soc.* **2006**, *128*, 7748-7749.
(91) Kalviri, H. A.; Gartner, F.; Ye, G.; Korobkov, I.; Baker, R. T. *Chem. Sci.* **2015**, *6*, 618-624.
(92) a) Li, Z.; He, T.; Liu, L.; Chen, W.; Zhang, M.; Wu, G.; Chen, P. *Chem. Sci.* **2017**, *8*, 781-788; b) Fu, Z.-C.; Xu, Y.; Chan, S. L.-F.; Wang, W.-W.; Li, F.; Liang, F.; Chen,

Y.; Lin, Z.-S.; Fu, W.-F.; Che, C.-M. *Chem. Commun.* **2017**; c) Xu, Q.; Chandra, M. *J. Alloys Compd.* **2007**, *446–447*, 729-732.
(93) a) Srinivas, G.; Travis, W.; Ford, J.; Wu, H.; Guo, Z.-X.; Yildirim, T. *J. Mater. Chem. A* **2013**, *1*, 4167-4172; b) Richard, J.; Cid, S. L.; Rouquette, J.; van der Lee, A.; Bernard, S.; Haines, J. *J. Phys. Chem. C* **2016**, *120*, 9334-9340.
(94) Shrestha, R. P.; Diyabalanage, H. V. K.; Semelsberger, T. A.; Ott, K. C.; Burrell, A. K. *Int. J. Hydrogen Energy* **2009**, *34*, 2616-2621.
(95) a) Valero-Pedraza, M. J.; Martín-Cortés, A.; Navarrete, A.; Bermejo, M. D.; Martín, Á. *Energy* **2015**, *91*, 742-750; b) Wright, W. R. H.; Berkeley, E. R.; Alden, L. R.; Baker, R. T.; Sneddon, L. G. *Chem. Commun.* **2011**, *47*, 3177-3179; c) Himmelberger, D. W.; Alden, L. R.; Bluhm, M. E.; Sneddon, L. G. *Inorg. Chem.* **2009**, *48*, 9883-9889.
(96) a) Kim, S.-K.; Han, W.-S.; Kim, T.-J.; Kim, T.-Y.; Nam, S. W.; Mitoraj, M.; Piekoś, Ł.; Michalak, A.; Hwang, S.-J.; Kang, S. O. *J. Am. Chem. Soc.* **2010**, *132*, 9954-9955; b) Kim, S.-K.; Kim, T.-J.; Kim, T.-Y.; Lee, G.; Park, J. T.; Nam, S. W.; Kang, S. O. *Chem. Commun.* **2012**, *48*, 2021-2023; c) Zhong, W.-d.; Tian, X.-k.; Yang, C.; Zhou, Z.-x.; Liu, X.-w.; Li, Y. *Int. J. Hydrogen Energy* **2016**, *41*, 15225-15235; d) Staubitz, A.; Robertson, A. P. M.; Manners, I. *Chem. Rev.* **2010**, *110*, 4079-4124.
(97) Chu, H.; Qiu, S.; Sun, L.; Xu, F. In *Advanced Materials for Renewable Hydrogen Production, Storage and Utilization*, **2015**.
(98) Xiong, Z.; Yong, C. K.; Wu, G.; Chen, P.; Shaw, W.; Karkamkar, A.; Autrey, T.; Jones, M. O.; Johnson, S. R.; Edwards, P. P.; David, W. I. F. *Nat. Mater.* **2008**, *7*, 138-141.
(99) Burrell, A. K.; Davis, B. J.; Thorn, D. L.; Gordon, J. C.; Baker, R. T.; Semelsberger, T. A.; Tumas, W.; Diyabalanage, H. V. K.; Shrestha, R. P.; Us Patents 7713506: **2010**.
(100) Luo, J.; Kang, X.; Wang, P. *Energy Environ. Sci.* **2013**, *6*, 1018-1025.
(101) Wu, C.; Wu, G.; Xiong, Z.; Han, X.; Chu, H.; He, T.; Chen, P. *Chem. Mater.* **2010**, *22*, 3-5.
(102) Chua, Y. S.; Wu, G.; Xiong, Z.; Karkamkar, A.; Guo, J.; Jian, M.; Wong, M. W.; Autrey, T.; Chen, P. *Chem. Commun.* **2010**, *46*, 5752-5754.
(103) Diyabalanage, H. V. K.; Shrestha, R. P.; Semelsberger, T. A.; Scott, B. L.; Bowden, M. E.; Davis, B. L.; Burrell, A. K. *Angew. Chem. Int. Ed.* **2007**, *46*, 8995-8997.
(104) Diyabalanage, H. V. K.; Nakagawa, T.; Shrestha, R. P.; Semelsberger, T. A.; Davis, B. L.; Scott, B. L.; Burrell, A. K.; David, W. I. F.; Ryan, K. R.; Jones, M. O.; Edwards, P. P. *J. Am. Chem. Soc.* **2010**, *132*, 11836-11837.
(105) Zhang, Q.; Tang, C.; Fang, C.; Fang, F.; Sun, D.; Ouyang, L.; Zhu, M. *J. Phys. Chem. C* **2010**, *114*, 1709-1714.
(106) a) Hügle, T.; Kühnel, M. F.; Lentz, D. *J. Am. Chem. Soc.* **2009**, *131*, 7444-7446; b) Sun, W.; Gu, Q.; Guo, Y.; Guo, Z.; Liu, H.; Yu, X. *Int. J. Hydrogen Energy* **2011**, *36*, 13640-13644.
(107) a) Moury, R.; Demirci, U. B.; Ichikawa, T.; Filinchuk, Y.; Chiriac, R.; van der Lee, A.; Miele, P. *Chem. Sus. Chem* **2013**, *6*, 667-673; b) Chua, Y. S.; Pei, Q.; Ju, X.; Zhou, W.; Udovic, T. J.; Wu, G.; Xiong, Z.; Chen, P.; Wu, H. *J. Phys. Chem. C* **2014**, *118*, 11244-11251.
(108) Luo, W.; Zakharov, L. N.; Liu, S.-Y. *J. Am. Chem. Soc.* **2011**, *133*, 13006-13009.
(109) Luo, W.; Campbell, P. G.; Zakharov, L. N.; Liu, S.-Y. *J. Am. Chem. Soc.* **2011**, *133*, 19326-19329.
(110) a) Soloveichik, G. L. *Mater. Matters* **2007**, *2.2*, 11-15; b) Rude, L. H.; Nielsen, T. K.; Ravnsbæk, D. B.; Bösenberg, U.; Ley, M. B.; Richter, B.; Arnbjerg, L. M.; Dornheim, M.; Filinchuk, Y.; Besenbacher, F.; Jensen, T. R. *Phys. Stat. Solid. (A)* **2011**, *208*, 1754-1773; c) Filinchuk, Y.; Chernyshov, D.; Dmitriev, V. In *Zeitschrift für Kristallographie*

International journal for structural, physical, and chemical aspects of crystalline materials **2008**; Vol. 223, p 649; d) Marks, T. J.; Kolb, J. R. *Chem. Rev.* **1977**, *77*, 263-293.
(111) Orgaz, E.; Membrillo, A.; Castañeda, R.; Aburto, A. *J. Alloys Compd.* **2005**, *404–406*, 176-180.
(112) Ravnsbæk, D.; Filinchuk, Y.; Cerenius, Y.; Jakobsen, H. J.; Besenbacher, F.; Skibsted, J.; Jensen, T. R. *Angew. Chem. Int. Ed.* **2009**, *48*, 6659-6663.
(113) Ley, M. B.; Paskevicius, M.; Schouwink, P.; Richter, B.; Sheppard, D. A.; Buckley, C. E.; Jensen, T. R. *Dalton Trans.* **2014**, *43*, 13333-13342.
(114) Edelstein, N. *Inorg. Chem.* **1981**, *20*, 297-299.
(115) Schlesinger, H. I.; Brown, H. C. *J. Am. Chem. Soc.* **1940**, *62*, 3429-3435.
(116) Züttel, A.; Wenger, P.; Rentsch, S.; Sudan, P.; Mauron, P.; Emmenegger, C. *J. Power Sources***2003**, *118*, 1-7.
(117) Orimo, S.; Nakamori, Y.; Kitahara, G.; Miwa, K.; Ohba, N.; Towata, S.; Züttel, A. *J. Alloys Compd.* **2005**, *404–406*, 427-430.
(118) Błoński, P.; Łodziana, Z. *Phys. Rev. B* **2014**, *90*, 054114.
(119) Nakamori, Y.; Li, H. W.; Kikuchi, K.; Aoki, M.; Miwa, K.; Towata, S.; Orimo, S. *J. Alloys Compd.* **2007**, *446–447*, 296-300.
(120) Chong, M.; Callini, E.; Borgschulte, A.; Zuttel, A.; Jensen, C. M. *RSC Adv.* **2014**, *4*, 63933-63940.
(121) Jaron, T.; Wegner, W.; Grochala, W. *Dalton Trans.* **2013**, *42*, 6886-6893.
(122) Ravnsbæk, D. B.; Ley, M. B.; Lee, Y.-S.; Hagemann, H.; D'Anna, V.; Cho, Y. W.; Filinchuk, Y.; Jensen, T. R. *Int. J. Hydrogen Energy* **2012**, *37*, 8428-8438.
(123) Payandeh GharibDoust, S.; Heere, M.; Sorby, M. H.; Ley, M. B.; Ravnsbaek, D. B.; Hauback, B. C.; Cerny, R.; Jensen, T. R. *Dalton Trans.* **2016**, *45*, 19002-19011.
(124) Friedrichs, O.; Kim, J. W.; Remhof, A.; Buchter, F.; Borgschulte, A.; Wallacher, D.; Cho, Y. W.; Fichtner, M.; Oh, K. H.; Zuttel, A. *Phys. Chem. Chem. Phys.* **2009**, *11*, 1515-1520.
(125) Zhang, Y.; Tian, Q.; Zhang, J.; Liu, S.-S.; Sun, L.-X. *J. Phys. Chem. C* **2009**, *113*, 18424-18430.
(126) Vajo, J. J.; Olson, G. L. *Scr. Mater.* **2007**, *56*, 829-834.
(127) Vajo, J. J.; Skeith, S. L.; Mertens, F. *J. Phys. Chem. B* **2005**, *109*, 3719-3722.
(128) Au, M.; Jurgensen, A. R.; Spencer, W. A.; Anton, D. L.; Pinkerton, F. E.; Hwang, S.-J.; Kim, C.; Bowman, R. C. *J. Phys. Chem. C* **2008**, *112*, 18661-18671.
(129) Li, H. W.; Kikuchi, K.; Nakamori, Y.; Miwa, K.; Towata, S.; Orimo, S. *Scr. Mater.* **2007**, *57*, 679-682.
(130) Srinivasan, S.; Escobar, D.; Jurczyk, M.; Goswami, Y.; Stefanakos, E. *J. Alloys Compd.* **2008**, *462*, 294-302.
(131) Barbaras, G. D.; Dillard, C.; Finholt, A. E.; Wartik, T.; Wilzbach, K. E.; Schlesinger, H. I. *J. Am. Chem. Soc.* **1951**, *73*, 4585-4590.
(132) Ranu, B. C. *Synlett* **1993**, *1993*, 885-892.
(133) Gutowska, A.; Li, L.; Shin, Y.; Wang, C. M.; Li, X. S.; Linehan, J. C.; Smith, R. S.; Kay, B. D.; Schmid, B.; Shaw, W.; Gutowski, M.; Autrey, T. *Angew. Chem. Int. Ed.* **2005**, *44*, 3578-3582.
(134) Gross, A. F.; Vajo, J. J.; Van Atta, S. L.; Olson, G. L. *J. Phys. Chem. C* **2008**, *112*, 5651-5657.
(135) Nale, A.; Pendolino, F.; Maddalena, A.; Colombo, P. *Int. J. Hydrogen Energy* **2016**, *41*, 11225-11231.
(136) Fu, H.; Wu, Y.; Chen, J.; Wang, X.; Zheng, J.; Li, X. *Inorg. Chem. Front.* **2016**, *3*, 1137-1145.

(137) Demirci, U. B.; Akdim, O.; Andrieux, J.; Hannauer, J.; Chamoun, R.; Miele, P. *Fuel Cells* **2010**, *10*, 335-350.
(138) a) Minkina, V. G.; Shabunya, S. I.; Kalinin, V. I.; Martynenko, V. V.; Smirnova, A. L. *Int. J. Hydrogen Energy* **2008**, *33*, 5629-5635; b) Şahin, Ö.; Dolaş, H.; Özdemir, M. *Int. J. Hydrogen Energy* **2007**, *32*, 2330-2336.
(139) Moussa, G.; Moury, R.; Demirci, U. B.; Şener, T.; Miele, P. *Int. J. Energy Res.* **2013**, *37*, 825-842.
(140) Xu, D.; Wang, H.; Guo, Q.; Ji, S. *Fuel Proc. Technol.* **2011**, *92*, 1606-1610.
(141) Dovgaliuk, I.; Hagemann, H.; Leyssens, T.; Devillers, M.; Filinchuk, Y. *Int. J. Hydrogen Energy* **2014**, *39*, 19603-19608.
(142) Schlesinger, H. I.; Brown, H. C.; Finholt, A. E.; Gilbreath, J. R.; Hoekstra, H. R.; Hyde, E. K. *J. Am. Chem. Soc.* **1953**, *75*, 215-219.
(143) Urgnani, J.; Torres, F. J.; Palumbo, M.; Baricco, M. *Int. J. Hydrogen Energy* **2008**, *33*, 3111-3115.
(144) a) Demirci, U. B.; Miele, P. *C. R. Chim.* **2014**, *17*, 707-716; b) Demirci, U. B.; Miele, P. *Phys. Chem. Chem. Phys.* **2010**, *12*, 14651-14665; c) Brack, P.; Dann, S. E.; Wijayantha, K. G. U. *Energy Sci. Eng.* **2015**, *3*, 174-188; d) Retnamma, R.; Novais, A. Q.; Rangel, C. M. *Int. J. Hydrogen Energy* **2011**, *36*, 9772-9790.
(145) Demirci, U. B. *Int. J. Hydrogen Energy* **2015**, *40*, 2673-2691.
(146) Zheng, X.; Wu, G.; Li, W.; Xiong, Z.; He, T.; Guo, J.; Chen, H.; Chen, P. *Energy Environ. Sci.* **2011**, *4*, 3593-3600.
(147) Guo, Y.; Jiang, Y.; Xia, G.; Yu, X. *Chem. Commun.* **2012**, *48*, 4408-4410.
(148) Guo, Y.; Wu, H.; Zhou, W.; Yu, X. *J. Am. Chem. Soc.* **2011**, *133*, 4690-4693.
(149) Soloveichik, G.; Her, J.-H.; Stephens, P. W.; Gao, Y.; Rijssenbeek, J.; Andrus, M.; Zhao, J. C. *Inorg. Chem.* **2008**, *47*, 4290-4298.
(150) Yang, Y.; Liu, Y.; Li, Y.; Gao, M.; Pan, H. *J. Phys. Chem. C* **2013**, *117*, 16326-16335.
(151) Tang, Z.; Tan, Y.; Gu, Q.; Yu, X. *J. Mater. Chem.* **2012**, *22*, 5312-5318.
(152) Jepsen, L. H.; Ley, M. B.; Černý, R.; Lee, Y.-S.; Cho, Y. W.; Ravnsbæk, D.; Besenbacher, F.; Skibsted, J.; Jensen, T. R. *Inorg. Chem.* **2015**, *54*, 7402-7414.
(153) Yuan, F.; Gu, Q.; Chen, X.; Tan, Y.; Guo, Y.; Yu, X. *Chem. Mater.* **2012**, *24*, 3370-3379.
(154) Gu, Q.; Gao, L.; Guo, Y.; Tan, Y.; Tang, Z.; Wallwork, K. S.; Zhang, F.; Yu, X. *Energy Environ. Sci.* **2012**, *5*, 7590-7600.
(155) Jaroń, T.; Orłowski, P. A.; Wegner, W.; Fijałkowski, K. J.; Leszczyński, P. J.; Grochala, W. *Angew. Chem. Int. Ed.* **2015**, *54*, 1236-1239.
(156) Sullivan, E. A.; Johnson, S. *J. Phys. Chem.* **1959**, *63*, 233-238.
(157) Guo, Y.; Xia, G.; Zhu, Y.; Gao, L.; Yu, X. *Chem. Commun.* **2010**, *46*, 2599-2601.
(158) Sørensen, R. Z.; Hummelshøj, J. S.; Klerke, A.; Reves, J. B.; Vegge, T.; Nørskov, J. K.; Christensen, C. H. *J. Am. Chem. Soc.* **2008**, *130*, 8660-8668.
(159) Chen, X.; Li, S.; Guo, Y.; Yu, X. *Dalton Trans.* **2011**, *40*, 9679-9689.
(160) Tan, Y.; Tang, Z.; Li, S.; Li, Q.; Yu, X. *Int. J. Hydrogen Energy* **2012**, *37*, 18101-18107.
(161) Chen, X.; Cai, W.; Guo, Y.; Yu, X. *Int. J. Hydrogen Energy* **2012**, *37*, 5817-5824.
(162) Zhang, P.; Xu, B.; Li, X.; Zeng, Y.; Meng, L. *Int. J. Hydrogen Energy* **2014**, *39*, 17144-17152.
(163) Li, Y.; Liu, Y.; Zhang, X.; Yang, Y.; Gao, M.; Pan, H. *Int. J. Hydrogen Energy* **2016**, *41*, 2788-2796.
(164) Chen, X.; Yuan, F.; Gu, Q.; Yu, X. *Dalton Trans.* **2013**, *42*, 14365-14368.

(165) Sun, W.; Chen, X.; Gu, Q.; Wallwork, K. S.; Tan, Y.; Tang, Z.; Yu, X. *Chem. Eur. J.* **2012**, *18*, 6825-6834.
(166) Yang, Y.; Liu, Y.; Li, Y.; Zhang, X.; Gao, M.; Pan, H. *J. Mater. Chem. A* **2015**, *3*, 11057-11065.
(167) Chu, H.; Wu, G.; Xiong, Z.; Guo, J.; He, T.; Chen, P. *Chem. Mater.* **2010**, *22*, 6021-6028.
(168) Chen, X.; Yuan, F.; Tan, Y.; Tang, Z.; Yu, X. *J. Phys. Chem. C* **2012**, *116*, 21162-21168.
(169) Tang, Z.; Yuan, F.; Gu, Q.; Tan, Y.; Chen, X.; Jensen, C. M.; Yu, X. *Acta Mater.* **2013**, *61*, 3110-3119.
(170) Yuan, F.; Gu, Q.; Guo, Y.; Sun, W.; Chen, X.; Yu, X. *J. Mater. Chem.* **2012**, *22*, 1061-1068.
(171) Yan, Y.; Li, H.-W.; Sato, T.; Umeda, N.; Miwa, K.; Towata, S.-i.; Orimo, S.-i. *Int. J. Hydrogen Energy* **2009**, *34*, 5732-5736.
(172) Callini, E.; Szilagyi, P. A.; Paskevicius, M.; Stadie, N. P.; Rehault, J.; Buckley, C. E.; Borgschulte, A.; Zuttel, A. *Chem. Sci.* **2016**, *7*, 666-672.
(173) Gennari, F. C.; Fernández Albanesi, L.; Rios, I. J. *Inorg. Chim. Acta* **2009**, *362*, 3731-3737.
(174) Huang, J.; Tan, Y.; Su, J.; Gu, Q.; Cerny, R.; Ouyang, L.; Sun, D.; Yu, X.; Zhu, M. *Chem. Commun.* **2015**, *51*, 2794-2797.
(175) Huang, J.; Tan, Y.; Gu, Q.; Ouyang, L.; Yu, X.; Zhu, M. *J. Mater. Chem. A* **2015**, *3*, 5299-5304.
(176) Huang, J.; Ouyang, L.; Gu, Q.; Yu, X.; Zhu, M. *Chem. Eur. J.* **2015**, *21*, 14931-14936.
(177) Yuan, F.; Chen, X.; Gu, Q.; Tang, Z.; Yu, X. *Int. J. Hydrogen Energy* **2013**, *38*, 5322-5329.
(178) Li, M.; Yuan, F.; Gu, Q.; Yu, X. *Int. J. Hydrogen Energy* **2013**, *38*, 9236-9242.
(179) Parry, R. W.; Schultz, D. R.; Girardot, P. R. *J. Am. Chem. Soc.* **1958**, *80*, 1-3.
(180) Li, M.; Gu, Q.; Li, X.; Yu, X. *Int. J. Hydrogen Energy* **2016**, *41*, 733-739.
(181) Roedern, E.; Jensen, T. R. *Inorg. Chem.* **2015**, *54*, 10477-10482.
(182) Jepsen, L. H.; Ley, M. B.; Filinchuk, Y.; Besenbacher, F.; Jensen, T. R. *ChemSusChem.* **2015**, *8*, 1452-1463.
(183) Li, L.; Huang, J.; Li, M.; Li, Q.; Ouyang, L.; Zhu, M.; Yu, X. *Int. J. Hydrogen Energy* **2013**, *38*, 16208-16214.
(184) Xia, G.; Gu, Q.; Guo, Y.; Yu, X. *J. Mater. Chem.* **2012**, *22*, 7300-7307.
(185) Li, M.; Xia, G.; Tan, Y.; Gu, Q.; Yu, X. *Int. J. Hydrogen Energy* **2014**, *39*, 11668-11674.
(186) Nakamori, Y.; Li, H. W.; Matsuo, M.; Miwa, K.; Towata, S.; Orimo, S. *J. Phys. Chem. Solids* **2008**, *69*, 2292-2296.
(187) Guo, Y.; Yu, X.; Sun, W.; Sun, D.; Yang, W. *Angew. Chem. Int. Ed.* **2011**, *50*, 1087-1091.
(188) Tang, Z.; Tan, Y.; Chen, X.; Ouyang, L.; Zhu, M.; Sun, D.; Yu, X. *Angew. Chem. Int. Ed.* **2013**, *52*, 12659-12663.
(189) Tang, Z.; Tan, Y.; Wu, H.; Gu, Q.; Zhou, W.; Jensen, C. M.; Yu, X. *Acta Mater.* **2013**, *61*, 4787-4796.
(190) Dovgaliuk, I.; Filinchuk, Y. *Int. J. Hydrogen Energy* **2016**, *41*, 15489-15504.

Chapter 2: Base-Metal Catalysts Based on Porous Layered Double Hydroxides for Alkaline-Free Sodium Borohydride Hydrolysis

A draft of this chapter has been published in: Mehdi Mostajeran, Vanessa Prévot, Sib S. Mal, Emily Mattiussi, Boyd R. Davis and R. Tom Baker, Int. J. Hydrogen Energy, ***2017****,* 42, 20092-20102.

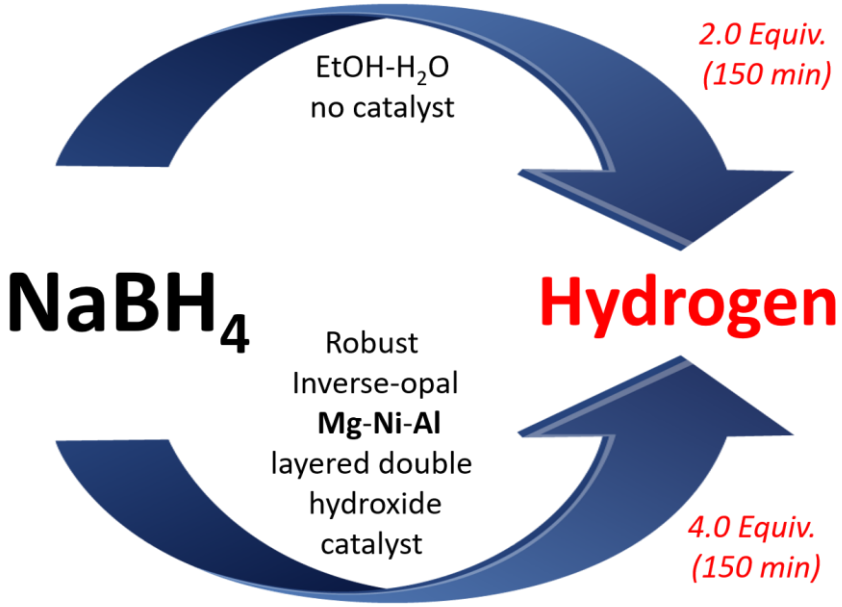

Author Contribution:

The TiO_2, γ-Al_2O_3 and BN supported base-metal catalysts were synthesized and tested for hydrolysis of $NaBH_4$ by Mal and Mattiussi. The LDOs and 3-DOM-Fe-Mg-Al catalysts were synthesized and tested by Mostajeran. The 3-DOM-Ni-Mg-Al (pore size: 190 and 500 nm) catalysts were prepared by Prévot and tested by Mostajeran. The manuscript was submitted and published by Mostajeran and Baker.

2.1. Abstract

Catalyzed hydrolysis of sodium borohydride (SBH) has demonstrated promise for generation of a pure hydrogen stream for use with fuel cells. In designing an improved continuous hydrogen generator that uses the substantial heat released in the hydrolysis reaction to more effectively separate the sodium borate by-product, we sought a robust base-metal catalyst that could tolerate the exothermic reaction under flow conditions. Working under base-free conditions in ethanol solvent we identified reduced nickel and iron-containing particles supported on layered double hydroxides (LDHs) as robust catalysts. Catalytic activity was enhanced further using high surface area hierarchical supports prepared using the '*inverse opal*' method. In particular, macroporous Ni-Mg-Al- and Fe-Mg-Al LDHs produced 0.4 and 1.0 mole of hydrogen per minute per mole of active metal of the supported catalyst in aqueous ethanol solvent.

2.2. Introduction

Polymer electrolyte membrane (PEM) fuel cells have emerged as one of the most efficient energy generators but their success in the portable power generation market depends on a convenient source of pure hydrogen fuel.[1] Hydrogen is an environmentally benign and gravimetrically energy-rich fuel that produces only water vapor effluent when combined with air in a PEM fuel cell.[2] The low volumetric energy density of hydrogen, however, requires expensive compression that also hampers its practical applications.[3] An alternative approach involves storage of hydrogen in so-called 'chemical hydrides' that offer thermal stability, high density and ease of high purity hydrogen release.[4] Although azacycloalkanes could serve as liquid fuels capable of *reversible* hydrogen storage,[5] the high temperatures (ca. 200 °C), long recharging times and precious metal catalysts required have limited their utility. In contrast, alkali metal borohydrides, MBH_4, where M is Li,[6] Na,[7] or K,[8] have been well studied as *irreversible* hydrogen sources (Equation 1) and metal-catalyzed hydrolysis of sodium borohydride has been demonstrated for transportation applications.[9]

$$NaBH_4 + (2+X)\,H_2O \longrightarrow NaBO_2 \cdot xH_2O + 4\,H_2 \qquad (1)$$

As the least expensive metal borohydride, sodium borohydride (SBH) is a stable solid at room temperature that is slowly hydrolyzed by moisture to produce minimal amounts of pure hydrogen.[10] As such, a catalyst is needed to increase the rate of reaction. Early investigations on SBH hydrolysis date back to 1953[11] utilizing cobalt(II) chloride as a

catalyst precursor that generates cobalt borides under the reaction conditions.[12] Consequently, there have been a plethora of studies using both precious- and base-metal heterogeneous catalysts.[7a,7c,7e,13] Following the work by Schlesinger et al.,[11] special attention has been dedicated to development of low-cost, highly active Co-B catalysts.[14] Copper supported nanostructured Co-B catalysts with high durability (80% of the original activity after 5 cycles) were reported to release ~8 $L(H_2)min^{-1}g^{-1}$.[15] Other supports such as reduced graphene oxide,[16] acidic montmorillonite,[17] metal-organic frameworks,[18] TiO_2,[19] γ-Al_2O_3[20] and polymeric microgels[21] along with several additives including Mo,[22] Ce,[19] Ni[7a] and P[23] have been investigated to enhance the activity of the Co-B catalysts mainly using alkaline aqueous $NaBH_4$ solutions.

The US DOE made a ***"no-go"*** recommendation in 2007 for SBH hydrolysis for transportation purposes[9] due to the need for added base and excess water to solubilize the borate by-product and the large heat of reaction which makes the fuel regeneration energy intensive. However, the amount of hydrogen that can be released from catalytic SBH/H_2O systems under ambient conditions exceeds that of most chemical hydrogen storage materials, making it an attractive candidate for portable power applications. In a recent review Demirci rightly notes that base-metal catalysts already achieve sufficient activity and that current research should be focused on catalyst lifetime, reaction engineering and scale-up and borate separation / recycling.[13d] Reactions of base-stabilized aqueous SBH solutions, for example, afford a sticky, hydrated sodium borate product that coats the catalyst in batch reactions and leads to plugging in flow applications. One proposed solution to this problem involves conducting the hydrolysis reaction in an alcohol solvent.[24] In one example, high conversion of SBH was obtained at low temperatures (27-35 ºC) in pure ethanol using acetic acid as a catalyst. (Equation 2).[25]

$$NaBH_4 + 4\,EtOH \longrightarrow NaB(OEt)_4 + 4\,H_2 \qquad (2)$$

More suitable hydrolysis conditions are proposed when an alcohol, particularly methanol or ethanol, is mixed with water:[19] **1)** Alcoholysis of SBH proceeds with higher rate than the aqueous systems, even under uncatalyzed conditions. **2)** Alcohol containing systems have lower freezing points than pure water which makes these systems more practical for subzero environments. **3)** The borate by-products ($NaB(OCH_3)_4$ and $NaB(OCH_2CH_3)_4$, are completely soluble in the methanol or ethanol solvent eliminating the plugging problems. **4)** These borate by-products are readily

hydrolyzed to methanol or ethanol, increasing the gravimetric energy density of the system.

To take advantage of these potential benefits we designed a continuous hydrogen generator that conducts the hydrolysis of SBH in aqueous ethanol solution without added base (Figure 2.1). The ethanol solvent (**1**) is pumped through a cartridge of solid SBH (**2**) and water (**3**) is injected just prior to the solution's entry into the solid catalyst cartridge (**4**). As the generated hydrogen (**5**) is fed to the fuel cell, the spent fuel solution is pumped to the outer jacket (**6**) where the heat produced by the SBH hydrolysis reaction then distills the ethanol which is condensed back to the solvent reservoir (**1**), allowing the solid sodium borate product to build up in the detachable spent fuel cartridge (**6**).

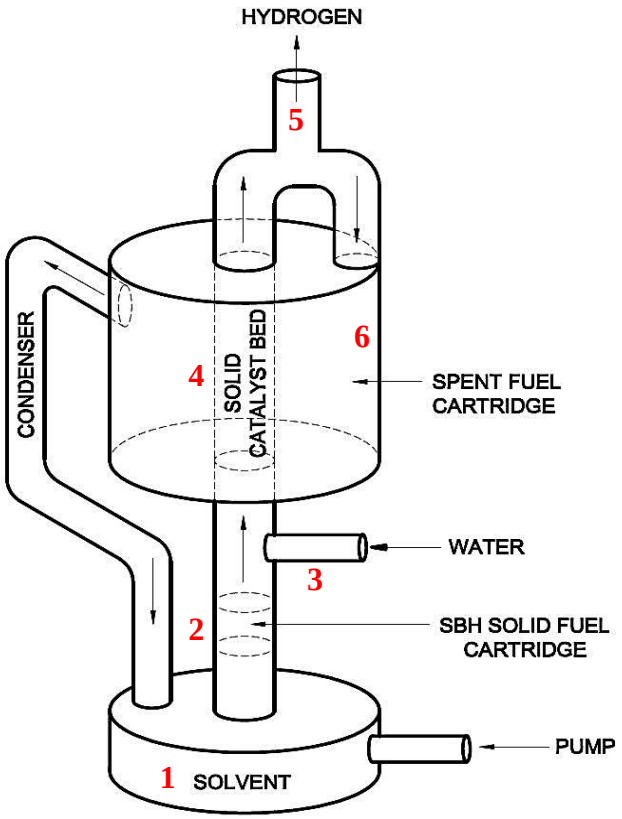

Figure 2.1. Prototype single-pass continuous reactor for hydrolysis of SBH.

The hydrolysis of $NaBH_4$ is highly exothermic (-210 kJ/mol H_2 based on the Equation 1) especially when excess water is used to generate hydrated sodium borate by-product, $NaBO_2{\cdot}xH_2O$.[22a,24c] Efficient capture of the released heat by the reactor's jacket should then provide enough energy to distill ethanol back to the reservoir (*cf.* for ethanol at RT: $C_{p,liquid}$= 112 J/molK and $\Delta_{vap}H$= 38 kJ/mol[26]). In contrast to its methanolysis reaction,[24a,24b] the reactivity of SBH with ethanol or water is sluggish at room

temperature thus limiting the hydrolysis reaction to the catalyst bed to ensure efficient reuse of the reaction heat. Moreover, ethanol is non-toxic and an 80% aqueous solution does not freeze until -59 ºC. Optimal operation of this generator will depend on the solvent flow rate, SBH particle size, and, most importantly, the activity and lifetime of the supported catalyst.

Herein, various base metal catalysts were investigated including layered double hydroxide matrices. To avoid particle attrition and catalyst bed plugging, we also prepared alternative porous layered double hydroxides and compared their performance.

Layered double hydroxides (LDHs), also known as hydrotalcite-like compounds (HTs), are synthesized through the formation of positively charged layers (including divalent and trivalent metal cations) with multivalent, compensating solvated anions intercalating between them.[27] These layers are easy and economical to prepare. Moreover, they are air- and water-stable compounds. Their lamellar nature, wide range of possible chemical compositions, tunable anion exchange capacity and highly versatile chemical properties have made LDHs excellent precursors for preparation of highly dispersed materials with high metal loadings.[28] Practically, several dopants can be introduced, during or after synthesis of LDHs, to improve their performance and catalytic activity.[29] In addition to a large number of applications for LDHs,[30] HT materials have been tested for hydrogen production through catalytic steam reforming of methane.[31] Kim and co-workers reported HT-based catalyst for SBH hydrolysis in which a 6 mol% Ce-doped Ni-Zn-Al-HT, prepared by co-precipitation, exhibited superior activity compared to the un-doped catalyst.[32] The Ce-doped HT released 2.6 $L(H_2)min^{-1}mol^{-1}$, using 0.12 wt.% catalyst loading at 50 ºC over 96 min.

Since most LDH applications are focused on their surface properties, substantial effort has been devoted to developing open, macroporous structures[33] with extended periodicity. Usually, classical LDHs are based on two-dimensional aggregated particles displaying mainly interparticle mesoporosity.[27a] Using a sacrificial template (such as a polymer), it is possible to prepare three-dimensionally ordered macroporous (3-DOM) hydrotalcites.[34] "Inverse opal" LDHs are formed through diffusion of an alcoholic solution of metal precursors through the interstitial voids of close-packed arrays of the template beads. These so called synthetic opals create a colloidal system of crystal spheres due to the fluid-solid transformation.[35] The impregnated opals are placed in a basic solution to let the LDH structure form by developing an interconnected, open 3-DOM structure around the compact template beads. Following removal of the 'opals'

by calcination or dissolution, a macroporous, interconnected inorganic network is obtained (Scheme 2.1).

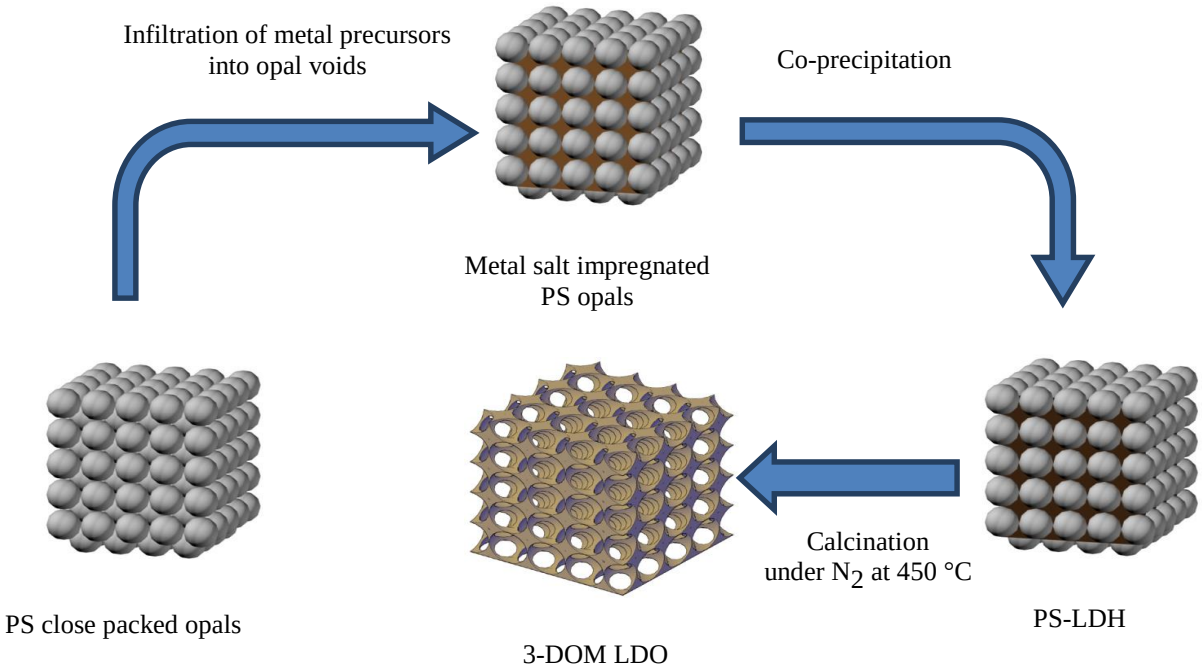

Scheme 2.1. Preparation of the macroporous inverse opal LDOs.

For this work, several base metals were tested and the most efficient SBH hydrolysis catalysts were supported on LDHs. The next step was to increase the surface area, the mass transport and hence the activity, of the most efficient LDH-supported catalysts by using polystyrene inverse opal strategy[36] to template a macroporous hierarchical catalyst for both high diffusion and mechanical stability with respect to liquid flow through the catalyst particle.

2.3. Materials and Methods

2.3.1. Chemicals

Inorganic precursors $Fe(NO_3)_3 \cdot 9H_2O$, $Mg(NO_3)_2 \cdot 6H_2O$ and Na_2MoO_4 were purchased from Alfa Aesar and used as received. $Al(NO_3)_3 \cdot 9H_2O$, $CuCl_2 \cdot 6H_2O$, $FeCl_3 \cdot 6H_2O$, $NiCl_2 \cdot 6H_2O$, $MnCl_2 \cdot 4H_2O$, potassium persulfate, styrene, boron nitride (BN) and sodium borohydride (SBH) were all purchased from Sigma-Aldrich and used without further purification. TiO_2 was from Degussa and all solvents and common chemicals such as NaOH and Na_2CO_3 were purchased from Fisher Scientific.

2.3.2. Preparation of Supported Base-Metal Catalysts

All operations were conducted under air and samples were stored in a MBraun nitrogen-filled glove box after preparation. According to previous methods of synthesizing supported metal/metal boride nanoparticles,[11,37] Fe/TiO_2 was prepared by adding solid $FeCl_3{\cdot}6H_2O$ (1 mmol, 0.27 g), TiO_2 (10 mmol, 0.80 g) and SBH (100 mmol, 3.78 g) to a 500 mL round-bottom flask. 25 mL of distilled water were slowly added and the mixture was stirred overnight with a magnetic stir bar until hydrogen evolution ceased. The mixture was subsequently filtered and air-dried. The particles obtained were then combined in a round-bottom flask with additional SBH (100 mmol, 3.78 g) and H_2O (25 mL) for a second reduction. After stirring for another 24 h, the mixture was filtered and the particles dried completely in air. Accordingly, the other M/TiO_2 solids were synthesized from $CuCl_2{\cdot}6H_2O$ (1 mmol, 0.14 g), $NiCl_2{\cdot}6H_2O$ (1 mmol, 0.24 g) or $MnCl_2{\cdot}4H_2O$ (1 mmol, 0.20 g) in place of $FeCl_3{\cdot}6H_2O$. A subsequent procedure using BN (10 mmol, 0.25 g) in place of TiO_2, afforded Fe/BN and Mn/Al_2O_3, was prepared similarly using $MnCl_2{\cdot}4H_2O$ (1 mmol, 0.20 g) and Al_2O_3 (10 mmol, 1.02 g).

2.3.3. Preparation of Layered Double Hydroxides (LDHs)

2.3.3.1. Preparation of Fe-Mg-Al-CO_3, Ni-Mg-Al-CO_3 and Ni-Al-CO_3 LDH

The syntheses were performed following the co-precipitation method reported previously.[34a,36c] Typically, for Fe-Mg-Al, an aqueous solution of metal nitrate [$Fe(NO_3)_3{\cdot}9H_2O$, $Mg(NO_3)_2{\cdot}6H_2O$ and $Al(NO_3)_3{\cdot}9H_2O$] with $[Mg^{2+}] + [Al^{3+}] = 1$ mol/L , Mg/Al = 2 and Fe/Al = 0.4 was added dropwise (1 drop every 2 seconds) to 50 mL deionized water while stirring. The *p*H of the solution was kept constant at 10±0.5 using a solution of 2 M NaOH and 0.5 M Na_2CO_3. For the Ni-Mg-Al phase, a 1M salt solution was used containing $Ni(NO_3)_2{\cdot}6H_2O$, $Al(NO_3)_3{\cdot}9H_2O$ and $Mg(NO_3)_2{\cdot}6H_2O$ in a molar ratio of Ni/Al=1 and Mg/Al=1. The solution was stirred for 25 h at room temperature, and then filtered. For the Ni-Al-CO_3 composition, a slightly modified method was followed. A 50 mL aqueous solution of $Ni(NO_3)_2{\cdot}6H_2O$ and $Al(NO_3)_3{\cdot}9H_2O$, where $[Ni^{2+}]+[Al^{3+}] = 1$ mol/L and Ni/Al = 3, was added dropwise to a 500 mL solution of 2 M NaOH and 0.5 M Na_2CO_3 while stirring. The pH of the solution was held at 10 by using a solution of 3 M NaOH. The mixture was stirred for 18 h at 65 ^oC, cooled to room temperature and filtered. The precipitations were washed with cold deionized water and air-dried overnight. Dried LDHs were subsequently calcined under N_2 (10 mL/min) at a heating rate of 1 ^oC/min to 450 ^oC. This elevated

temperature was sustained for 1 h. The resultant Layered Double Oxide (LDO) was cooled to room temperature under N_2. In the next step, the LDOs were treated with SBH in water for 24 h, filtered again, and washed with deionized water. These three operations were each applied twice. Finally, the resulting LDO was air-dried overnight.

2.3.3.2. Preparation of Fe-Mg-Al-MoO_4 LDH

The Fe-Mg-Al LDH from 2.3.1 was added to an aqueous solution of Na_2MoO_4 (0.5 g in 50 mL deionized water) at room temperature and left stirring for 24 h to rebuild the LDH layers with MoO_4^{2-} intercalated between them. Calcination was performed under N_2, applying the same method to obtain the LDO.

2.3.4. Preparation of 3-DOM LDOs

2.3.4.1. Polystyrene close-packed arrays (polystyrene opals)

Polystyrene beads were prepared through an 'emulsifier-free' system reported elsewhere.[38] Three different batches were obtained containing monodispersed polystyrene beads of 190, 500 and 540 nm (± 10 nm) particle size respectively according to dynamic light scattering measurements. To prepare the close-packed arrays of the colloidal polystyrene beads, approximately 3 g (2% wt.) of the suspension solution was centrifuged at 1400 or 2000 rpm for 12 h. Then the liquid phase was decanted, and the packed opals were slowly air-dried.

2.3.4.2. Preparation of 3-DOM-Fe-Mg-Al and 3-DOM-Ni-Mg-Al LDOs

1 g of the packed opals was filled with 6 mL of an ethanol/water solution (1:1) of the metal salt precursors for 48 hours. $Fe(NO_3)_3 \cdot 9H_2O$, $Mg(NO_3)_2 \cdot 6H_2O$ and $Al(NO_3)_3 \cdot 9H_2O$ were used for Fe-Mg-Al with [Mg]+[Al]=1 M, Mg/Al=2 and Fe/Al=0.4) while for Ni-Mg-Al a solution containing $Ni(NO_3)_2 \cdot 6H_2O$, $Mg(NO_3)_2 \cdot 6H_2O$ and $Al(NO_3)_3 \cdot 9H_2O$ with a Ni:Mg:Al ratio of 1:1:1 was involved. Successful infiltration was indicated by the colour change of the white opals to the orange or green hue of the impregnating solution. Any excess solution was removed and the opals were air-dried. Then they were placed in a 2M NaOH solution for 24 h, filtered, washed with cold water and allowed to air-dry. 3-DOM-Fe-Mg-Al LDO was prepared using polystyrene beads of 540 nm size and Ni-Mg-Al LDOs were obtained using both 190 and 500 nm beads. Finally, the polymeric phase was removed through calcination. With a ramp of 1 ^oC/min, the sample was heated from room temperature to 450 ^oC under 5 mL/min of dried air. The highest temperature was maintained for 1 h. The resulting PS-templated

LDO was then treated twice with SBH in water for 24 h, filtered, washed with deionized water and air-dried overnight.

2.3.5. SBH Hydrolysis Reactions

Hydrogen evolution was measured volumetrically using a simple inverted burette or an automated burette designed after Zheng et al. [39]. All chemicals and the catalyst were added to a dry 3-neck Schlenk flask equipped with a Teflon-coated stir bar under a constant flow of N_2. Sodium borohydride (0.050 g, 1.3 mmol; 0.6 wt.%, with respect to the water:ethanol solvent) and the solid catalyst (0.100 g) were placed in a round bottom Schlenk flask. The flask was then placed in an oil bath preheated to the desired temperature. A water-cooled condenser was attached on top of the flask to capture evaporating solvents, and reduce the temperature of hydrogen gas. The condenser was connected to a gas burette to collect and measure the amount of gas liberated during the hydrolysis reaction either automatically or through displacement of degassed silicon oil. The solvent was added to the reaction vessel with a dropping funnel at a rate of 5 mL every 2 minutes. After the reaction, the flask was cooled and the solid residue was separated by centrifugation. The same conditions were applied for control reactions. For evaluating the reusability, the catalyst was collected from the reaction mixture after each cycle via centrifugation and air-dried overnight. The chemical quantities needed for each subsequent cycle were determined based on the amount of collected catalyst. Initial reaction rates were estimated from plots of ln(fraction of H_2 volume generated) vs. time over the first 15 min of reaction. Note that the volume of H_2 measured in each experiment is a combination of catalyzed and un-catalyzed release.

2.3.6. Characterization

A ZetaNano ZS (Malvern) device was used for the dynamic light scattering (DLS) to define the polystyrene particle sizes. To determine the surface area of each material nitrogen adsorption–desorption isotherms were measured at −196 ºC using a Micromeritics ASAP 2020 automated gas analyzer. Field Emission Scanning Electron Microscope (FESEM) and Transmission Electron Microscope (TEM) images were acquired using a JEOL JSM-7500F FESEM and a JEOL JEM-2100F FTEM microscope operated at an accelerating voltage and an emission current of 5 kV and 20 μA, respectively. The TEM microscope was equipped with an ultra-high resolution pole-piece operating at 200kV. An Oxford Energy Dispersive X-ray spectrometer (EDX) attached to the JEM-2100F microscope was used to determine the elemental

composition of the particles. Powder X-ray diffraction patterns were recorded on a X'Pert Pro Philips diffractometer with a diffracted beam graphite monochromator and a Cu Kα radiation source in the 2θ range of 2-70°. Calcinations were carried out using a Lindberg Blue M Mini-Mite Tube Furnace (model TF55035A-1). ICP-MS measurements were conducted on a Varian Vistra-PRO spectrometer.

2.4. Results and Discussion

2.4.1. SBH Hydrolysis using Supported Base-Metal Heterogeneous Catalysts

Control experiments were first carried out to determine the amount of hydrogen produced from hydrolysis of SBH in ethanol and ethanol-water mixtures without catalyst (Figure 2.2).

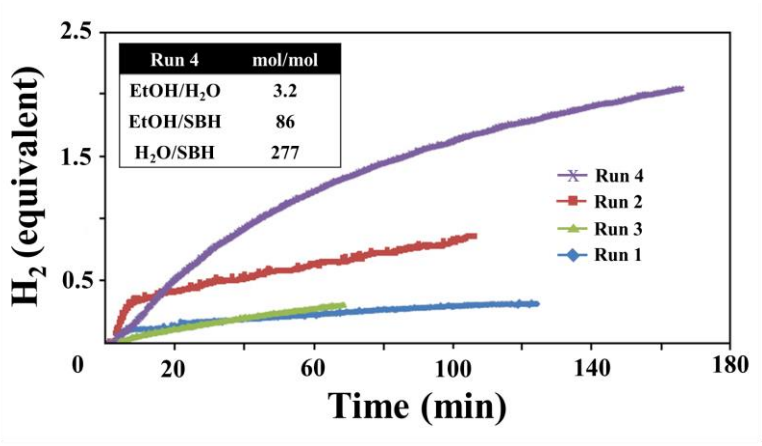

Figure 2.2. Sodium borohydride (SBH) hydrolysis control reactions. All of the reactions contained 0.05 g SBH. Run 1: 3 mL EtOH, 22 ˚C, Run 2: 5 mL EtOH, 50 ˚C, Run 3: 5 mL EtOH, 5 mL water, 22 ˚C, Run 4: 5 mL EtOH, 5 mL water, 50 ˚C. Inset: Molar ratios of reagents in run 4 (most reactive reaction medium).

In order to control the reaction temperature and mimic the staged water addition in the hydrogen generator described above, water was added slowly over the course of the reaction (5 mL every 2 minutes, until the entire solution was added).

As shown in Figure 2.2, the highest rate of hydrogen release was from ethanol at 50 °C (run 2) whereas the highest volume of hydrogen release was achieved with a 1:1 ratio of EtOH:H_2O (5 mL each) at 50 °C (run 4). Experiments using substoichiometric amounts of water in ethanol produced less hydrogen more slowly. Supported catalysts were prepared by treatment of an aqueous solution of the metal chloride with $NaBH_4$ in a slurry of the titania, alumina or boron nitride support. Since the concentration of the reducing agent (used to prepare the catalyst) was shown to have a significant impact on

the hydrogen release performance,[40] the catalysts were treated two times with excess $NaBH_4$ to ensure a full reduction.

Six different supported base-metal catalysts were prepared, and tested in the hydrolysis reactions by monitoring the reaction profiles (Figure 2.3) to determine viable base metals to be loaded on LDHs for further investigation. While most catalysts effect the immediate hydrogen release from SBH, after 20 min the performance of the Mn catalysts has fallen off and the most active Ni/TiO_2 catalyst appears to be deactivated after 1 h, in contrast to the Fe catalysts that are able to release the full 4 equivalents over 3 h. ICP analysis of the spent Ni/TiO_2 catalyst shows only 1.55 wt.% Ni remaining on the catalyst (compared to ca. 7 wt.% loading) indicative of catalyst leaching into the aqueous ethanol.

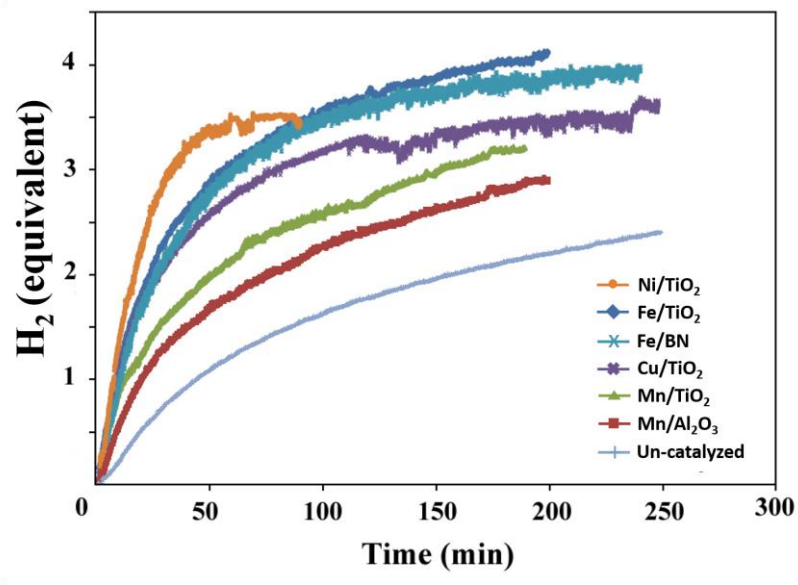

Figure 2.3. Hydrogen release curves for SBH hydrolysis using supported base-metal catalysts. Reaction conditions: 0.10 g solid catalyst (10 wt% metal catalyst loaded on support), 0.05 g SBH, 5 mL EtOH, 5 mL H_2O and 50 °C.

Selected catalysts were characterized via TEM, including elemental analysis by EDX to determine the amount of metal present at the surface (Figure 2.4). For the Fe/TiO_2 catalyst, metal particles tended to agglomerate in the aqueous ethanol, leading to higher average concentrations of Fe at the surface (Figures. 2.4a and 2.4b), whereas little change was observed with the Ni/TiO_2 catalyst (Figures. 2.4c and 2.4d). From these results Ni and Fe were selected for further investigation in order to increase their activity (*i.e.* to be loaded on a more robust support with higher surface area). Since LDHs are interesting materials for catalysis with enhanced mechanical (i.e. thermal stability) and chemical (*i.e.* versatile composition and high active surface area)

properties, several Ni- and Fe-substituted LDH samples were prepared and reduced using SBH in water.

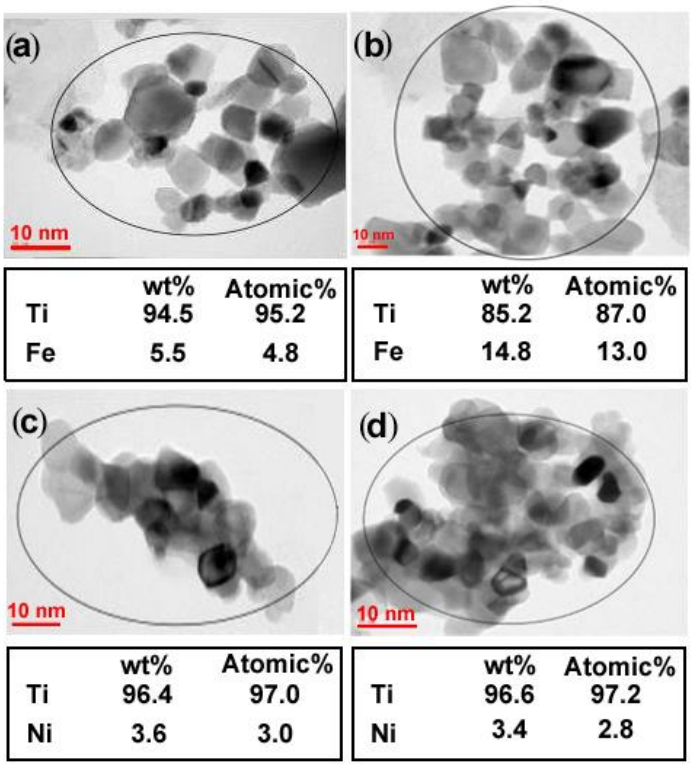

Figure 2.4. TEM images of M/TiO_2 catalysts and typical Ti/M surface ratios prior to (a,c) and after (b,d) SBH hydrolysis reaction in ethanol-water solvent.

2.4.2. Synthesis of Reduced Base-Metals on LDOs

Due to the supersaturation conditions used in the constant pH co-precipitation method, the resultant base-metal LDHs exhibited a strongly aggregated morphology with low surface area and low porosity.[41] In this study, Fe-Mg-Al-CO_3, Fe-Mg-Al-MoO_4, Ni-Mg-Al-CO_3 and Ni-Al-CO_3 LDHs were prepared.[36c,41-42] To assess the effect of interlayer spaces on the catalytic activity of LDH catalysts, Fe-Mg-Al-MoO_4 was selected to be compared with Fe-Mg-Al-CO_3 in which the former has a larger distance between the hydrotalcite layers due to the larger intercalated molybdate anions. As illustrated in Figure 2.5 for the Ni-Mg-Al-CO_3 chemical composition, X-ray diffraction confirmed the hexagonal lattice of hydrotalcite-like compounds with no other crystalline phases being detected.[36c,41] It should be underlined that even though the mother solution for the Ni-Al LDH prepared by co-precipitation (and aged at 65 ^oC),[42b] contained Ni/Al in a molar ratio of 3, ICP data showed a mass distribution of 6.74% Al and 57.38% Ni. Such higher Ni/Al ratio (3.9 vs. 3) evidences lower precipitation of Al^{3+} into the LDH structure under the used synthetic conditions. In contrast, the observed

molar ratio in Ni-Mg-Al (1.1:1:1) correspond closely correlation to its aging solution (1:1:1). Subsequent calcination removes CO_2 and water from the CO_3^{2-} counter ions to leave μ-oxo bridges between the layers, transforming the LDHs into LDOs. Such structural transformation is clearly observed by XRD pattern (Figure 2.5) as described previously.[27a]

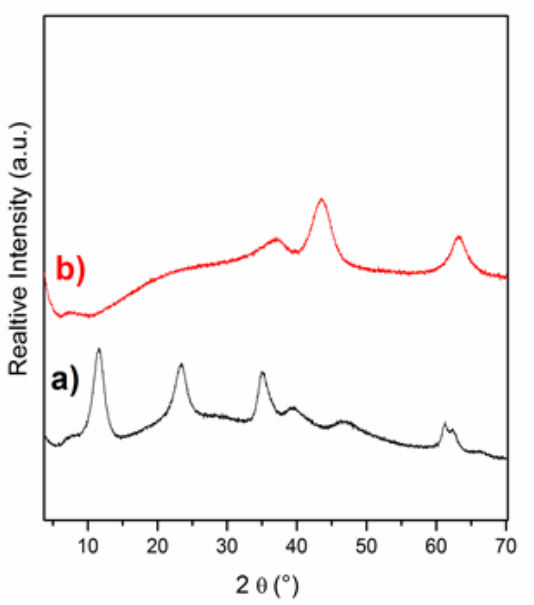

Figure 2.5. XRD patterns of the Ni-Mg-Al-CO_3 a) before and b) after calcination.

After treating with SBH in water, reduced metal particles are formed on the outer surface of the layers (upon reduction to their zero-valent state) and the layers rearrange. It has been proposed that the surrounding layers prevent metal particles from aggregating.[36c] As expected, the surface area was relatively low; BET surface area of Fe-Mg-Al (treated twice with SBH) was measured to be 4 m^2/g, while the BJH adsorption average pore diameter was 62 nm. Field Emission Scanning Electron Microscope (FESEM) images of the porous structures of Fe-Mg-Al (A) and Ni-Mg-Al (B) are shown in Figure 2.6. Metal loading of the LDOs, determined by inductively coupled plasma (ICP), showed that Fe-Mg-Al contained 8.9% Fe, 18.8% Mg and 9.9% Al, in accordance with the original metal precursor solution (Mg/Al and Fe/Al molar ratios of 2 and 0.4, respectively).[43]

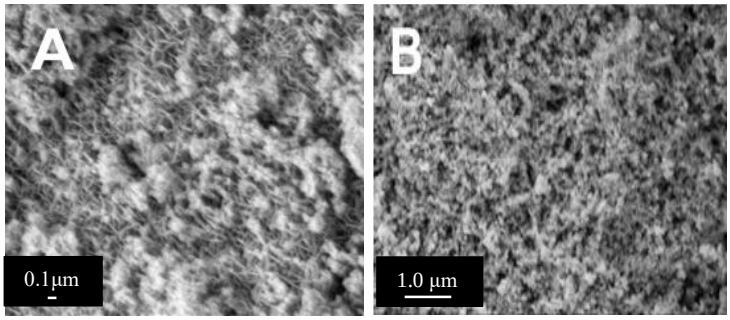

Figure 2.6. FESEM image of the morphology of the Fe-Mg-Al (A) and Ni-Mg-Al (B) LDOs after treatment with SBH.

2.4.3. Base-Metals Supported on LDOs as Catalysts

The activity of the synthesized Ni- and Fe-substituted LDOs toward the hydrolysis of SBH was assessed under identical reaction conditions (Figure 2.7).

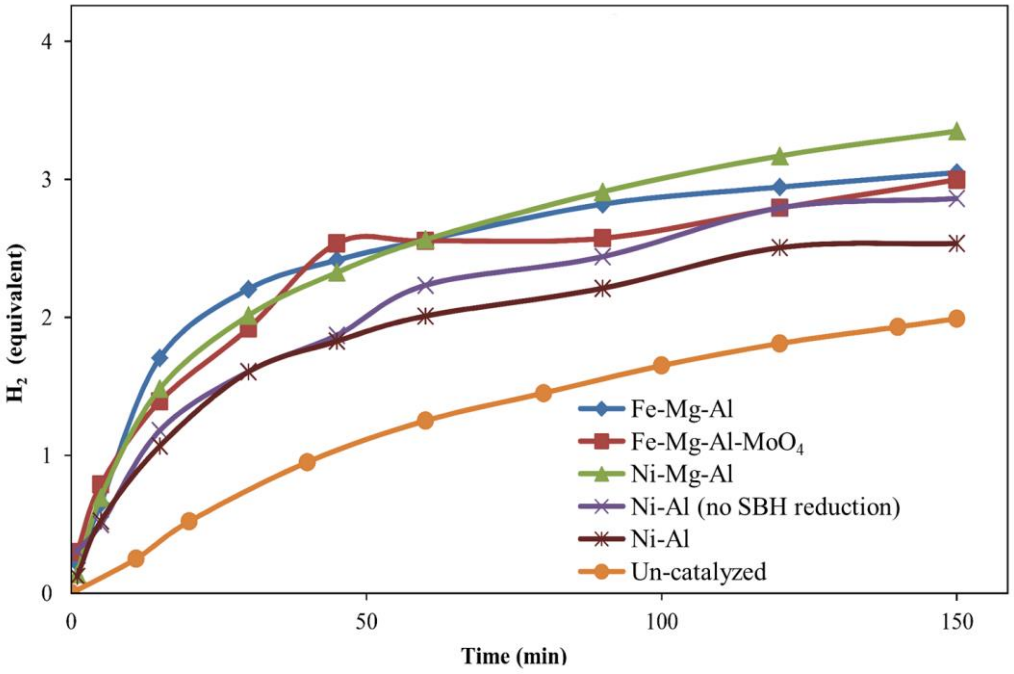

Figure 2.7. Activity of the different supported catalysts for the hydrolysis of sodium borohydride. Reaction condition: 0.05 g SBH, 0.10 g Catalyst, 50 ^{o}C and EtOH/H_2O: 1/1.

The Fe-Mg-Al catalyst had the greatest initial activity, producing 3.2 equivalents of hydrogen over 150 minutes but the stability of the Ni-Mg-Al catalyst was slightly better with a higher rate and extent after 2 hr (3.4 equiv). The Fe-Mg-Al-MoO_4 catalysts showed a similar activity, producing nearly 3 equiv. of hydrogen. In contrast, the Ni-Al catalyst gave only 2.3 equiv. H_2 after 150 min. Although the Ni-Al catalysts showed the same initial activity (*i.e.* before 50 min), the catalyst which was not treated with SBH released slightly higher amount of hydrogen (2.5 equiv.) which is still lower than that of Fe containing catalysts. These observations suggest a beneficial role for Mg in the high

catalytic activity of Ni-Al LDH catalysts. Reuse of the Fe-Mg-Al catalyst showed a slight increase in H_2 production (Figure 2.8). ICP analysis of the catalyst after the 3rd cycle shows it now contains 9.3% Fe, 18.6% Mg and 0.5% Al indicating that much of the Al content has been washed from the structure after this third run.

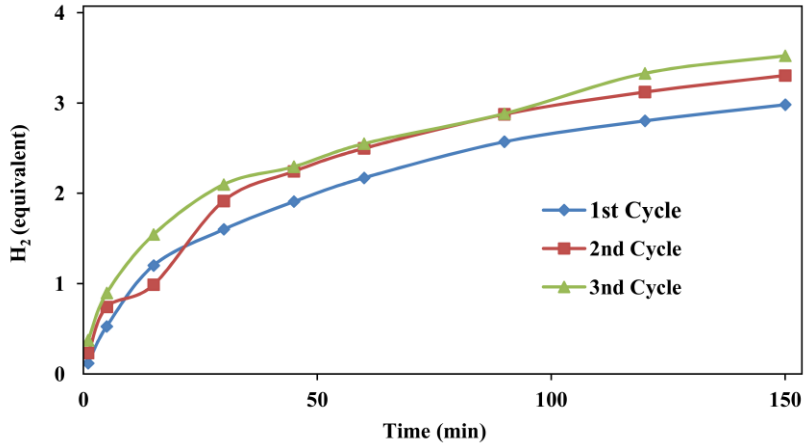

Figure 2.8. Reusability of the Fe-Mg-Al LDO catalyst. Reaction conditions: 0.05 g SBH, 0.10 g Catalyst, 50 ^{o}C and EtOH/H_2O: 1/1.

2.4.4. Base Metals on Inverse-Opal LDOs

As the moderate activity of the supported base metal catalysts is likely due to their poor surface area, one approach to obtaining a macroporous, high surface area LDO support is to use a polystyrene template in the inverse opal method [36b,42a]. During the process, addition of ethanol facilitated the infiltration of the aqueous mixed-metal salt solution into the voids, and after reaction with NaOH and LDH co-precipitation the resulting salt by-products (Na_2CO_3 and NaCl) were easily removed by washing. As the last step, the LDH-impregnated polystyrene arrays were calcined to remove the polymeric phase. The macroporous sizes are directly linked to the diameter of the starting polystyrene beads. Subsequently, to prepare the active sites, the calcined hydrotalcites were then treated twice with a solution of SBH. The evident pores and channels are obvious and indicate the formation of the 3-DOM LDO structure. The porous matrices of the calcined product demonstrate that the close-packed arrays are maintained during the infiltration and reduction (Figure 2.9).

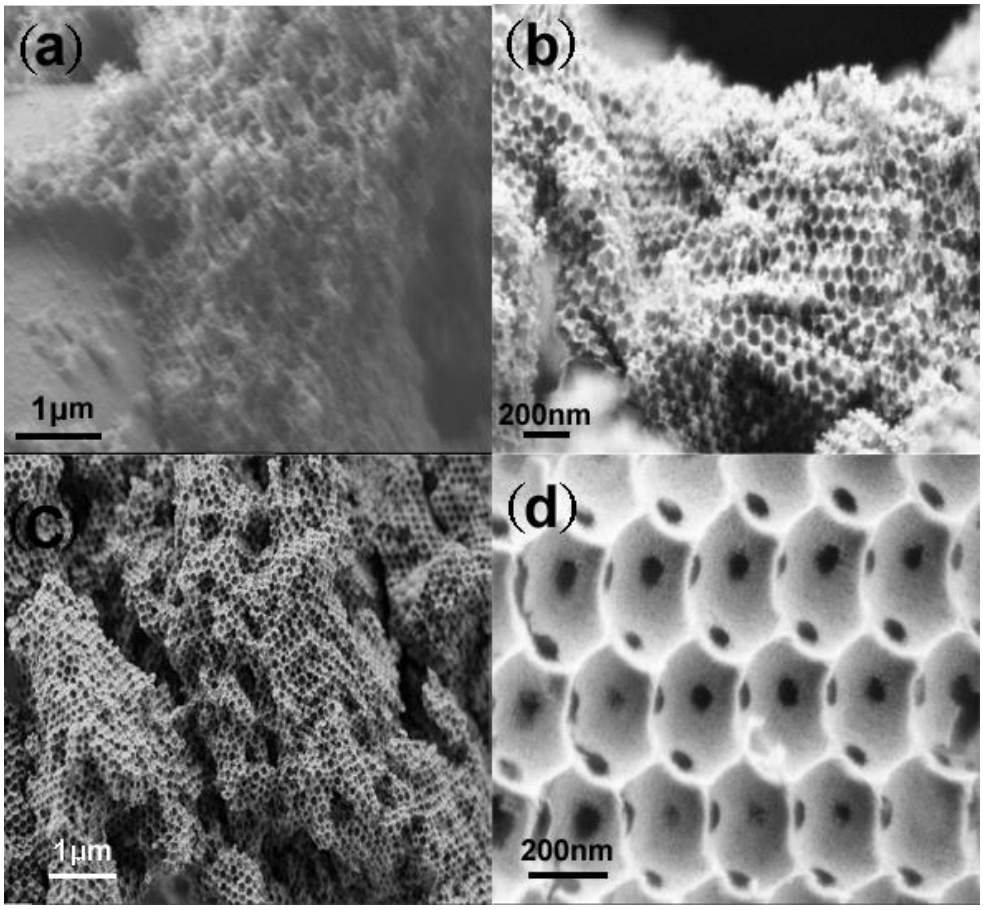

Figure 2.9. FESEM pictures: (a) 3-DOM-Fe-Mg-Al with 15 nm por size, (b) 3-DOM-Ni-Mg-Al with 115 nm pore size, (c) and (d) 3-DOM-Ni-Mg-Al with 451 nm pore size and the windows between the macropores of the LDOs after 2x SBH treatment and drying under vacuum at room temperature.

The BET active surface area for the as-synthesised 3-DOM-Fe-Mg-Al is measured to be 109 m^2/g, which represents a significant increase compared to the classical LDH with the same metal components. In addition, BJH adsorption average pore diameter (4V/A) is determined to be 15.4 nm (after treatment twice with SBH). It should be noted that macroporosity is not measured by the nitrogen adsorption technique, and the average pore size achieved corresponds to the leftover mesoporosity in the structure. This suggests that almost 75% of the mesopores in the pristine LDO's structure have been transformed to macropores. It is thus concluded that the porosity of the new LDH is hierarchically ordered. ICP analysis indicates the composition of this LDO as 10.0% Al, 18.1% Mg, and 8.3% Fe, by weight. This is in close agreement to the mother solution ratios. Two other 3-DOM LDOs with almost the same compositions, but different pore size, were also synthesized (Table 2.1; Figure 2.9c,d). Since the impregnation solution was the same for both LDOs, except the average size of the opals, they show a very similar composition.

Table 2.1. Characterization of the inverse opal Ni-Mg-Al LDOs

entry	3-DOM LDOs	Pore size (nm)	Wall thickness (nm)	Composition (wt.%)			Ratio (mol/mol)		
				Mg	Ni	Al	Mg/Ni	Ni/Al	Mg/Al
1	3-DOM-Ni-Mg-Al	115 ±10	26 ± 5	12.1	32.8	11.0	0.9	1.4	1.2
2	3-DOM-Ni-Mg-Al	451 ±10	21 ± 5	12.1	32.5	11.4	0.9	1.3	1.2

2.4.5. SBH Hydrolysis Catalyzed by Base Metals on Inverse-Opal LDOs

Base metal-substituted polystyrene-based LDOs (PS-LDO) with open 3D macroporous structures display a significantly higher rate and extent of hydrogen release from SBH hydrolysis (Figure 2.10).

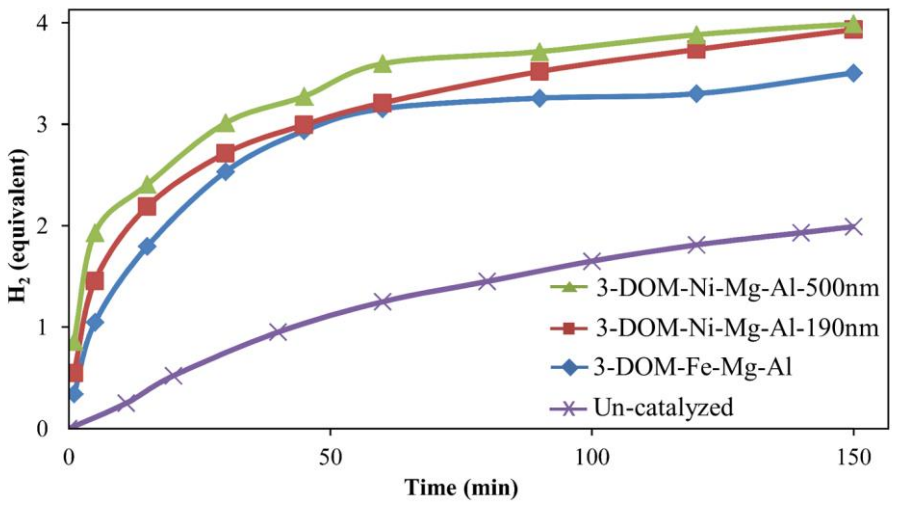

Figure 2.10. Activity of 3-DOM-LDOs for the hydrolysis of SBH. Reaction conditions: 0.05 g SBH, 0.10 g catalyst, 50 ^{o}C and EtOH/H_2O: 1/1.

3-DOM-Fe-Mg-Al produces 3.50 equivalents of hydrogen after 150 minutes, relative to 2.98 equivalents released by the classical LDO with the same metal composition. This illustrates an enhancement in the rate of the hydrolysis reaction to 1.0 mol(H_2)min^{-1}mol$^{-1}_{Fe}$ for the former from 0.7 mol(H_2)min^{-1}mol$^{-1}_{Fe}$ for the latter. The rates of the reactions have been calculated based on the amounts of hydrogen produced in the first 15 min of the hydrolysis reaction shown in Figure 2.11.

Although the 3-DOM-Ni-Mg-Al catalyst with 190 nm pore size exhibited a slightly slower initial rate, the extent of H_2 release was identical with the 500 nm pore size catalyst after 150 min (3.9 and 4.0 equiv. H_2, respectively). In other words, these 3-DOM catalysts released 0.3 and 0.4 mol(H_2)min^{-1}mol$^{-1}_{Ni}$, indicating that macropore size does not drastically affect their performance. The previously reported un-doped Ni-Zn-

Al hydrotalcite-like catalysts released about 0.1 mol(H_2)$min^{-1}mol^{-1}_{Ni}$ during 150 min at 25 °C[32] (amounts of released hydrogen from these catalysts were adjusted to conduct an accurate comparison to the 3-DOM catalysts in this study.)

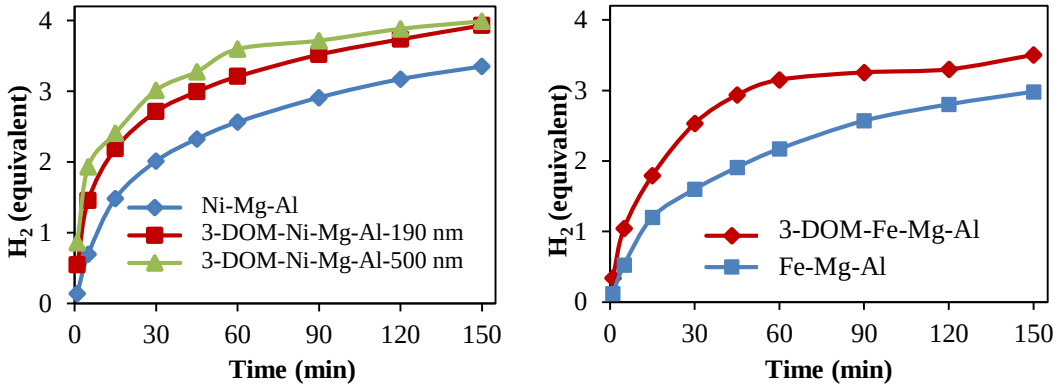

Figure 2.11. Comparison of the catalytic activity of classical *vs.* 3-DOM LDOs of Ni-Mg-Al (left) and Fe-Mg-Al (right) in the SBH hydrolysis reaction. Reaction conditions: 0.05 g SBH, 0.10 g catalyst, 50 °C and EtOH/H_2O: 1/1.

As well as being inexpensive and easy to prepare, the 3-DOM-Fe-Mg-Al catalyst still functions after multiple cycles (Figure 2.12), in spite of noticeable leaching of Al (metal composition after the third cycle was 0.6% Al, 3.5% Fe and 4.4% Mg by ICP). Although the focus of this work was on the preparation of a robust catalyst, the hierarchical 3-DOM-Fe-Mg-Al catalyst clearly demonstrates enhanced activity vs. the non-templated variants.

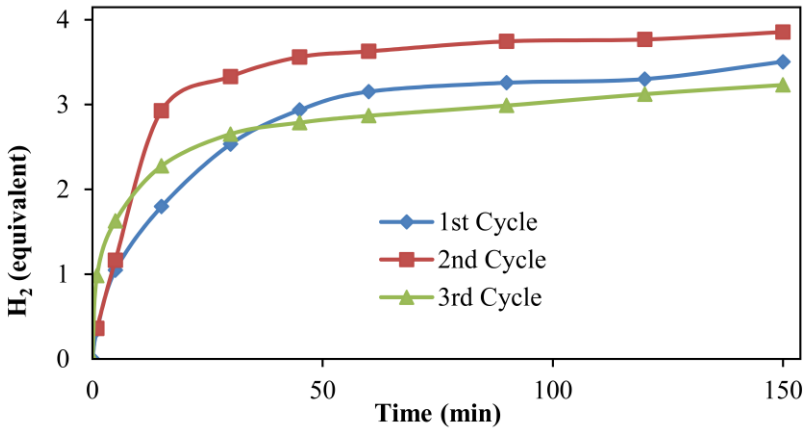

Figure 2.12. Recyclability of 3-DOM-Fe-Mg-Al. Reaction condition: 0.05 g SBH, 0.10 g catalyst, 50 °C and EtOH/H_2O: 1/1.

The ICP results of the Fe-Mg-Al-LDO and 3-DOM-Fe-Mg-Al catalysts after the 3rd hydrolysis cycle reveals significant aluminum leaching in addition to Mg and Al leaching for the latter. It has been observed that the pH of the SBH hydrolysis reactions increases along with the reaction progress due to formation of alkaline borate by-

products,[44] even using acidic catalysts such as sulfated silica.[45] Dealumination may thus occur in our experiments through dissolution in the hot alkaline H_2O/EtOH solvent.

2.5. Conclusions

Several solid supported catalysts containing non-precious metals have been prepared, characterized and tested for eventual use in a portable hydrogen generator using aqueous ethanol solvent in the absence of base. Analysis of the catalysts was based on the $NaBH_4$ hydrolysis initial reaction rate and the total amount of hydrogen liberated. TiO_2, γ-Al_2O_3 and BN supported base-metal catalysts, prepared by reduction with $NaBH_4$, were tested in the $NaBH_4$ hydrolysis reactions indicating the higher activity of Fe and Ni catalysts (vs. Mn and Cu). In order to obtain a more robust catalyst, different Fe and Ni containing layered double hydroxides were prepared and their corresponding calcined oxides, Fe-Mg-Al- and Ni-Mg-Al LDOs, also showed promising activity for the hydrolysis reaction, producing up to 3.4 equiv. of hydrogen. The inverse opal method was then employed to increase their surface area using polystyrene beads (inverse opal) as the template. 3-DOM-Fe-Mg-Al, 3-DOM-Ni-Mg-Al (pore size: 190 nm) and 3-DOM-Ni-Mg-Al (pore size: 500 nm) could release 1.0, 0.3 and 0.4 $mol(H_2)min^{-1}mol^{-1}_{Active\ metal}$ at 50 ºC which is significantly higher than that previously reported for our untemplated catalysts and for Zn-Al and un-doped Ni-Zn-Al hydrotalcite-like catalysts.[32,46] It was observed that the catalytic activity of the inverse opal LDOs was largely maintained after three cycles, in spite of significant Al leaching. The hierarchical structure of these highly porous materials thus makes them potential candidates to be used in a flow reactor for the base-free hydrolysis of sodium borohydride in ethanol solvent. In future, the catalysts need to be tested under flow conditions to examine their mechanical properties and long-term activity. Moreover, ceria doping[32] of these novel 3-DOM catalysts will be performed in order to assess effects on activity and lifetime.

2.6. References

(1) Narayan S.R., Valdez TI. *Electrochem. Soc. Interfaces* **2008**, *17*, 40-45.
(2) Amendola, S. C.; Sharp-Goldman, S. L.; Janjua, M. S.; Spencer, N. C.; Kelly, M. T.; Petillo, P. J.; Binder, M. *Int. J. Hydrogen Energy* **2000**, *25*, 969-975.
(3) a) Eberle, U.; Felderhoff, M.; Schüth, F. *Angew. Chem. Int. Ed.* **2009**, *48*, 6608-6630; b) Ferreira, M. J. F.; Gales, L.; Fernandes, V. R.; Rangel, C. M.; Pinto, A. M. F. R. *Int. J. Hydrogen Energy* **2010**, *35*, 9869-9878.
(4) Luo, W.; Campbell, P. G.; Zakharov, L. N.; Liu, S.-Y. *J. Am. Chem. Soc.* **2011**, *133*, 19326-19329.

(5) a) Crabtree, R. H. *Energy Environ. Sci.* **2008**, *1*, 134-138; b) Cooper, A.; Pez, G. US Patent 7101530, **2006**; c) Cui, Y.; Kwok, S.; Bucholtz, A.; Davis, B.; Whitney, R. A.; Jessop, P. G. *N. J. Chem.* **2008**, *32*, 1027-1037; d) Teichmann, D.; Arlt, W.; Wasserscheid, P. *Int. J. Hydrogen Energy* **2012**, *37*, 18118-18132; e) Sotoodeh, F.; Smith, K. J. *Can. J. Chem. Eng.* **2013**, *91*, 1477-1490.
(6) Weng, B.; Wu, Z.; Li, Z.; Yang, H. *J. Power Sources* **2012**, *204*, 60-66.
(7) a) Brack, P.; Dann, S. E.; Wijayantha, K. G. U. *Energy Sci. Eng.* **2015**, *3*, 174-188; b) Mahmood, J.; Jung, S.-M.; Kim, S.-J.; Park, J.; Yoo, J.-W.; Baek, J.-B. *Chem. Mater.* **2015**, *27*, 4860-4864; c) Eugénio, S.; Demirci, U. B.; Silva, T. M.; Carmezim, M. J.; Montemor, M. F. *Int. J. Hydrogen Energy* **2016**, *41*, 8438-8448; d) Nunes, H. X.; Ferreira, M. J. F.; Rangel, C. M.; Pinto, A. M. F. R. *Int. J. Hydrogen Energy* **2016**, *41*, 15426-15432; e) Minkina, V. G.; Shabunya, S. I.; Kalinin, V. I.; Smirnova, A. *Int. J. Hydrogen Energy* **2016**, *41*, 9227-9233.
(8) Xu, D.; Wang, H.; Guo, Q.; Ji, S. *Fuel Proc. Technol.* **2011**, *92*, 1606-1610.
(9) Demirci, U. B.; Akdim, O.; Andrieux, J.; Hannauer, J.; Chamoun, R.; Miele, P. *Fuel Cells* **2010**, *10*, 335-350.
(10) Yadav, M.; Xu, Q. *Energy Environ. Sci.* **2012**, *5*, 9698-9725.
(11) Schlesinger, H. I.; Brown, H. C.; Finholt, A. E.; Gilbreath, J. R.; Hoekstra, H. R.; Hyde, E. K. *J. Am. Chem. Soc.* **1953**, *75*, 215-219.
(12) Wu, F.; Li, T.; Yang, X. R.; Li, C. M.; Fan, M. Q.; Shu, K. *Instrum. Sci. Technol.* **2016**, *44*, 425-434.
(13) a) Roy, S.; Pachfule, P.; Xu, Q. *Eur. J. Inorg. Chem.* **2016**, *2016*, 4353-4357; b) Lin, K.-Y. A.; Chang, H.-A. *Chem. Eng. J.* **2016**, *296*, 243-251; c) Marchionni, A.; Bevilacqua, M.; Filippi, J.; Folliero, M. G.; Innocenti, M.; Lavacchi, A.; Miller, H. A.; Pagliaro, M. V.; Vizza, F. *J. Power Sources* **2015**, *299*, 391-397; d) Borohydride hydrolysis catalyst reports from 2000-2013: Demirci, U. B. *Int. J. Hydrogen Energy* **2015**, *40*, 2673-2691.
(14) Results from 2010-2013 on Co-based borohydride hydrolysis catalysts: Demirci, U. B.; Miele, P. *Phys. Chem. Chem. Phys.* **2014**, *16*, 6872-6885.
(15) Wang, Y.; Li, T.; Bai, S.; Qi, K.; Cao, Z.; Zhang, K.; Wu, S.; Wang, D. *Int. J. Hydrogen Energy* **2016**, *41*, 276-284.
(16) Krishna, R.; Fernandes, D. M.; Dias, C.; Ventura, J.; Freire, C.; Titus, E. *Int. J. Hydrogen Energy* **2016**, *41*, 11498-11509.
(17) Shavi, R.; Jadhav, A. H.; Lee, K.; Seo, J. G. *J. Nanosci. Nanotechnol.* **2016**, *16*, 10980-10985.
(18) Chen, Y.-Z.; Xu, Q.; Yu, S.-H.; Jiang, H.-L. *Small* **2015**, *11*, 71-76.
(19) Chang, J.; Tian, H.; Du, F. *Int. J. Hydrogen Energy* **2014**, *39*, 13087-13097.
(20) Li, Z.; Li, H.; Wang, L.; Liu, T.; Zhang, T.; Wang, G.; Xie, G. *Int. J. Hydrogen Energy* **2014**, *39*, 14935-14941.
(21) Sahiner, N.; Yasar, A. O. *Int. J. Hydrogen Energy* **2014**, *39*, 10476-10484.
(22) a) Zhuang, D.-W.; Dai, H.-B.; Zhong, Y.-J.; Sun, L.-X.; Wang, P. *Int. J. Hydrogen Energy* **2015**, *40*, 9373-9381; b) Ke, D.; Tao, Y.; Li, Y.; Zhao, X.; Zhang, L.; Wang, J.; Han, S. *Int. J. Hydrogen Energy* **2015**, *40*, 7308-7317.
(23) Fernandes, R.; Patel, N.; Miotello, A. *Int. J. Hydrogen Energy* **2009**, *34*, 2893-2900.
(24) a) Lo, C.-t. F.; Karan, K.; Davis, B. R. *Ind. Eng. Chem. Res.* **2007**, *46*, 5478-5484; b) Lo, C. t. F.; Karan, K.; Davis, B. R. *Ind. Eng. Chem. Res.* **2009**, *48*, 5177-5184; c) Zhang, J.; Fisher, T. S.; Gore, J. P.; Hazra, D.; Ramachandran, P. V. *Int. J. Hydrogen Energy* **2006**, *31*, 2292-2298; d) Ramya, K.; Dhathathreyan, K. S.; Sreenivas, J.; Kumar, S.; Narasimhan, S. *Int. J. Energy Res.* **2013**, *37*, 1889-1895.

(25) Arzac, G. M.; Fernández, A. *Int. J. Hydrogen Energy* **2015**, *40*, 5326-5332.
(26) NIST Chemistry WebBook: www.webbook.nist.gov.
(27) a) Forano, C.; Costantino, U.; Prévot, V.; Gueho, C. T. In *Developments in Clay Science*; Faïza, B., Gerhard, L., Eds.; Elsevier: **2013**; Volume 5, p 745-782; b) Debecker, D. P.; Gaigneaux, E. M.; Busca, G. *Chem. Eur. J.* **2009**, *15*, 3920-3935.
(28) Noda P, C.; Pérez, C. A.; Henriques, C. A.; Monteiro, J. L. F. *Appl. Catal. A Gen.* **2004**, *272*, 229-240.
(29) Iqbal, K.; Iqbal, A.; Kirillov, A. M.; Wang, B.; Liu, W.; Tang, Y. *J. Mater. Chem. A* **2017**, *5*, 6716-6724.
(30) Wang, Q.; O'Hare, D. *Chem. Rev.* **2012**, *112*, 4124-4155.
(31) a) Basile, F.; Benito, P.; Fornasari, G.; Vaccari, A. *Appl. Clay Sci.* **2010**, *48*, 250-259; b) Dewoolkar, K. D.; Vaidya, P. D. *Int. J. Hydrogen Energy* **2016**, *41*, 6094-6106.
(32) Tamboli, A. H.; Jadhav, A. R.; Chung, W.-J.; Kim, H. *Energy* **2015**, *93, Part 1*, 955-962.
(33) Géraud, E.; Prévot, V.; Ghanbaja, J.; Leroux, F. *Chem. Mater.* **2006**, *18*, 238-240.
(34) a) Géraud, E.; Prévot, V.; Leroux, F. *J. Phys. Chem. Solids* **2006**, *67*, 903-908; b) Géraud, E.; Rafqah, S.; Sarakha, M.; Forano, C.; Prevot, V.; Leroux, F. *Chem. Mater.* **2008**, *20*, 1116-1125; c) Woodford, J. J.; Dacquin, J.-P.; Wilson, K.; Lee, A. F. *Energy Environ. Sci.* **2012**, *5*, 6145-6150; d) Martin, J.; Jack, M.; Hakimian, A.; Vaillancourt, N.; Villemure, G. *J. Electroanal.Chem.* **2016**, *780*, 217-224.
(35) Liu, B.; Jin, Z.; Qu, X.; Yang, Z. *Macromol. Rapid Commun.* **2007**, *28*, 322-328.
(36) a) Halma, M.; Castro, K. A. D. d. F.; Prévot, V.; Forano, C.; Wypych, F.; Nakagaki, S. *J. Mol. Catal. A Chem.* **2009**, *310*, 42-50; b) Prevot, V.; Forano, C.; Khenifi, A.; Ballarin, B.; Scavetta, E.; Mousty, C. *Chem. Commun.* **2011**, *47*, 1761-1763; c) Zhao, M.-Q.; Zhang, Q.; Zhang, W.; Huang, J.-Q.; Zhang, Y.; Su, D. S.; Wei, F. *J. Am. Chem. Soc.* **2010**, *132*, 14739-14741.
(37) Glavee, G. N.; Klabunde, K. J.; Sorensen, C. M.; Hadjipanayis, G. C. *Langmuir* **1994**, *10*, 4726-4730.
(38) Goodwin, J. W.; Hearn, J.; Ho, C. C.; Ottewill, R. H. *Col. Polym. Sci* **1974**, *252*, 464-471.
(39) Zheng, F.; Rassat, S. D.; Helderandt, D. J.; Caldwell, D. D.; Aardahl, C. L.; Autrey, T.; Linehan, J. C.; Rappé, K. G. *Rev. Sci. Instrum.***2008**, *79*, 084103.
(40) Wang, Y.; Lu, Y.; Wang, D.; Wu, S.; Cao, Z.; Zhang, K.; Liu, H.; Xin, S. *Int. J. Hydrogen Energy* **2016**, *41*, 16077-16086.
(41) Adachi-Pagano, M.; Forano, C.; Besse, J.-P. *J. Mater. Chem.* **2003**, *13*, 1988-1993.
(42) a) Choudary, B. M.; Jaya, V. S.; Reddy, B. R.; Kantam, M. L.; Rao, M. M.; Madhavendra, S. S. *Chem. Mater.* **2005**, *17*, 2740-2743; b) He, L.; Huang, Y.; Wang, A.; Wang, X.; Chen, X.; Delgado, J. J.; Zhang, T. *Angew. Chem. Int. Ed.* **2012**, *51*, 6191-6194.
(43) Han, Y.; Liu, Z.-H.; Yang, Z.; Wang, Z.; Tang, X.; Wang, T.; Fan, L.; Ooi, K. *Chem. Mater.* **2008**, *20*, 360-363.
(44) Fernandes, V. R.; Pinto, A. M. F. R.; Rangel, C. M. *Int. J. Hydrogen Energy* **2010**, *35*, 9862-9868.
(45) Manna, J.; Roy, B.; Sharma, P. *J. Power Sources* **2015**, *275*, 727-733.
(46) These rates can be compared with those of the best porous supported metal catalysts for ammonia-borane hydrolysis: Umegaki, T.; Xu, Q.; Kojima, Y. *Materials* **2015**, *8*, 4512.

Chapter 3: Solution-Based Routes to Ammine Metal Borohydrides: Formation of Ammonia-Borane

This chapter has been partially published in: Mehdi Mostajeran, David J. Wolstenholme, Chris Frazee, G. Sean McGrady and R. Tom Baker, Chemical Communications, ***2016****, 52, 2851-2854.*

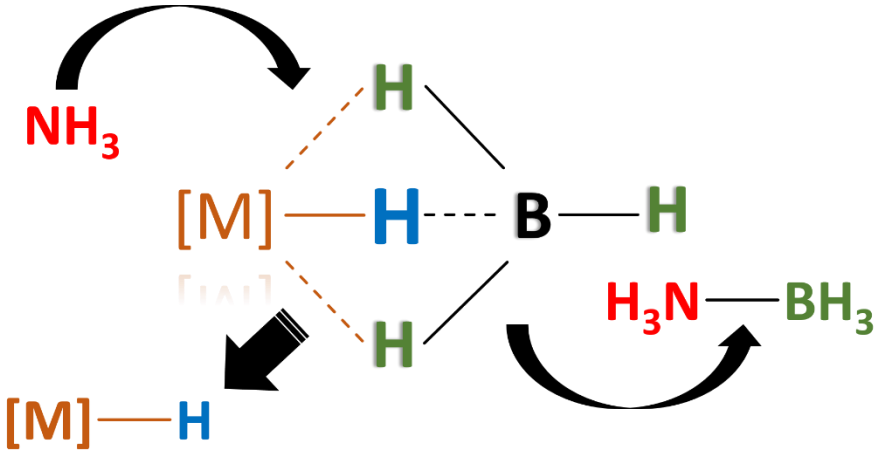

Author Contribution:

Mostajeran performed all the experiments. Wolstenholme, Frazee and McGrady assisted in manuscript preparation by giving comments and advices in addition to revision of the final draft. The manuscript was prepared and submitted by Mostajeran and Baker.

3.1. Abstract

Ammine metal borohydrides (AMBs) have recently commanded attention as low-temperature hydrogen sources. As an alternative to widely used mechanochemical synthesis that affords mixtures with salt co-products, we have been investigating solution synthesis routes to obtain pure AMBs. Here we show that reactions of MCl_n + $nNaBH_4$ with ammonia in thf afford ammonia-borane (AB) via borane abstraction from M-coordinated borohydride. The amount of AB formed correlates roughly with the metal ion electronegativity and AMB thermal stability, except for reducible metals such as Ti, which affords nearly 3 equiv. of AB per Ti.

3.2. Introduction

Development of the hydrogen economy will be enhanced by safe and efficient H_2 storage methods and materials.[1] Lightweight metal borohydrides, $[M(BH_4)_m]$, contain large amounts of hydrogen (10-15 wt%), but are plagued by high desorption temperatures and, in some cases, formation of toxic and potentially explosive diborane.[2] These shortcomings led to the development of ammine metal borohydrides $[M(BH_4)_m{\cdot}nNH_3$; AMBs][3-14] that exploit protic N-H and hydridic B-H bonds to reduce the energy barriers for low temperature hydrogen release.[15] Currently, the majority of AMBs are synthesised through ball-milling of $MCl_m{\cdot}nNH_3$ with Li/$NaBH_4$. One drawback of this method is the retention of Li/NaCl in the mixture, which decreases the efficiency of the material to serve as a hydrogen source by imposing ‘‘dead mass’’[16] and perhaps also by introducing additional reaction pathways to volatile contaminants such as diborane and ammonia. In this paper we show that solution synthesis of AMBs in tetrahydrofuran (thf) can be accompanied by formation of ammonia-borane (NH_3BH_3; AB).

3.3. Materials and Methods

3.3.1. Chemicals

YCl_3 (99.99%), $AlCl_3$ (99.99%), $MgCl_2$ (98%), $LiBH_4$ (95%), VCl_3 (99%), $LaCl_3$ (99.99%) and $ZnCl_2$ (99.99%) were purchased from Alfa Aesar®. $CaCl_2$ (96%), $TiCl_3$ (>95%) and $NaBH_4$ (98%) were purchased from Sigma Aldrich®. $AlCl_3$, $MgCl_2$ and $CaCl_2$ were dried and deoxygenated under vacuum at 110 °C for 3 h, then transferred and stored in the glove box. Other chemicals were transferred directly to the glove box and used without further treatment. Ammonia gas (99.99%) was obtained from Linde and dried by passing through a NaOH bed immediately before use.

3.3.2. Characterization

All experiments and manipuations were conducted under the strict exclusion of oxygen and moisture, using nitrogen gas and standard Schlenk and glove box (MBraun LABmaster 130) techniques. Levels of O_2 and H_2O were kept below 1 ppm. All solvents were deoxygenated by sparging with nitrogen, and were dried on columns of activated alumina using a J. C. Meyer (formerly Glass Contour®) solvent purification system. Benzene-d6 (C_6D_6) was dried by stirring over activated alumina (ca. 10 wt. %) overnight, followed by filtration. All solvents were stored over activated 4 Å molecular sieves (heated at ca. 250 °C for >10 hours in vacuo). ^{11}B and ^{11}B decoupled ^{1}H solution NMR spectra were recorded using a Bruker Avance spectrometer (300 MHz) at room temperature (21-23 °C). Solid state ^{11}B NMR spectra were collected using Bruker Avance spectrometers (200, 400 and 500 MHz) at room temperature (21-23 °C). $NaBH_4$ was used as a reference (δ = –42.1 ppm) to tune the parameters and the spectrometer for the ^{11}B MAS NMR experiments. Nonetheless, the resonance for residual $NaBH_4$ present in most of the reactions appears at –42.7 ppm in the solid state. Unless otherwise stated, the spinning rate for the MAS NMR experiments was 10 KHz for the 400 MHz Bruker spectrometer (4 mm BN rotor) and 25 KHz for the 500 MHz Bruker spectrometer (2.5 mm BN rotor). FT-IR spectra were collected using a Thermo Nicolet NEXUS 670 FT-IR instrument.

3.3.3. Synthesis of $Y(BH_4)_3$

Yttrium borohydride [$Y(BH_4)_3$] was prepared by the reaction of YCl_3 and 4 equiv. of $NaBH_4$ in refluxing thf for 2 days under N_2. Colourless $Y(BH_4)_3(thf)_3$ powder was isolated after removing thf *in vacuo*. This powder was then extracted repeatedly with dry toluene to ensure no contamination by $NaBH_4$ or NaCl. After removal of the toluene, washing with hexanes and drying, the product was yellow with an approximate stoichiometry of $[Y(BH_4)_3(thf)_2]n$ as determined by ^{11}B NMR spectroscopy.

3.3.4. Reaction of Pure $[Y(BH_4)_3(thf)_2]_n$ with Ammonia in thf

Yellow $[Y(BH_4)_3(thf)_2]_n$ 0.118 g, 0.43 mmol) was loaded into a Schlenk flask and dissolved in 30 g of dry thf, yielding a clear yellow solution. The flask was briefly evacuated for 2-3 seconds, and dry NH_3 was introduced to the flask, causing an immediate precipitation of a colourless solid. The mixture was stirred vigorously for 2 hours, briefly evacuated, refreshed with ammonia gas and stirred for another 2 hours. Finally, the flask was transferred into the glove box and its contents were filtered using a glass funnel

equipped with a frit. The solid (**1**) was dried *in vacuo* and the colourless filtrate was analysed by ^{11}B NMR spectroscopy.

3.3.5. General Procedure for the Reaction of Ammonia with a Mixture of MCl_n + *n*$NaBH_4$ in thf.

Solid MCl_n and *n* equiv. of $NaBH_4$ were loaded into a Schlenk flask equipped with a Teflon stir bar and 30 g dry thf. The flask was evacuated for 2-3 seconds and dry ammonia was introduced into the flask, causing immediate precipitation of a colourless solid (unless otherwise stated). The reaction was stirred for 2 days with little apparent change (the atmosphere of the flask was refreshed with ammonia twice during this period). Then the flask was transferred to the glove box and the mixture filtered. The solid (m) was dried *in vacuo* and characterised by solid-state ^{11}B NMR and FT-IR spectroscopy; the filtrate was analysed by solution ^{11}B NMR spectroscopy.

3.3.5.1. Magnesium

Colourless solid $MgCl_2$ (0.109 g, 1.12 mmol) and $NaBH_4$ (0.085 g, 2.24 mmol) were mixed together in a Schlenk flask with 30 g of dry thf, and ammonia was added. Rapid formation of a colourless powder (**4**) was observed as the result of adding ammonia. The mixture was filtered to obtain 259 mg of solid. Analysis of the filtrate by ^{11}B NMR showed 0.37 equiv. AB/Mg.

3.3.5.2. Calcium

Colourless solid $CaCl_2$ (0.138 g, 1.12 mmol) and $NaBH_4$ (0.085 g, 2.24 mmol) were placed in a Schlenk flask along with 30 g thf and ammonia was added as above. In this case the reaction was slower than the others. Stirring for 3 hours caused precipitation of a colourless powder (**5**). The mixture was filtered to obtain 236 mg of solid. Analysis of the filtrate by ^{11}B NMR spectroscopy showed 0.20 equiv. AB/Ca. The thf solvent was removed from the filtrate in vacuo to afford 17 mg solid.

3.3.5.3. Zinc

Colorless solid $ZnCl_2$ (0.153 g, 1.12 mmol) and $NaBH_4$ (0.085 g, 2.24 mmol) were loaded into a Schlenk flask along with 30 g of dry thf, and ammonia was added as above, causing immediate precipitation of a colourless powder (**6**). The mixture was filtered to obtain 286 mg of solid. Analysis of the filtrate by ^{11}B NMR spectroscopy showed 0.01 equiv. AB/Zn.

3.3.5.4. Aluminum

Colourless solid $AlCl_3$ (0.149 g, 1.12 mmol) and $NaBH_4$ (0.130 g, 3.36 mmol) were loaded in a Schlenk flask along with 30 g of dry thf. As the result of adding ammonia to the flask a colourless powder (**7**) precipitated. The mixture was filtered to obtain 347 mg of solid. Analysis of the filtrate by ^{11}B NMR spectroscopy showed 0.47 equiv. AB/Al. The thf solvent was removed from the filtrate *in vacuo* to afford 13 mg solid.

3.3.5.5. Vanadium

Violet solid VCl_3 (0.182 g, 1.12 mmol) and $NaBH_4$ (0.130 g, 3.36 mmol) were loaded into a Schlenk flask with 30 g of dry thf, resulting in a dark violet solution. As the result of adding ammonia to the flask, a dark brown powder (**8**) precipitated. The mixture was filtered to obtain 390 mg of solid. Analysis of the filtrate by ^{11}B NMR spectroscopy showed 1.35 equiv. AB/V.

3.3.5.6. Titanium

Purple solid $TiCl_3$ (0.173 g, 1.12 mmol) was placed in a Schlenk flask along with $NaBH_4$ (0.130 g, 3.36 mmol) and 30 g of dry thf, to give a purple suspension. As the result of adding ammonia to the flask a colourless powder (**9**) precipitated. The mixture was filtered to obtain 307 mg of 9. Analysis of the filtrate by ^{11}B NMR spectroscopy showed 3.1 equiv. AB/Ti. The thf solvent was then removed from the filtrate *in vacuo* to afford 72 mg solid. The solid was dried *in vacuo* and the filtrate was analysed by ^{11}B NMR spectroscopy.

3.3.5.7. Yttrium

Colourless solid YCl_3 (0.223 g, 1.14 mmol) and $NaBH_4$ (0.135 g, 3.49 mmol) were loaded into a Schlenk flask equipped with a Teflon stir bar, and 30 g of dry thf was added with stirring. Addition of ammonia to the flask gave a colourless precipitate (**3**). The mixture was filtered, washed with thf and dried to obtain 405 mg of 5. Analysis of the filtrate by ^{11}B NMR spectroscopy showed 0.25 equiv. AB/Y, but no evidence of soluble Y product. The thf solvent was then removed from the filtrate *in vacuo* to afford 9 mg of solid AB.

3.3.5.8. Lanthanum

Colorless solid $LaCl_3$ (0.275 g, 1.12 mmol) and $NaBH_4$ (0.130 g, 3.36 mmol) were loaded in a Schlenk flask with 30 g of dry thf, and ammonia was added as above, causing immediate precipitation of a colourless powder (**10**). The mixture was filtered to obtain

430 mg of solid. Analysis of the filtrate by ^{11}B NMR spectroscopy showed 0.09 equiv. AB/La.

3.3.5.9. Lithium

Colourless solid $LiBH_4$ (0.077 g, 0.30 mmol) was placed in a Schlenk flask with 30 g of dry thf and ammonia was added. Soon after introducing ammonia to the flask a colorless gel formed. Analysis of the solution after filtration by ^{11}B NMR spectroscopy showed 0.02 equiv. AB/Li.

3.3.5.10. Sodium

Colorless solid $NaBH_4$ (0.130 g, 3.36 mmol) was loaded into a Schlenk flask with 30 g of dry thf and ammonia was added as above. The presence of ammonia caused all the $NaBH_4$ to dissolve, giving a clear colourless solution. Analysis of the solution by ^{11}B NMR spectroscopy showed 0.01 equiv. AB/Na.

3.3.6. Effect of Solvent on the Reaction of YCl_3 + 3 $NaBH_4$ with Ammonia

Colorless solid YCl_3 (0.275 g, 1.12 mmol) and $NaBH_4$ (0.130 g, 3.36 mmol) were loaded in a Schlenk flask with 30 g of dry solvent, and ammonia was added as above, causing immediate precipitation of a colourless powder.

3.3.6.1. Dichloromethane (DCM)

Addition of ammonia to the flask gave a colourless precipitate. The mixture was filtered, washed with DCM and dried to obtain 470 mg of solid. Analysis of the filtrate by ^{11}B NMR spectroscopy showed 0.11 equiv. AB/Y. The DCM solvent was then removed from the filtrate *in vacuo* to afford 8 mg of solid AB.

3.3.6.2. Pyridine (py)

Addition of ammonia to the flask gave a colourless precipitate. The mixture was filtered, washed with py and dried to obtain 465 mg of solid. Analysis of the filtrate by ^{11}B NMR spectroscopy showed predominate formation of pyridine-borane (-11.4 ppm; J_{BH}= 100 Hz) along with some AB (Figure A1.12; 0.24 equiv. AB + pyridine-borane/Y). The pyridine solvent was then removed from the filtrate *in vacuo* to afford 61 mg of a solid mixture of AB and pyridine.

3.3.6.3. Dimethylsulfoxide (DMSO)

Addition of ammonia to the flask gave a colourless precipitate. The mixture was filtered, washed with DMSO and dried to obtain 235 mg of solid. Analysis of the filtrate

by ^{11}B NMR spectroscopy showed 0.24 equiv. AB/Y. Due to the high boiling point of DMSO (189 °C), no evaporation was conducted.

3.4. Results and Discussion

3.4.1. Experimental Observations

We began our investigation with the yttrium AMB, $Y(BH_4)_3(NH_3)_4$, **1**, prepared initially by Yu et al. by ball-milling a mixture of $YCl_3(NH_3)_4$ and 3 equiv. $LiBH_4$.[13] In order to avoid formation of 'ate' complexes and to facilitate separation of the salt co-product, we prepared the known complex, $Y(BH_4)_3(thf)_3$[17] from YCl_3 and 3 equiv. of $NaBH_4$ in thf solution (Figure A1.1). Subsequent treatment of a thf solution of this complex with ammonia gas produced immediate precipitation of a colourless solid, **2**. After filtration, the ^{11}B NMR spectrum of the filtrate contained two resonances in a 1:1 ratio (Figure A1.2). The quintet resonance at -26.6 ppm (J_{BH}= 85 Hz) is due presumably to an unidentified yttrium borohydride complex (*cf.* $Y(BH_4)_3(thf)_3$ in thf is at -23.6 ppm, 85 Hz), whereas the quartet at -22.3 ppm (J_{BH}= 93 Hz) can be assigned to AB (ca. 0.2 equiv. per Y using an external $BF_3{\cdot}Et_2O$ standard). The FT-IR spectrum of 2 (Figure A3.1) shows minor differences when compared to a pure sample of **1** (prepared by treatment of $Y(BH_4)(thf)_3$ with liquid NH_3 at -50 °C). The ^{11}B MAS NMR spectrum of **2** consists of a minor amount of AB at -22.6 ppm and two Y-BH_4 resonances at -27.9 and -37.9 ppm in a 26:1 ratio (Figure A2.1). Although Yu et al. assigned two similar resonances at -28.6 and -39.0 ppm to Y-coordinated and outer-sphere borohydrides in the tetra-ammoniate salt, $[Y(BH_4)_2(NH_3)_4]BH_4$ (2:1 ratio),[13] a more recent study by Jensen et al. reports these resonances to arise from the tetra- and heptaammoniates, respectively.[18] In concert with this assignment, we found that the pure solid product obtained from reaction of $Y(BH_4)_3(thf)_3$ with liquid ammonia gave rise to a single ^{11}B NMR resonance at -27.3 ppm due to 1 (Figure A2.2).

We next investigated the generality of AB formation accompanying the synthesis of most known AMBs in thf solution (Table 3.1). A solution or suspension of the metal chloride and $NaBH_4$ was treated with ammonia, and the resulting solid and filtrate were then characterized by IR and NMR spectroscopy. Note that under these reaction conditions, both thf and ammonia adducts of the metal halides will be reacting with the borohydride salt. For the yttrium reaction, a mixture of 223 mg anhydrous YCl_3 and 135 mg $NaBH_4$ in 30 g of dry thf was treated with excess ammonia to afford 405 mg of a colourless solid, **3**.

Table 3.1. Formation of ammonia-borane during synthesis of AMBs.

Element	Ionic radius, Å[a]	Zhang Electronegativity[b]	Zhang Lewis acidity[c]	Amount of AB formed (equiv./metal)
Li[d]	0.92	0.94	1.97	0.02
Na[d]	1.18	0.96	1.38	0.01
Mg	0.89	1.21	1.40	0.37
Ca	1.12	1.03	1.59	0.20
Zn	0.74	1.43	0.66	0.01
Al	0.53	1.50	3.04	0.47
Ti[e]	0.67	1.41	1.69	3.10
V[e]	0.78	0.61	1.09	1.35
Y	1.02	1.21	1.47	0.25
La[d]	1.17	1.21	0.85	0.09

[a] Ref. 19a. [b] Ref. 19b. [c] Ref. 20. [d, e] Oxidation state: 3+.

The ^{11}B NMR spectrum (Figure A1.3) of the filtrate shows formation of AB and a small amount of unreacted $NaBH_4$ but none of the soluble Y-BH_4 by-product observed above. Integration of the spectrum vs. the $BF_3{\cdot}Et_2O$ standard indicated ca. 99% conversion of $NaBH_4$ and the formation of 0.28 mmol AB (0.25 equiv. vs. Y). Comparison of the FT-IR spectra of solids **2** and **3** (Figure A3.2) again suggests contamination of the desired Y AMB product **1**.

Reactions of divalent metal chlorides with $NaBH_4$ and ammonia afforded varying amounts of AB. In the case of Mg, in addition to the resonance for unreacted $NaBH_4$ (at -42.7 ppm), the resonance centred at -38.2 ppm in the solid-state ^{11}B MAS NMR (Figure A2.4) could be assigned to the tetra-ammoniate, $Mg(BH_4)_2(NH_3)_4$ **4**, on the basis of the estimated ammonia uptake (Table 3.2).[21]

The ^{11}B NMR spectrum of the filtrate yielded an estimate of 0.37 equiv. of AB vs. Mg. In contrast, the Ca reaction afforded $Ca(BH_4)_2(NH_3)_2$ **5** (sharp singlet at -35.1 vs. -34.7 ppm in the literature).[7a] While only 0.2 equiv. of AB (vs. Ca) were produced in this reaction, a new Ca-coordinated BH_4 resonance was observed in the solution ^{11}B NMR spectrum at -36.9 ppm (J_{BH}= 82Hz) (Figure A1.5). For the heavier divalent metal, $Zn(BH_4)_2(NH_3)_2$[10b] is reported to exhibit a ^{11}B MAS NMR resonance at -44.1 ppm. However, in our reaction this is only a minor product (-44.3 ppm), with the major product **6** giving rise to two resonances at -36.8 ppm and -38.5 ppm in a ratio of 1:2 (Figure A2.6). We have observed this AMB with formula $Zn_3(BH_4)_6(NH_3)_8$ previously from treatment of isolated $Zn(BH_4)_2(thf)_2$ with liquid ammonia; full characterization will be published elsewhere. In this reaction only 0.01 equiv. of AB (*vs.* Zn) were formed (Figure A1.6), indicating the potential to prepare a pure sample of **6** using the thf solution method.

Table 3.2. Estimate of ammonia uptake in reactions of MCl_n + *n* $NaBH_4$ with ammonia.

Element M	Wt. of insoluble solid (mg)	Wt. – *n* NaCl	Calc'd Wt. of $M(BH_4)_n$	NH_3 uptake (equiv/M)	Mass Difference (calc'd NH_3 equiv)
Ca	236	105	78	1.5	13 (0.7)
Mg	259	128	60	3.5	65 (3.4)
Zn	286	155	107	2.5	48 (2.5)
Al	347	150	80	4.0	68 (3.6)
Ti	307	110	103	0.5	0 (0)
V	390	193	197	0	78 (4.0)
Y	405	205	152	3.0	47 (2.5)
La	475	279	205	3.9	71 (3.7)

Reactions with trivalent metal chlorides shed additional light on the factors leading to AB formation. The ^{11}BMAS NMR spectrum of the colourless solid obtained from the Al reaction showed two overlapping resonances centred at -35.8 and -37.0 ppm in a ratio of ca. 2.5:1 that can be assigned to a mixture of $Al(BH_4)_3(NH_3)_4$[6d] (-36.9 ppm) and $Al(BH_4)_3(NH_3)_6$[6e] (-36.7 ppm). Analysis of the reaction filtrate gave an estimate of 0.47 equiv. of AB (*vs.* Al) (Figure A1.7). As seen for yttrium, the lanthanum reaction afforded one major product **7** with a ^{11}B MAS NMR resonance at -24.1 ppm which matches that of the product obtained from reaction of $La(BH_4)_3(thf)_3$ with liquid ammonia. In contrast to Y, however, the La reaction in thf produced less than 0.1 equiv. of AB (*vs.* La).

The most remarkable results were obtained from the V and Ti reactions. ^{11}B MAS NMR spectroscopic analysis of the brown solid **8** obtained from the reaction of 1:3 VCl_3: $NaBH_4$ with ammonia in thf gave a series of broad peaks between -13.7 and 38.1 ppm that includes resonances typical of 3-coordinate boron (Figure A2.9).[22] While the paramagnetic d^2 V^{3+} ion likely prevents observation of V-coordinated borohydride NMR resonances, the spectrum suggests that the reaction also involves some dehydrocoupling. In this reaction 1.35 equiv. of AB (vs. V) were produced. In the remarkable reaction of $TiCl_3$ + $3NaBH_4$ with ammonia, formation of nearly 3 equiv. of AB (vs. Ti) was observed along with colourless solid **9**. Indeed, evaporation of the filtrate and drying in vacuo afforded 72 mg of colourless solid (*cf.* 2.53 mmol AB= 78 mg). The FT-IR spectrum of solid **9** clearly indicates the presence of B-H units although only a weak, broad feature is observed in the N-H stretching region (Figure A3.4). Both tetra- and tricoordinate boron environments are clearly observed in the ^{11}B MAS NMR spectrum of solid **9** (Figure 3.1).

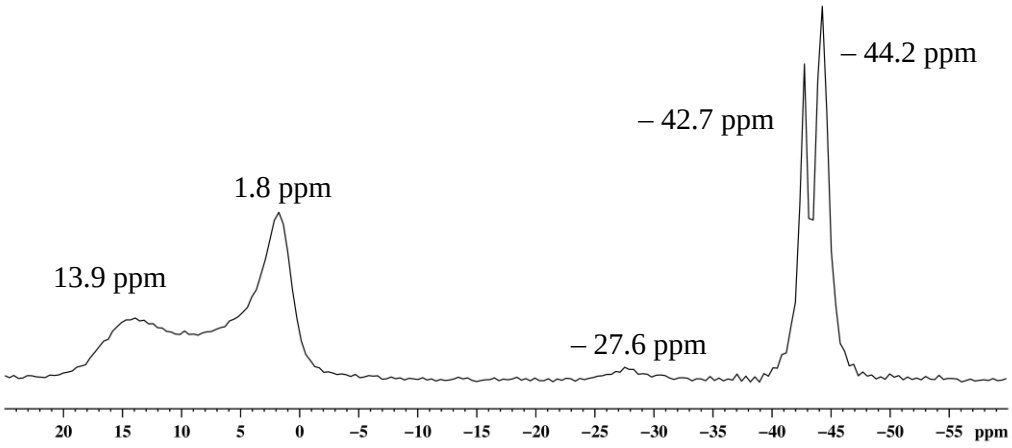

Figure 3.1. ^{11}B MAS NMR (128 MHz, ν_R= 10 KHz) of solid **9** obtained from $TiCl_3/3NaBH_4$ and NH_3 in thf.

Three different environments can be identified: a major broad peak spans 1.8 to 13.9 ppm, indicative of 3-coordinate boron, a weak resonance at -27.6 ppm may be due to a BH_3 unit, and a major BH_4 resonance appears at -44.2 ppm, *i.e.*, upfield of $NaBH_4$. Ti^{3+} is a paramagnetic d^1 ion, and ^{11}B NMR spectra of its monomeric borohydride derivatives are not typically observed.[23] Formation of colourless solid **9** and the presence of a sharp borohydride resonance are both suggestive of accompanying redox chemistry. EPR spectroscopy is currently being applied to investigate this reaction further, and the results will be published in due course.

3.4.2. Trends, Origin and Correlations in AB Formation by Each Metal

In these one-pot reactions, ammonia adducts of MCl_n appear to react more readily with $NaBH_4$ than do the pure MCl_n reagents in thf.[10b] Nonetheless, the results described above indicate that formation of AB usually accompanies attempts to prepare pure AMBs using thf solution routes. Reactions of $Cp_2Zr(BH_4)_2$ with an amine base to afford amine-borane and $Cp_2ZrH(BH_4)$ were reported by Bird and Wallbridge et al.,[24] and Nöth et al. noted that dissolution of $Ti(BH_4)_3$ in pyridine afforded pyridine-borane.[25] However, this reaction pathway has not been recognised in recent work investigating AMBs as hydrogen storage media.[8] As can be seen in Figure 3.2a, the amount of AB formed with the s- and p-block metals correlates roughly with the Zhang electronegativity[19b] with the exception of Zn, which shows the least tendency to produce the amine-borane adduct. In this respect, the electronegativity of the metal centre in a series of AMBs was also recently correlated with their thermal decomposition temperature.[26] This suggests that AB may be formed as an intermediate in the decomposition of these hydrogen storage candidates, possibly through generation of $M\text{-}NH_2BH_3$ units derived from

dehydrocoupling of M-H + AB. In contrast, little correlation is found with the metal ion Lewis acidity as calculated by Zhang[20a] (Figures A4.2 and A4.3).

As can be seen in Figure 3.2b, the ionic radii for the d-block metal derivatives display a strong correlation with the amount of AB formed in these reactions, with the exception of $[Zn_3(BH_4)_6(NH_3)_8]$.

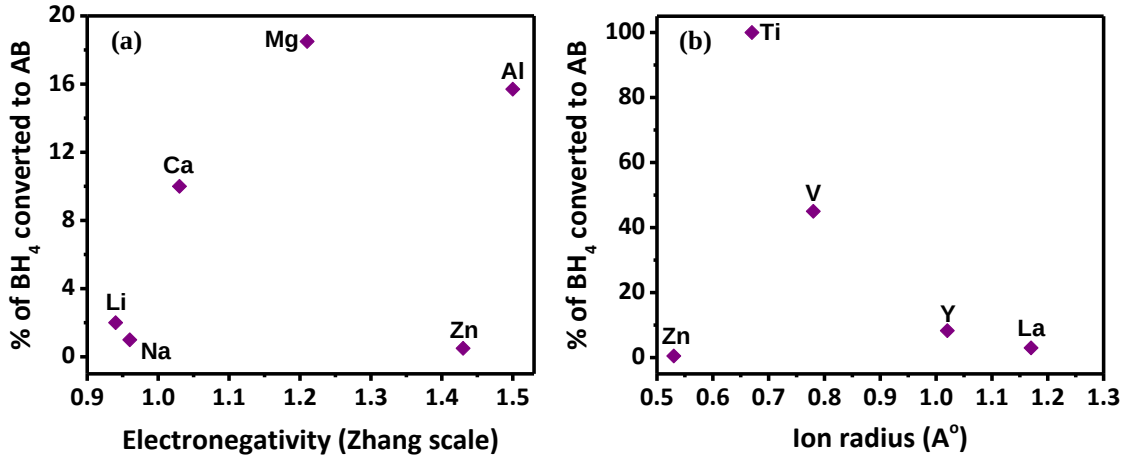

Figure 3.2. Correlation between the amount of AB produced in reactions of MCln + *n*$NaBH_4$ with NH_3 vs. (a) Zhang electronegativity of the s- and p-block metal ions, and (b) ionic radius of the d-block metal ions.

This indicates a pronounced increase in the formation of AB as the ionic radius decreases. Closer inspection of this behaviour shows that the redox-inactive d^0 and d^{10} complexes yield small amounts of AB (<0.25 equiv.), whereas the d^1 (Ti) and d^2 (V) derivatives engage in a competitive dehydrocoupling process, leading to appreciable quantities of the amine-borane adduct. If we consider the reaction as a nucleophilic abstraction of borane from the coordinated borohydride ligand, the relative stability of the metal borohydride *vs.* metal hydride should be one thermodynamic factor to be considered. While we do not yet fully understand this trend, it is interesting to consider that these are the only redox-active metals on the list. The presence of these non-bonding electrons may also confer a kinetic advantage by increasing the lability of the ligands within their metal coordination sphere.

At the request of a referee, the experimental thermal stability (T_{dec}) of some of the AMBs is plotted against the amount of AB obtained for each metal (Figure 3.3). The strong correlation suggests that more stable AMBs are less susceptible to AB formation. As reported above, Zn and the reducible transition metals (*i.e.* Ti and V) are exceptions to this trend.

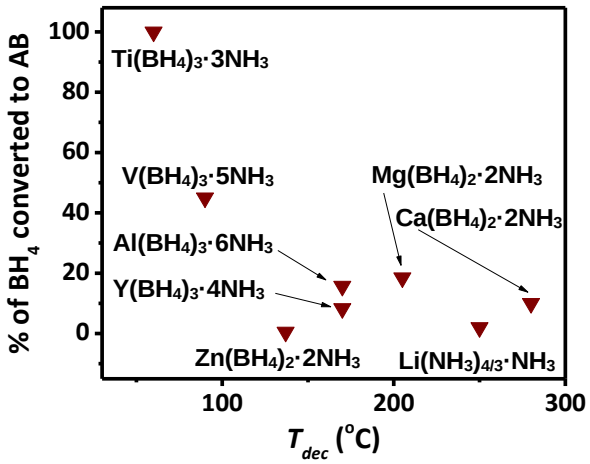

Figure 3.3. Correlation between the amount of AB produced *vs.* the decomposition onset temperature (T_{dec}) of each AMB.

3.4.3. Solvent Effect

To consider the effect of solvent polarity on the formation of AB, YCl_3 was treated with 3 equiv. of $NaBH_4$ in dichloromethane (DCM, ε = 9.1), pyridine (py, ε = 12.3) and dimethyl sulfoxide (DMSO, ε = 46.7) (Table 3.3).

Table 3.3. Estimate of ammonia uptake in reactions of YCl_3 + 3 $NaBH_4$ with ammonia in different solvents.[a]

solvent	Wt. of Reagents	Wt. of Insoluble	Wt. – n NaCl	Calc'd Wt. of $Y(BH_4)_3$	NH_3 uptake (equiv/M)[b]	Mass Difference (calc'd NH_3 equiv)[c]
thf	358	405	205	152	2.8	47 (2.5)
DCM	358	470	270	152	6.2	112 (5.8)
DMSO	358	235	35	152	--[d]	--[d]
Pyridine	358	465	265	152	5.9	107 (5.6)

[a] Calculation assumes all chloride in MCl_n ends up as NaCl. [b] Calculation based on formation of $M(BH_4)_n(NH_3)_m$. [c] Calculation based on excess mass obtained vs. mol MCl_n employed. [d] No evaporation was made due to the high boiling point of DMSO.

Only 0.1 equiv. of AB were formed in DCM while 1.6 equiv. were obtained in DMSO (Figures A1.11 and A1.13). Notably, ^{11}B NMR spectroscopy indicated that the heptaammoniate Y-AMB, $Y(BH_4)_3{\cdot}7NH_3$,[18] is favoured in DCM (*vs*. the tetra-ammoniate in thf; Figure A2.12). The result in pyridine solvent is complicated by formation of pyridine-borane (PyB) that could arise from both direct reaction with a Y-BH_4 group and the known pyridine reaction with ammonia-borane.[27] A total of 0.24 equiv./Y of AB + PyB was formed in this reaction (Figure A1.12). The increased amount of AB formation observed in DMSO *vs.* thf may be attributed to the stronger donor power of the former that could facilitate the borane abstraction.

3.5. Conclusions

In summary, we have shown that solution synthesis of ammine metal borohydrides in thf is accompanied by formation of ammonia-borane via ammonia abstraction of borane from a metal-coordinated borohydride ligand. An inspection of ^{11}B MAS NMR spectra for a number of AMBs prepared by mechanochemical means also provides evidence for AB formation.[6b,f,13] Although AB is observed as a by-product for each metal studied here, the solution method offers a potentially efficient route to prepare the desired AMBs directly and cleanly from their corresponding metal borohydrides in liquid ammonia or dimethylsulfide[18] solvents at low temperatures. Further investigations along these lines are in progress in our labs.

3.6. References

(1) a) Chen, P.; Zhu, M. *Mater. Today* **2008**, *11*, 36-43; b) Hamilton, C. W.; Baker, R. T.; Staubitz, A.; Manners, I. *Chem. Soc. Rev.* **2009**, *38*, 279-293; c) Chua, Y. S.; Chen, P.; Wu, G.; Xiong, Z. *Chem. Commun.* **2011**, *47*, 5116-5129.
(2) a) Orimo, S.-i.; Nakamori, Y.; Eliseo, J. R.; Züttel, A.; Jensen, C. M. *Chem. Rev.* **2007**, *107*, 4111-4132; b) Li, H.-W.; Yan, Y.; Orimo, S.-i.; Züttel, A.; Jensen, C. M. *Energies* **2011**, *4*, 185-214.
(3) Li: a) Sullivan E. A.; Johnson S. *J. Phys. Chem.* **1959**, 63, 233-238; b) Johnson S. R.; David W. I. F.; Royse D. M.; Sommariva M.; Tang C. Y.; Fabbiani F. P. A.; Jones M. O.; Edwards P. P. *Chem. - Asian J.* **2009**, 4, 849-854; c) Gao L.; Guo Y. H.; Xia G. L.; Yu X. B. *J. Mater. Chem.* **2009**, 19, 7826-7829; d) Guo Y.; Xia G.; Zhu Y.; Gao L.; Yu X. *Chem. Commun.* **2010**, 46, 2599-2601; e) Zhong B.; Huang X. X.; Wen G.; Zhang X. D.; Bai H. W.; Zhang T.; Yu H. M. *Solid State Commun*. **2010**, 150, 1552-1555; f) Guo Y. H.; Sun W. W.; Guo Z. P.; Liu H. K.; Sun D. L.; Yu X. B. *J. Phys. Chem. C* **2010**, 114, 12823-12827; g) Chen X.; Li S.; Guo Y.; Yu X. *Dalton Trans*. **2011**, 40, 9679-9689; h) Tan Y.; Guo Y.; Li S.; Sun W.; Zhu Y.; Li Q.; Yu X. *J. Mater. Chem*. **2011**, 21, 14509-14515; i) Zheng X.; Wu G.; Li W.; Xiong Z.; He T.; Guo J.; Chen H.; Chen P. *Energy Environ. Sci.* **2011**, 4, 3593-3600; j) Tang Z.; Tan Y.; Chen X.; Yu X. *Chem. Commun.* **2012**, 48, 9296-9298; k) Kumar S.; Taxak M.; Krishnamurthy N. *Int. J. Hydrogen Energy* **2012**, 37, 3283-3291; l) Chen X.; Cai W.; Guo Y.; Yu X. *Int. J. Hydrogen Energy* **2012**, 37, 5817-5824; m) Tan Y.; Tang Z.; Li S.; Li Q; Yu X. *Int. J. Hydrogen Energy* **2012**, 37, 18101-18107.
(4) Na: Kravchenko O. V.; Khafizova G. M.; Burdina K. P.; Semenenko K. N. *Zh. Obshch. Khim.* **1992**, 62, 2401-2406.
(5) Mg: a) Wagner R. I.; Grant L. R. **US Pat**., 4,604,271 **1986**; b) Soloveichik G.; Her J.-H.; Stephens P. W.; Gao Y.; Rijssenbeek J.; Andrus M.; Zhao J. C., *Inorg. Chem*. **2008**, 47, 4290-4298; c) Gao L.; Guo Y. H.; Li Q.; Yu X. B. *J. Phys. Chem. C* **2010**, 114, 9534-9540; d) Sun W.; Chen X.; Gu Q.; Wallwork K. S.; Tan Y.; Tang Z.; Yu X. *Chem. - Eur. J.* **2012**, 18, 6825-6834; e) Yang Y.; Liu Y.; Li Y.; Gao M.; Pan H. *Chem. - Asian J.* **2013**, 8, 476-481; f) He T.; Wu H.; Chen J.; Zhou W.; Wu G.; Xiong Z.; Zhang T; Chen P. *Phys. Chem. Chem. Phys*. **2013**, 15, 10487-10493; g) Yang Y.; Liu Y.; Li Y.; Gao M.; Pan H. *J. Phys. Chem. C* **2013**, 117, 16326-16335; h) Yuan P.-F.; Wang F.; Sun Q.; Jia Y.; Guo Z. X. *Int. J. Hydrogen Energy* **2013**, 38, 2836-2845; i) Chen X.; Yuan F.; Gu Q.; Tan Y.; Liu H.; Dou S.; Yu X. *Int. J. Hydrogen Energy* **2013**, 38, 16199-16207.

(6) Al: a) Kravchenko O. V.; Kravchenko S. E. *Zh. Obshch. Khim*. **1989**, 59, 1935-1939; b) Guo Y.; Yu X.; Sun W.; Sun D.; Yang W., *Angew. Chem., Int. Ed*. **2011**, 50, 1087-1091; c) Guo Y.; Wu H.; Zhou W.; Yu X., *J. Am. Chem. Soc*. **2011**, 133, 4690-4693; d) Guo Y.; Jiang Y.; Xia G.; Yu X., *Chem. Commun*. **2012**, 48, 4408-4410; e) Tang Z.; Tan Y.; Wu H.; Gu Q.; Zhou W.; Jensen C. M.; Yu X. *Acta Mater*. **2013**, 61, 4787-4796; f) Tang Z.; Tan Y.; Chen X.; Ouyang L.; Zhu M.; Sun D.; Yu X. *Angew. Chem., Int. Ed*. **2013**, 52, 12659-12663.
(7) Ca: a) Chu H.; Wu G.; Xiong Z.; Guo J.; He T.; Chen P. *Chem. Mater*. **2010**, 22, 6021-6028; b) Tang Z.; Tan Y.; Gu Q.; Yu X. *J. Mater. Chem*. **2012**, 22, 5312-5318; c) Chen X.; Yuan F.; Tan Y.; Tang Z.; Yu X. *J. Phys. Chem. C* **2012**, 116, 21162-21168.
(8) Ti: Yuan F.; Gu Q.; Chen X.; Tan Y.; Guo Y.; Yu X. *Chem. Mater*. **2012**, 24, 3370-3379.
(9) V: a) Tang Z.; Yuan F.; Gu Q.; Tan Y.; Chen X.; Jensen C. M.; Yu X. *Acta Mater*. **2013**, 61, 3110-3119; b) Yuan F.; Chen X.; Gu Q.; Tang Z.; Yu X. *Int. J. Hydrogen Energy* **2013**, 38, 5322-5329.
(10) Zn: a) Xia G.; Gu Q.; Guo Y.; Yu X. *J. Mater. Chem*. **2012**, 22, 7300-7307; b) Gu Q., Gao L.; Guo Y.; Tan Y.; Tang Z.; Wallwork K. S.; Zhang F.; Yu X. *Energy Environ. Sci*. **2012**, 5, 7590-7600.
(11) Co: Li L.; Huang J.; Li M.; Li Q.; Ouyang L.; Zhu M.; Yu X. *Int. J. Hydrogen Energy* **2013**, 38, 16208-16214.
(12) Nb: Li M.; Yuan F.; Gu Q.; Yu X. *Int. J. Hydrogen Energy* **2013**, 38, 9236-9242.
(13) Y: Yuan F.; Gu Q.; Guo Y.; Sun W.; Chen X.; Yu X., *J. Mater. Chem*. **2012**, 22, 1061-1068.
(14) Zr: a) Huang J.; Tan Y.; Su J.; Gu Q.; Cerny R.; Ouyang L.; Sun D.; Yu X.; Zhu M. *Chem. Commun*. **2015**, 51, 2794-2797; b) Huang J.; Tan Y.; Gu Q.; Ouyang L.; Yu X.; Zhu M. *J. Mater. Chem. A* **2015**, 3, 5299-5304.
(15) Chen X.; Zhao J.-C.; Shore S. G. *Acc. Chem. Res*. **2013**, 46, 2666-2675.
(16) Jaroń T.; Orłowski P. A.; Wegner W.; Fijałkowski K. J.; Leszczyński P. J.; Grochala W. *Angew. Chem., Int. Ed*. **2015**, 54, 1236-1239.
(17) a) Segal B. G.; Lippard S. J. *Inorg. Chem*. **1978**, 17, 844-850; b) Lobkovskii É. B.; Kravchenko S. E.; Kravchenko O. V. *J. Struct. Chem*. **1983**, 23, 582-586.
(18) Jepsen L. H.; Ley M. B.; Černý R.; Lee Y.-S.; Cho Y. W.; Ravnsbak D.; Besenbacher F.; Skibsted J.; Jensen T. R. *Inorg. Chem*. **2015**, 54, 7402-7414.
(19) a) Shannon R. *Acta Crystallogr., Sect. A: Cryst. Phys., Diffr., Theor. Gen. Crystallogr*. **1976**, 32, 751-767; b) Zhang Y. *Inorg. Chem*. **1982**, 21, 3886-3889.
(20) a) Zhang Y., *Inorg. Chem*. **1982**, 21, 3889-3893; b) Yang Y.; Liu Y.; Wu H.; Zhou W.; Gao M.; Pan H. *Phys. Chem. Chem. Phys*. **2014**, 16, 135-143.
(21) The ^{11}B NMR resonance of the solid hexa-ammoniate is reported at -37.1 ppm (ref. 5c).
(22) Stowe A. C.; Shaw W. J.; Linehan J. C.; Schmid B.; Autrey T., *Phys. Chem. Chem. Phys.* **2007**, 9, 1831-1836.
(23) Nöth H.; Schmidt M. *Organometallics* **1995**, 14, 4601-4610.
(24) Bird P. H.; Wallbridge M. G. H. *J. Chem. Soc*. **1965**, 3923-3928.
(25) Franz K.; Fusstetter H.; Nöth H. *Z. Anorg. Allg. Chem*. **1976**, 427, 92-132.
(26) Jepsen L. H.; Ley M. B.; Lee Y.-S.; Cho Y. W.; Dornheim M.; Jensen J. O.; Filinchuk Y.; Jorgensen J. E.; Besenbacher F.; Jensen T. R. *Mater. Today* **2014**, 17, 129-135.
(27) a) Baldwin R. A.; Washburn R. M., *J. Org. Chem*. **1961**, 26, 3549-3550; b) Ramachandran P. V.; Kulkarni A. S., *RSC Adv*. **2014**, 4, 26207-26210.

Chapter 4: Base-Metal Nanoparticle-Catalyzed Hydrogen Release from Ammine Yttrium and Lanthanum Borohydrides

*A draft of this thesis has been published in: Mehdi Mostajeran, Eric Ye, Serge Desgreniers, and R. Tom Baker, Chem. Mater., **2017**, 29, 742-751.*

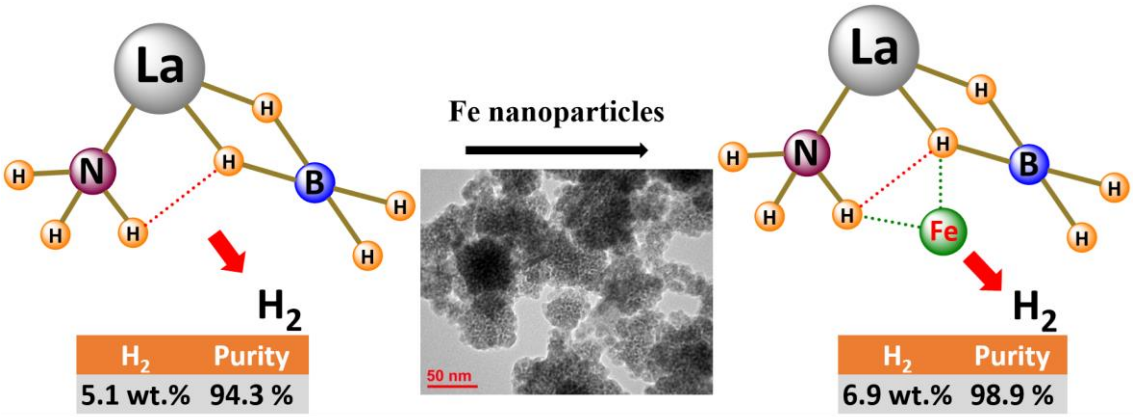

Authors Contribution:

Mostajeran conducted all the experiments presented in this chapter. Ye performed all the MAS NMRs and assisted in preparation of the manuscript for the ^{1}H DQF and ^{1}H 2D DQ MAS NMR experiments. Calculation of unit cells and structural parameters was executed by Desgreniers. The manuscript was prepared and submitted by Mostajeran and Baker.

4.1. Abstract

Solid ammine metal borohydrides [$M(BH_4)_m(NH_3)_n$, AMBs] are promising materials for low temperature, high capacity hydrogen generation. Retention of metal halide co-products, arising from typical mechanochemical synthetic methods, are shown to have negative impacts on dehydrogenation properties of yttrium AMB. Halide-free yttrium and lanthanum AMBs, $M(BH_4)_3(NH_3)_4$, have been synthesized directly by treatment of MCl_3 with 3 equiv. of $NaBH_4$ in thf followed by filtration, cooling and exposure to liquid ammonia. The peak dehydrogenation temperature of the Y analog decreased from previously reported 179 to 160 °C while the ammonia peak temperature increased from 86 to 165 °C. To enhance the dehydrogenation properties and increase the selectivity of gas formation from these AMBs, base-metal nanoparticle catalysts, M'NPs; M' = Fe, Co, Ni and Cu) were employed. Preparation of the M'NPs from $M'Cl_2$ and liquid hexylamine-borane allowed for separation of the B-Cl by-products by subsequent solvent washing. Sonication of the M'NPs in toluene followed by addition of the solid AMB afforded composite AMB-M'NP-BN solids. Thermolysis data indicated a 3-fold reduction in ammonia release from the Y-Co and 4-fold for the La-Fe composite. The purity of the released hydrogen was estimated to be 97.9 mol% for Y-Co and 98.9 mol% for La-Fe.

4.2. Introduction

Hydrogen has been introduced as a clean, renewable and sustainable energy for the future.[1] Its high energy density (142 MJ/kg) offers a potentially efficient replacement for fossil fuel combustion and complement to electricity for portable power applications.[1-2] Improved materials are required, however, to mitigate the low volumetric storage density of H_2 gas.[3] Among reported materials,[4] metal borohydrides, MBHs, have demonstrated some of the highest gravimetric hydrogen storage capacities.[5] However, their application has been hampered by high dehydrogenation temperatures (*e.g.* 380 °C for $LiBH_4$),[6] sluggish kinetics,[7] and formation of diborane and other toxic impurities.[8] In addition to some of the first row transition metal borohydrides,[9] of relevance to this work, yttrium borohydride, $Y(BH_4)_3$ (9.1 wt.% hydrogen) is reported to undergo H_2 release starting at *ca.* 185 °C, with 7.8 wt.% H_2 production up to 500 °C.[10] While lanthanum metal has also been used to dope other MBH systems to release hydrogen under more favorable conditions,[7,11] $La(BH_4)_3$ (6.5 wt.% hydrogen)[10b,12] is reported to release

2.9 wt.% hydrogen with no diborane from $LaCl_3 \cdot LiBH_4$ (1:3) between 200 and 400 °C.[13]

More recently, ammine metal borohydrides (AMBs, $[M(BH_4)_m(NH_3)_n]$)[14] have attracted attention due to their enhanced dehydrogenation properties (*i.e.* lower desorption temperature for hydrogen and absence of diborane) aided by intra- and intermolecular $B\text{-}H^{\delta-}\cdots{}^{\delta+}H\text{-}N$ interactions between their $(BH_4)^-$ and NH_3 ligands.[15] Coordination of ammonia to yttrium in $Y(BH_4)_3 \cdot 4NH_3$ for instance, lowers the hydrogen release onset to *ca.* 60 °C producing 9.3 wt. % hydrogen up to 300 °C.[16] Thermolysis of this AMB, however, is accompanied by substantial ammonia release that would be detrimental to the fuel cell catalyst. Although the detailed thermolysis mechanisms of AMBs are not yet fully understood, use of metal catalysts may improve the selectivity of H_2 release,[17] affording purer hydrogen streams.

One structural model of Y-AMB, $[Y(BH_4)_2(NH_3)_4]BH_4$, was first introduced by Yu et al.[16] in which $(BH_4)^-$ ligands are present in a 2:1 ratio of coordinated vs. outer-sphere ligands (based on the presence of two distinct B environments at -28.9 and -30 ppm in the ^{11}B MAS NMR and a Rietveld powder diffraction refinement). In this model the local geometry around Y was distorted octahedral and all the NH_3 ligands were coordinated directly to the metal center. In contrast, further investigation by Jensen et al.[18] revealed that all the $(BH_4)^-$ and NH_3 ligands are coordinated to Y and that the previous work analyzed a mixture of the tetra- and hepta-ammoniates.

The most common synthetic method for AMBs is ball-milling of metal chloride ammoniates with $M''BH_4$ (M''= Li, Na and K) under an inert atmosphere. Incorporation of the alkali metal chloride "dead mass",[19] in the AMB product, however, reduces the gravimetric storage capacity and may even affect production of volatile by-products such as ammonia or diborane.[20] We reported recently that solution synthesis of AMBs in tetrahydrofuran (thf) at room temperature can be accompanied by formation of ammonia-borane (AB).[21] Several other strategies for MBHs[10a-c,19,22] and AMBs[18,23] have been reported for synthesis of salt-free AMBs but a more general method is needed.

In this study, we show that pure Y and La AMBs, $M(BH_4)_3(NH_3)_4$, can be prepared directly from the corresponding metal borohydrides in liquid ammonia. Dehydrogenation properties of these pure AMBs are improved somewhat over the AMB-alkali metal chloride mixtures and improved even further by addition of base-metal (Fe, Co) nanoparticle catalysts.

4.3. Materials and Methods

4.3.1. General Procedures

Experiments were conducted under nitrogen, using Schlenk techniques or a nitrogen-filled MBraun glove box maintaining the level of oxygen and water below 0.1 ppm. All solvents were deoxygenated by purging with nitrogen. Toluene, hexanes, diethyl ether and tetrahydrofuran (thf) were dried on columns of activated alumina using a J. C. Meyer (formerly Glass Contour®) solvent purification system. Benzene-d_6 (C_6D_6) was dried by stirring over activated alumina (ca. 10 wt. %) overnight, followed by filtration. Ammonia gas (99.99%) was purchased from Linde Canada and dried by passing through a NaOH bed before use.

4.3.2. Chemicals

Yttrium(III) chloride (99.9%), lanthanum(III) chloride (99.9%), cobalt(II) chloride (97%), iron(II) chloride (98%), toluene, tetrahydrofuran (Alfa Aesar), sodium borohydride (98%), copper(II) chloride (97%), and bis(1,5-cyclo-octadiene)nickel (98%) were used as received. Both 1-butyl-3-methylimidazolium trifluoromethanesulfonate ([BMIM][OTf]) and tetradecyl(trihexyl)-phosphonium bis(triflamide) ([$P_{6.6.6.14}$]NTf_2) ionic liquids were provided by Cytec Canada. n-Hexylamine-borane was prepared using a literature procedure.[24]

4.3.3. Characterization

^1H and ^{11}B solution NMR spectra were recorded on a 300 MHz Bruker Avance instrument at room-temperature (21-23 °C). NMR chemical shifts are reported for ^{11}B relative to $BF_3{\cdot}OEt_2$ (sealed capillary) at 0 ppm and for ^1H from the protic impurities in the C_6D_6. The ^{11}B solid-state MAS NMR spectra were acquired on a Bruker Avance III 400 MHz spectrometer at room temperature and referenced to $NaBH_4$ (δ= -42.1 ppm). The samples were spun at 10 kHz using 4 mm ZrO_2 rotors. The ^1H solid-state NMR spectra were acquired on a Bruker Avance 500 MHz spectrometer at room temperature using adamantane as a reference (δ= 1.63 ppm). The samples were spun at 31.3 kHz using 2.5 mm Zr rotors. The double quantum filtering (DQF) pulse sequence, Back-to-Back (BaBa),[25] was used to recouple the dipolar coupling between protons, from which their relative mobility can be deduced. All samples for solid-state NMR experiments were packed in a nitrogen-filled glove box with oxygen and water levels maintained below 0.1 ppm. FT-IR spectra were obtained as Nujol mulls using a Thermo Nicolet

NEXUS 670 FT-IR instrument and 25x4 mm NaCl plates. PXRD data were collected on a Rigaku Ultima IV diffractometer equipped with a Cu Kα radiation source (λ = 1.541836 Å) and a graphite monochromator. Scanning of the 2θ range was performed from 5 to 50° at 0.5 °/min. Samples were grinded using an agate stone mortar and pestle in a nitrogen-filled glovebox to obtain fine particles. Then the samples were loaded in an air-tight sample holder and mounted on the spectrometer to measure the PXRD patterns at RT. Initial unit cells and structural parameters for both compounds were first obtained by a full-pattern fitting in software FOX.[26] Definitive refinements of the positions and orientations of the $(BH_4)^-$ and NH_3 molecular units were not attempted. Unit cell parameters were refined by a full-pattern fitting and resulting X-ray diffraction patterns were plotted using FullProf.[27] Results are shown in Figures A6.1 and A6.2. Scanning electron microscopy (SEM) images were taken to elicit the size and distribution of the base-metal nanoparticles using a JSM-7500F FESEM (JEOL), and transmission electron (TEM) images were obtained using a JEM-2100F FETEM (JEOL). The thermogravimetric analyzer (Q500 TGA, TA instruments) was coupled with a mass spectrometer (Thermostar, Pfeiffer Vacuum). Air-free samples were prepared using Tzero aluminum lids and pans and heated at 5 °C/min under a flow of N_2. Differential scanning calorimetry measurements were run using a TA Instruments Q2000 with a heating rate of 5 °C/min using Tzero aluminum lids and pans under a flow of N_2.

4.3.4. Synthesis of $Y(BH_4)_3(thf)_2$ and $La(BH_4)_3(thf)_3$

MCl_3 (M= Y, La) and excess sodium borohydride (1:4) were refluxed in dry thf for 3 days under nitrogen. After filtration to remove NaCl, absence of chloride in the filtrate was confirmed by the $AgNO_3$ test. The thf filtrate was then evaporated *in vacuo* and the resulting solid extracted into toluene over 3 days using a Soxhlet. Upon removal of the toluene solvent *in vacuo* and drying at 40 °C for 3 h, the stoichiometry of the resulting yellow $[Y(BH_4)_3(thf)_2]$ and colorless $[La(BH_4)_3(thf)_3]$ powders was determined by integration of the ^1H NMR spectra. The powders were placed in screw cap vials and stored in the glove box fridge at -30 °C before use.

4.3.5. Synthesis of $M(BH_4)_3(NH_3)_4$ [M= Y (1) and La (2)]

In thf solution: Dry ammonia was bubbled through a solution of 118 mg (0.43 mmol) $[Y(BH_4)_3(thf)_2]$ in 30 mL of dry thf in a round bottom Schlenk flask for 1 h resulting in rapid precipitation of a colorless solid. The volume was then reduced to 20 mL to remove ammonia and the mixture filtered, washed with thf and dried *in vacuo* at 40 °C

for 3 h, yielding 62 mg of solid **A.** The filtrate was analyzed by ^{11}B and ^{1}H NMR spectroscopy and the solid was characterized by ^{11}B MAS NMR, powder XRD and FTIR. The La analog was prepared similarly from 100 mg (0.25 mmol) $[La(BH_4)_3(thf)_3]$ to give 61 mg (97% yield) solid **B**.

In liquid ammonia (LNH_3): 426 mg (1.53 mmol) solid $[Y(BH_4)_3(thf)_2]$ were placed in a Schlenk flask equipped with a Teflon-coated stir bar under nitrogen. The flask was cooled to -50 °C using an isopropanol/dry ice cold bath and dry NH_3 gas was condensed into the flask until the solid was dissolved. After 4 h stirring at -50 °C, excess ammonia was evaporated to yield 288 mg (93% yield) of **1** as a colorless solid. The solid was dried further at 43 °C for 2 hours and stored in the fridge of the glovebox at -30 °C. The La analog was prepared similarly from 700 mg (1.73 mmol) $[La(BH_4)_3(thf)_3]$ to give 429 mg (97% yield) **2** and stored in the glove box fridge at -30 °C after drying at 43 °C for 2 hours.

4.3.6. In-situ Direct Synthesis of AMB/M'NPs Composites (M'NPs= Fe, Co, Cu, Ni)

In a screw cap vial equipped with a Teflon stir bar, the desired amount of $M'Cl_2$ or $Ni(COD)_2$ (5 or 25 mol% with respect to the initial amounts of **1** or **2**) were added in ~5 mL of toluene in the glovebox. Then 100 mg of **1** or **2** was added to the vial after grinding in an agate mortar and pestle and stirred for 15 hours at RT in the glove box. Filtration of the suspension resulted in a light gray powder and a clear solution. The solid was dried under reduced pressure at 40 °C for 2 hours and stored in the fridge of the glovebox at -30 °C.

4.3.7. Synthesis of Base-metal Nanoparticles (M'NPs; M'= Fe, Co, Cu) Using Neat n-Hexylamine-borane

In a screw cap vial equipped with a Teflon stir bar, 100 mg $M'Cl_2$ was treated with 5 equiv. of n-hexylamine-borane. The resulting paste was stirred overnight with appearance of a black color indicating formation of the M'NPs. Subsequently, 1 mL of dry toluene was added to the vial and stirred for another 2-3 hours. The resulting solid M'NPs were then separated by centrifugation at 4000 rpm for 30 min., washed with 3 X 1 mL of toluene, dried under reduced pressure, and stored in the glove box at RT.

4.3.8. Synthesis of AMB-M'NP Composites

In a screw cap vial equipped with a Teflon stir bar, the desired amount of M'NPs (5 wt.% with respect to the initial weight of **1** or **2**) were added in ~5 mL of toluene in the glovebox. The vial was then sealed, shipped out of the glovebox and sonicated for 5 minutes to increase particle dispersion. The final suspension was stable for about 15 min and precipitation of fine particles was observed after that period. Then 100 mg of **1** or **2** was added to the vial after shipping in the vial to the glovebox and stirred for 15 hours at RT. Filtration of the suspension resulted in a light gray powder and a clear solution. The solid was dried under reduced pressure at 40 °C for 2 hours and stored in the fridge of the glovebox at -30 °C.

4.3.9. Determination of Hydrogen Extent and Purity from Thermolysis of AMB-M'NP Composites

To measure the extent and purity of the released gas from **1** and **2**, 100 mg of each sample was heated to 200 °C under a slow flow of N_2 in a round-bottom Schlenk flask while the off-gas was bubbled through a standard 0.1 M HCl solution. To achieve the full contact of the bubbles with the standard solution, the discharging stream passed through a ceramic bubble diffuser in a 100 mL Schlenk tube while the standard solution was stirring vigorously. Back-titration of this solution with a standard 0.1 M NaOH solution after the heat treatment indicated the amount of NH_3 released from the sample. Combining these results with those obtained from TGA-MS allowed for an estimate of the extent of the hydrogen stream released from each sample.

4.3.10. Thermolysis of AMB-M'NP composites in ionic liquids (ILs)

The ionic liquids [BMIM][OTf] and $[P_{6.6.6.14}]NTf_2$ were dried under reduced pressure at 60 °C for 24 hours. For the latter, 1 mL hexylamine-borane was added to 100 mL of the IL, stirred overnight and dried under reduced pressure at 60 °C for another 12 hours. Water content of both ILs was confirmed to be < 100 ppm by ^{1}H NMR spectroscopy. In a screw cap vial equipped with a Teflon stir bar, 30 mg of **1** or **2**, 5 wt.% of the M'NPs and 2 g of the dried ionic liquid were stirred for 15 hours. Samples were taken from these stable suspensions for TGA-MS analysis.

4.4. Results and discussion

4.4.1. Solution synthesis of pure Y- and La AMBs

Halide-free MBHs, ($M(BH_4)_3(thf)_n$, M= Y and La) were synthesized in tetrahydrofuran (thf) through salt metathesis reactions of $NaBH_4$ and MCl_3 (4:1,[10d] eqn. 1) followed

by filtration of insoluble NaCl. After thf removal, the solid was extracted continuously into toluene using a Soxhlet to separate the product from unreacted $NaBH_4$. Subsequent removal of the toluene and drying at 40 °C *in vacuo*, yielded pure $Y(BH_4)_3(thf)_2$ and $La(BH_4)_3(thf)_3$ as fine powders. Quantitative ^1H NMR measurements of the resulting solids in C_6D_6 revealed that the number of thf ligands was 2 for the yellow Y powder (**1**) and 3 for the colorless La solid (**2**). ^{11}B solution NMR spectra showed a quintet (J_{BH}= 85 Hz) at -24.5 and -19.7 ppm for the Y and La borohydride products, **1** and **2**, respectively (Figures A1.14 and A1.15).

$$MCl_3 + 3\ NaBH_4 \xrightarrow[\text{reflux}]{\text{thf}} M(BH_4)_3(thf)_n + 3\ NaCl \qquad (1)$$
$$M = Y,\ La$$

Attempted preparation of known $Y(BH_4)_3(NH_3)_4$, **1**,[23,26] from the reaction of NH_3 gas with $Y(BH_4)_3(thf)_2$ in thf solution was hampered by competing ammonia-borane formation (0.25 equiv. per Y) as reported previously.[21] The ^{11}B MAS NMR spectrum of the resulting solid **A** showed a major resonance at -27.9 ppm due to **1** and a minor resonance at -37.9 ppm (assigned to the hepta-ammoniate yttrium borohydride)[18] in a 26:1 ratio while an unidentified soluble Y borohydride product (quintet at -26.6 ppm; J_{BH} = 85 Hz) was observed in the filtrate. In contrast, synthesis of the La analog in thf yielded < 0.1 equiv. of AB (*vs.* La) and a colorless solid **B** which exhibited a single ^{11}B MAS NMR resonance at -22.6 ppm attributed to $La(BH_4)_3(NH_3)_4$, **2** (*vide infra*).

In a second approach to isolate pure AMBs, ammonia was condensed onto the MBH complexes at -50 °C and the mixture stirred for 4 hours. Powder X-ray diffraction (PXRD) data of the resulting AMBs confirmed the absence of NaCl or $NaBH_4$ (Figures A6.1 and A6.2). Additionally, ^{11}B MAS NMR spectra contained a single resonance for the $M(BH_4)_3(NH_3)_4$ products **1** and **2** (Figure A2.13). The N-H bond stretch at 3264-3356 cm^{-1} in the IR spectrum of **2** is typical for coordinated ammonia and the B-H bond stretching and bending vibrations at 2429 cm^{-1} and 1159 cm^{-1} are consistent with $(BH_4)^-$ units coordinated directly to the metal center (Figure A3.12).[18]

The crystal structure of **1** obtained by Jensen et al.[18] and validated by DFT calculations indicated that all of the $(BH_4)^-$ and NH_3 ligands are directly coordinated to the metal center in a distorted trigonal bipentagonal geometry (unit cell indexed here also for the isostructural La analogue; Table 4.1).

Table 4.1. Room temperature structural data obtained from the full-pattern Rietveld refinements.

Compound	$Y(BH_4)_3(NH_3)_4$	$La(BH_4)_3(NH_3)_4$
Space group	$Pna2_1(33)$	$Pna2_1(33)$
a (Å)	12.2084(3)	12.433(3)
b (Å)	7.0870(2)	7.2955(2)
c (Å)	11.374(3)	11.645(3)
V ($Å^3$)	984.12(4)	1056.3(4)
Z	4	4

While the axial and equatorial borohydride ligands give rise to a single broad resonance in the solid-state (^1H) δ 0.37 (Y), 0.92 (La) and ^{11}B NMR spectra, distinct N-H resonances are observed by ^1H MAS NMR spectroscopy (Figure 4.1).

The minor sharp resonance at -0.07 ppm was shown to be due to mobile protons of an ammonia impurity in the double quantum-filtered NMR experiment (Figure 4.1a,c).[10a,28] For M = Y the distinct broad N-H resonance at δ 4.36 is assigned to the axial ammonia ligand that also is involved in unique N-H···H-B interactions (Figure 4.1b; Tables A6.1 and A6.2). Deconvolution of the overlapping peaks confirmed the similarity of the axial and equatorial borohydride chemical shifts and the contribution of the unique equatorial ammonia ligand to the single broad resonance at δ 2.35 (Figure A2.14).

In an additional ^1H 2D DQ MAS NMR experiment the correlation peak for protons that are interacting with each other will be observed with a chemical shift in the DQ dimension equal to the sum of their chemical shifts in the single quantum (SQ) dimension. As can be seen in Figure 4.2, the strong correlation peak for the new La AMB **2** with a chemical shift of ~2 ppm in the DQ dimension suggests that it results from the interaction of two nearby H atoms with chemical shift of ~1 ppm in the SQ dimension.

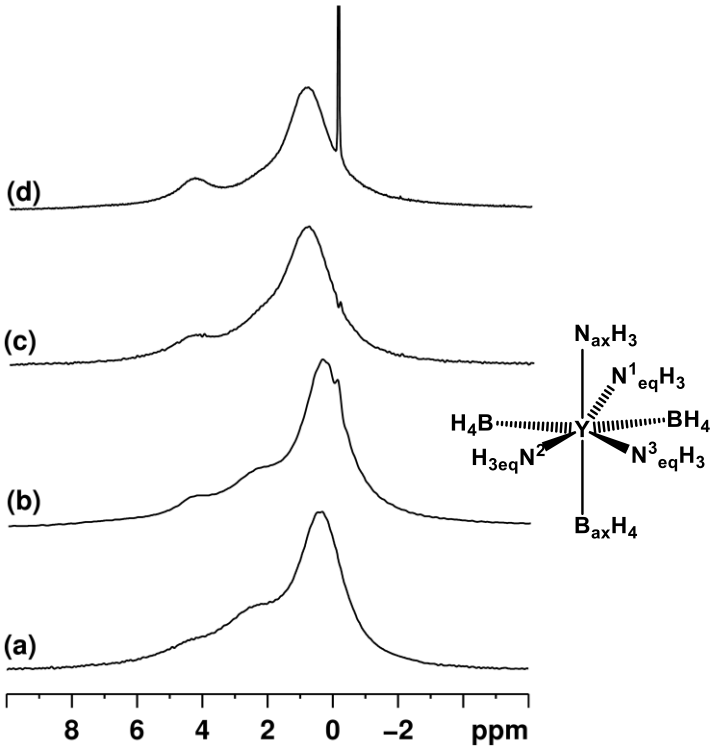

Figure. 4.1. ^{1}H MAS NMR spectra (500 MHz, υ_R = 31.25 KHz) of pristine $Y(BH_4)_3(NH_3)_4$ (**1**; a and b) and $La(BH_4)_3(NH_3)_4$ (**2**; c and d). The (b) and (d) spectra are standard ^{1}H MAS NMR and (a) and (c) spectra are the corresponding ^{1}H DQF MAS NMR spectra.

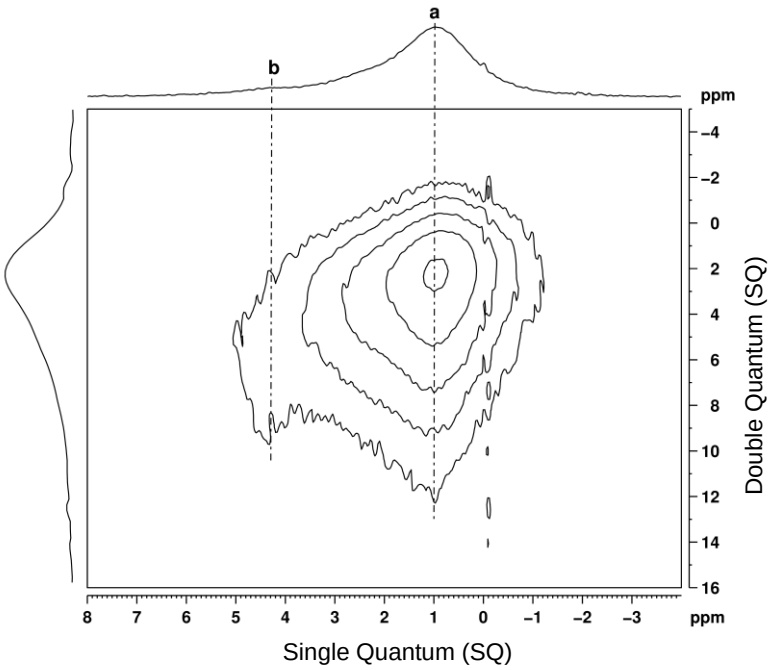

Figure 4.2. ^{1}H 2D DQ MAS NMR of $La(BH_4)_3(NH_3)_4$ (500 MHz, υ_R = 31.25 kHz).

Hence, strong proton dipolar coupling interactions exist among the $(BH_4)^-$ ligands. Along the dashed line (a) in Figure 4.2, the strong correlation peak presents a long tail toward the high chemical shift. This is the combination of many correlation peaks

which are attributed to the interactions of $(BH_4)^-$ hydrides and coordinated NH_3 protons, as indicated by the chemical shift in the DQ dimension. Consistently, the interaction between $(BH_4)^-$ hydrides and coordinated NH_3 protons has also been observed along the dashed line (b). Although the correlation peak between coordinated NH_3 protons is not resolved very well due to the relatively low intensity, the 2D ^1H DQ MAS NMR spectrum clearly shows that all five types of rigid protons are well mixed. Based on this observation we can conclude that all borohydride and ammonia ligands remain bonded to the metal center in agreement with the structure reported by Jensen and co-workers for $Y(BH_4)_3(NH_3)_4$.[18]

4.4.2. Thermolysis of Y and La AMBs

Thermolysis of pure AMBs, **1** and **2,** was monitored by thermogravimetric (TG) analysis with mass spectroscopic analysis of the evolved gases (Figure 4.3 and Table 4.2). No traces of diborane or other volatile borane species were observed from thermolysis of pristine or catalyzed AMBs. Concurrent release of H_2 and NH_3 proceeds through several steps during heating from 25 to 200 °C.[15] Closer inspection of the TG profile for **1** reveals at least a triple step process (Figure A5.1): I) *50-95 °C* (with onset release for NH_3 at 70 °C) in which 2.1 wt.% hydrogen with a small amount of ammonia is released. This step is illustrated as a very broad exothermic peak centered at 86.4 °C in the DSC profile of **1** (Figure 4.4). II) *95-140 °C.* In this step the major content of the 3.6% weight loss is H_2 which is accompanied by a minor amount of NH_3. The exothermic nature of dehydrogenation, which is the case in many AMBs, prevents the process from being reversible.[29] III) *140-200 °C* (with 5.4% weight loss) in which the MS analysis of the evolved gas shows a major peak for H_2 at 160 °C; however, NH_3 release also reached its peak at 155 °C with a smaller shoulder at 175 °C. Thermal features in this range are two exothermic peaks at 158.9 and 194.5 °C and one endothermic event at 179.8 °C shown in the DSC profile of **1** (Figure 4.4).

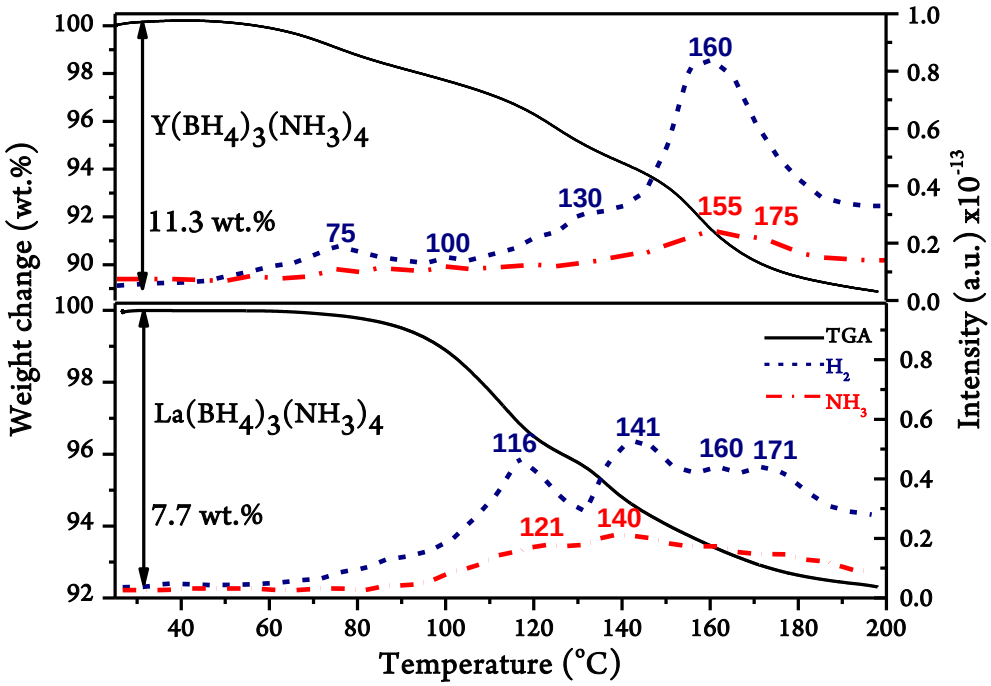

Figure 4.3. TGA-MS results for dehydrogenation of $Y(BH_4)_3(NH_3)_4$ (**1**) and $La(BH_4)_3(NH_3)_4$ (**2**) in the temperature range of RT to 200 °C (ramp = 5 °C/min) under N_2.

Table 4.2. Dehydrogenation results of as synthesized $Y(BH_4)_3(NH_3)_4$ and $La(BH_4)_3(NH_3)_4$.[a]

Parameter	$Y(BH_4)_3(NH_3)_4$	$La(BH_4)_3(NH_3)_4$
Total weight loss (%)	11.1	7.7
H_2 onset (°C)	45	55
H_2 peak (°C)	160	141
H_2 (wt.%)	7.7	5.1
NH_3 onset (°C)	70	85
NH_3 peak (°C)	165	140
NH_3 (wt.%)	3.4	2.6

[a] TGA-MS data has been collected from heating the samples under N_2 from RT to 200 °C with ramp of 5 °C/min.

The large exothermic feature (194.5 °C) can be attributed to the sudden increase in H_2 release as the DSC measurements were conducted in closed vessels vs. the TGA experiments carried out under a dynamic flow of N_2.[16] We are also unsure whether the endothermic feature at 179.8 °C is a melting event or a decomposition step.[10d,30]

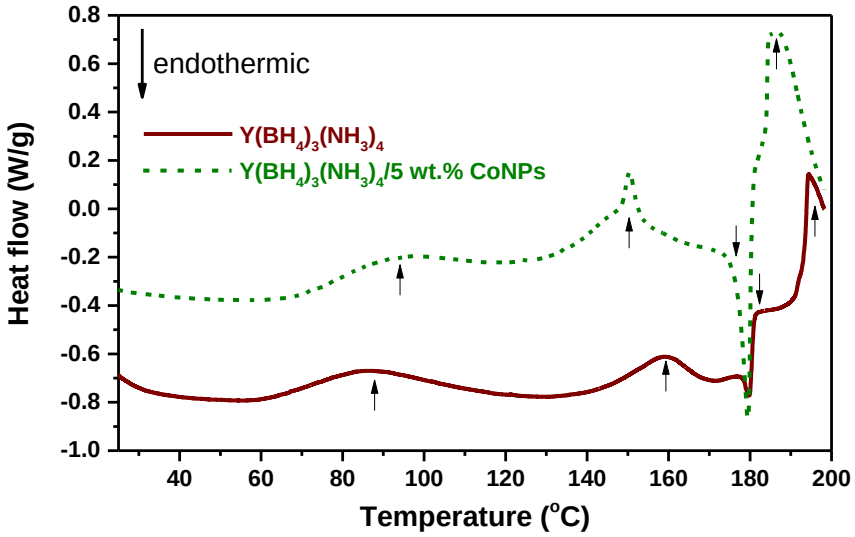

Figure 4.4. DSC results of $Y(BH_4)_3(NH_3)_4$, **1,** and Y-AMB/Co composite on heating from RT to 200 °C under N_2 (ramp = 5 °C/min).

A total of 11.7 % weight loss is observed for **1** which is ~8% lower than the sample prepared by ball milling of $YCl_3{\cdot}4NH_3{\cdot}3LiBH_4$ (over the same temperature range and ignoring the LiCl dead mass).[16] The amount of H_2 released from **1** was measured to be 7.7 wt.% (95.1 mol% pure). Improvements in kinetic properties (e.g. elevating the NH_3 peak temperature from previously reported 86 °C to 155 °C for the Y AMB in this work) along with purer released hydrogen (90.5 mol% for **1** synthesized through ball-milling)[16] clearly emphasize the negative influence of metal halide impurities on dehydrogenation of **1**.

Thermal dehydrogenation of **2** resulted in 7.7 % total weight loss which was achieved in four steps (Figures 4.3 and A5.2): I) *50-85 °C* with 0.4 % weight loss which is pure hydrogen with no ammonia contamination. One broad exothermic peak can be detected with a peak at 72.8 °C in the DSC profile of **2** (Figure 4.5) indicates the exothermic nature of pure hydrogen release which was also observed for $Ti(BH_4)_3{\cdot}3NH_3$[31] and $NaZn(BH_4)_3{\cdot}2NH_3$[32]. II) *85-128 °C* (onset release for NH_3 at 85 °C) in which 3.7% weight loss with simultaneous release of H_2 and NH_3 is observed. One small exothermic feature was observed at 91 °C in this temperature range. III) *128-151 °C*. The 2.0 % weight loss over this range consists of both H_2 and NH_3 while an intense exothermic peak was observed at 135.7 °C. IV) 151-200 °C in which 1.6% weight loss and diminishing NH_3 release were observed. Thermal events in this range consist of two exothermic peaks at 154.2 and 161.1 °C and a minor endothermic peak at 157.4 °C (Figure 4.5). Indeed, the dehydrogenation process of **2** seems to be more complicated than **1** and occurs through several intermediates that could release 5.1 wt.% hydrogen and 2.6

wt.% ammonia (Table 4.2) consistent with the determined hydrogen purity of 94.3 mol% (*vide supra*).

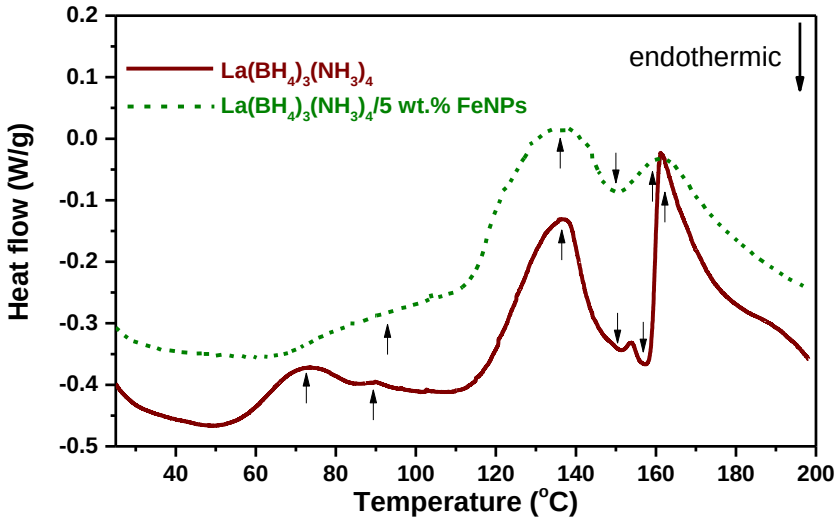

Figure 4.5. DSC results of $La(BH_4)_3(NH_3)_4$, **2,** and La-AMB/Fe composite on heating from RT to 200 °C under N_2 (ramp = 5 °C/min).

To shed more light on the dehydrogenation mechanisms of **1** and **2**, ^{11}B MAS NMR spectra of the pristine and heated AMBs were obtained. The spectrum of **1** heated to 200 °C includes a broad resonance at -23.8 ppm which is typical of sp^3 coordination (*cf.* ^{11}B NMR resonance for NH_3-BH_3 is at -23 ppm) and a two-peaked resonance at 21.7 assigned to trigonal sp^2 B coordination (Figure 4.6). In a similar trend the ^{11}B MAS NMR spectrum of heated **2** includes sp^3 boron at -17.7 ppm and a small shoulder at -30.3 ppm (more typical of borohydride) along with a two-peaked resonance at 16.1 ppm for sp^2 B (Figure 4.7). The extensive dihydrogen bonding networks that are the norm in typically insoluble AMBs likely give rise to facile intermolecular H_2 loss pathways (vs. intramolecular formation of M-NH_2BH_3). Although models for this process are rare, Harder demonstrated[33] that ammonia-borane dehydrogenation in a dicalcium model complex afforded a stable $[NH\text{-}BH\text{-}NH\text{-}BH_3]^{2-}$ fragment that would be consistent with our NMR results and studies by Guo et al. that indicated initial loss of two N-H bonds per ammonia.[23]

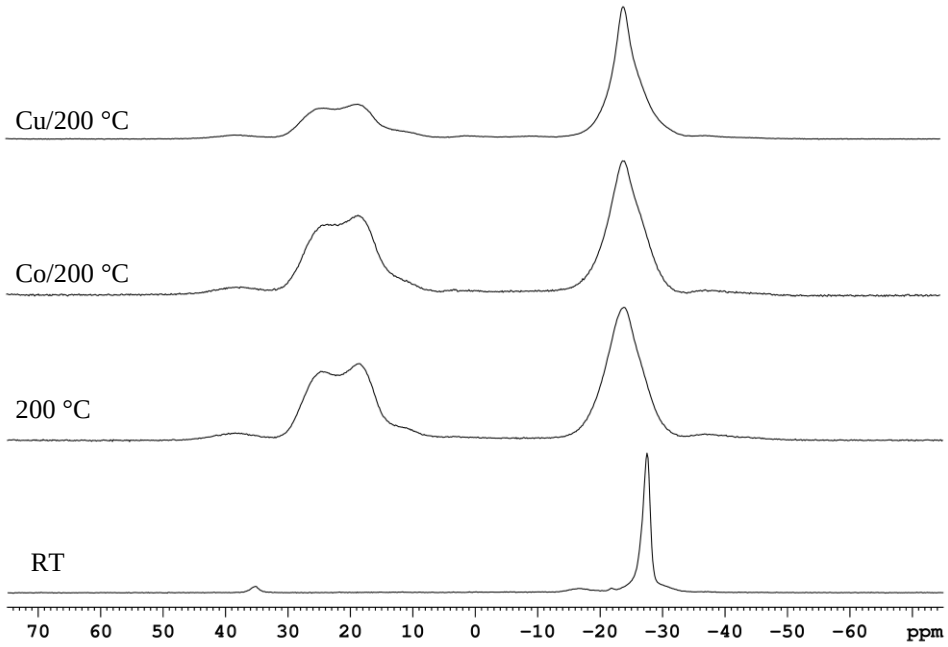

Figure 4.6. ^{11}B MAS NMR spectra (128 MHz, υ_R = 10 KHz) of dehydrogenation of $Y(BH_4)_3(NH_3)_4$ (pristine and catalyzed).

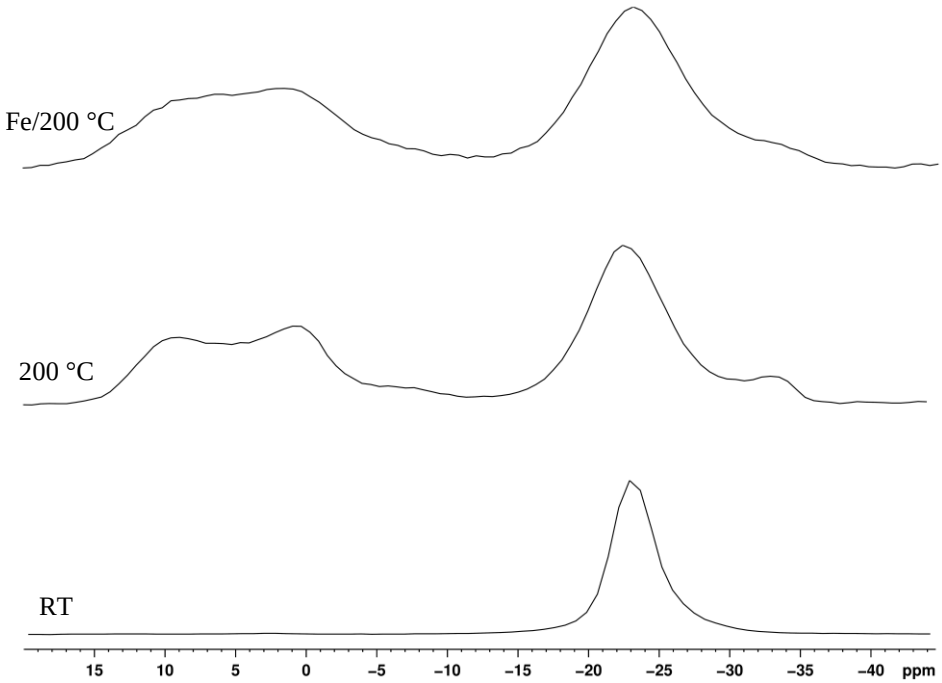

Figure 4.7. ^{11}B MAS NMR spectra (128 MHz, υ_R = 10 KHz) of dehydrogenation of $La(BH_4)_3(NH_3)_4$ (pristine and catalyzed).

In the infrared spectra of **1** and **2** the B-H (2334-2382 cm^{-1}) and N-H (3163-3336 cm^{-1}) stretching vibrations are reduced significantly upon heating (Figures A3.11 and A3.12). The appearance of B-N vibrations at 845 cm^{-1} is a clear indication of characteristic AMB dehydrogenation pathways that are responsible for releasing hydrogen at lower temperatures.

4.4.3. Thermolysis of AMB-M'NP Mixtures

Complementing reports of improved kinetic and thermodynamic hydrogen storage properties of MBHs through additives or catalysts,[8] significant results have also been obtained for AMBs.[34] Double-cation AMBs such as $Li_2Al(BH_4)_5{\cdot}6NH_3$[35] are capable of releasing >10 wt.% H_2 below 120 °C and AB modified Zn-AMB, $NaZn(BH_4)_3{\cdot}4NH_3BH_3$,[36] released 11.6 wt.% of H_2 on heating to 250 °C with a peak at 85 °C. In a recent report the Lewis acidic metal additive $ZnCl_2$ enhanced the hydrogen purity from ball-milled $CrCl_3{\cdot}3NH_3/3LiBH_4$ (7.4 wt.% H_2 with a purity of 98.9 mol%).[37] More relevant to the present work, Chen et al. showed that ball-milling 2.6 mol% $CoCl_2$ with $Li(NH_3)BH_4$ and $Li(NH_3)_2BH_4$ led to enhanced hydrogen release and purity, albeit in a closed system.[17]

In this study inexpensive, earth-abundant metal nanoparticles (M'NPs) including Co, Cu, Fe and Ni are investigated as catalysts in an attempt to favor release of hydrogen over ammonia. First, base-metal dichlorides were added directly to a toluene suspension of AMBs. Appearance of a black suspension after about 18 hours stirring at RT was a visual indicator of the formation of M'NPs. Filtration of this suspension yielded a dark gray powder and a colorless filtrate confirming full loading of the M'NPs onto the AMB particles without formation of soluble B-containing by-products (from ^{11}B NMR).[38] Note, however, that this method for M'NP incorporation necessarily decomposes some of the AMB and introduces chloride impurities. For the Y-AMB complex, for example, the reducing metal borohydride ligands likely form Y-coordinated $(BClH_3)^-$ and/or $(BCl_2H_2)^-$ anions in addition to hydrogen and the reduced base transition metal. In contrast, the Ni NPs were produced by thermal decomposition of the $Ni(COD)_2$ precursor at room temperature without noticeable AMB decomposition.

Thermolysis of the Y-AMB/M'NP mixtures shows significant effects on the H_2 release properties. While lower weight loss was observed in all cases with 5 mol% of the studied base-metal catalysts, the onset temperatures for H_2 release increased by 15-20 °C (Table 4.3).

Table 4.3. Effects of catalyst on dehydrogenation of as synthesized $Y(BH_4)_3(NH_3)_4$.[a]

	$Y(BH_4)_3(NH_3)_4$/5 mol% Catalyst			$Y(BH_4)_3(NH_3)_4$/25 mol% Catalyst		
	Weight loss (%)	H_2 (On-set/Peak) °C	NH_3 (On-set/Peak) °C	Weight loss (%)	H_2 (On-set/Peak) °C	NH_3 (On-set/Peak) °C
none	11.1	45/160	75/165	11.1	45/160	75/165
$CoCl_2$	9.0	60/170	85/155	8.9	50/150	60/150
$CuCl_2$	9.4	60/155	140/155	9.1	60/125	90/119
$FeCl_2$	9.3	65/170	90/150	9.3	60/155	60/150
$Ni(COD)_2$	10.5	65/170	75/165	10.4	60/170	75/165

[a] All results were obtained by TGA-MS analysis from samples heated from RT to 200 °C under nitrogen (ramp= 5 °C/min).

Table 4.4. Effect of different amounts of catalyst on dehydrogenation of as synthesized $La(BH_4)_3(NH_3)_4$.[a]

	$La(BH_4)_3(NH_3)_4$/5 mol% Catalyst			$La(BH_4)_3(NH_3)_4$/25 mol% Catalyst		
	Weight loss (%)	H_2 (Onset/Peak) °C	NH_3 (Onset/Peak) °C	Weight loss (%)	H_2 (Onset/Peak) °C	NH_3 (Onset/Peak) °C
none	7.7	55/140	85/140	7.7	55/140	85/140
$CoCl_2$	12.2	60/170	70/130	10.7	55/170	70/130
$CuCl_2$	12.3	60/170	70/125	10.7	65/115	85/135
$FeCl_2$	12.0	50/165	75/125	11.9	50/115	70/125
$Ni(COD)_2$	13.0	55/175	80/130	13.0	60/180	80/140

[a] All the results were obtain by TGA-MS analysis from samples heated from RT to 200 °C under nitrogen (ramp= 5 °C/min).

H_2 release peak temperatures also increased slightly except for Cu. Interestingly, ammonia onset release also undergoes a modest temperature increase except for Cu which jumps from 75 to 140 °C (Figure A5.3). TGA-MS results for the Y-Cu mixture indicate that nearly 5 wt.% pure hydrogen is released up to 140 °C (Figure A5.4). Using higher amounts of catalyst decreased the peak temperature for H_2 release while the onset remains almost the same (except for Ni, Table 4.3). Again Cu shows a remarkable activity as peak temperatures for H_2 and NH_3 release are decreased to 125 °C and 119 °C respectively (Figure A5.8).

Using the base-metal catalysts with La-AMB also altered the gas release kinetics and selectivity (Table 4.4). In contrast to the Y-AMB, catalyzed H_2 release from La-AMB showed higher weight loss *vs.* the pristine La-AMB. Higher catalyst concentrations (25 mol%) again gave decreased weight loss confirming the efficiency of these catalysts to

lower ammonia contamination in the evolved H_2 streams from AMBs.[37] Using 5 mol% catalyst, onset for H_2 remained constant while the peak release temperature increased in all cases. When applying 25 mol% catalyst loadings H_2 onset release did not change markedly; however, the release peak temperature was dramatically decreased from 140 °C for pure **2** to 115 °C with Cu and Fe. Lower NH_3 onset and peak temperatures were observed when $CuCl_2$ and $FeCl_2$ were used as catalysts. Although the temperature range in which hydrogen is the only released gas is smaller for La-AMB when catalysts are used, more favorable kinetics are observed for gas release. While the advantage of in situ reduction technique for preparation of nanoparticles was the ease of MNP generation, these *in situ*-produced MNPs were not characterized in detail as we moved on to prepare the MNPs separately (using n-hexylamine-borane) so as to maintain the pure AMB structure.

4.4.4. Synthesis of M'NP-BN Composites

In order to obtain purer AMB/M'NP composites, we sought to prepare the M'NPs independently. Although a number of techniques have been reported for the synthesis of base-metal nanoparticles,[39] the reactivity of our AMBs precluded those using polar solvents or strongly donating reducing agents. While previous work using ammonia-borane and metal halides was attractive,[40] this technique affords insoluble by-products and we already showed that the presence of chloride can adversely affect the AMB hydrogen release properties. As a result, we turned to liquid n-hexylamine-borane (HxAB)[24] which imparts additional solubility to B-Cl containing by-products in non-polar solvents.

Metal dichlorides were added directly to neat HxAB and a rapid color change confirmed formation of M'NPs (tan to black for $FeCl_2$, brown to reddish brown for $CuCl_2$ and blue to dark green for $CoCl_2$). The ^{11}B NMR spectrum of the toluene filtrate showed resonances indicative of $nHxNH_2{\cdot}BH_2Cl$ as well as dehydrogenated B(sp2)-containing products (Figures A1.17-19). TEM images showed the resulting 2 nm Fe and Co nanoparticles supported on insoluble $[BNH_x]_n$ particles (Figure 4.8).[41] In contrast, Cu afforded larger elliptical particles ~50 nm in diameter.

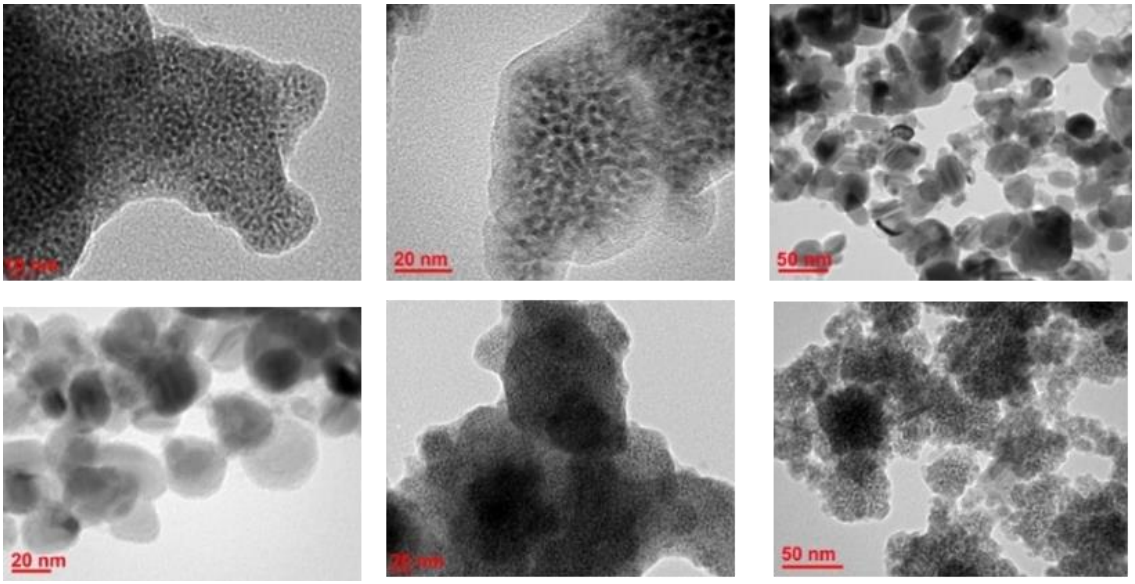

Figure 4.8. TEM images of Co (left), Fe (middle) and Cu (right) NPs prepared by neat HxAB.

4.4.5. Preparation of AMB-M'NP-BN Composites

AMBs are not soluble in non-protic polar solvents, due to their extensive intra- and intermolecular hydrogen bonding networks between N-H and B-H bonds, and they react with protic solvents such as water or alcohols to produce hydrogen gas. Moreover, Y-AMB decomposes in boiling thf to H_2, AB, an unknown Y-BH_4 complex (-40 ppm, q, J_{BH}= 81 Hz), and a colorless precipitate (Figure A1.16). In contrast, heat treatment of **1** in toluene gave only a minor amount of AB so we chose this solvent for immobilizing the synthesized M'NPs on the AMBs. To maximize dispersion, the M'NPs were sonicated for 5 minutes and then stirred with the AMBs overnight at RT. Filtration of this suspension yielded a gray powder (Figure A7.1) and a colorless solution indicating all the M'NPs were loaded on the AMB particles. ^{11}B NMR analysis of the solution filtrate for each catalysts showed only a trace of AB.

4.4.6. Thermolysis of AMB-M'NP-BN Composites

Thermolysis of the new composites now showed the best performance for the Y/Co and La/Fe combinations (Figures A5.19-22). Heating the Y/Co composite (5 wt.% Co) gave 8.9 % weight loss which is 2.2 % lower than pure Y AMB **1** in keeping with the extra mass of Co**.** Released ammonia was decreased by 3-fold (Figure 4.9 and Table 4.5) and the MS results confirmed desorption of ~1.5 wt.% pure hydrogen from 55-100 °C (Figure 4.9). A total of 7.6 wt.% hydrogen (97.9 mol% pure) was released from RT to 200 °C. Comparison of the DSC profile of this composite with that of **1** (Figure 4.4) revealed that the exothermic peak at 86.4 °C shifted to 91.5 °C which can be assigned

to the increased NH_3 release onset temperature in the Y/Co composite. Other exothermic peaks at 158.9 and 194.5 °C are shifted to 150.7 and 186.1 °C, respectively, whereas the endothermic peak at 179.8 °C remained the same (179.4 °C; Figure 4.4). Insensitivity of this peak to the presence of the catalyst suggests a melting event which could allow for more efficient contact of **1** with Co NPs causing the large shifts in the high-temperature exothermic peaks.

Thermolysis of the Y/Cu composite gave 7.7 % total weight loss including 5.6 wt.% H_2. Compared to pure **1**, ammonia release is decreased by only 1.5 times. Lower efficiency of the Y/Cu composite may be due to the larger Cu nanoparticles that reduce productive interactions with the Y AMB solid.

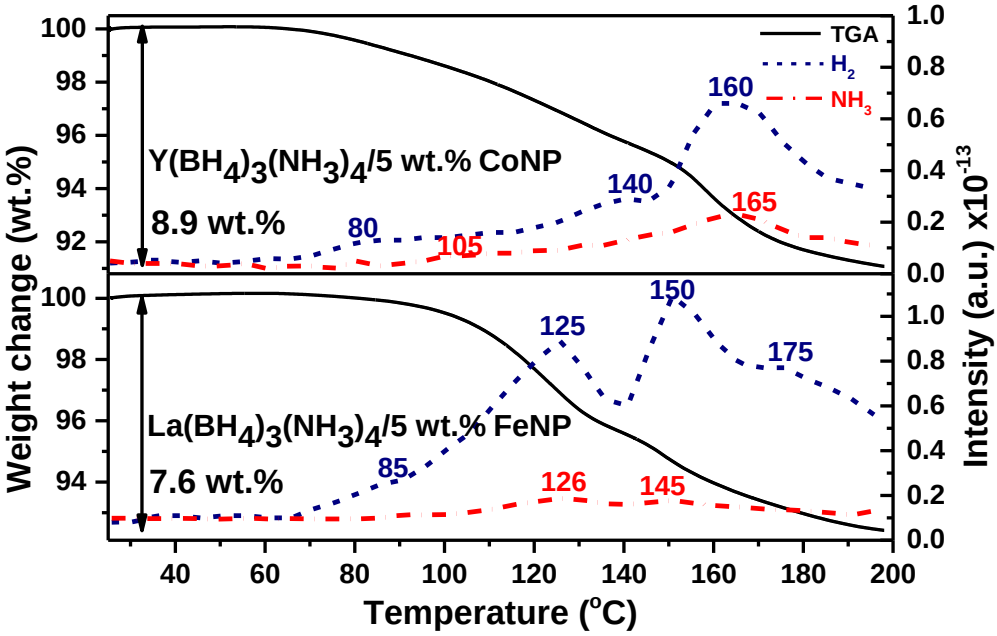

Figure 4.9. TGA-MS results for dehydrogenation of Y/Co and La/Fe AMB-M'NP-BN composites from RT to 200 °C (ramp = 5 °C/min) under N_2.

^{11}B MAS NMR and IR spectroscopic analysis of the composites heated to 200 °C suggests that similar products are formed in the catalyzed and uncatalyzed reactions (Figures. 4.6, 4.7, A3.11, A3.12). The heated Y/Co composite shows a new feature in the FTIR spectrum at 1164 cm^{-1} which does not exist in heated pure **1,** indicating the alteration of B-H bonds under the effect of catalysts. This is further confirmed the purer H_2 streams from catalyzed **1** and **2** indicated in the TGA-MS results.

The TGA-MS results for the La/Fe composite show that hydrogen and ammonia are released almost simultaneously throughout heating to 200 °C (Figure 4.9). A total of 7.6 % weight loss was observed while the composition of the evolved gas was 6.9 wt.% H_2

and only 0.7 wt.% NH_3 (Table 4.5). Decreasing the released ammonia by nearly 4-fold generated the purest H_2 stream in this study (98.9 mol%). Fe NPs resulted in a smoother dehydrogenation for **2** as can be seen in its DSC profile (Figure 4.5). The exothermic peak between 57.8-84.3 °C changed to a broader peak spanning the range of 63.9-114.2 °C. The other exothermic peaks at 135.7 and 161.1 °C did not change noticeably (134.7 and 161.7 °C), and no melting event could be detected.

4.4.7. Thermolysis of AMB-M'NP Composites in Ionic Liquids

Previous reports demonstrated that thermolysis of ammonia-borane in ionic liquids (ILs) affords more than twice as much hydrogen than heating in the solid state or in ether solvents in which it is soluble.[42] Moreover, we showed previously that >7 wt.% hydrogen could be released from metal-catalyzed AB dehydrogenation in the [EMIM][$EtSO_4$] IL at 80 °C (EMIM = 1-ethyl-3-methylimidazolium).[43] Even if our AMBs are not soluble in ILs, the IL-supported M'NPs should increase the chances for each AMB particle to undergo catalyzed (vs. uncatalyzed) thermolysis. Starting with the most commonly employed imidazolium ILs, we found that 1-butyl-3-methylimidazolium trifluoromethanesulfonate, [BMIM][OTf] will not support the Fe nanoparticle synthesis using nHxAB. However, previously synthesized FeNPs formed a stable suspension in this IL. Addition of this suspension to the La-AMB gave a black paste after stirring overnight. Subsequent thermolysis of this sample showed only 0.8% weight loss upon heating from RT to 200 °C with the IL and IL+FeNP suspension showing 0.3% and 0.2% weight loss over the same range. Along with concurrent release of small amounts of H_2 and NH_3, several other unidentified volatile products were released between 50 and 150 °C.

We turned next to the more thermally stable phosphonium-based IL,

Table 4.5. Dehydrogenation results of catalyzed and un-catalyzed Y-BA (1) and La-BA (2).

	Y-AMB	Y-AMB/Co NP	Y-AMB/Cu NP	La-AMB	La-AMB/Fe NP
Weight loss (%)	11.1	8.9	7.7	7.7	7.6
H_2 onset (°C)	45	55	85	55	65
H_2 peak (°C)	160	160	185	141	150
H_2 wt.%	7.7	7.6	5.6	5.1	6.9
NH_3 onset (°C)	70	100	115	85	85
NH_3 peak (°C)	165	165	180	140	145
NH_3 (wt.%)	3.4	1.3	2.1	2.6	0.7

[a] All the results were obtain by TGA-MS analysis from samples heated from RT to 200 °C under nitrogen (ramp= 5 °C/min).

tetradecyl(trihexyl)phosphonium bistriflamide, $[P_{6.6.6.14}]NTf_2$, with less sterically accessible activated C-H bonds. Heat treatment of the dried IL resulted in only 0.1% weight loss and no gases could be detected. Mixing $FeCl_2$ and excess HxAB in $[P_{6.6.6.14}]NTf_2$ gave rise to a black suspension of FeNPs. No precipitation was observed even after several days sitting at room temperature in the glove box, proving the positive stabilizing effect of this IL on the M'NPs. Upon addition of **2** to the suspension of FeNPs in $[P_{6.6.6.14}]NTf_2$, 11.2% weight loss was observed in total during heating from RT to 200 °C (Figure 4.10). While no ammonia could be detected (based on MS results), hydrogen evolution was evident from 60–200 °C with the peak at 121 °C. The large observed weight loss, however, corresponded to formation of significant amounts of several unidentified volatile products starting from 72°C. Indeed, thermolysis of the Fe NPs in the IL alone gave 6.8 % weight loss to 200°C (Figure A5.24), indicates the unexpectedly high reactivity of FeNPs for degradation of $[P_{6.6.6.14}]NTf_2$.

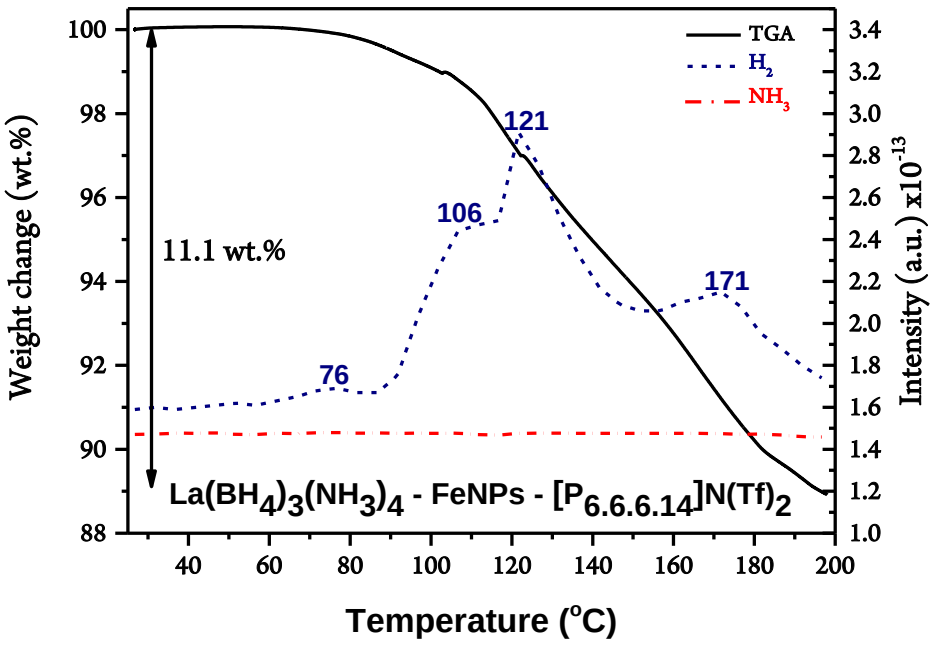

Figure 4.10. TGA-MS results for dehydrogenation of La/Fe composite in $[P_{6.6.6.14}]NTf_2$ from RT to 200°C (ramp = 5 °C/min) under N_2.

4.5. Conclusions

Pure tetra-ammoniates of yttrium- and lanthanum borohydride were synthesized through condensation of liquid ammonia (-50 °C) on halide-free yttrium and lanthanum borohydride thf adducts. Absence of metal halide impurities and/or excess $Li/NaBH_4$ gave improved dehydrogenation behavior of these AMBs vs. mixtures obtained by ball-milling. Moreover, composites of these AMBs with Fe and Co nanoparticles, prepared

using neat liquid hexylamine-borane, released a significantly purer hydrogen stream due to suppression of ammonia evolution. As both materials are solids, however, it is difficult to ensure that every AMB dehydrogenation event benefits from physical access to the added nanoparticle catalyst. While the ionic liquids tested herein did not effectively address this limitation, recent progress in diaminoboronium ionic liquids[44] may offer more compatible reaction media and further investigations are currently underway along these lines.

4.6. References

(1) Cipriani, G.; Di Dio, V.; Genduso, F.; La Cascia, D.; Liga, R.; Miceli, R.; Ricco Galluzzo, G. *Int. J. Hydrogen. Energy* **2014**, *39*, 8482-8494.
(2) Graetz, J. *Chem. Soc. Rev.* **2009**, *38*, 73-82.
(3) Mulder, G.; Hetland, J.; Lenaers, G. *Int. J. Hydrogen. Energy* **2007**, *32*, 1324-1331.
(4) a) Moussa, G.; Moury, R.; Demirci, U. B.; Şener, T.; Miele, P. *Int. J. Energy Res.* **2013**, *37*, 825-842; b) Durbin, D. J.; Malardier-Jugroot, C. *Int. J. Hydrogen. Energy* **2013**, *38*, 14595-14617.
(5) Orimo, S.-i.; Nakamori, Y.; Eliseo, J. R.; Züttel, A.; Jensen, C. M. *Chem. Rev.* **2007**, *107*, 4111-4132.
(6) Züttel, A.; Rentsch, S.; Fischer, P.; Wenger, P.; Sudan, P.; Mauron, P.; Emmenegger, C. *J. Alloys Compd.* **2003**, *356–357*, 515-520.
(7) Zhang, B. J.; Liu, B. H.; Li, Z. P. *J. Alloys Compd.* **2011**, *509*, 751-757.
(8) Li, H.-W.; Yan, Y.; Orimo, S.-i.; Züttel, A.; Jensen, C. M. *Energies* **2011**, *4*, 185-214.
(9) Soloveichik, G. L. *Mater. Matters* **2007**, *2.2*, 11-16.
(10) a) Segal, B. G.; Lippard, S. J. *Inorg. Chem.* **1978**, *17*, 844-850; b) Bernstein, E. R.; Chen, K. M. *Chem. Phys.* **1975**, *10*, 215-228; c) Yan, Y.; Li, H.-W.; Sato, T.; Umeda, N.; Miwa, K.; Towata, S.-i.; Orimo, S.-i. *Int. J. Hydrogen. Energy* **2009**, *34*, 5732-5736; d) Ravnsbæk, D. B.; Filinchuk, Y.; Černý, R.; Ley, M. B.; Haase, D. r.; Jakobsen, H. J.; Skibsted, J. r.; Jensen, T. R. *Inorg. Chem.* **2010**, *49*, 3801-3809; e) Frommen, C.; Aliouane, N.; Deledda, S.; Fonneløp, J. E.; Grove, H.; Lieutenant, K.; Llamas-Jansa, I.; Sartori, S.; Sørby, M. H.; Hauback, B. C. *J. Alloys Compd.* **2010**, *496*, 710-716.
(11) Qiang Sun, W.; Fan, M.-Q.; Fei, Y.; Pan, H.; Wang, L. L.; Yao, J. *Sci. World J.* **2012**, *2012*, 6.
(12) a) Gafurov, B. A.; Mirsaidov, I. U.; Nasrulloeva, D. Kh.; Badalov, A. *Russ. J. Phys. Chem. A* **2013**, 87, 1601−1606.; b) Robert, D.; Kondracka, M.; Okuda, J. *Dalton Trans.* **2008**, 2667-2669; c) Ley, M. B.; Jørgensen, M.; Černý, R.; Filinchuk, Y.; Jensen, T. R. *Inorg. Chem.* **2016**, *55*, 9748-9756.
(13) Ley, M. B.; Boulineau, S.; Janot, R.; Filinchuk, Y.; Jensen, T. R. *J. Phys. Chem. C* **2012**, *116*, 21267-21276.
(14) Jepsen, L. H.; Ley, M. B.; Lee, Y.-S.; Cho, Y. W.; Dornheim, M.; Jensen, J. O.; Filinchuk, Y.; Jørgensen, J. E.; Besenbacher, F.; Jensen, T. R. *Mater. Today* **2014**, *17*, 129-135.
(15) Song, Y.; Wu, F.; Zheng, X.; Ma, X.; Fang, F.; Guo, Y. *Chem. Commun.* **2015**, *51*, 1104-1107.

(16) Yuan, F.; Gu, Q.; Guo, Y.; Sun, W.; Chen, X.; Yu, X. *J. Mater. Chem.* **2012**, *22*, 1061-1068.
(17) a) Zheng, X.; Wu, G.; Li, W.; Xiong, Z.; He, T.; Guo, J.; Chen, H.; Chen, P. *Energy Environ. Sci.* **2011**, *4*, 3593-3600; b) Zheng, X.; Chua, Y.; Xiong, Z.; Chen, W.; Jiang, Z.; Wu, G.; Chen, P. *Int. J. Hydrogen. Energy* **2015**, *40*, 4573-4578.
(18) Jepsen, L. H.; Ley, M. B.; Černý, R.; Lee, Y.-S.; Cho, Y. W.; Ravnsbæk, D.; Besenbacher, F.; Skibsted, J.; Jensen, T. R. *Inorg. Chem.* **2015**, *54*, 7402-7414.
(19) Jaroń, T.; Orłowski, P. A.; Wegner, W.; Fijałkowski, K. J.; Leszczyński, P. J.; Grochala, W. *Angew. Chem. Int. Ed.* **2015**, *54*, 1236-1239.
(20) Jaron, T.; Wegner, W.; Grochala, W. *Dalton Trans.* **2013**, *42*, 6886-6893.
(21) Mostajeran, M.; Wolstenholme, D. J.; Frazee, C.; McGrady, G. S.; Baker, R. T. *Chem. Commun.* **2016**, *52*, 2581-2584.
(22) Lobkovskii, É. B.; Kravchenko, S. E.; Kravchenko, O. V. *J. Struct. Chem.* **1983**, *23*, 582-586.
(23) a) Guo, Y.; Yu, X.; Sun, W.; Sun, D.; Yang, W. *Angew. Chem. Int. Ed.* **2011**, *50*, 1087-1091; b) Tang, Z.; Tan, Y.; Chen, X.; Ouyang, L.; Zhu, M.; Sun, D.; Yu, X. *Angew. Chem.* **2013**, *125*, 12891-12895; c) Soloveichik, G.; Her, J.-H.; Stephens, P. W.; Gao, Y.; Rijssenbeek, J.; Andrus, M.; Zhao, J. C. *Inorg. Chem.* **2008**, *47*, 4290-4298.
(24) Framery, E.; Vaultier, M. *Heteroat. Chem.* **2000**, *11*, 218-225.
(25) a) Schnell, I.; Spiess, H. W. *J. Magn. Reson.* **2001**, *151*, 153-227; b) Brown, S. P.; Schnell, I.; Brand, J. D.; Müllen, K.; Spiess, H. W. *J. Mol. Struct.* **2000**, *521*, 179-195.
(26) Favre-Nicolin, V.; Cerny, R. *J. Appl. Crystallogr.* **2002**, *35*, 734-743.
(27) Rodríguez-Carvajal, J. *Newsletter* **2001**, *26*, 12-19.
(28) In the Back-to-Back (BaBa) experiment, the intensity of the double quantum coherence (DQC) depends on the product of coupling strength and the excitation time. Therefore, a DQC based on strong dipolar coupling will be efficiently excited in short recoupling time. Mobile protons with weak or no dipolar coupling will be absent from the DQF MAS NMR spectra due to inefficient excitation. This makes it possible to distinguish a mobile proton from those rigid ones by comparing the ^{1}H MAS NMR with ^{1}H DQF MAS NMR spectra.
(29) Yang, Y.; Liu, Y.; Li, Y.; Zhang, X.; Gao, M.; Pan, H. *J. Mater. Chem. A* **2015**, *3*, 11057-11065.
(30) a) Jaron, T.; Grochala, W. *Dalton Trans.* **2011**, *40*, 12808-12817; b) Park, K.; Lee, H.-S.; Remhof, A.; Lee, Y.-S.; Yan, Y.; Kim, M.-Y.; Kim, S. J.; Züttel, A.; Cho, Y. W. *Int. J. Hydrogen. Energy* **2013**, *38*, 9263-9270.
(31) Yuan, F.; Gu, Q.; Chen, X.; Tan, Y.; Guo, Y.; Yu, X. *Chem. Mater.* **2012**, *24*, 3370-3379.
(32) Xia, G.; Gu, Q.; Guo, Y.; Yu, X. *J. Mater. Chem.* **2012**, *22*, 7300-7307.
(33) a) Spielmann, J.; Jansen, G.; Bandmann, H.; Harder, S. *Angew. Chem. Int. Ed.* **2008**, *47*, 6290-6295; b) Spielmann, J.; Harder, S. *J. Am. Chem. Soc.* **2009**, *131*, 5064-5065.
(34) Pons, V.; Baker, R. T.; Szymczak, N. K.; Heldebrant, D. J.; Linehan, J. C.; Matus, M. H.; Grant, D. J.; Dixon, D. A. *Chem. Commun.* **2008**, 6597-6599.
(35) Guo, Y.; Wu, H.; Zhou, W.; Yu, X. *J. Am. Chem. Soc.* **2011**, *133*, 4690-4693.
(36) Li, M.; Xia, G.; Tan, Y.; Gu, Q.; Yu, X. *Int. J. Hydrogen. Energy* **2014**, *39*, 11668-11674.
(37) Li, M.; Gu, Q.; Li, X.; Yu, X. *Int. J. Hydrogen. Energy* **2016**, *41*, 733-739.
(38) In contrast, pure Y-AMB (**1**) decomposes in thf and Et_2O to AB and a soluble, uncharacterized Y BH_4 complex

(39) a) Pachón, L. D.; Rothenberg, G. *Appl. Organomet. Chem.* **2008**, *22*, 288-299; b) Janiak, C. *Z. Naturforsch. B: J. Chem. Sci.* **2013**, 68, 1059-1089.
(40) a) Pelletier, F.; Ciuculescu, D.; Mattei, J.-G.; Lecante, P.; Casanove, M.-J.; Yaacoub, N.; Greneche, J.-M.; Schmitz-Antoniak, C.; Amiens, C. *Chem. Eur. J.* **2013**, *19*, 6021-6026; b) Zheng, N.; Fan, J.; Stucky, G. D. *J. Am. Chem. Soc.* **2006**, *128*, 6550-6551; c) Kalidindi, S. B.; Sanyal, U.; Jagirdar, B. R. *Inorg. Chem.* **2010**, *49*, 3965-3967.
(41) The homogeneous elemental constitution of the BN support was confirmed by EDX measurements using the TEM instrument.
(42) Himmelberger, D. W.; Alden, L. R.; Bluhm, M. E.; Sneddon, L. G. *Inorg. Chem.* **2009**, *48*, 9883-9889.
(43) Wright, W. R. H.; Berkeley, E. R.; Alden, L. R.; Baker, R. T.; Sneddon, L. G. *Chem. Commun.* **2011**, *47*, 3177-3179.
(44) Davis, J. H.; Ruether, T.; Dorman, S. C. *Electrochem. Soc. Trans.***2013**, *50*, 293-299.

Chapter 5: Double-Cation Alkali Metal-Zinc AMBs: Solution Synthesis and Dehydrogenation of $KZn(BH_4)_3(NH_3)_3$

This chapter will be included in: M. Mostajeran, M. A. Reynen, N. Brar and R. T. Baker, 2017, under preparation.

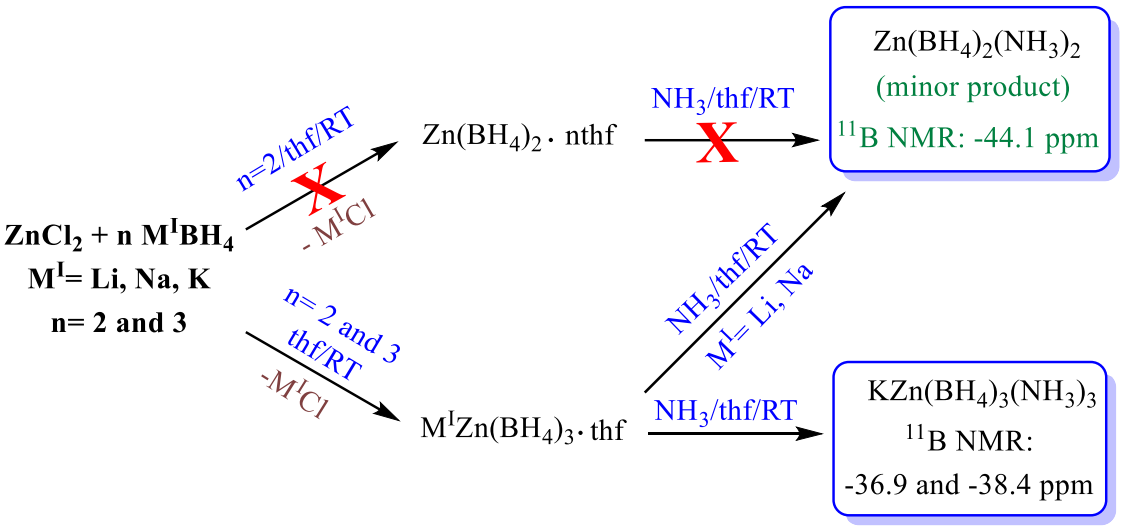

Author Contribution:

The experiments for synthesis and characterization of Zn-AMBs using $NaBH_4$ were performed by undergraduate students Reynen and Brar and completed by Mostajeran. All the experiments presented for $ZnCl_2/LiBH_4$ and $ZnCl_2/KBH_4$ were conducted by Mostajeran. The manuscript is under preparation by Mostajeran and Baker.

5.1. Abstract:

Chloride-free, double-cation alkali metal-zinc borohydride complexes were prepared from $ZnCl_2$ and $M^I(BH_4)$ in ether solvents (M^I= Li, Na, K) and used to prepare ammine metal borohydride solid products. The Zn-AMB products were characterized by powder X-ray diffraction, TGA-MS, FT-IR and ^{11}B MAS NMR techniques. Heating a mixture of 5 wt.% BN-supported Fe nanoparticles and $KZn(BH_4)_3(NH_3)_3$ gave a fourfold reduction in the amount of released ammonia, affording a purer hydrogen stream (98.9 mol%) as compared to the uncatalyzed thermolysis (97.0 mol%).

5.2. Introduction

In Chapter 3 we suggested that the weak Zn-H bond strength (cf. 85 kJ/mol in gas phase ZnH) may contribute to the stability of its coordinated borohydride ligands in the presence of ammonia. As a result, Zn AMBs should be promising thermal hydrogen sources if we can suppress co-production of ammonia gas. In this chapter we first confirm that solution routes from $ZnCl_2$ and alkali metal borohydrides afford primarily double-cation metal borohydride products that have been reported previously to include $[Zn(BH_4)_3]^-$, $[Zn(BH_4)_4]^{2-}$, $[Zn_2(BH_4)_5]^-$ and $[Zn_3(BH_4)_8]^{2-}$ anions.[1] Treatment of these complexes with ammonia yields a series of double-cation M^I–Zn AMBs that are characterized along with their dehydrogenation properties (M^I= Li, Na, K). Finally, base metal catalysts are added in order to suppress ammonia formation.

Although zinc borohydride is used as a reducing agent in organic chemistry, it is rarely prepared as a pure material. For the synthesis of pure $Zn(BH_4)_2$, the method of Schlesinger et al. from ZnH_2 and diborane[2] was soon supplanted by the somewhat more convenient zinc dialkoxide + diborane route from Nöth and co-workers.[3] Attempts to completely remove the coordinated ether solvent to obtain pure material result in partial decomposition. In an alternative strategy Nöth's group later showed,[1] along with two other groups,[4] that simple metathesis reactions of Zn dihalides and alkali metal borohydrides yielded double-cation products (Eq. 1-3) and that 3-4 equiv. of borohydride reagent were required to ensure formation of halide-free products.

$$ZnCl_2 + 3\ LiBH_4 \longrightarrow LiZn(BH_4)_3 + 2\ LiCl \quad (1)$$

$$ZnCl_2 + 4\ LiBH_4 \longrightarrow Li_2Zn(BH_4)_4 + 2\ LiCl \quad (2)$$

$$3\ ZnCl_2 + 8\ KBH_4 \longrightarrow K_2Zn_3(BH_4)_8 + 6\ KCl \quad (3)$$

Similar Zn borohydride materials were prepared by mechanochemical techniques (ball-milling) as mixtures with the alkali metal halide co-products. In one example a mixture obtained from $ZnCl_2$ and 2 equiv. of $NaBH_4$ released 12 wt.% of mixed hydrogen and diborane from heating in the range of 85-140 °C.[5] In testing a series of heterogeneous catalysts[6] with the $Zn(BH_4)_2$/2NaCl mixture, a commercial nanoNi catalyst (1.5 mol% loading) decreased both the decomposition temperature (by 20-40 °C) and the amount of released volatile boranes (illustrated by 10% weight loss until 200 °C).[7] Bimetallic Zn-BHs such as $LiZn_2(BH_4)_5$,[8] and $NaZn(BH_4)_3$[7a] have also been prepared and their hydrogen release behaviour studied.[9]

While reaction of zinc borohydride with ammonia is reported to give the tetra-ammine salt, $[Zn(NH_3)_4](BH_4)_2$],[3] alternative formulations were prepared more recently by ball-milling. The diammoniate, $Zn(\kappa^2\text{-}BH_4)_2(NH_3)_2$, first prepared by Yu et al. from $ZnCl_2(NH_3)_2$ and 2 equiv. of $LiBH_4$, was structurally characterized by a Rietveld analysis on the LiCl-containing mixture.[9] As is typically the case for AMBs, the molecular units are connected in the crystal by a series of dihydrogen bonds with H-H distances between 1.91 and 2.30 Å. The authors claimed a release of 8.9 wt% (not including the LiCl) pure hydrogen at 115 °C within 15 min. In a second report from the same group, an ether solution of "purified" $NaZn(BH_4)_3$ was treated with ammonia at 0°C to afford a new AMB proposed to be $NaZn(BH_4)_3(NH_3)_2$ on the basis of elemental analysis and a Rietveld analysis of the solid. The structure they proposed includes one "outer-sphere" borohydride anion and a $[NaZn(BH_4)_2(NH_3)_2]^+$ cation. To obtain a pure hydrogen stream they ball-milled their AMB with one equivalent of $ZnCl_2$ and then claimed a release of >7.9 wt% (not including the $ZnCl_2$) below 110°C.

In this study we investigate reactions of ammonia with double-cation Zn borohydrides prepared from solution. Attempts are then made to use both heterogeneous and homogeneous catalysts to suppress ammonia formation.

5.3. Materials and Method

5.3.1. General procedures

Experiments were conducted under nitrogen, using Schlenk techniques or a nitrogen-filled MBraun glove box maintaining the level of oxygen and water below 0.1 ppm. All solvents were deoxygenated by purging with nitrogen. Toluene, diethyl ether and tetrahydrofuran were dried on columns of activated alumina using a J. C. Meyer (formerly Glass Contour®) solvent purification system. Benzene-d_6 (C_6D_6) was dried

by stirring over activated alumina (ca. 10 wt. %) overnight, followed by filtration. Ammonia gas (99.99%) was prepared from Linde Canada and dried by passing through a NaOH bed upon using. ^{11}B solution state NMR spectra were recorded on a 300 MHz Bruker Avance instrument at room temperature (21-23 °C). The NMR chemical shifts are reported for ^{11}B relative to $BF_3{\cdot}OEt_2$ (sealed capillary) at 0 ppm and for ^{1}H from the protic impurities in the C_6D_6. The solid state ^{11}B and ^{1}H spectra were collected on a 400 MHz Bruker Avance instruments at room temperature (21–23 °C). Sodium borohydride and adamantane were used as references (δ –42.06 and 1.63 ppm) for ^{11}B and ^{1}H MAS NMRs to tune the parameters and the spectrometer. Unless otherwise stated, the spinning rate for the MAS NMR experiments was 10 KHz for the 400 MHz Bruker spectrometer (4 mm ZrO_2 rotor). FT-IR spectra were collected by a Thermo Nicolet NEXUS 670 FT-IR instrument using 25x4 mm NaCl plates and Nujol oil for air/moisture sensitive compounds. All powder X-ray diffraction (PXRD) analysis performed from a Rigaku Ultima IV diffractometer equipped with a Cu Kα radiation source (λ = 1.541836 Å) and a graphite monochromator. Scanning of the 2θ range was performed from 5 to 50° with the speed of 0.5 °/min. Samples were grinded using an agate stone mortar and pestle in a nitrogen-filled glovebox to obtain fine particles. Then the samples were loaded in an airtight sample holder and mounted on the spectrometer to measure the PXRD patterns at RT. To conduct thermal gravimetric analysis coupled to mass spectrometer (TGA-MS) a thermogravimetric analyzer (Q500 TGA, TA instruments) and a MS spectrometer (Thermostar, PFeiffer Vacuum) were used. Air-free samples were prepared using Tzero aluminum lids and pans and heated at 5 °C/min under a flow of N_2. Differential scanning calorimetry measurements were obtained by a Q2000 (TA instruments) analyzer using hermetic aluminum lids and pans during heating rate of 5 °C/min under a flow of N_2.

5.3.2. Chemicals

Zinc(II) chlroride (Sigma-Aldrich, 98%), Lithium borohydride (Alfa aesar, 95%), Sodium borohydride (Sigma-Aldrish, 98%), Potassium borohydride (Acros, 98%) were used as received. Heterogeneous BN-supported, base-metal nanoparticle catalysts were prepared as detailed in Chapter 4. $(RhClcod)_2$ (Strem Chemicals, 98%), Wilkinson's catalyst (98%, Sigma-Aldrich) were used as received. Ir-POCOP-H_2 was prepared based on a previously reported method.[10]

5.3.3. Synthesis of Double-cation Zinc AMBs, $M^{I}Zn(BH_4)_3(NH_3)_3$

***Li*:** $ZnCl_2$ (250 mg, 1.8 mmol) and 3 equiv. of $LiBH_4$ (124 mg, 5.4 mmol) were stirred in 30 mL of dry diethyl ether overnight in a round bottom Schlenk flask. After filtration to remove LiCl (152 mg, 3.6 mmol), ammonia was added to the flask at RT resulting in rapid precipitation of a colorless solid. The volume was reduced to 20 mL to remove ammonia and the mixture filtered, washed with thf and dried in vacuo at RT for 3 h, yielding 303 mg of a colorless solid. The filtrate was analyzed by ^{11}B and ^{1}H NMR spectroscopy and the solid was characterized by ^{11}B MAS NMR, powder XRD and FTIR.

***Na*:** Under similar conditions $ZnCl_2$ and 3 equiv. of $NaBH_4$ (624 mg, 5.4 mmol) were stirred overnight in 30 mL of dry thf. Ammonia was then added after removing NaCl (207 mg, 3.55 mmol), resulting in precipitation of 328 mg of a colorless solid.

K: $ZnCl_2$ and 4 equiv. of KBH_4 (396 mg, 7.2 mmol) were stirred in 30 mL of dry thf for overnight. After filtration of KCl and unreacted KBH_4 (364 mg), the solution was cooled to 0 °C and ammonia was bubbled through it for 15 min yielding, after filtration and drying, 374 mg of a colorless solid.

5.3.4. Determination of Hydrogen Extent and Purity from Thermolysis of AMB-MNP Composites

The total weight loss was measured from TG results. The MS was calibrated using $Co(NH_3)_6Cl_2$[11] as the standard. Different amounts (3 data points) of cobalt salt were analysed by TGA-MS (from RT-500 °C with a heating ramp of 5°C/min) and the surface areas for the NH_3 peaks were plotted against the numbers of moles of ammonia that could be released under the tested reaction conditions, preparing a calibration curve. During the thermolysis of the Zn-AMB samples, the actual concentrations of ammonia were calculated through fitting to the calibration curve and from there the number of moles of hydrogen could be calculated.

5.3.5. Synthesis of AMB-MNP (M= Fe, Co, Cu) Composites

In a screw cap vial equipped with a Teflon stir bar, the desired amount of MNPs (5 wt.% with respect to the initial weight of **1** or **2**) were added in ~5 mL of toluene in the glovebox. The vial was then sealed, shipped out of the glovebox and sonicated for 5 minutes to increase particle dispersion. The final suspension was stable for about 15 min and precipitation of fine particles was observed after that period. After returning the vial to the glovebox, 100 mg of the Zn AMB solid was added to the vial and stirred

for 15 hours at RT. Filtration of the resulting suspension gave a a light gray powder and a clear solution. The solid was dried under reduced pressure at 40 °C for 2 hours and stored in the glovebox fridge at -30 °C.

5.3.6. Dehydrogenation with Homogeneous Catalysts

In a screw cap vial equipped with a Teflon stir bar, the desired amount of catalysts (1 mol%) and $KZn(BH_4)_3(NH_3)_3$ were added to ~5 mL of thf in the glovebox. The vial was then sealed and stirred (or heated if necessary) in the glovebox for the mentioned periods of time. After the reaction the vials were cooled to RT and both the solid and filtrate were analysed by ^{11}B NMR spectroscopy.

5.4. Results and Discussion

5.4.1. Reactions of $ZnCl_2$ with M^IBH_4 (M^I = Li, Na, K)

In our initial study from Chapter 3, the one-pot reaction of excess ammonia gas with a 1:2 ratio of $ZnCl_2$:$NaBH_4$ in thf indicated adsorption of ~2.5 equiv. of ammonia per Zn. The ^{11}B MAS NMR spectrum of the solid (**1**) showed 3 major resonances at -36.8, -38.5 and -42.7 with a small shoulder at -44.2 ppm. A similar reaction in which the $ZnCl_2$:$NaBH_4$ mixture was first stirred overnight showed the same resonances (**2**, Figure A2.15). From Yu's work the minor resonance could be assigned to the neutral Zn AMB, $Zn(BH_4)_2(NH_3)_2$ (**Zn-1**).[9] In his double-cation paper, Yu reported two resonances for $NaZn(BH_4)_3(NH_3)_2$ (**Zn-2**) at -38.4 and -42.0 ppm with a relative ratio of 1:2 assigned to the outer-sphere and Zn-coordinated BH_4 ligands.[8] Closer inspection of his ^{11}B MAS NMR spectrum, however, reveals the presence of another peak at ~ -36 ppm that was left unexplained. In fact the peak at -42 ppm can be assigned to $NaBH_4$ and the resonances we observe at -36.8 and -38.5 ppm are due to **Zn-2**. This observation confirms the preference for forming $NaZn(BH_4)_3$ in solution, presumably with some unreacted $ZnCl_2$. Overnight stirring of 1.7, 1.8 and 1.9 equivalent of $NaBH_4$ with $ZnCl_2$ in thf afforded grey suspensions, indicative of partial reduction of divalent zinc to metal, while producing stoichiometric amounts of NaCl (based on added $NaBH_4$). Since the major product is expected to be soluble $NaZn(BH_4)_3(thf)_n$, the unreacted portion of added $ZnCl_2$ should have been remained soluble in thf. The ^{11}B MAS NMR spectra of the solids (**3**, **4** and **5**) are shown in Figure 5.1.

While the intensity of the peaks at -36.8 and -38.5 ppm is almost identical within the 3 samples, more **Zn-1** was formed when using 1.7 equiv. of $NaBH_4$ (solid **3**). While the

Bragg's peaks for NaCl are absent in the PXRD profile of **3** (Figure A6.3), characteristic peaks for both **Zn-1** and **Zn-2** indicate more than one phase (through comparison to the reported PXRDs). These results clearly show that formation of **Zn-1** is less favoured by the solution route when higher concentrations of BH_4 are available.

Room temperature overnight stirring of the 1:3 $ZnCl_2$:$NaBH_4$ mixture in thf did not result in the observation of a gray color which means no reduction to metallic Zn. The excess borohydride ligands in thf seem to prevent zinc reduction probably by saturating

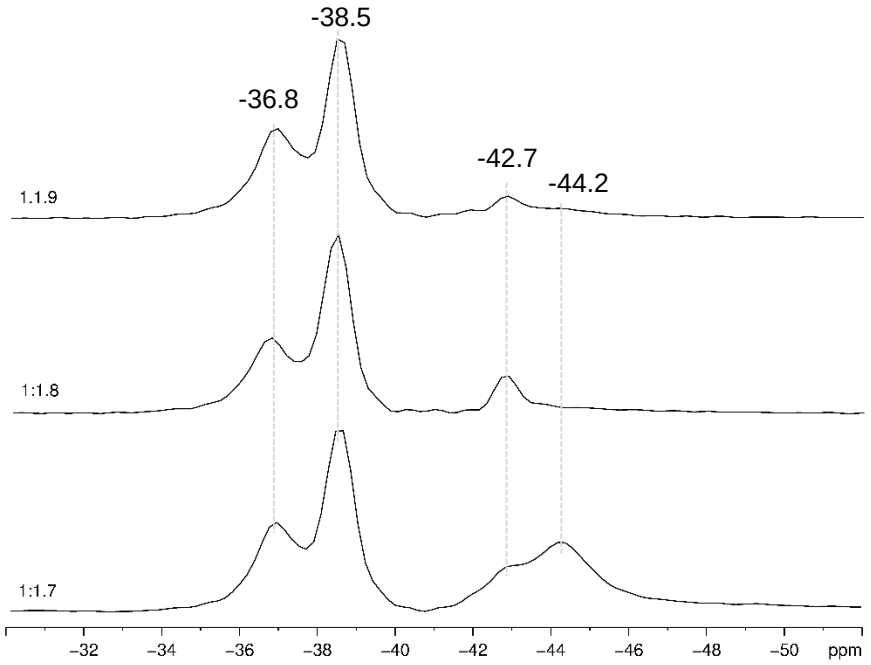

Figure 5.1. ^{11}B MAS NMR spectra (128 MHz, ν_R= 10 KHz) of solids **3**, **4** and **5** (Zn-AMB solids isolated from the reaction of ammonia with solution filtrates from the reaction of $ZnCl_2$ with >2 equiv. of $NaBH_4$ in thf at RT).

its coordination capacity. To further investigate the highest possible number of coordinated BH_4 ligands, $ZnCl_2$ was stirred with various ratios of MBH_4 (M'=Li, Na and K) in thf and monitored by ^{11}B NMR (Figure 5.2). The yield of NaCl measured in each reaction was based on the amount of used M'BH_4 indicative of complete metathesis reactions with $ZnCl_2$.

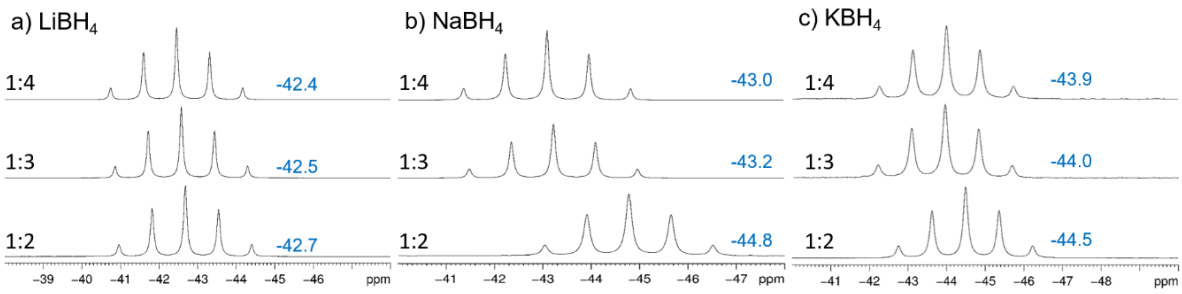

Figure 5.2. ^{11}B NMR spectra (96 MHz, C_6D_6) of solutions obtained after reaction of $ZnCl_2$ with different ratios of M'BH_4 (M'= Li, Na, K; 1:2, 1:3 and 1:4) in thf at RT. All spectra are referenced to $BF_3{\cdot}OEt_2$ at 0 ppm and J_{BH} values are 83 Hz.

As can be seen from Figure 5.2, regardless of the source of BH_4 ligands, the difference in chemical shifts is negligible between "1:3" and "1:4" reactions while it is remarkable between "1:2" and "1:3" reactions. These results suggest the formation of double-cation products such as M'$Zn(BH_4)_3$ (M'=Li, Na and K). It should be noted that while KBH_4 is insoluble in thf at RT, $LiBH_4$ and $NaBH_4$ have chemical shifts of -41.5 and -42.6 ppm, respectively. Further investigations by Nöth indicated that solution synthesis of pure $Zn(BH_4)_2$ in ether is problematic due to its additional reaction with LiCl (forming $Li[Zn(BH_4)_2Cl]$). However, using 3 equiv. (*vs.* Zn) of MBH_4 (M= Li and Na) gives the chloride-free products.[12]

Evaporation of the thf solvent from the 1:3 $ZnCl_2$:$NaBH_4$ reaction under reduced pressure and drying for 13 hrs gave a grey solid (**6**). While no peak was observed for $NaBH_4$ (at ~ -42.1 ppm) in the ^{11}B MAS NMR analysis of **6** (Figure 5.3), one major resonance was observed at -45.1 ppm and 2 minor ones at -41.7 and -47.8 ppm.

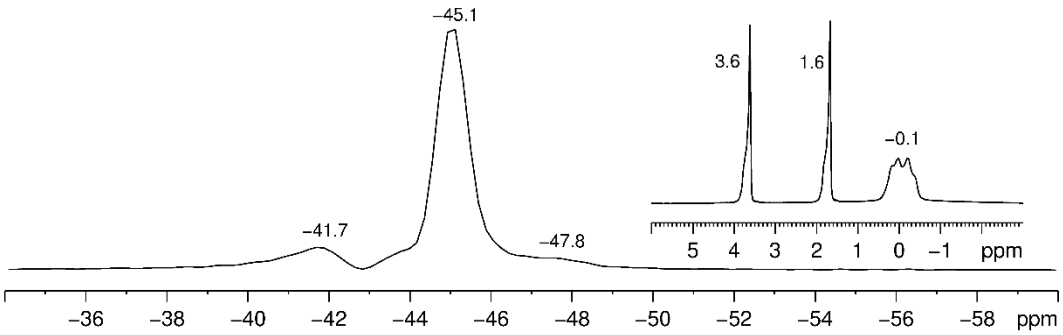

Figure 5.3. ^{11}B MAS NMR (128 MHz, ν_R= 10 KHz) of the solid **6** obtained from the reaction of 1:3 $ZnCl_2$:$NaBH_4$ in thf. Inset: ^{1}H MAS NMR (128 MHz, ν_R= 10 KHz) of the $NaZn(BH_4)_3(thf)_n$.

The two resonances assigned to $NaZn(BH_4)_3(thf)_n$ by Yu are at -42 and -45.3 ppm in a 2:1 ratio.[8] However, in the ^{11}B MAS NMR spectrum in Figure 5.3 the resonances at -

41.7 and -45.1 ppm are clearly not in a 2:1 ratio. Combining this result with that from the solution NMR data suggests the presence of a second phase such as $NaZn_2(BH_4)_5$.

As both KCl and KBH_4 are insoluble in thf, solution synthesis of Zn-AMB with KBH_4 allowed us to estimate the exact number of BH_4 ligands on Zn through the weight of the initial precipitate. Using $ZnCl_2$:KBH_4 in a 1:4 ratio the weight of the filtered salts was consistent with 2 equiv. of KCl and one equiv. of unreacted KBH_4, confirming the $KZn(BH_4)_3$(thf) formula (the single thf molecule was confirmed by integrating the ^{1}H MAS NMR resonances vs. those of the borohydride ligands. This contrasts with the ball-milling preparation of $KZn(BH_4)_3$ in which always a mixture of products (including $K_2Zn(BH_4)_xCl_{4-x}$) was obtained even when $ZnCl_2$:KBH_4 was used in a 1:3 ratio.[13] The B-H bond stretching vibrations are well presented in the FT-IR spectrum of $KZn(BH_4)_3$ in the range of 2100-2500 cm^{-1} (Figure A3.13).

5.4.2. Reactions of M^I-Zn Borohydrides with Ammonia

Addition of ammonia to a clear thf filtrate from the reaction of $ZnCl_2$ with 3 equiv. of $NaBH_4$ affords a colorless solid (**7**). The ^{11}B MAS NMR spectrum of **7** (Figure 5.4) exhibits the same set of peaks as previously observed for **3**, **4** and **5**. The solution ^{11}B NMR of the filtrate shows one resonance at -43.3 ppm (J_{BH}= 81 Hz). The simulated relative intensity of the resonances in the ^{1}H MAS NMR spectrum of **7** indicates a slightly higher ratio for the N-H peaks at 3.1 ppm (vs. B-H).

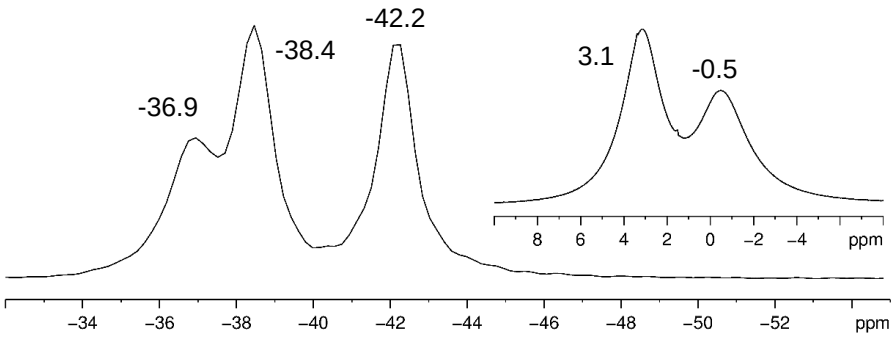

Figure 5.4. ^{11}B MAS NMR spectrum (128 MHz, ν_R= 10 KHz) of the solid (**7**) obtained from ammonia addition to solution filtrate of 1:3 $ZnCl_2$ and $NaBH_4$ in thf at RT. Inset: ^{1}H MAS NMR spectrum (400 MHz, ν_R= 10 KHz) of the same sample.

Comparing the ^{11}B MAS NMR spectrum of $NaZn(BH_4)_3$ and the solid **7** (Figures 5.3 and 5.5) reveals a considerable amount of $NaBH_4$ in the latter. As no $NaBH_4$ was observed in the $NaZn(BH_4)_3$ starting material, it must have been formed during the formation of Zn-AMB product perhaps in a process like that in Eq. 4. As there is not a

corresponding amount of neutral **Zn-1** formed, this observation provides additional evidence for multizinc complexes such as $NaZn_2(BH_4)_5$.

$$Na_2Zn_3(BH_4)_8 + 7\,NH_3 \longrightarrow NaZn(BH_4)_3(NH_3)_3 + 2\,Zn(BH_4)_2(NH_3)_2 + NaBH_4 \qquad (4)$$

Attempts to wash the excess $NaBH_4$ from the solid **7** to obtain a pure sample of **Zn-2** were not successful (Fig 5.5).

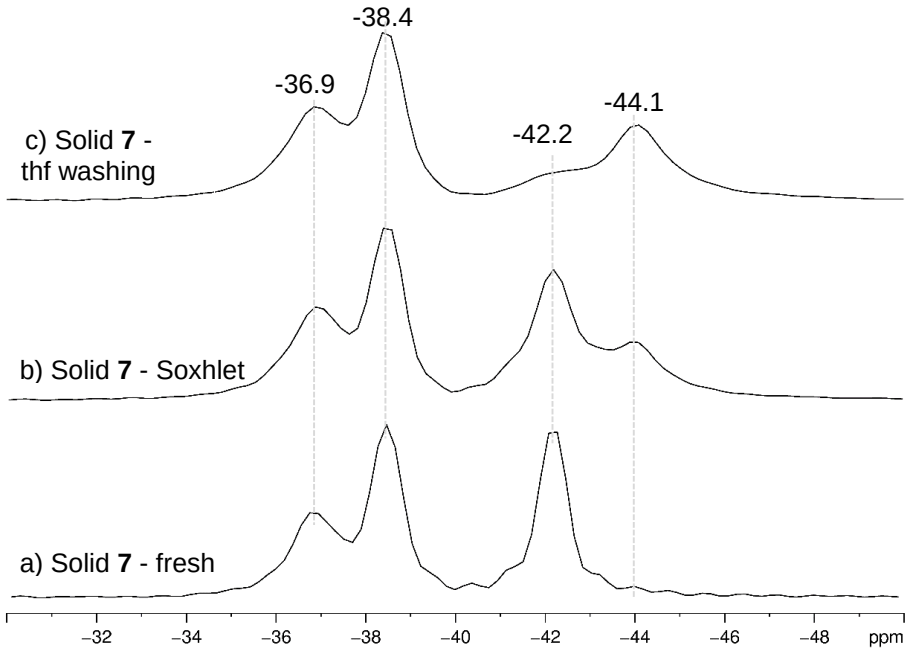

Figure 5.5. ^{11}B MAS NMR spectrum (128 MHz, ν_R= 10 KHz) of a) the as-synthesized solid **6**, b) Solid **8** obtained from Soxhlet extraction of **7** with thf for 18 hrs and c) Solid **9** obtained from extensive room-temperature thf washing of solid **7**.

Soxhlet extraction with thf for 18 hrs resulted in the formation of a black solid (**8**, *i.e.* massive zinc reduction); AB and a quintet at -43.3 ppm (J_{BH}= 82 Hz) were observed in the ^{11}B NMR spectrum of the solution. Washing the solid with a large volume (300 mL) of thf at RT also caused partial decomposition of the Zn-AMB product (solid **9**) with formation of a grey solid and a quintet at -43.3 ppm (J_{BH}= 82 Hz). While the amount of $NaBH_4$ was clearly reduced, more of the neutral Zn-AMB was formed, probably through partial decomposition of the $NaZn(BH_4)_3(NH_3)_n$. Due to the limited solubility of the $NaBH_4$ in thf, determination of its exact amount was not possible. Therefore, $LiBH_4$ in diethyl ether (DEE) was used to study this reaction as LiCl is not soluble in DEE[14] while $LiBH_4$ is completely soluble.

Reaction of $ZnCl_2$ with $LiBH_4$ (1:3) is reported to give $LiZn(BH_4)_3$[1] and a stoichiometric amount of LiCl in DEE. Addition of ammonia at RT yields a colorless

solid (**10,** Figure 5.6). Similar to the Zn-AMB sample prepared from $NaBH_4$, the ^{11}B MAS NMR spectrum of **10** shows more than one compound in the mixture. The ^{11}B NMR analysis of the DEE filtrate indicates the presence of ~0.5 equiv. of free $LiBH_4$, suggesting coordination of 2.5 equiv. BH_4 to each Zn atom as in the $LiZn_2(BH_4)_5$ complex characterized in the solid state.[7a] Thus, reactions of this complex with ammonia also produce a mixture of two Zn-AMB compounds, presumably $LiZn(BH_4)_3(NH_3)_n$, $LiZn_2(BH_4)_5(NH_3)_n$, and free $LiBH_4$.

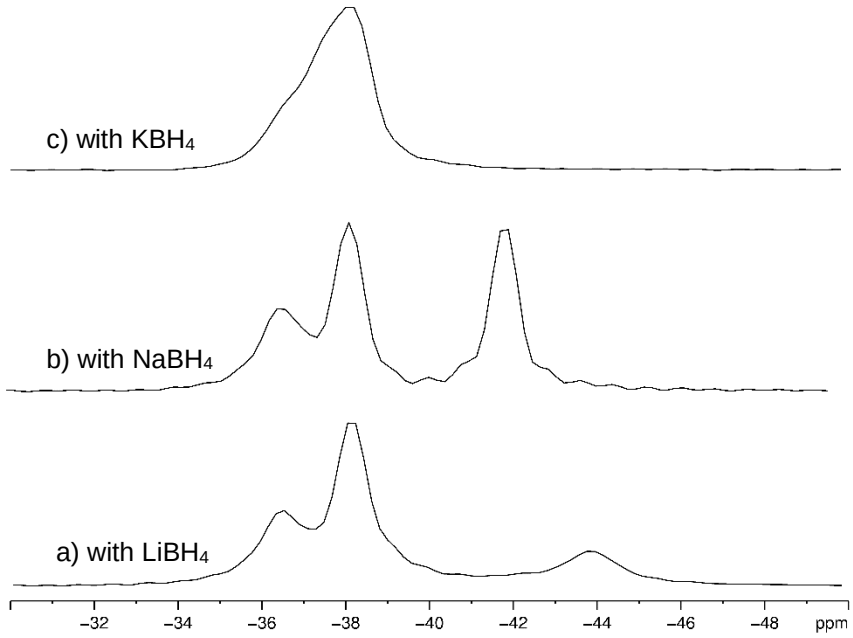

Figure 5.6. The ^{11}B MAS NMR spectra (128 MHz, ν_R= 10 KHz) of the solids derived from $ZnCl_2$ + 3 M^IBH_4 + ammonia. M^I = Li (**10**, a), Na (**7**, b) and K (**11**, c).

Reaction of ammonia gas with the $KZn(BH_4)_3$ afforded a colorless precipitate (**Zn-3**) and a clear solution. Analysis of the weight difference during this reaction (reactant *vs.* final Zn-AMB solid) indicates uptake of 3 equiv. of NH_3 per Zn, suggesting the formula of $KZn(BH_4)_3(NH_3)_3$. It should be emphasized that KBH_4 in thf does not uptake any ammonia or produce any AB. The ^{11}B NMR spectrum of the solution also showed no AB while 2 major broad peaks were observed in the ^{11}B MAS NMR spectrum (Figure 5.6c). Free KBH_4 with δ= -38 ppm[15] overlaps with the resonances at -36.5 and -38.4 ppm. Importantly, none of the neutral complex **Zn-1** is observed. Nonetheless, monitoring the ammonia reaction with $KZn(BH_4)_3$ by powder XRD clearly indicates formation of additional KBH_4 (Figure 5.7).

5.4.3. Thermal Decomposition of $KZn(BH_4)_3$·thf and $KZn(BH_4)_3(NH_3)_3$

Thermolysis of $KZn(BH_4)_3$·thf (8.1 wt.% hydrogen capacity without thf) indicates a decomposition onset at 90 ^oC (Figure 5.8) which is significantly lower than that of KBH_4 (~680 ^oC).[16] A total of 32.1% weight loss was observed in the range of 89-148 °C during heating from RT to 200 °C (5 °C/min). In contrast to $NaZn(BH_3)_3$, no trace of BH_3 (m/z= 14) was detected. However, concurrent release of H_2 (m/z= 2) and B_2H_6

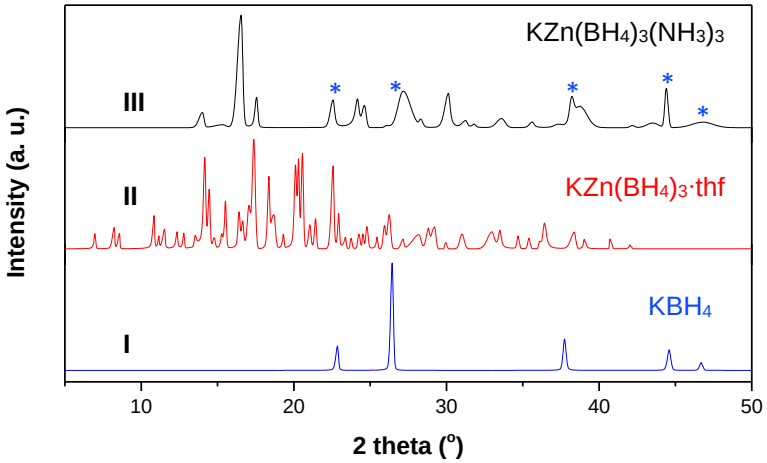

Figure 5.7. PXRD profiles of KBH_4 (I), as synthesized $KZn(BH_4)_3$·thf (II) and as synthesized $KZn(BH_4)_3(NH_3)_3$ (III) obtained at RT. Bragg's peaks of KBH_4 are marked with asterisks.

(m/z= 27) was observed starting from 92 °C (in the ratio of 15:1), consistent with the proposed decomposition mechanism reported by Jensen.[13] While B_2H_6 release subsided at 164 °C, hydrogen evolution was still on-going and expected to continue beyond 200 °C.

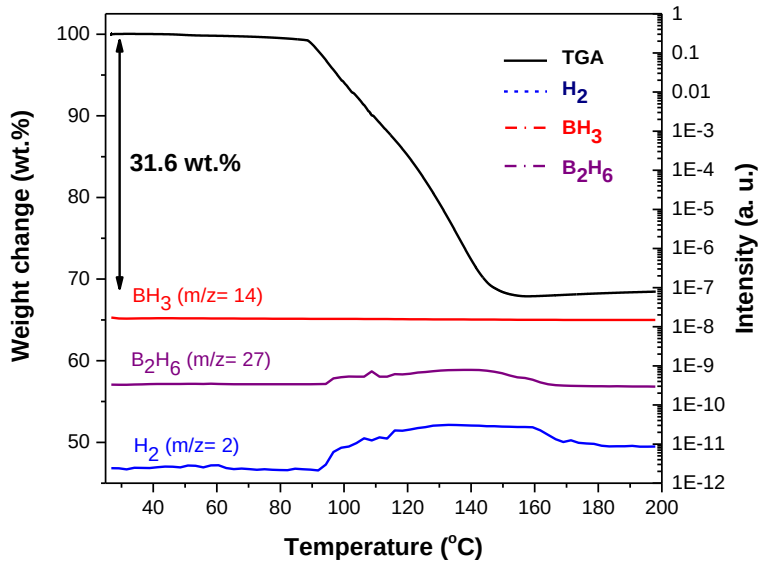

Figure 5.8. TGA-MS results for thermal dehydrogenation of $KZn(BH_4)_3$·thf upon heating from RT to 200 °C (ramp = 5 °C/min) under N_2.

Release of hydrogen proceeds through a single step with a peak at 132 °C which is slightly lower than for $NaZn(BH_4)_3$ (140 °C). It should be noted that the observed large weight loss from $KZn(BH_4)_3$·thf is partially due to release of coordinated thf (m/z= 72). The coordinated thf molecule accounts for 32.6 wt.% however, the exact amount of remaining thf in the $KZn(BH_3)_3$ solid after extended drying under vacuum was unknown. Consequently, the observed weight loss consisted of H_2, B_2H_6 and thf. With respect to the complexity of the released gas stream from $KZn(BH_4)_3$·thf, the amount and purity of the released hydrogen was not determined.

As expected, oordination of NH_3 to $KZn(BH_4)_3$·thf alters significantly its hydrogen release behaviour. Total observed weight loss for **Zn-3** was 14.5% and no boron-containing gases were detected upon heating from RT to 200 °C (Figure 5.9). Hydrogen release began at 50 °C and continued even after 200 °C. In contrast, ammonia was released only between 73-145 °C. As confirmed by the MS results, a total of 12.1 wt.% hydrogen (97.0 mol% pure H_2) was released over this temperature range (Figure 5.9 and Table 5.1).

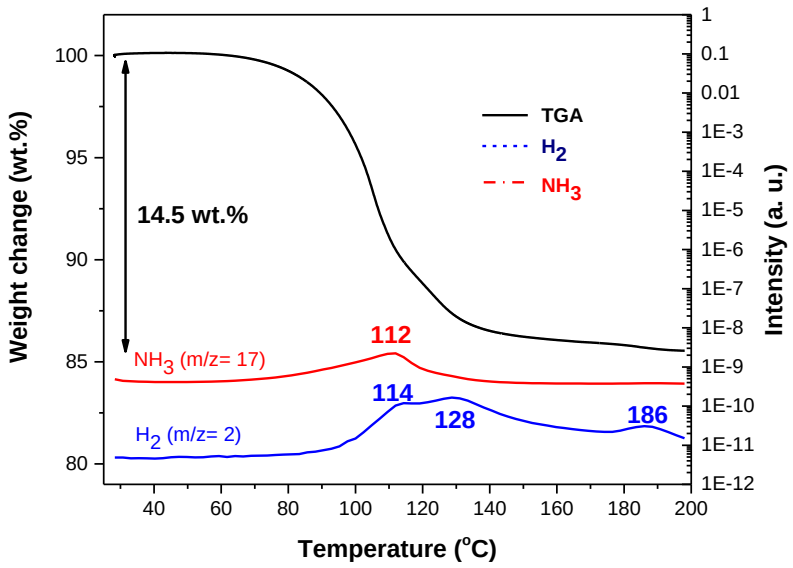

Figure 5.9. TGA-MS results for thermal decomposition of $KZn(BH_4)_3(NH_3)_3$ from RT to 200 °C under N_2 (ramp= 5 °C/min).

Table 5.1. Hydrogen release results of catalysed and uncatalyzed $KZn(BH_4)_3(NH_3)_3$ (**Zn-3**)

	10	**10/FeNPS**	**10/CoNPS**	**10/CuNPS**
Total Weight Loss (%)	14.6	6.4	9.1	12.7
H_2 Onset (^{o}C)	50	41	41	43
H_2 Peak (^{o}C)	128	99	108	128
H_2 (wt.%)	12.1	5.8	6.7	10.2
H_2 Purity (mol%)	97	98.8	95.9	97.2
NH_3 Onset (^{o}C)	56	55	63	55
NH_3 Peak (^{o}C)	112	92	106	106
NH_3 (wt.%)	2.5	0.6	2.4	2.5

All results were obtained by TGA-MS analysis from samples heated from RT to 200 °C (Ramp= 5 °C/min) under nitrogen.

Major thermal events for **Zn-3** over this temperature range occurred at 105, 124 and 184 °C (Figure A5.26) in line with the TG results indicating a three-step process: *I) 25-108 °C:* The first endothermic event, which is centred at 67 °C in the DSC profile of $KZn(BH_4)_3(NH_3)_3$ (Figure 5.10). This can be attributed to the initial hydrogen release step (50-98 °C) which also includes the onset temperature for NH_3 release at 73 °C.

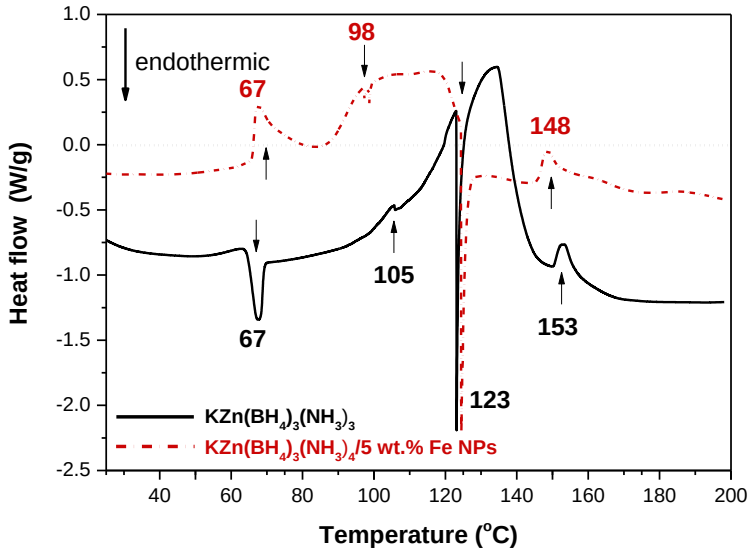

Figure 5.10. DSC profile of $KZn(BH_4)_3(NH_3)_4$, **11**, and KZn-AMB/FeNPs composite on heating from RT to 200 °C under N_2 (ramp = 5 °C/min).

The next small exothermic event over this range was observed at 105 °C, the ammonia release peak temperature. The ^{11}B MAS NMR spectrum of **Zn-3** heated to 70 °C for 30 minutes indicated partial decomposition of $KZn(BH_4)_3(NH_3)_3$ with respect to the observation of sp^2 boron species in the range of 10-21 ppm. Moreover, 2 new peaks centred at -42.1 and -43.7 ppm were also apparent (Figure 5.11a) which disappeared at

100 °C. While the resonance at -43.7 ppm could be attributed to **Zn-1** as a decomposition intermediate, the peak at -38.1 ppm can be assigned to KBH_4 as its dehydrogenation initiates at much higher temperatures. Simultaneous reduction in the intensity of the N-H (3.1 ppm) and B-H bonds (-0.2 ppm), as evidenced by the ^1H MAS NMR results (Figure 5.11b), confirms that hydrogen originates from the combination of N-H···H-B during the thermolysis of AMBs. *II) 108-128 °C:* The most significant thermal event in this step is observation of **Zn-3**'s melting point at ~123 °C (Figure 5.10) and also a two-step hydrogen release process spanning from 114 and 128 °C. This observation shows that hydrogen release is dominant in this range, which is also facilitated by melting of ZMB particles, albeit with small amount of ammonia contamination. *III) 128-200 °C:* NH_3 ceased to release at ~145 °C and so pure hydrogen

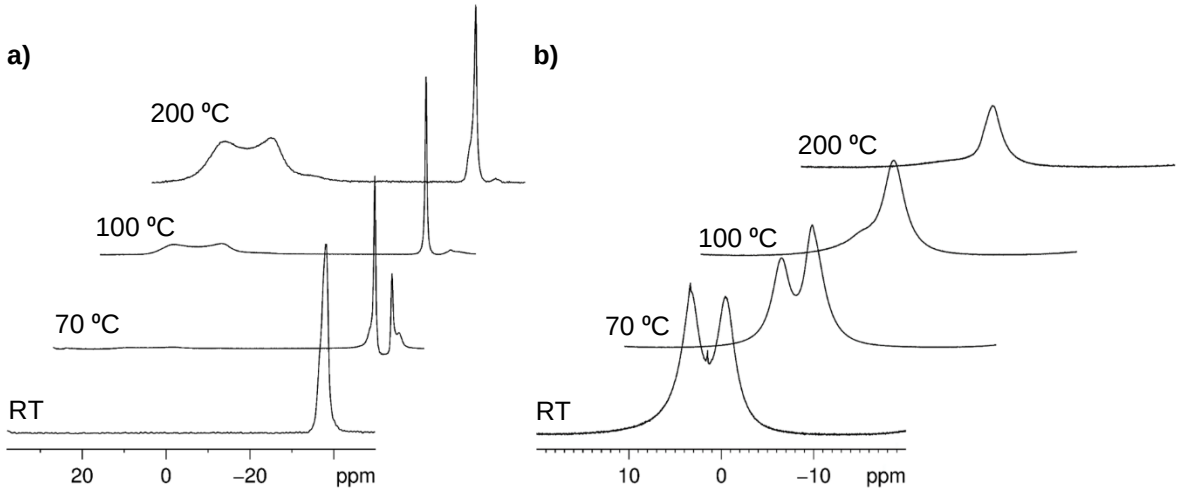

Figure 5.11. ^{11}B MAS NMR (left, 128 MHz, ν_R= 10 KHz) and ^1H MAS NMR (right, (400 MHz, ν_R= 10 KHz) of uncatalyzed $KZn(BH_4)_3(NH_3)_3$ heated at 70, 100 and 200 °C under static N_2 (i.e. in the glovebox) for 30 minutes.

(~1 wt.% according to the MS results) is released after this point with a peak temperature at 184 °C (Figure 5.9). In line with the MS results, the DSC profile shows a small exothermic event 153 °C which can be attributed to the peak in H_2 release in this step. The N-H bonds are converted almost entirely at 200 °C (Figure 5.11b) and the observed B-H resonance is due to the presence of KBH_4 which is completely stable under these thermal condition.

5.4.4. Catalytic thermolysis of $KZn(BH_4)_3(NH_3)_3$

In addition to our results from Chapter 4, enhanced dehydrogenation of $Li(NH_3)BH_4$ and $Li(NH_3)_2BH_4$ was reported using a catalytic amount of $CoCl_2$ in a closed system.[8]

Note that the active catalytic species are reduced metallic CoNPs, formation of which necessarily decomposes some of the AMB particles and introduces chloride impurities. To improve the hydrogen release properties of **Zn-3**, Zn-AMB/M'NP-BN composites were prepared through overnight stirring of the Zn-AMB suspensions with sonicated M'NPs-BN. A colorless solution filtrate in each case was a clear indication of full immobilization of the M'NPs-BN on the Zn-AMB particles.[18]

Consistent with the suppression of ammonia release, all the composites exhibited lower total weight loss (uncorrected for the catalyst) compared to the pristine $KZn(BH_4)_3(NH_3)_3$ (Figure 5.12). Comparison of the data shown in Table 5.1 indicates that the CuNPs resulted in the highest weight loss (12.7 %) while the FeNPs resulted in the highest purity of hydrogen stream, 98.8 mol%, albeit with the lowest weight loss. While the onset temperature for hydrogen release was not affected significantly by any catalyst, the peak release temperature for hydrogen was decreased by 34 °C using 5 wt.% FeNPs. More importantly, FeNPs decreased the amount of released ammonia by nearly fourfold, affording 5.9 equiv. hydrogen (98.8 mol% pure) as confirmed by the MS results.

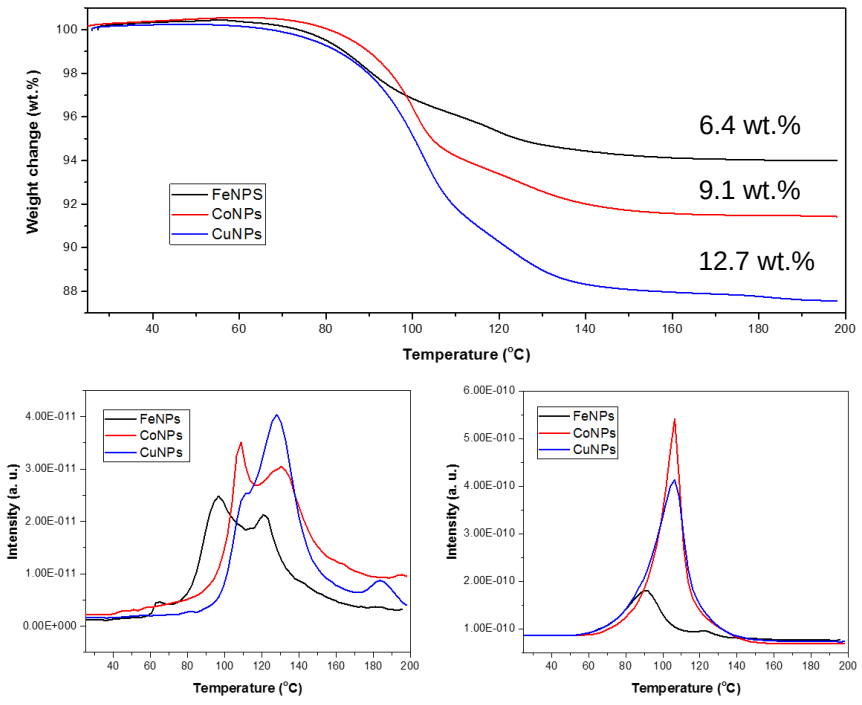

Figure 5.12. TGA-MS results for dehydrogenation of $KZn(BH_4)_3(NH_3)_3$/M′NP-BN composites from RT to 200 °C (ramp = 5 °C/min) under N_2 where M'= Fe, Co and Cu.

The major thermal events during the thermolysis of the $KZn(BH_4)_3(NH_3)_3$/FeNPs composite occur at 58, 87 and 119 °C (Figure A5.27) which are clearly lower than that of uncatalyzed **Zn-3**. Decomposition of $KZn(BH_4)_3(NH_3)_3$/FeNPs proceeds through 3

steps: I) *45-98 °C*: With the ammonia's onset release temperature at 55 °C, the majority of the observed 3.4% weight loss in this step was determined to be hydrogen with peaks at 68 and 94 °C. As can be seen in Figure 5.12, the hydrogen peak temperature was lowered from 128 °C for the pristine $KZn(BH_4)_3(NH_3)_3$ to 94 °C by the use of 5 wt.% FeNPs. II) *98-127 °C*: Concurrent release of hydrogen and ammonia was observed in this range while the ammonia release reached its peak at 92 °C. A total of 2.2% weight loss was observed in this step. III) *127-200* °C: Ammonia release stopped at 127 °C so the ~1% weight loss in this range was pure hydrogen.[18]

As mentioned earlier,[18,19] lack of homogeneous dispersion of the M'NPs-BN solid catalysts limits it contact with the AMB particles to the surface atoms. Mild dehydrocoupling of primary and secondary amine-boranes (25-45 °C) was reported to proceed remarkably with transition metal catalysts in toluene, in which AB is not soluble. Inspired by the use of homogeneous catalysts reacting at the liquid-solid interface, several active dehydrogenation catalysts were tested with $KZn(BH_4)_3(NH_3)_3$ (Figure 5.13).[19-20]

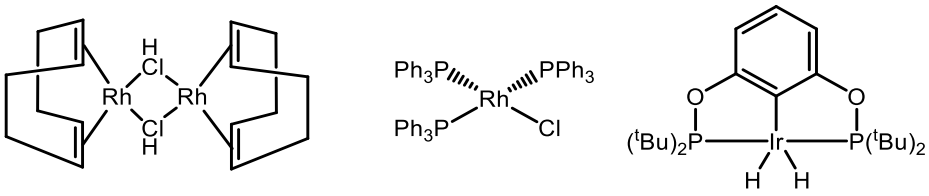

Figure 5.13. The tested homogeneous catalysts for dehydrogenation of Zn-AMB: $(RhClcod)_2$ (left), the Wilkinson's catalyst (middle) and IrPOCOP-H_2 (right).

The $[RhCl(cod)]_2$ catalyst turned immediately from orange to black in thf upon addition of $KZn(BH_4)_3(NH_3)_3$. Rapid formation of Rh nanoparticles (or small clusters) was followed by slow immobilization onto the AMB particles (*i.e.* heterogeneous catalyst). However, stirring this mixture for 1 hour in thf at RT indicated formation of AB (q, -22.3 ppm, J_{BH}=95 Hz), a small quartet at -24.5 ppm (J_{BH}= 87 Hz) and a new peak at -45.0 ppm (J_{BH}= 83 Hz) in the ^{11}B solution NMR spectrum (Figure A1.20). After 1 day of stirring at RT, the peak at -45.0 ppm disappeared and AB dehydrogenation products were observed in the range of 25-30 ppm.

Wilkinson's catalyst also darkened the solution after addition of the $KZn(BH_4)_3(NH_3)_3$. After stirring for 1 hour at RT 2 resonances were observed in the ^{11}B NMR spectrum at -38.2 and -45.0 ppm in addition to AB at -22.3 ppm (Figure A1.21). The AB peak started to grow on extending the reaction time along with formation of AB dehydrogenation products. While $KZn(BH_4)_3(NH_3)_3$ is quite stable in

thf, this evidence suggests that AB is a decomposition intermediate in its solution-based dehydrogenation using these catalysts.

Ir-POCOP-H_2 was synthesized from the reaction of Ir-POCOP-HCl and hydrogen gas in benzene using 1.1 equiv. of NaO^{t}Bu as a base.[10] Dark red crystals of Ir-POCOP-H_2 turned to yellow in thf immediately after the addition of the Zn-AMB. After one hour during which no further color change was observed, the ^{11}B NMR spectrum of the thf solution displayed a peak at -22.3 ppm for AB and a quintet at -44.0 ppm (J_{BH}= 81 Hz) (Figure A1.22). Overnight stirring resulted in a pale-green solution but little change in the NMR spectrum, indicating the slower dehydrogenation profile with Ir-POCOP-H_2.

Hydrogen is crucial for the IrPOCOP-H_2 catalysts to remain active. Therefore, dehydrogenation reactions with this catalyst were conducted in a closed vial in the glove box. Heating the $KZn(BH_4)_3(NH_3)_3$/IrPOCOP-H_2 in toluene for 4 hours at 60 °C did not initiate a remarkable activity. While the FT-IR spectra of this solid is identical to the un-catalyzed $KZn(BH_4)_3(NH_3)_3$ treated under the same conditions (not shown), solution NMR data of both exhibited a quintet at -45.0 ppm (J_{BH}= 84 Hz). The ^{11}B MAS NMR results obtained from both of the solids isolated after these reactions also indicated the formation of $Zn(BH_4)_2(NH_3)_2$ at -44.1 ppm which was slightly higher for the catalyzed sample (Figure A2.16). Prolonged heating time (1 day under similar reaction conditions) showed the presence of the same resonance at -45.0 ppm (J_{BH}=84 Hz) while a new resonance at -38.3 ppm and traces of **Zn-1** along with dehydrogenated products could be detected in the ^{11}B MAS NMR spectra in addition to the previous peaks (Figure A2.16).

5.5. Conclusions

Choride-free $KZn(BH_4)_3(NH_3)_3$ was produced through addition of NH_3 to the solution obtained from the reaction of $ZnCl_2$ and excess KBH_4 in thf. Formation of KBH_4 after the ammonia reaction suggests the presence of a second MBH phase, likely $KZn_2(BH_4)_5$ and/or $K_2Zn_3(BH_4)_8$.[21] Further investigations along these lines are on-going in our laboratories to isolate and structurally characterize these Zn borohydrides. While Cu NPs gave the highest extent of H_2 release, Fe NPs gave a four-fold reduction in NH_3 release, yielding a purer hydrogen stream (99 vs. 97 mol% uncatalyzed). While Rietveld analysis of powder X-ray data for $KZn(BH_4)_3(NH_3)_3$ is in progress, further investigation focuses on further purification of these Zn-AMBs.

5.6. References

(1) Nöth, H.; Wiberg, E.; Winter, L. P. *Z. Anorg. Allg. Chem.* **1971**, *386*, 73-86.
(2) Barbaras, G. D.; Dillard, C.; Finholt, A. E.; Wartik, T.; Wilzbach, K. E.; Schlesinger, H. I. *J. Am. Chem. Soc.* **1951**, *73*, 4585-4590.
(3) Nöth, H.; Wiberg, E.; Winter, L. P. *Z. Anorg. Allg. Chem.* **1969**, *370*, 209-223.
(4) a) Hagenmuller, P.; Rault, H. *C. R. Seances Acad. Sci.* **1959**, *248*, 2758; b) Mikheeva, V. I.; Mal'tseva, N. N.; Alekseeva, L. S. *Zh. Neorg. Khim.* **1968**, *13*, 1303-1308.
(5) Jeon, E.; Cho, Y. *J. Alloys Compd.* **2006**, *422*, 273-275.
(6) Srinivasan, S.; Escobar, D.; Goswami, Y.; Stefanakos, E. *Int. J. Hydrogen Energy* **2008**, *33*, 2268-2272.
(7) a) Ravnsbæk, D.; Filinchuk, Y.; Cerenius, Y.; Jakobsen, H. J.; Besenbacher, F.; Skibsted, J.; Jensen, T. R. *Angew. Chem. Int. Ed.* **2009**, *48*, 6659-6663; b) Černý, R.; Chul Kim, K.; Penin, N.; D'Anna, V.; Hagemann, H.; Sholl, D. S. *J. Phys. Chem. C* **2010**, *114*, 19127-19133.
(8) Xia, G.; Gu, Q.; Guo, Y.; Yu, X. *J. Mater. Chem.* **2012**, *22*, 7300-7307.
(9) Gu, Q.; Gao, L.; Guo, Y.; Tan, Y.; Tang, Z.; Wallwork, K. S.; Zhang, F.; Yu, X. *Energy Environ. Sci.* **2012**, *5*, 7590-7600.
(10) Göttker-Schnetmann, I.; White, P. S.; Brookhart, M. *Organometallics* **2004**, *23*, 1766-1776.
(11) Ingier-Stocka, E.; Bogacz, A. *J. Thermal Anal.* **1989**, *35*, 1373-1386.
(12) Nöth, H. *Angew. Chem.* **1961**, *73*, 371-383.
(13) Černý, R.; Ravnsbæk, D. B.; Schouwink, P.; Filinchuk, Y.; Penin, N.; Teyssier, J.; Smrčok, L. u.; Jensen, T. R. *J. Phys. Chem. C* **2012**, *116*, 1563-1571.
(14) Cotton, F. A.; Koch, S.; Mertis, K.; Millar, M.; Wilkinson, G. *J. Am. Chem. Soc.* **1977**, *99*, 4989-4992.
(15) Heyn, R. H.; Saldan, I.; Sorby, M. H.; Frommen, C.; Arstad, B.; Bougza, A. M.; Fjellvag, H.; Hauback, B. C. *Phys. Chem. Chem. Phys.* **2013**, *15*, 11226-11230.
(16) Paskevicius, M.; Ley, M. B.; Sheppard, D. A.; Jensen, T. R.; Buckley, C. E. *Phys. Chem. Chem. Phys.* **2013**, *15*, 19774-19789.
(17) a) Schlesinger, H. I.; Burg, A. B. *Chemical Reviews* **1942**, *31*, 1-41; b) Zheng, X.; Chua, Y.; Xiong, Z.; Chen, W.; Jiang, Z.; Wu, G.; Chen, P. *Int. J. Hydrogen Energy* **2015**, *40*, 4573-4578.
(18) Mostajeran, M.; Ye, E.; Desgreniers, S.; Baker, R. T. *Chem. Mater.* **2017**, *29*, 742-751.
(19) Jaska, C. A.; Temple, K.; Lough, A. J.; Manners, I. *J. Am. Chem. Soc.* **2003**, *125*, 9424-9434.
(20) Smythe, N. C.; Gordon, J. C. *Eur. J. Inorg. Chem.* **2010**, *2010*, 509-521.
(21) Ravnsbæk, D. B.; Sørensen, L. H.; Filinchuk, Y.; Reed, D.; Book, D.; Jakobsen, H. J.; Besenbacher, F.; Skibsted, J.; Jensen, T. R. *Eur. J. Inorg. Chem.* **2010**, *2010*, 1608-1612.

Chapter 6. Conclusions and Future Directions

6.1. *Thesis* Outlook

The work presented in this *Thesis* provides a promising perspective for developing catalysts with superior mechanical and thermal stability for the hydrolysis of sodium borohydride (**Chapter 2**) and also contributes significantly to the area of synthesis and catalytic dehydrogenation of AMBs (**Chapters 3-5**). In this chapter these advances are considered in the context of the current state of the art and suggestions are made for future opportunities.

6.2. Catalytic Hydrolysis of $NaBH_4$

Sodium borohydride ($NaBH_4$) is the least expensive metal borohydride and is air-stable although it reacts slowly with water. As noted in **Chapter 2**, the plethora of catalyst studies over the last 3 decades have established sufficient activity even with base metals, leading to an increased focus on catalyst stability and separation of the sodium borate by-product. Our long-term objective for **Chapter 2** was to develop active porous catalysts to allow for one-pass conversion of $NaBH_4$ in aqueous ethanol solvent to be tested in fuel cells for underground mine forklifts with our industry collaborator (Kingston Process Metallurgy Inc.). In collaboration with Professor Vanessa Prévot from Université Clermont Auvergne in France, polystyrene-templated Fe- and Ni-containing Layered Double Oxides (3-DOM LDOs) with high surface area were prepared using the inverse-opal technique and examined as catalysts for $NaBH_4$ hydrolysis in ethanol. The hierarchical 3-DOM-Fe-Mg-Al catalyst gave an enhanced hydrolysis rate (1.0 $mol(H_2)min^{-1}mol^{-1}_{Fe}$) compared to the non-templated catalyst with similar ions (0.7 $mol(H_2)min^{-1}mol^{-1}_{Fe}$). Similarly, the 3-DOM-Ni-Mg-Al catalysts with 190 and 500 nm pore size released 0.3 and 0.4 $mol(H_2)min^{-1}mol^{-1}_{Ni}$ respectively.

The studies reported in this *Thesis* lay the groundwork for the development of an efficient portable hydrogen generator. Although a change in priorities for our industry collaborator precluded our testing in the prototype hydrogen generator, the next step needed would be catalyst lifetime testing using a flow system. This would allow for achievement of the proper balance of surface area and catalyst particle porosity. Observed leaching of trivalent aluminum may suggest replacement in the LDH structure with trivalent boron that would eventually afford a stable catalyst composition. As a result, metal borate metal organic framework materials (MOFs) may also be long-lived catalysts

under flow conditions. Moreover, to close the hydrogen cycle for portable power applications, researchers should focus on additional applications for the sodium borate co-product.

6.3. Hydrogen Release from Ammine Metal Borohydrides

In spite of their irreversibility, ammine metal borohydrides are promising lightweight solid hydrogen sources with storage capacities typically in excess of 10 wt%.[1] Although the addition of protic N-H bonds to the existing hydridic B-H bonds allows for drastically reduced hydrogen release onset temperatures compared to the corresponding metal borohydrides, synthetic routes to pure materials are badly needed. Torben Jensen and co-workers introduced a low-temperature route from the metal halide, alkali metal borohydride and ammonia gas using dimethylsulfide solvent that could be practical with efficient recycling of the toxic solvent.[2] In light of our discovery of accompanying formation of ammonia-borane in thf solvent (**Chapter 3**), however, detailed investigations will be needed to see if similar reactions occur in SMe_2. If we assume that AB formation arises from nucleophilic abstraction of borane form the metal co-ordinated borohydride, this leaves behind a metal hydride that is likely to undergo further reaction with ammonia to generate hydrogen and a metal amide M-NH_2. If a single abstraction occurs, the resulting materials, such as those in **Chapter 3**, may also be promising hydrogen storage materials containing nearly equal numbers of N-H and B-H groups (Eq. 1). In fact mixtures of $LiNH_2$ and elected MBHs have been demonstrated by others to lower H_2 release temperatures and yield less volatile impurities.[3]

$$Y(BH_4)_3 + 4\ NH_3 \longrightarrow H_2 + Y(NH_2)(BH_4)_2(NH_3)_3 \qquad \text{Eq. 1}$$

Another fascinating aspect of the results of the work presented in **Chapter 3** is the different behaviour of the elements with regard to ammonia-borane formation. For the main group elements the trend (Zn << Ca < Mg < Al) correlated not with Lewis acidity but with electronegativity. From a thermodynamic viewpoint we can also compare the E-H bond energies (in kJ/mol)[4] (Zn:85 << Ca:167 < Mg:218 < Al:265) which also correlate reasonably well (Figure 6.1). Unique behaviour was also observed with the easily reduced transition metals such as Ti and V that produced sp^2 boron products, clearly warranting further investigation, including reaction monitoring with Electron Paramagnetic Resonance (EPR) spectroscopy. In work by our collaborator Professor Sean McGrady and his student, addition of $TiCl_3$ and 3 eq. of $LiBH_4$ in dimethylsulfoxide was claimed to give a near quantitative yield of ammonia-borane.

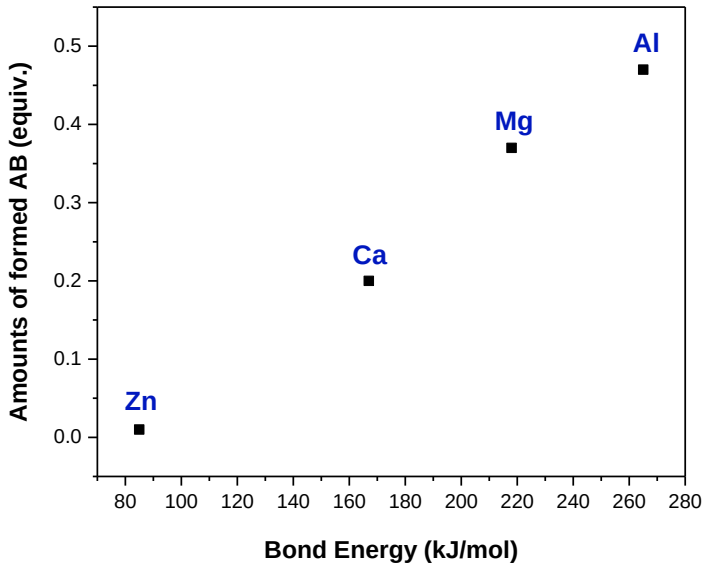

Figure 6.1. The correlation between the amounts of formed AB and the metal-hydride bond energies for (M= Zn, Ca, Mg, Al) in the reaction of ammonia with MCl_n + *n* $NaBH_4$ in thf at RT.

In **Chapter 4** pure samples of $(M(BH_4)_3(NH_3)_4$, M=Y, La) were obtained by reaction of purified $M(BH_4)_3$ with liquid ammonia at -50°C. To suppress ammonia release upon heating some novel BN-supported base-metal nanoparticle catalysts (MNPs) were prepared using liquid hexylamine-borane. Deposition of these MNPs onto solid Y and La AMBs gave a three-fold reduction of ammonia release for Y-AMB/Co NPs and a four-fold for La-AMB/Fe NPs composites. In spite of this improvement (98-99 mol% pure H_2), it was difficult to ensure full physical contact of every AMB particle to the added solid catalyst. While attempts to achieve this contact via use of an ionic liquid reaction medium proved unsuccessful, additional opportunities for improvement include: **I)** Dehydrogenation of nanoconfined AMBs in porous materials as reported by Yu et al. for $[Al(NH_3)_6](BH_4)_3$ in a polystyrene matrix,[5] could be applied to additional examples including the Y and La AMBs that contain the same number of N-H and B-H bonds; **II)** In-situ generation of MNP/NP composites, *i.e.* by ammonia treatment of $M(BH_4)_n$ in the presence of colloidal base metal NPs in solution at low temperatures or in liquid hexylamine-borane; **III)** Exploration of eutectic mixtures of AMBs with amine-boranes or metal amidoborates could generate liquid mixtures prior to significant H_2 loss. These lightweight mixtures may allow for ammonia suppression in the absence of heavier catalysts; **IV)** Detailed mechanistic studies of H_2 loss from AMBs by combining detailed

vibrational and multinuclear MAS NMR spectroscopic monitoring (^{139}La, ^{2}H [$(BD_4)^-$ or ND_3] and ^{15}N) with DFT calculations.

Following up on the unique property of Zn in producing only trace AB in the reaction of $ZnCl_2$ with 2 equiv. of $NaBH_4$ in thf at room temperature, investigations on solution synthesis of Zn-AMBs products were detailed in **Chapter 5**. In contrast to solid-state synthetic routes that yielded neutral $Zn(BH_4)_3(NH_3)_2$ (+ 2 equiv. of LiCl) from $ZnCl_2(NH_3)_2$ + 2 equiv. of $LiBH_4$, our work showed that solution routes lead invariably to double-cation borohydride products such as $M^IZn(BH_4)_3$ and likely even $M^IZn_2(BH_4)_5$ (M^I = Li, Na, K) even when sub-stoichiometric amounts of borohydride were employed. Consequently, while addition of ammonia gas to the thf solution, yielded $KZn(BH_4)_3(NH_3)_3$ in high yields without the formation of AB, some contamination by KBH_4 was unavoidable. In contrast, $M^IZn(BH_4)_3$ prepared from $LiBH_4$ or $NaBH_4$ afforded a mixture of the $M^IZn(BH_4)_3(NH_3)_n$ salt and neutral $Zn(BH_4)_2(NH_3)_2$. Using 5 wt.% FeNPs resulted in a fourfold reduction in the amount of released ammonia which led to a more pure hydrogen stream (98.9 mol%) compared to the uncatalyzed thermolysis (97.0 mol%). Moreover, ^{11}B MAS NMR results suggest a different decomposition pathway to that observed for Y and La. Ongoing research on this project should include a Rietveld analysis of powder X-ray data for $KZn(BH_4)_3(NH_3)_3$.

6.4. Final Remarks

Even though inexpensive and widely available renewable sources of hydrogen are not yet available, the thermodynamics of water splitting and non-toxic nature of the hydrogen and oxygen produced point to the importance of hydrogen in our future energy mix. Our work has focused primarily on catalysis solutions for hydrogen generation with a focus on portable power applications. While borohydride hydrolysis generates a pure H_2 stream at a rate controlled by the catalyst, the need for more long-lived catalysts and efficient separation of the borate by-products remains.

Our work on solution generation of pure ammine metal borohydrides uncovered an important side-reaction of AB formation that could even play a role in their H_2 release mechanisms. We showed additionally that catalysts can suppress ammonia formation even though it is not apparent that the final dehydrogenated material is any different than that obtained from the uncatalyzed thermolysis.

Although it is generally accepted that H_2 release from AMBs originates from a combination of N-H and B-H bonds, additional studies with labeled borohydride and

ammonia are needed to evaluate the released gas as a function of temperature. In addition, the utility of AMBs as versatile H_2 sources will also likely depend on effective chemical regeneration protocols such as that developed for AB.[6]

Since the work presented in this Thesis was being conducted over the past 5 years, magnificent progress has been made in the synthesis and chemistry of AMBs as novel dihydrogen-bonded solid materials. Ongoing research will likely also take advantage of their multi-functional chemical properties.

6.5. References

(1) Paskevicius, M.; Jepsen, L. H.; Schouwink, P.; Cerny, R.; Ravnsbaek, D. B.; Filinchuk, Y.; Dornheim, M.; Besenbacher, F.; Jensen, T. R. *Chem. Soc.Rev.* **2017**, *46*, 1565-1634.
(2) Jepsen, L. H.; Ley, M. B.; Černý, R.; Lee, Y.-S.; Cho, Y. W.; Ravnsbæk, D.; Besenbacher, F.; Skibsted, J.; Jensen, T. R. *Inorg. Chem.* **2015**, *54*, 7402-7414.
(3) Klebanoff, L.; In: *Hydrogen Storage Technology: Materials and Applications* CRC Press: New York, pp 133-212, **2016**.
(4) Wiberg, N.; Holleman, A. F.; Wiberg, E.; In: *Inorg. Chem.* Academic Press: San Diego, CA, p. 256, **2001**.
(5) Tang, Z.; Tan, Y.; Chen, X.; Ouyang, L.; Zhu, M.; Sun, D.; Yu, X. *Angew. Chem. Int. Ed.* **2013**, *52*, 12659-12663.
(6) Sutton, A. D.; Burrell, A. K.; Dixon, D. A.; Garner, E. B.; Gordon, J. C.; Nakagawa, T.; Ott, K. C.; Robinson, J. P.; Vasiliu, M. *Science* **2011**, *331*, 1426-1429.

Solution NMR Data

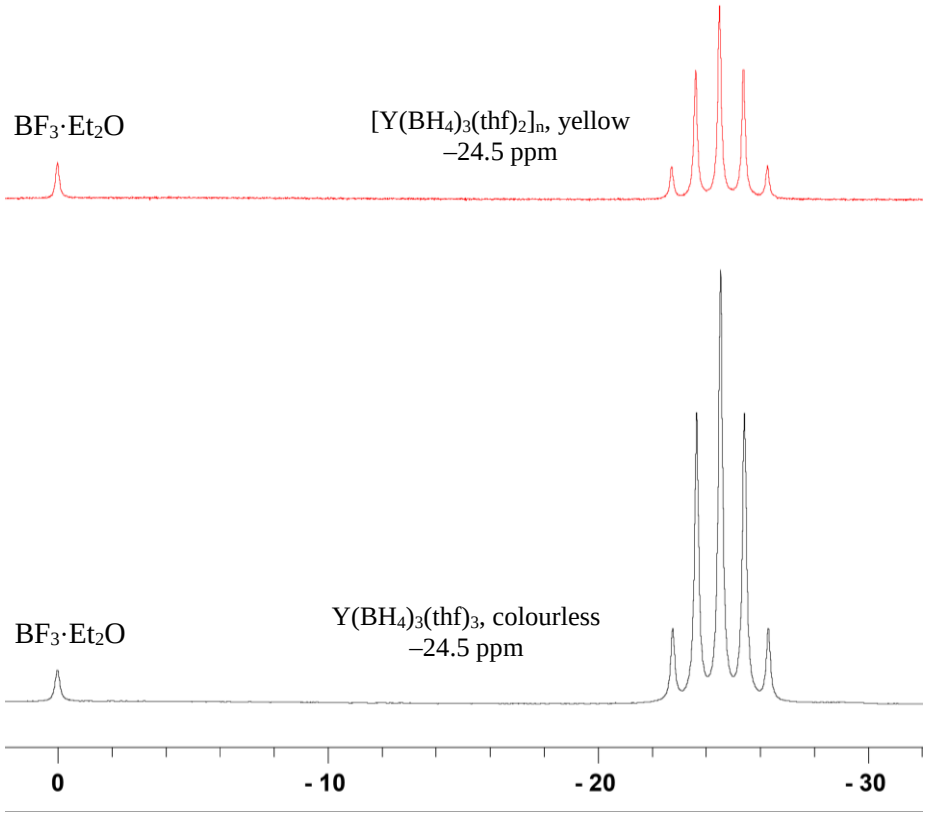

Figure. A1.1. $^{11}B\{^{1}H\}$ NMR (96 MHz, C_6D_6) spectra of $Y(BH_4)_3(thf)_3$ and $[Y(BH_4)_3(thf)_2]_n$ in toluene in the presence of $BF_3{\cdot}OEt_2$ internal standard in a glass capillary.

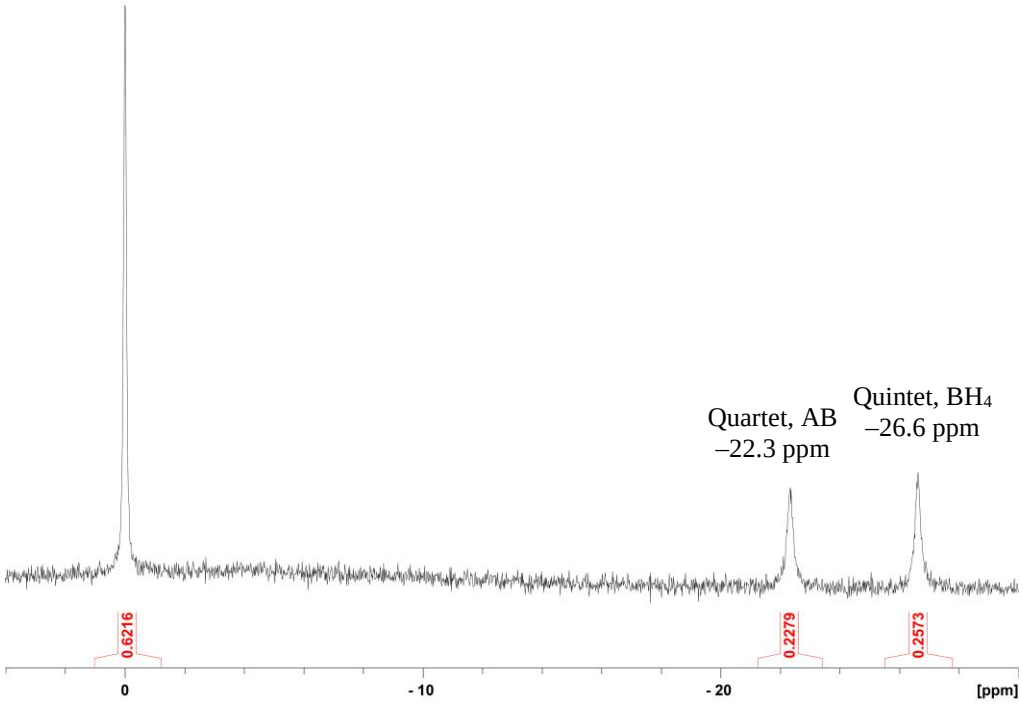

Figure A1.2. $^{11}B\{^{1}H\}$ NMR (96 MHz, C_6D_6) spectrum of the thf filtrate from the reaction of ammonia gas with pure $Y(BH_4)_3(thf)_3$. Resonance at 0 ppm is from $BF_3{\cdot}OEt_2$ in a glass capillary.

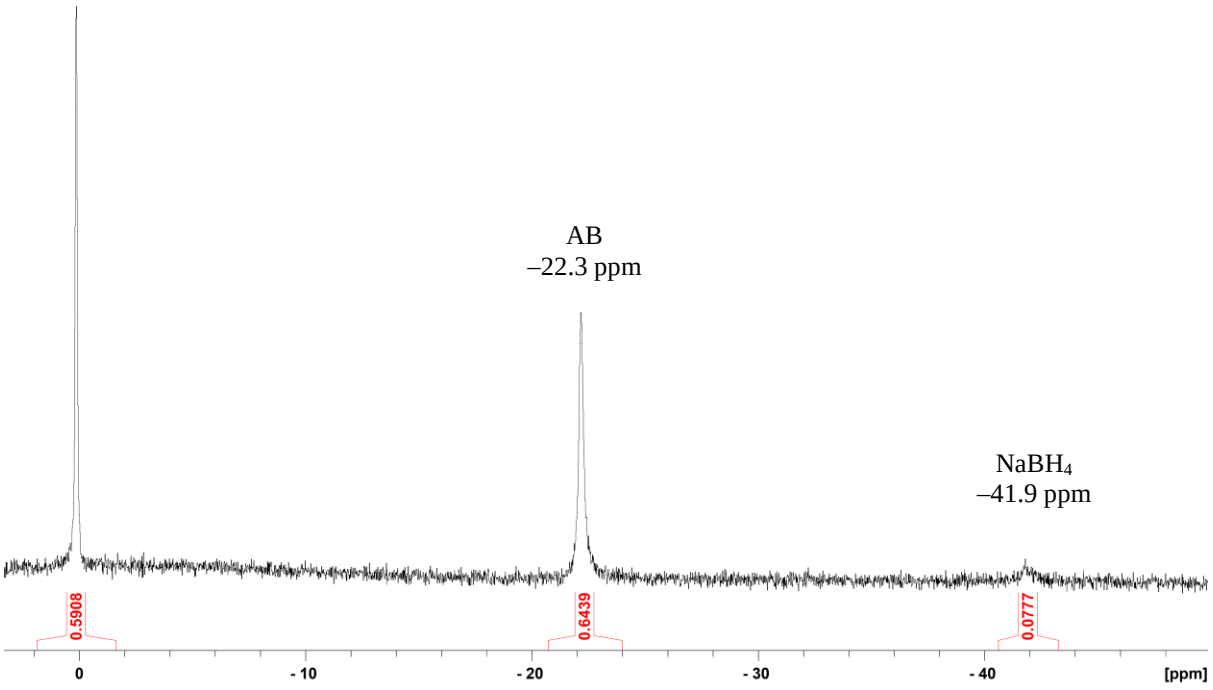

Figure A1.3. $^{11}B\{^{1}H\}$ NMR (96 MHz, C_6D_6) of the reaction of ammonia with a 1:3 mixture of YCl_3 and $NaBH_4$ in thf.

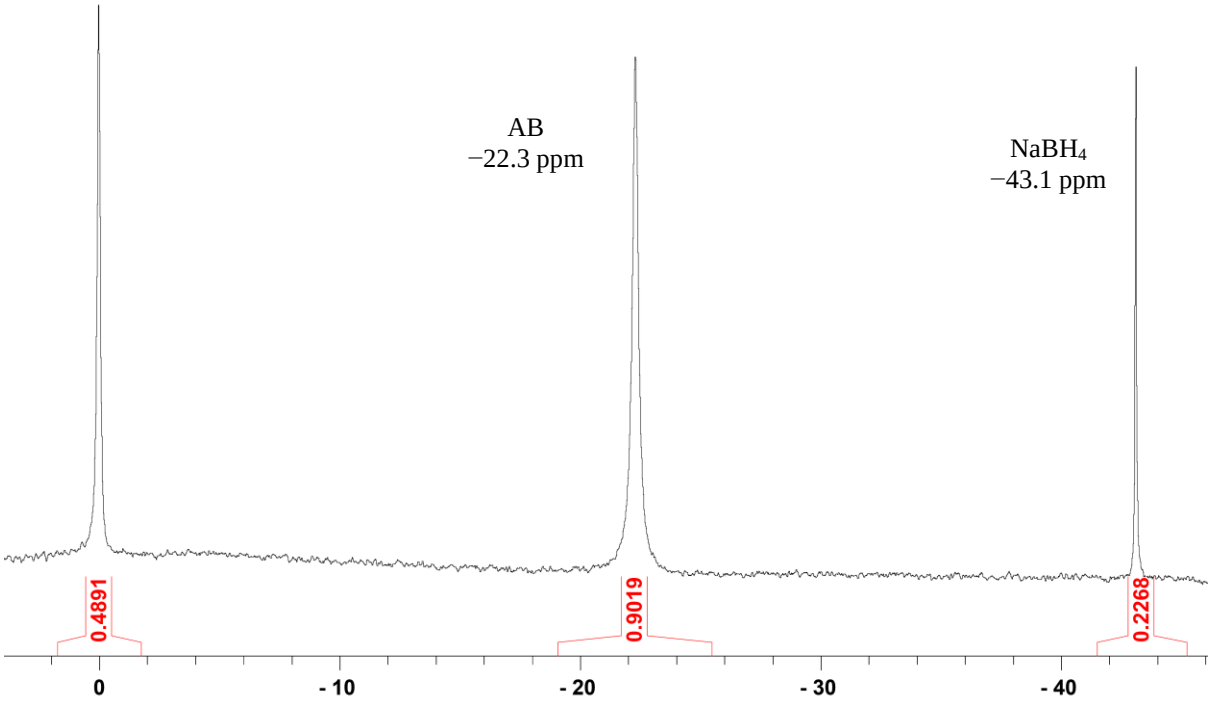

Figure A1.4. $^{11}B\{^{1}H\}$ NMR (96 MHz, C_6D_6) spectrum of the thf filtrate from the reaction of $MgCl_2$ and $NaBH_4$ with ammonia.

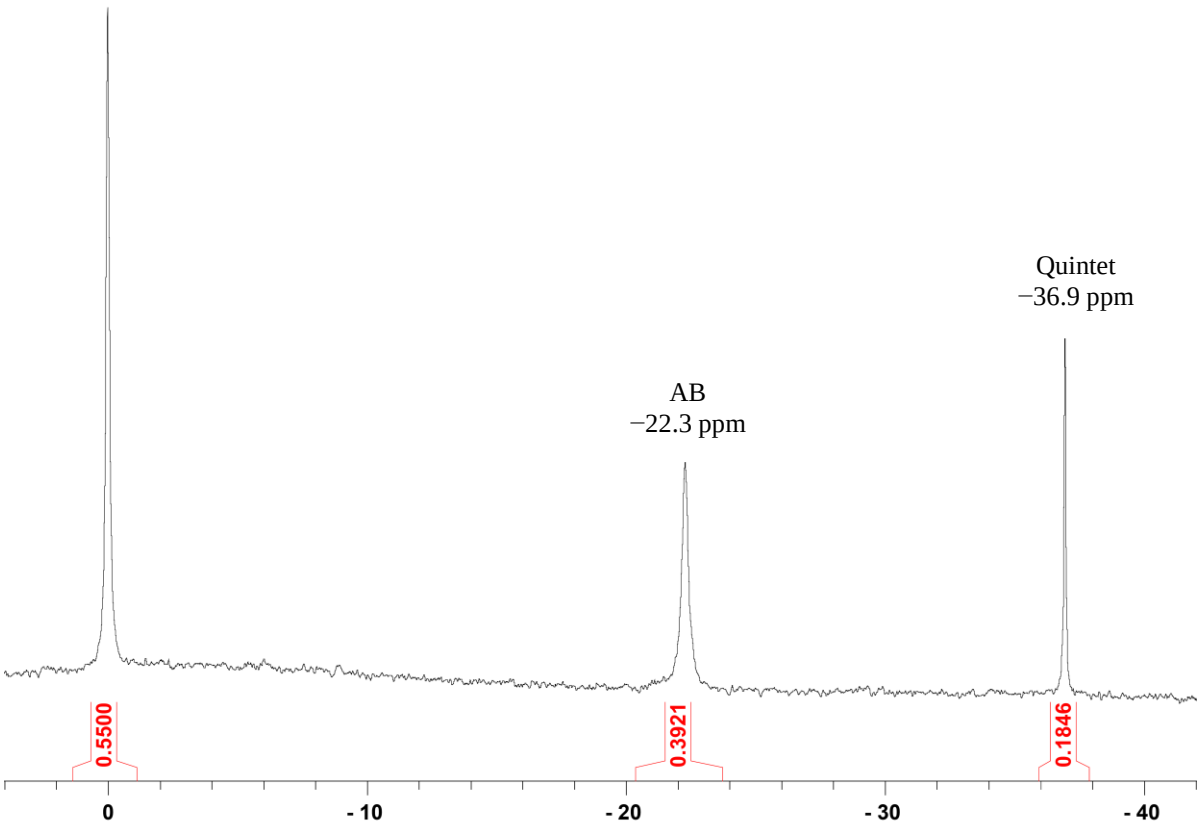

Figure A1.5. $^{11}B\{^{1}H\}$ NMR (96 MHz, C_6D_6) spectrum of the thf filtrate from the reaction of $CaCl_2$ and $NaBH_4$ with ammonia.

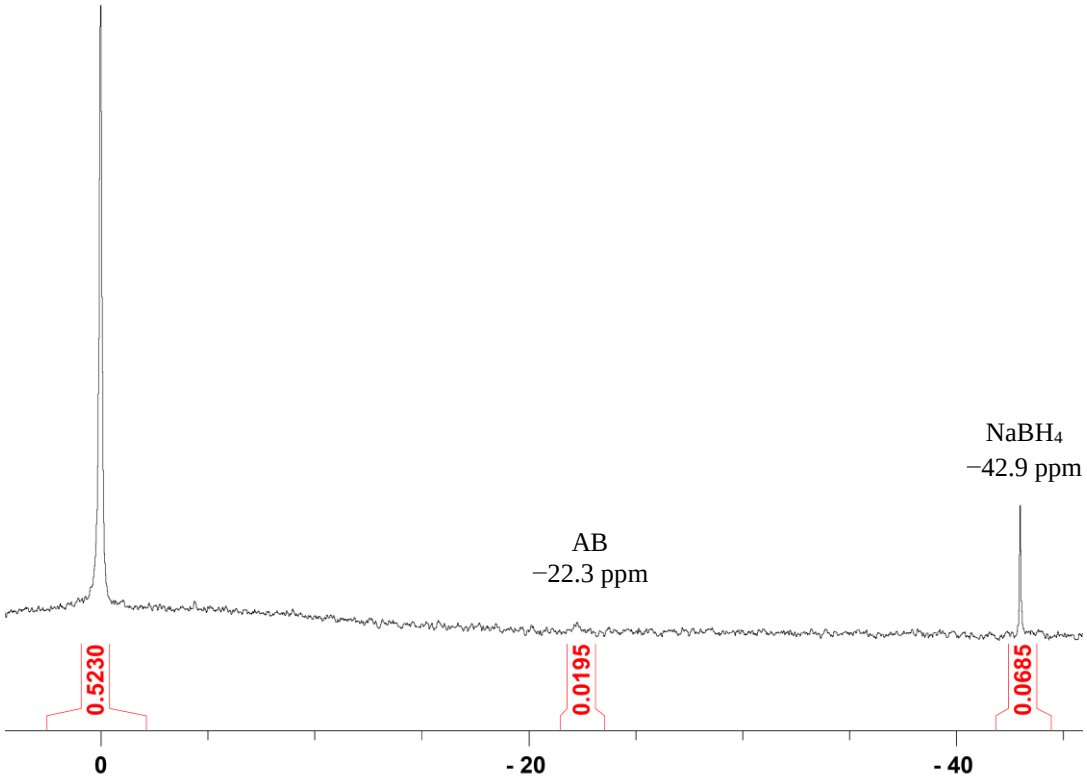

Figure A1.6. $^{11}B\{^{1}H\}$ NMR (96 MHz, C_6D_6) spectrum of the thf filtrate from the reaction of $ZnCl_2$ and $NaBH_4$ with ammonia.

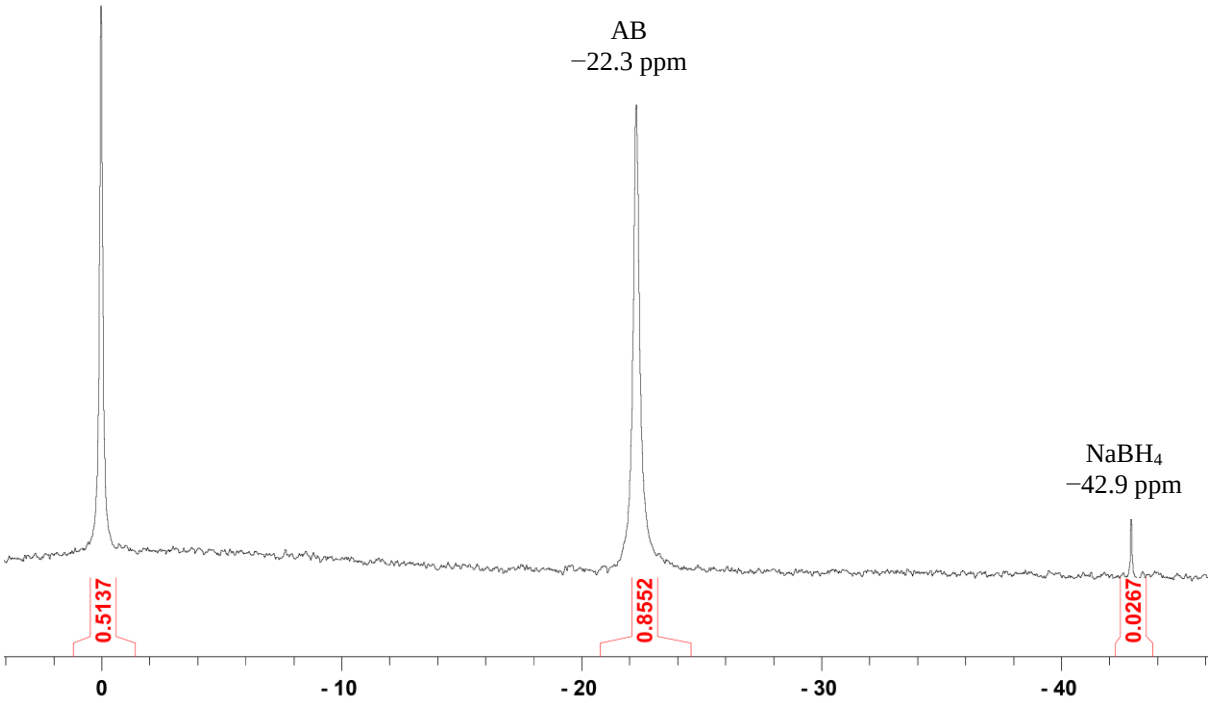

Figure A1.7. $^{11}B\{^{1}H\}$ NMR (96 MHz, C_6D_6) spectrum of the thf filtrate from the reaction of $AlCl_3$ and $NaBH_4$ with ammonia.

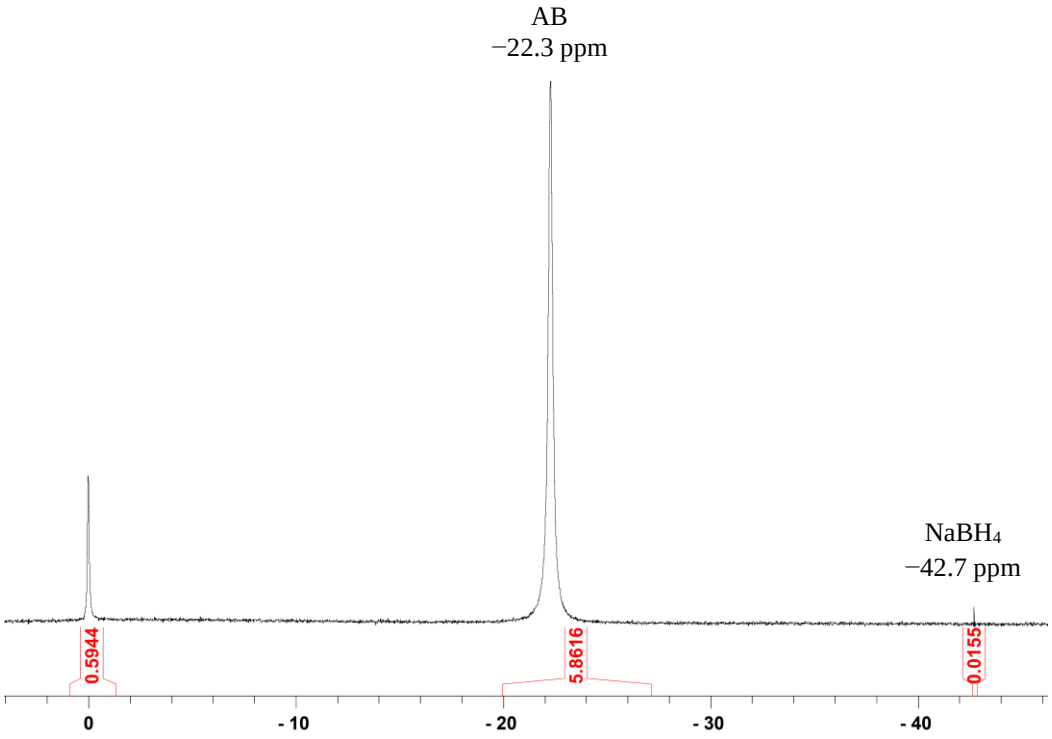

Figure A1.8. $^{11}B\{^{1}H\}$ NMR (96 MHz, C_6D_6) spectrum of the thf filtrate from the reaction of $TiCl_3$ and $NaBH_4$ with ammonia.

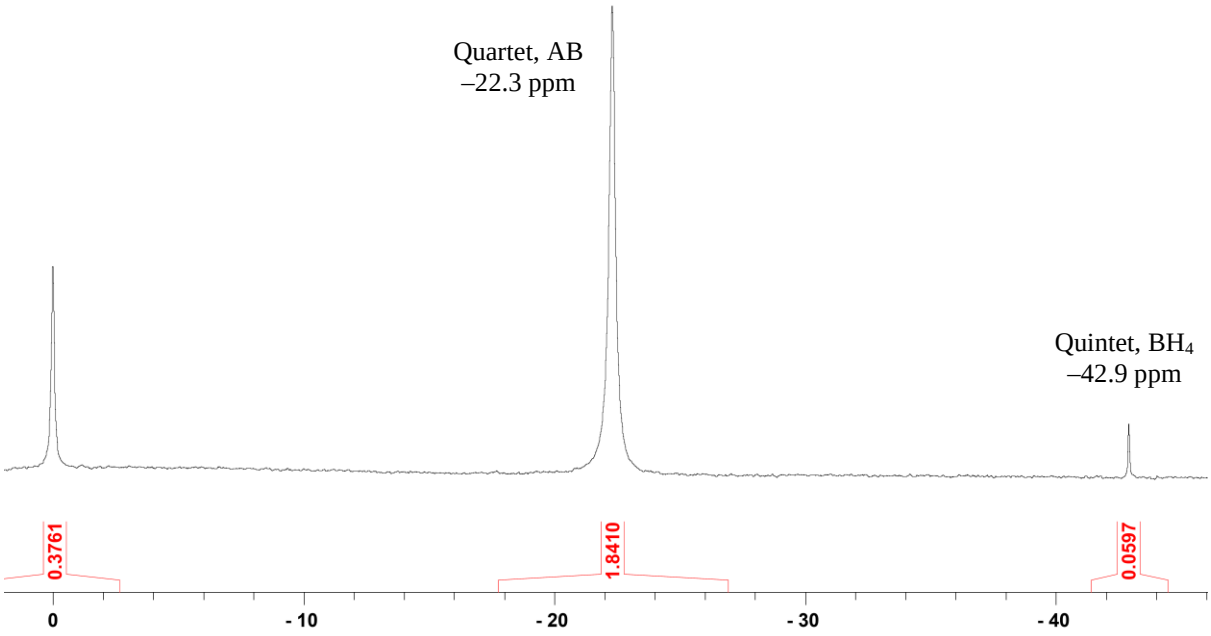

Figure A1.9. $^{11}B\{^{1}H\}$ NMR (96 MHz, C_6D_6) spectrum of the thf filtrate from the reaction of VCl_3 and $NaBH_4$ with ammonia.

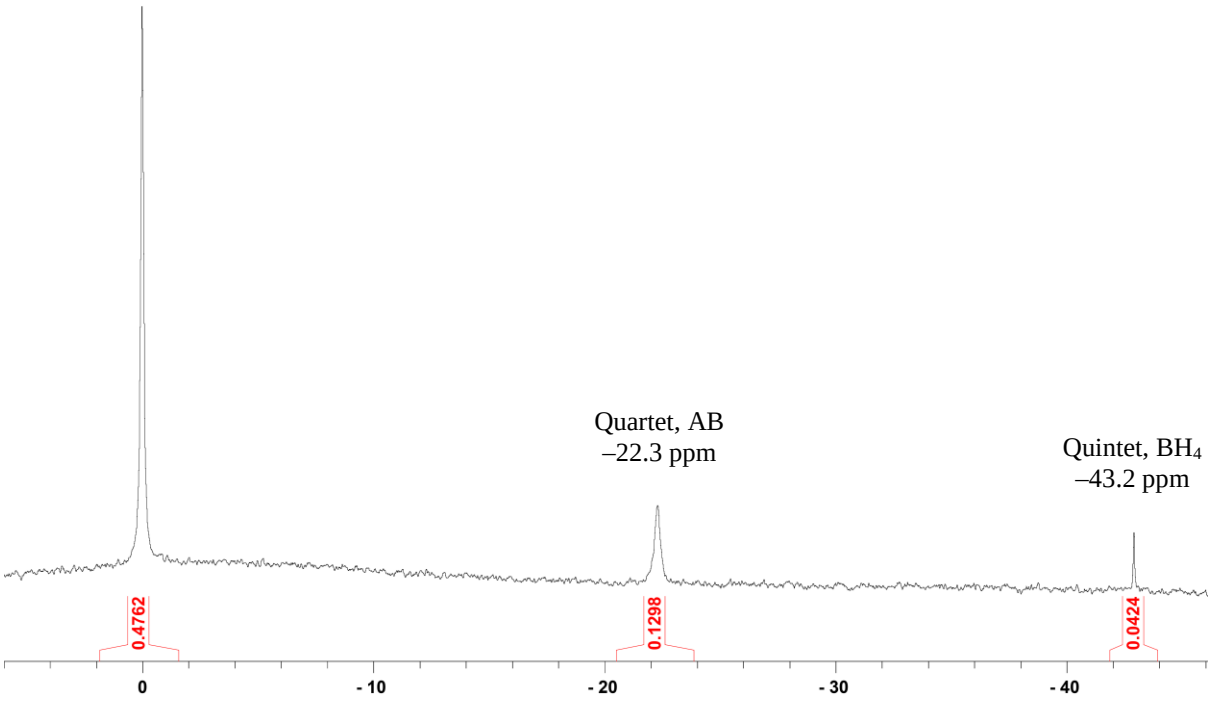

Figure A1.10. $^{11}B\{^{1}H\}$ NMR (96 MHz, C_6D_6) spectrum of the thf filtrate from the reaction of $LaCl_3$ and $NaBH_4$ with ammonia.

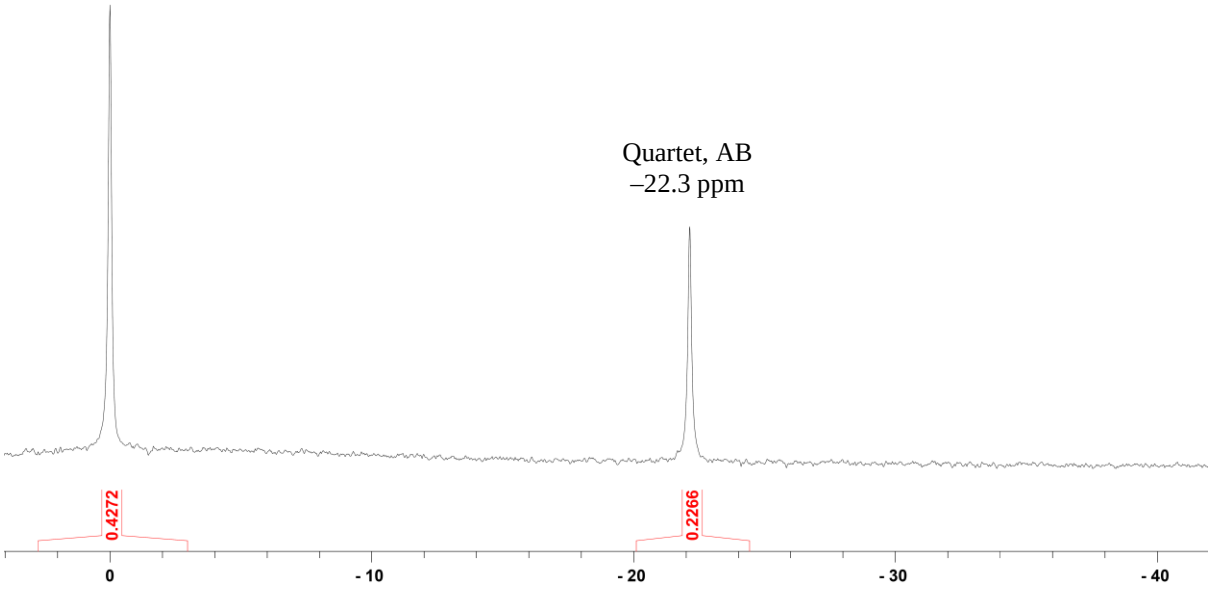

Figure A1.11. $^{11}B\{^{1}H\}$ NMR (96 MHz, C_6D_6) spectrum of the CH_2Cl_2 filtrate from the reaction of YCl_3 and $NaBH_4$ with ammonia.

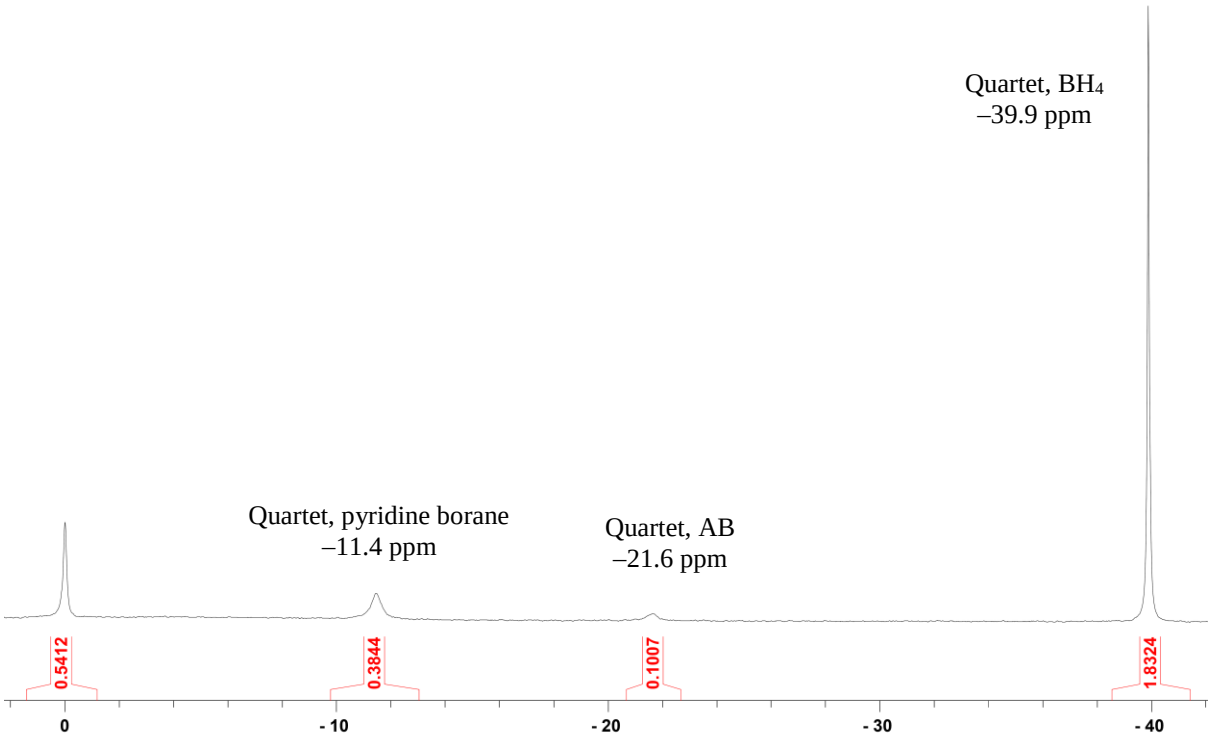

Figure A1.12. $^{11}B\{^{1}H\}$ NMR (96 MHz, C_6D_6) spectrum of the pyridine filtrate from the reaction of YCl_3 and $NaBH_4$ with ammonia.

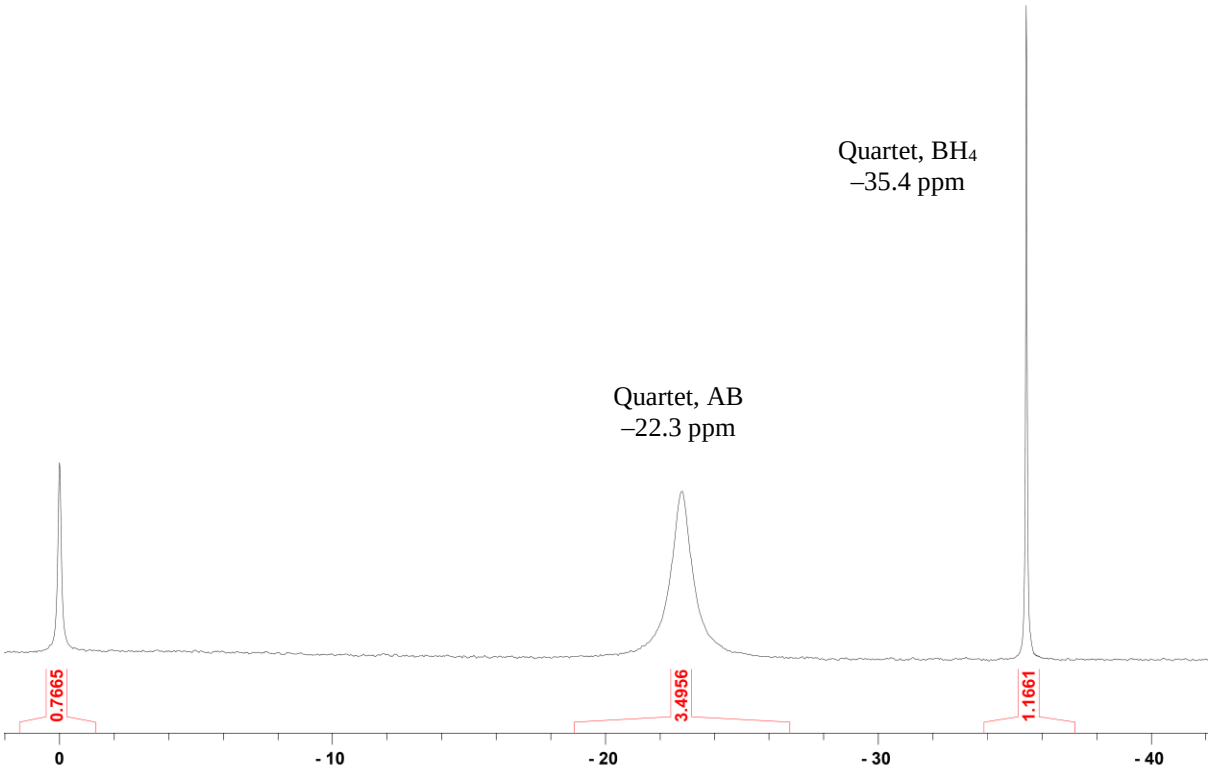

Figure A1.13. $^{11}B\{^{1}H\}$ NMR (96 MHz, C_6D_6) spectrum of the dimethyl sulfoxide filtrate from the reaction of YCl_3 and $NaBH_4$ with ammonia.

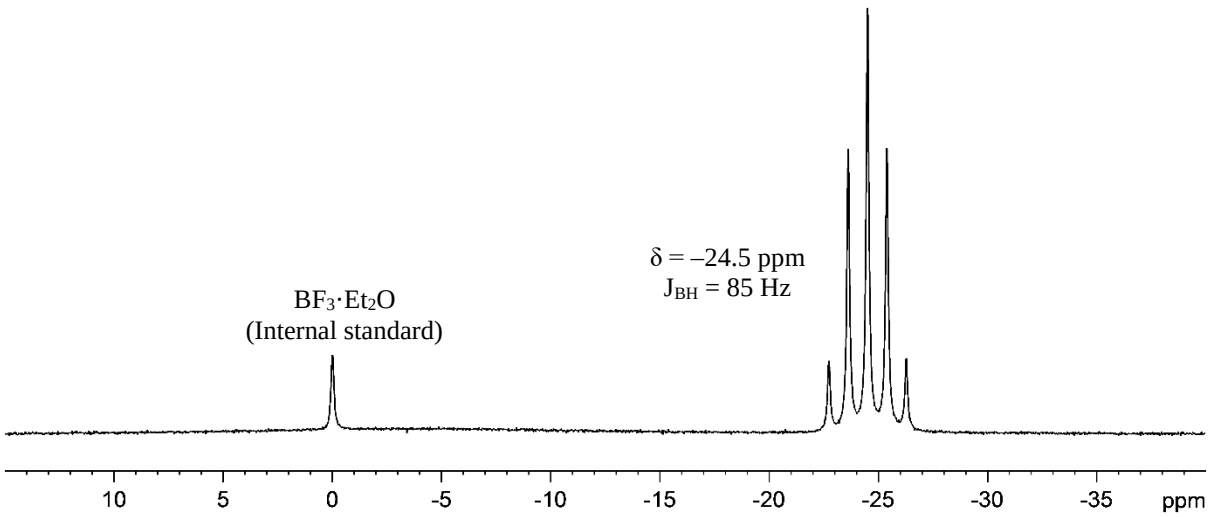

Figure A1.14. ^{11}B NMR spectrum (96 MHz, C_6D_6) of $Y(BH_4)_3(thf)_2$ in toluene.

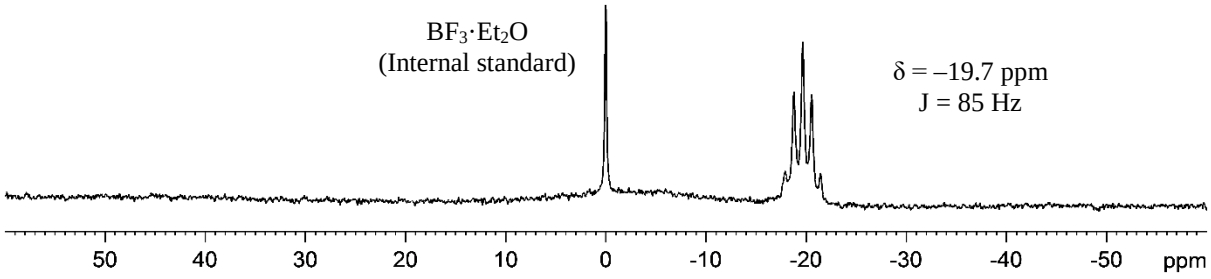

Figure A1.15. ^{11}B NMR spectrum (96 MHz, C_6D_6) of $La(BH_4)_3(thf)_3$ in toluene.

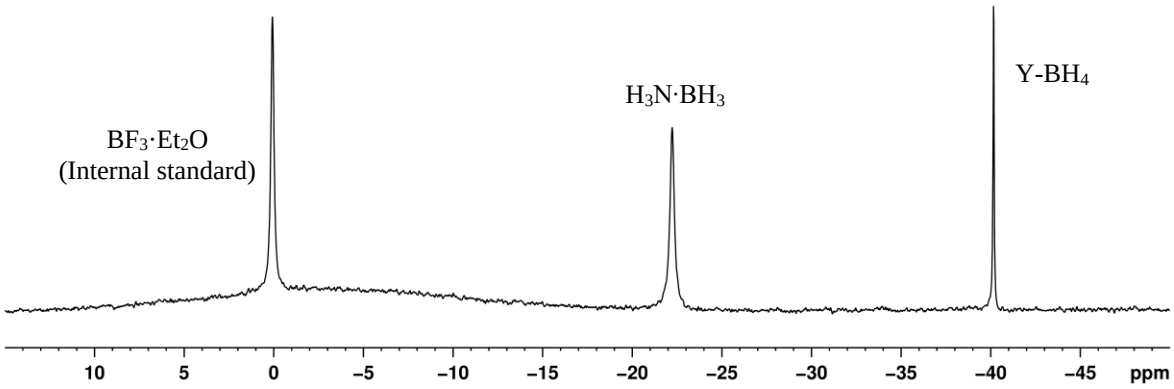

Figure A1.16. $^{11}B\{^1H\}$ NMR spectrum (96 MHz, C_6D_6) of the solution obtained from heating $Y(BH_4)_3(NH_3)_4$ in boiling thf for 18 hours.

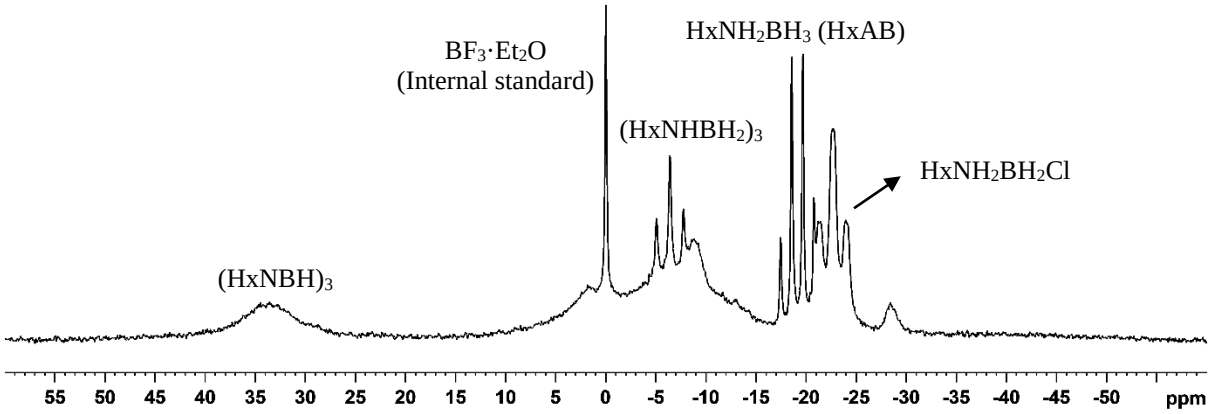

Figure A1.17. ^{11}B NMR spectrum (96 MHz, C_6D_6) of overnight reaction of neat HxAB with $FeCl_2$.

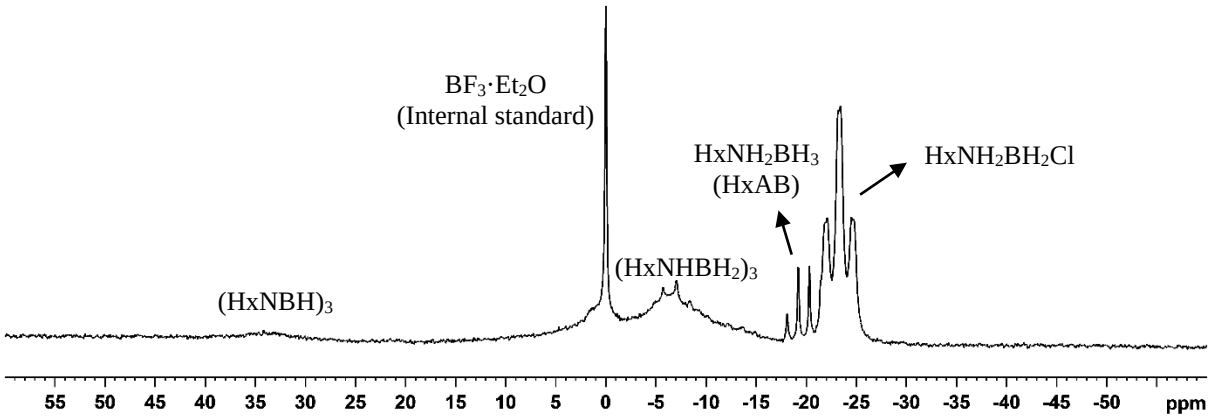

Figure A1.18. ^{11}B NMR spectrum (96 MHz, C_6D_6) of overnight reaction of neat HxAB with $CoCl_2$.

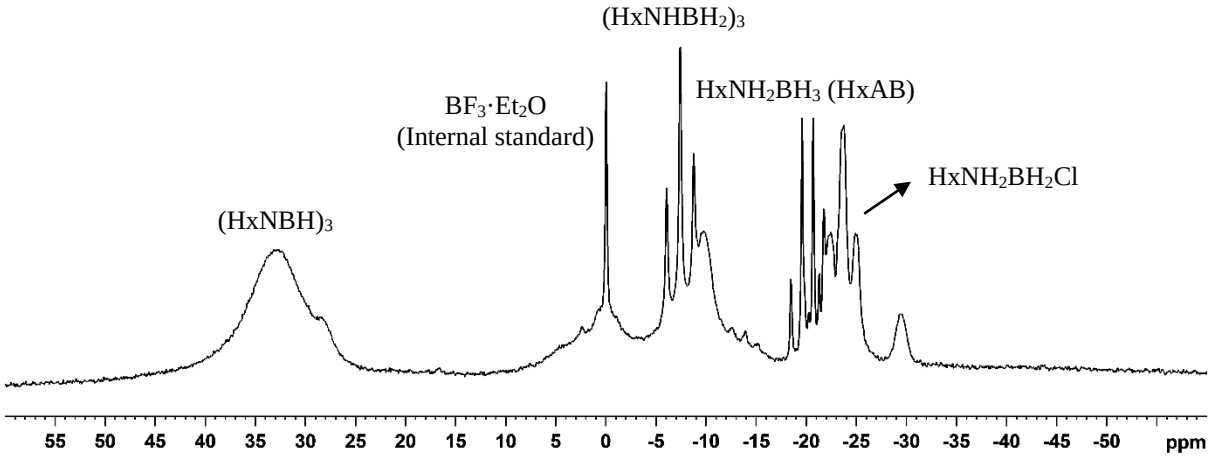

Figure A1.19. ^{11}B NMR spectrum (96 MHz, C_6D_6) of overnight reaction of neat HxAB with $CuCl_2$.

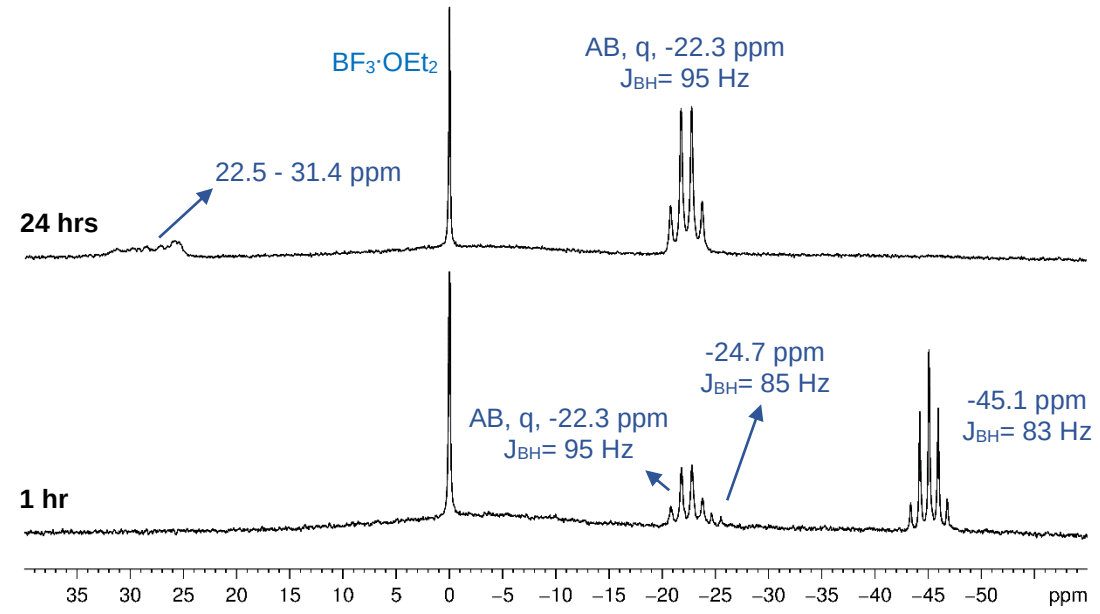

Figure A1.20. ^{11}B NMR (96 MHz, C_6D_6) spectrum of the solution obtained after RT stirring of **Zn-4** with 1 mol% $(RhClcod)_2$.

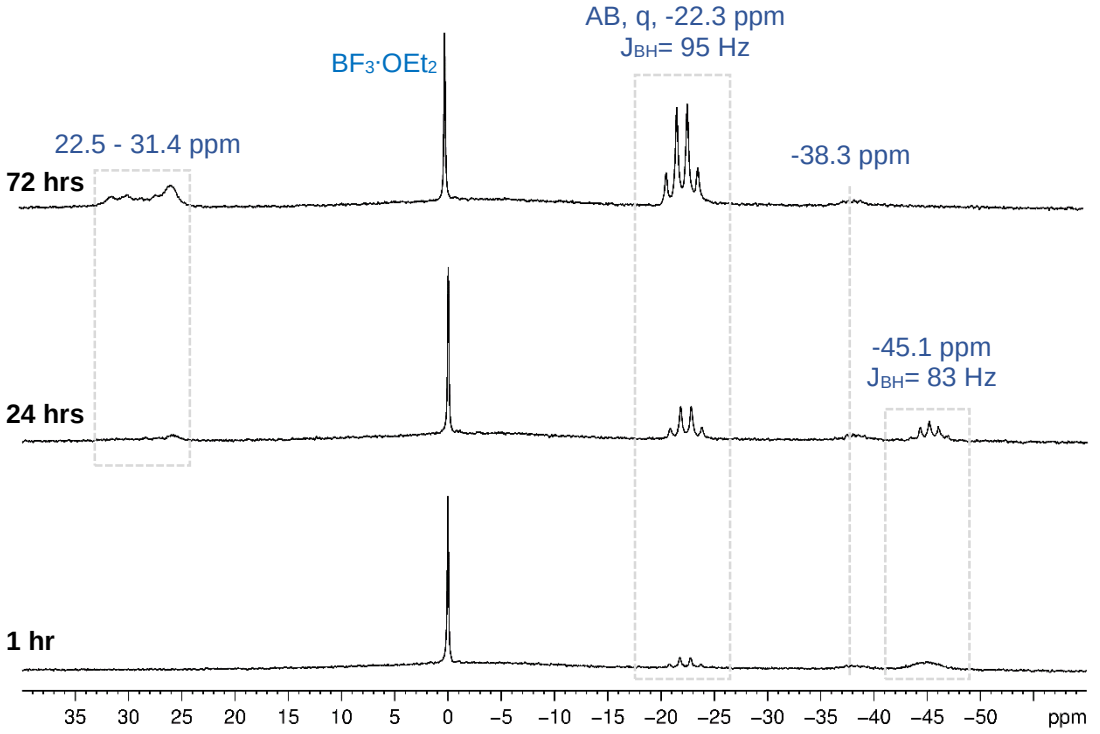

Figure A1.21. ^{11}B NMR (96 MHz, C_6D_6) spectrum of the solution obtained after RT stirring of **Zn-4** with 1 mol% of the Wilkinson's catalyst.

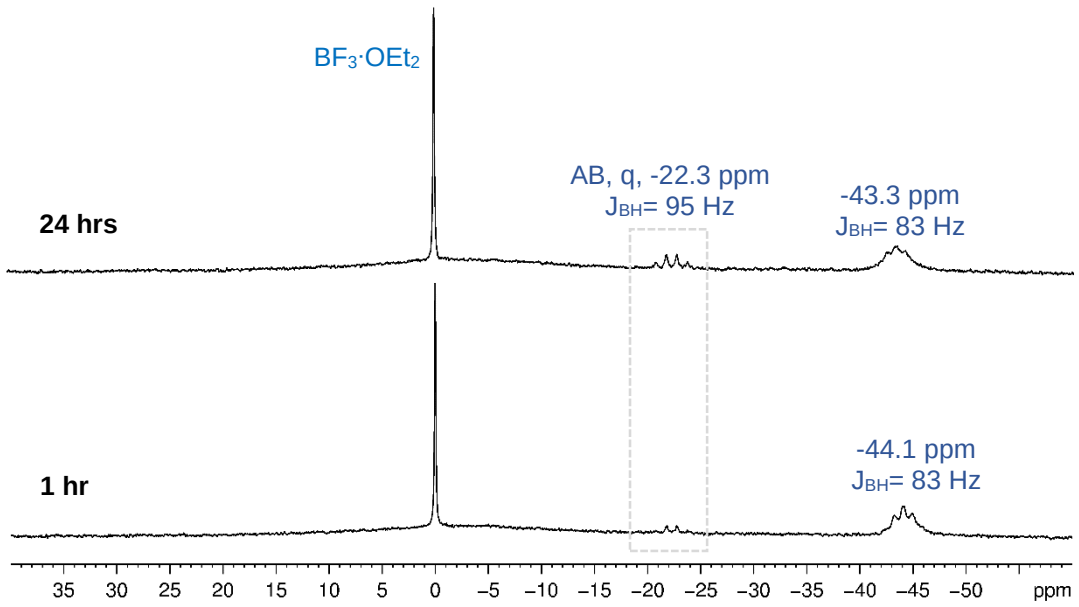

Figure A1.22. ^{11}B NMR (96 MHz, C_6D_6) spectrum of the solution obtained after RT stirring of **Zn-4** with 1 mol% of Ir-POCOP-H_2.

Magic Angle Spinning (MAS) NMR Data

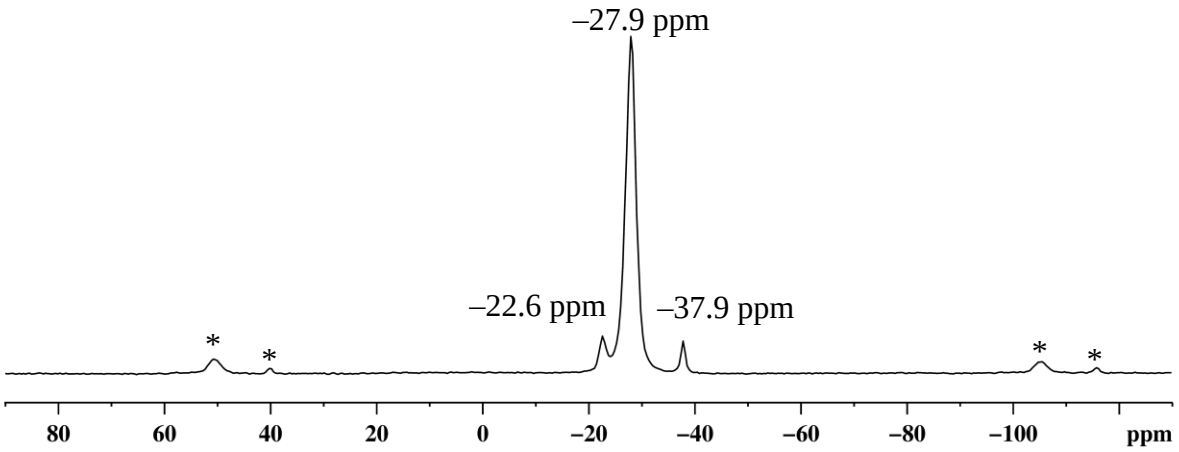

Figure A2.1. ^{11}B MAS NMR (128 MHz) spectrum of the solid 2 isolated from the reaction of ammonia and $Y(BH_4)_3(thf)_3$ in thf (* spinning sidebands).

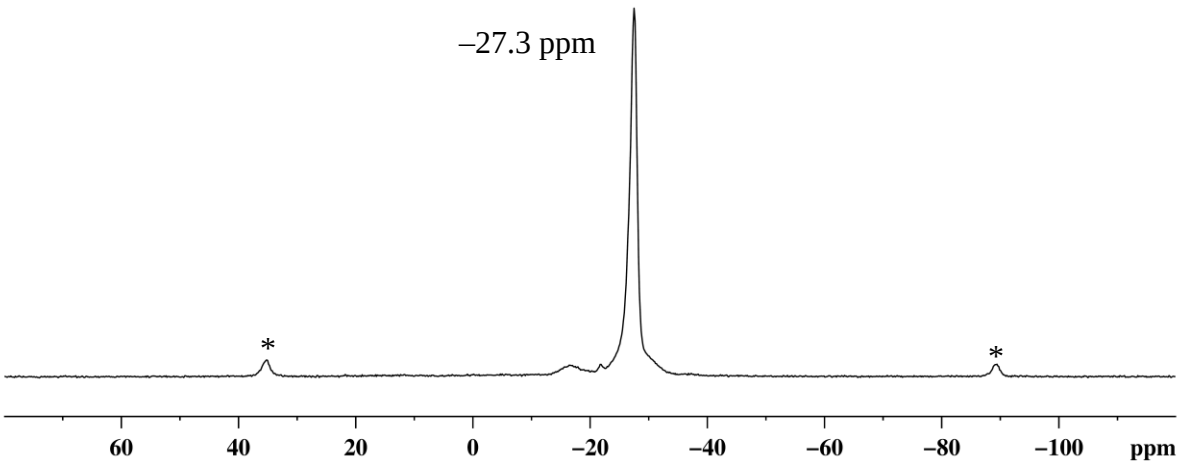

Figure A2.2. ^{11}B MAS NMR (160 MHz) spectrum of $Y(BH_4)_3(NH_3)_4$ (1) prepared through the reaction of pure $[Y(BH_4)_3(thf)_3]_n$ in liquid ammonia at –50 °C (* spinning sidebands).

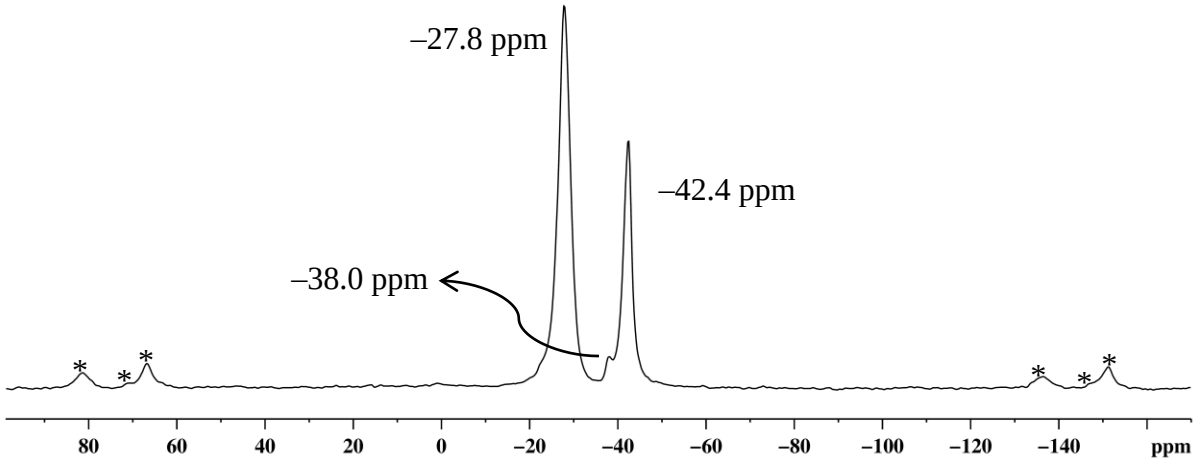

Figure A2.3. ^{11}B MAS NMR (128 MHz) spectrum of the solid 3 isolated from the reaction of ammonia and a 1:3 ratio of YCl_3 and $NaBH_4$ in thf (* spinning sidebands).

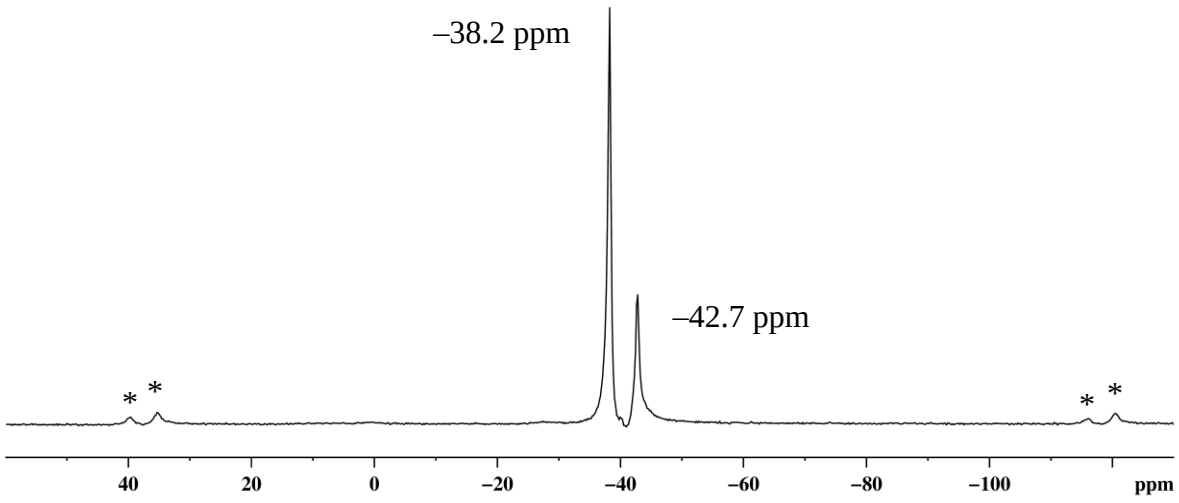

Figure A2.4. ^{11}B MAS NMR (128 MHz) spectrum of the thf filtrate from the reaction of $MgCl_2$ and $NaBH_4$ (1:2) with ammonia (* spinning sidebands).

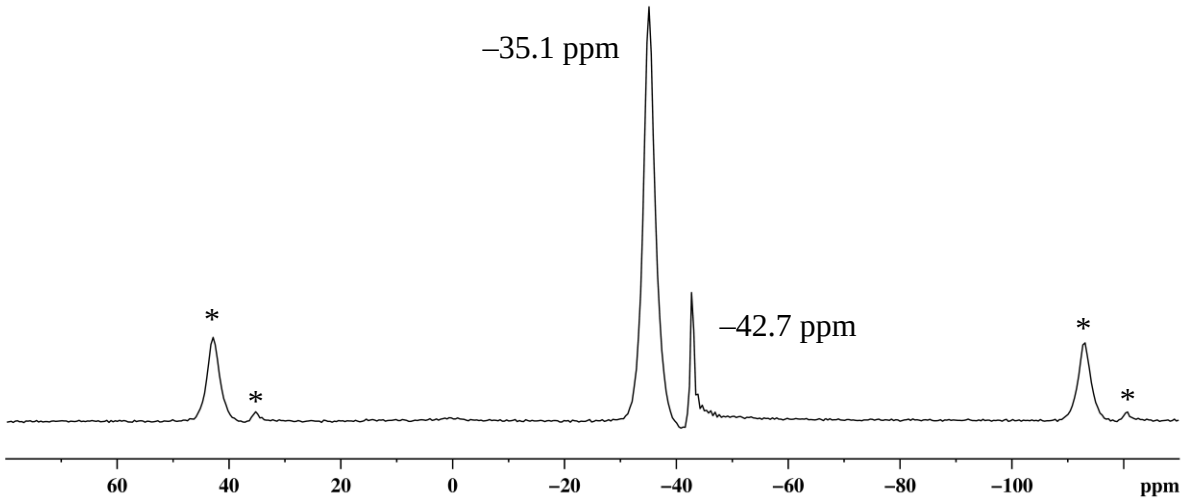

Figure A2.5. ^{11}B MAS NMR (128 MHz) spectrum of the solid isolated from the reaction of ammonia and a 1:2 ratio of $CaCl_2$ and $NaBH_4$ in thf (* spinning sidebands).

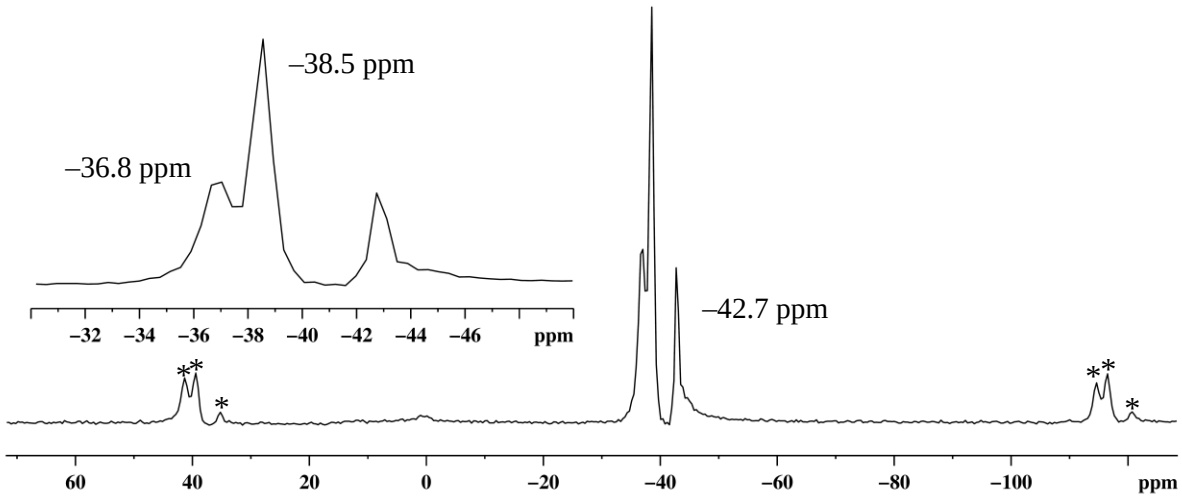

Figure A2.6. ^{11}B MAS NMR (128 MHz) spectrum of the solid isolated from the reaction of ammonia and a 1:2 ratio of $ZnCl_2$ and $NaBH_4$ in thf (* spinning sidebands).

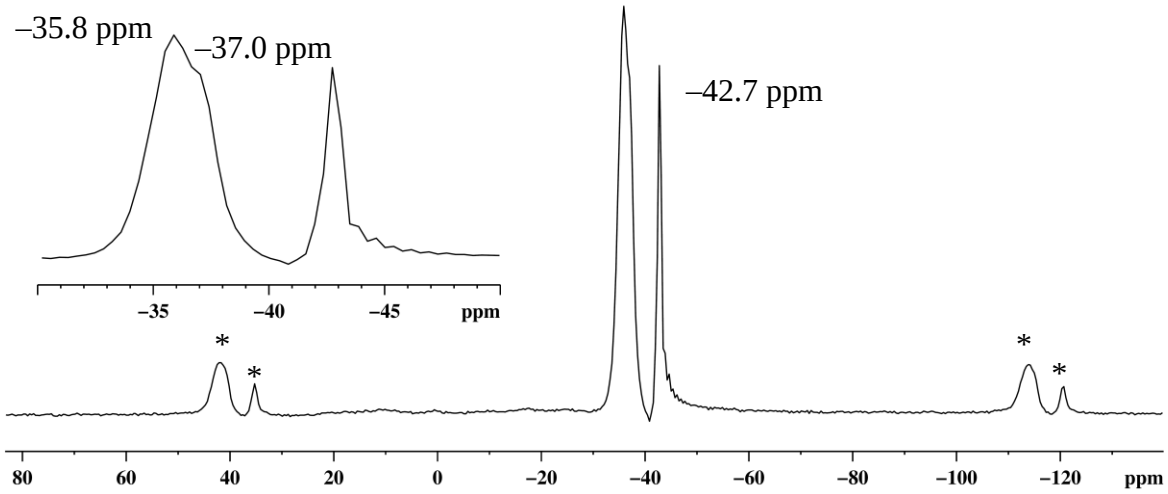

Figure A2.7. ^{11}B MAS NMR (128 MHz) spectrum of the solid isolated from the reaction of ammonia and a 1:3 ratio of of $AlCl_3$ and $NaBH_4$ in thf (* spinning sidebands).

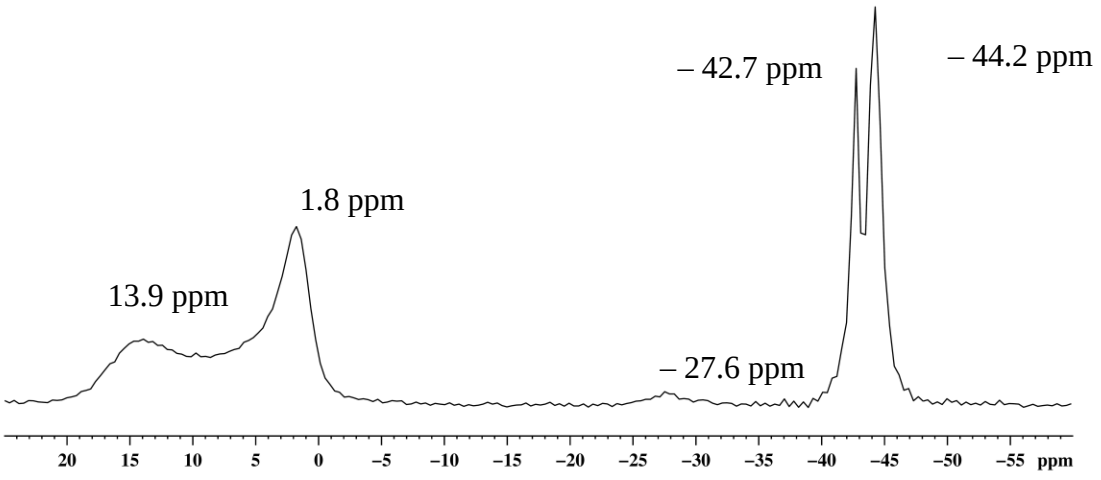

Figure A2.8. ^{11}B MAS NMR (128 MHz) spectrum of the solid isolated from the reaction of ammonia and a 1:3 ratio of $TiCl_3$ and $NaBH_4$ in thf.

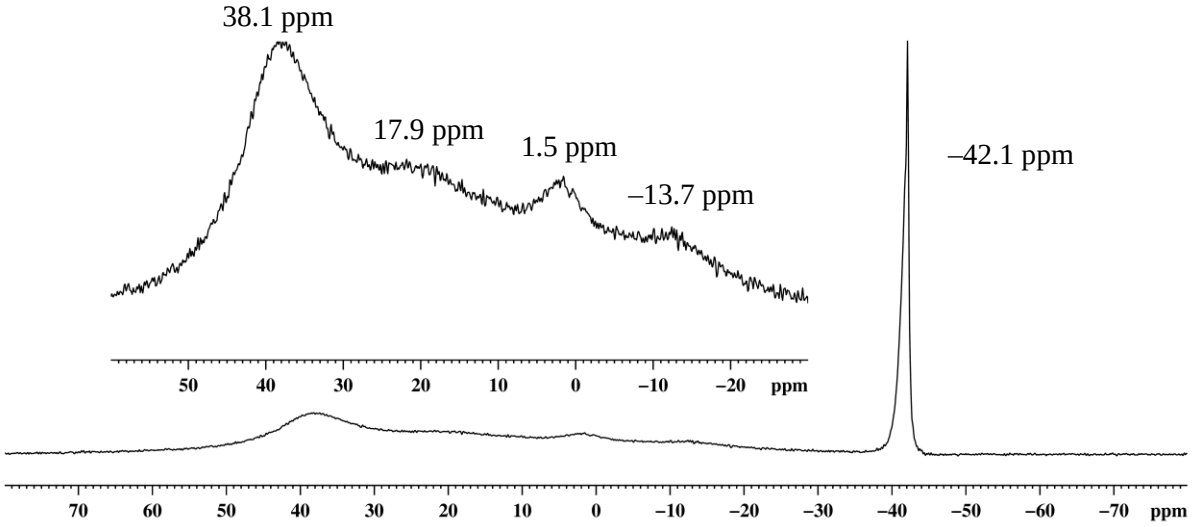

Figure A2.9. ^{11}B MAS NMR (160 MHz) spectrum of the solid isolated from the reaction of ammonia and a 1:3 ratio of VCl_3 and $NaBH_4$ in thf.

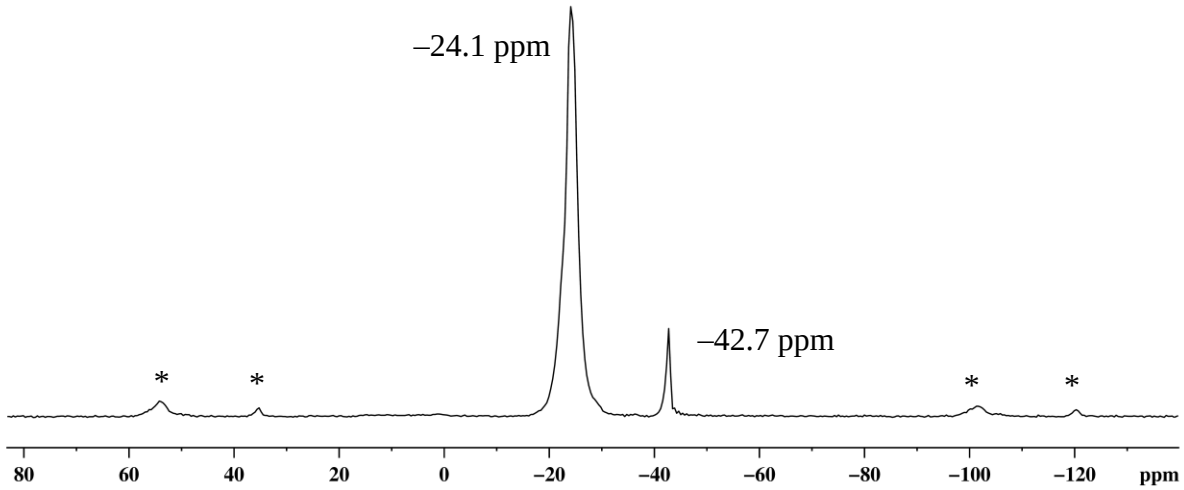

Figure A2.10. ^{11}B MAS NMR (128 MHz) spectrum of the solid isolated from the reaction of ammonia and a 1:3 ratio of $LaCl_3$ and $NaBH_4$ with ammonia (* spinning sidebands).

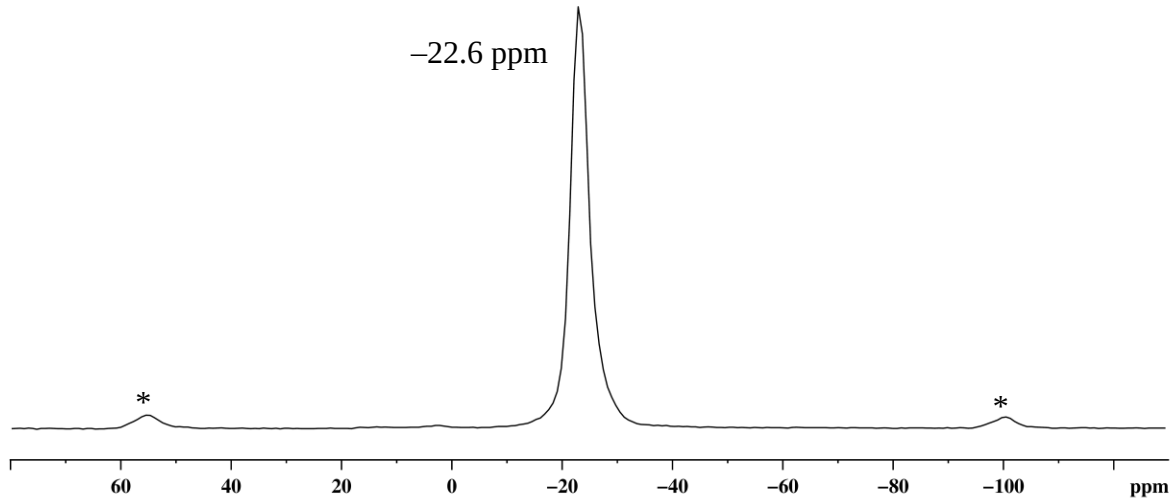

Figure A2.11. ^{11}B MAS NMR (128 MHz) spectrum of $La(BH_4)_3(NH_3)_4$ prepared through the reaction of pure $La(BH_4)_3(thf)_3$ in liquid ammonia at –50 °C (* spinning sidebands).

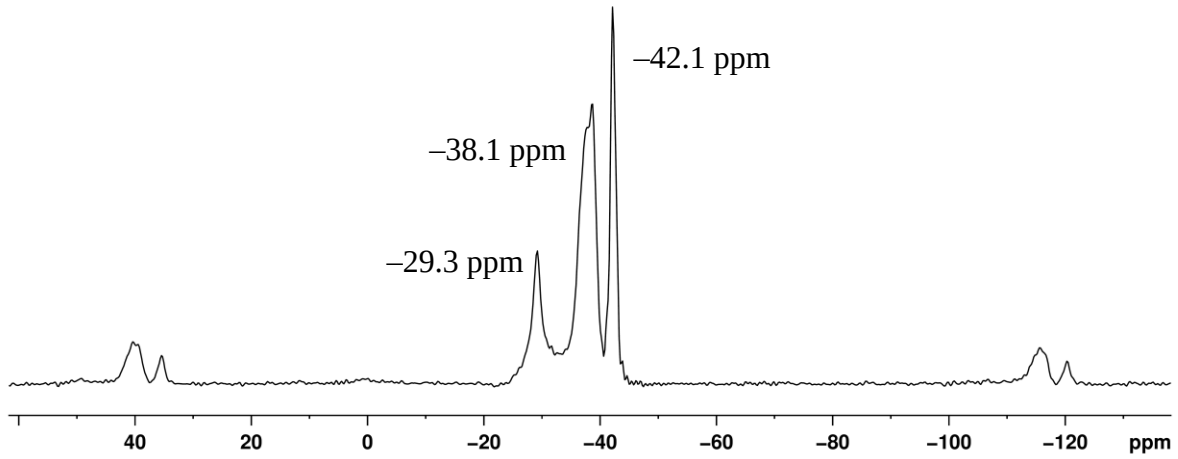

Figure A2.12. ^{11}B MAS NMR (128 MHz) spectrum of the solid isolated from the reaction of ammonia and a 1:3 ratio of YCl_3 and $NaBH_4$ in CH_2Cl_2 (* spinning sidebands).

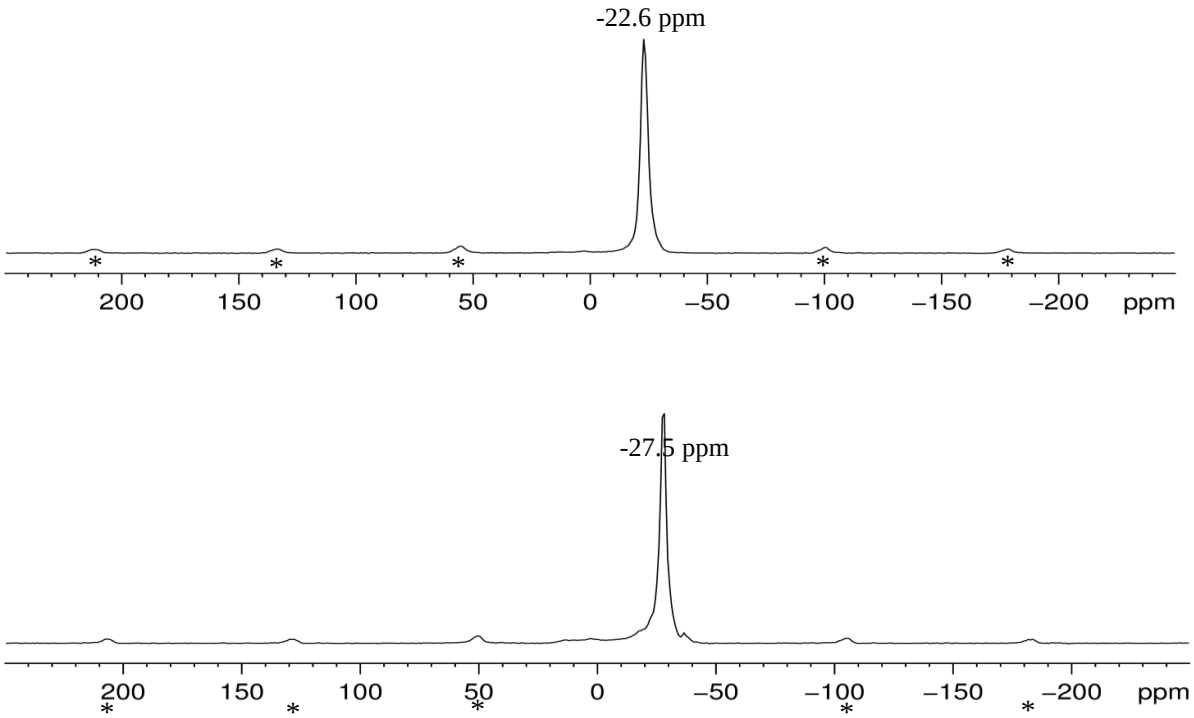

Figure A2.13. Solid state ^{11}B MAS NMR spectra (128 MHz, υ_R= 10 KHz) of fresh $Y(BH_4)_3(NH_3)_4$ (bottom) and $La(BH_4)_3(NH_3)_4$ (top) obtained from the reaction of $Y(BH_4)_3{\cdot}2thf$ and $La(BH_4)_3{\cdot}3thf$ with liquid NH_3 at –50 °C for 4 h. (* = spinning side bands).

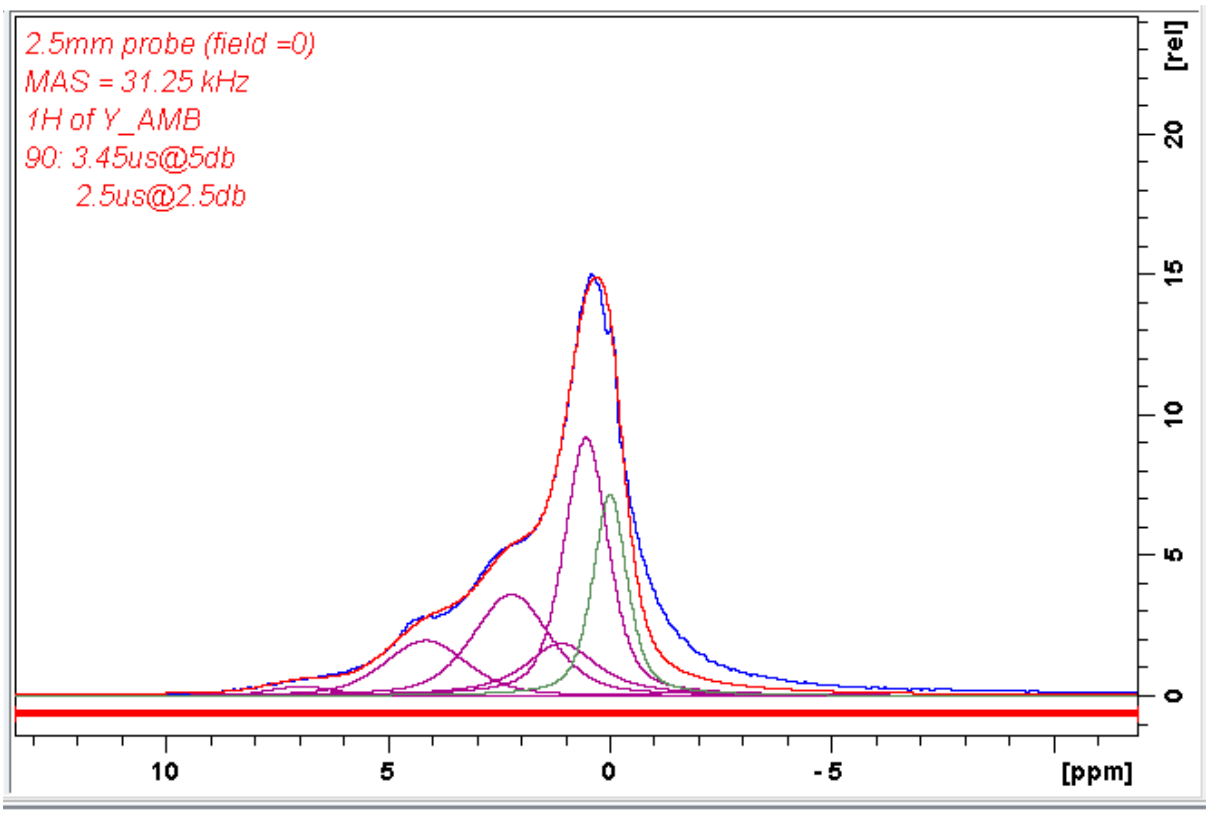

Figure A2.14. Deconvolution of the ^{1}H MAS NMR (500 MHz, υ_R= 31.25 KHz) of pure $Y(BH_4)_3(NH_3)_4$ using TopSpin 3.0. The red line is the fitted spectrum while the blue line is the spectrum obtained from the spectrometer. The simulated sites and their information are summarized in the table below.

Site	Chemical Shift (ppm)	Integral (#H)	Assigned Group	# of units
1	4.2	3.01	NH_3	1
2	2.3	5.85	NH_3	2
3	1.1	2.98	NH_3	1
4	0.6	8.06	BH_4	2
5	0.0	4.15	BH_4	1

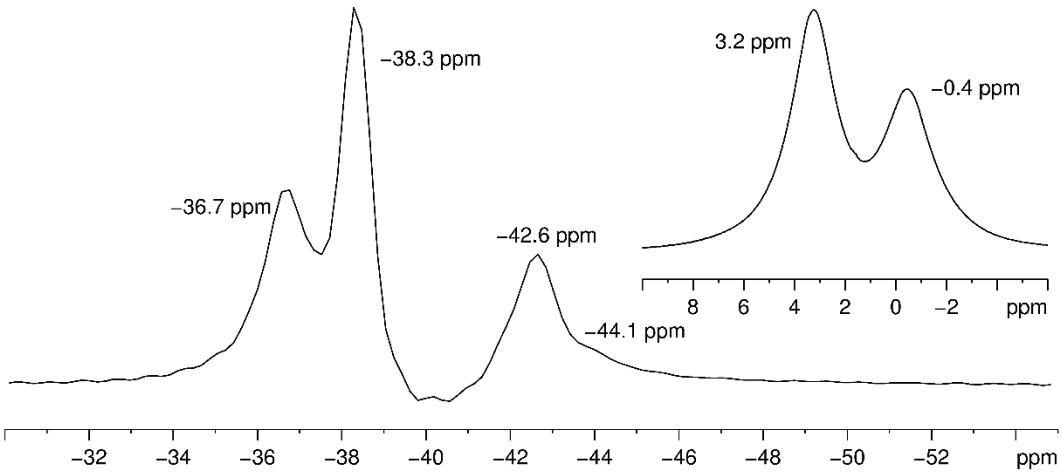

Figure A2.15. ^{11}B MAS NMR (128 MHz, ν_R= 10 KHz) spectrum of the solid which was isolated after the addition of ammonia to a solution filtrate of 1:2 $ZnCl_2$ and $NaBH_4$ in thf at RT. Inset: ^{1}H MAS NMR (400 MHz, ν_R= 10 KHz) of the same sample.

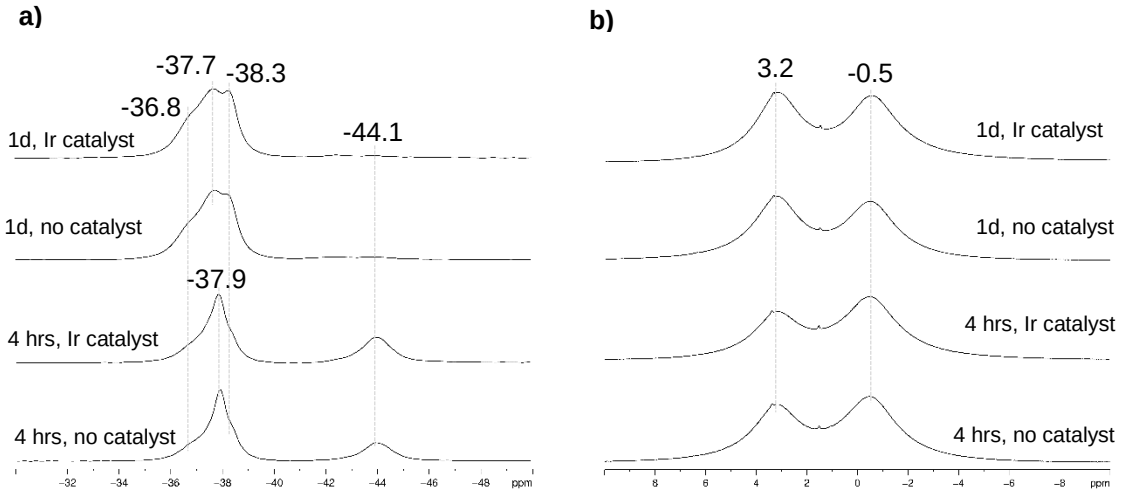

Figure A2.16. ^{11}B MAS NMR (128 MHz, ν_R= 10 KHz) spectrum of the solid which was isolated after the addition of ammonia to a solution filtrate of 1:2 $ZnCl_2$ and $NaBH_4$ in thf at RT. Inset: ^{1}H MAS NMR (400 MHz, ν_R= 10 KHz) of the same sample.

FT-IR Spectra

All FT-IR spectra were recorded as Nujol mulls between NaCl plates.

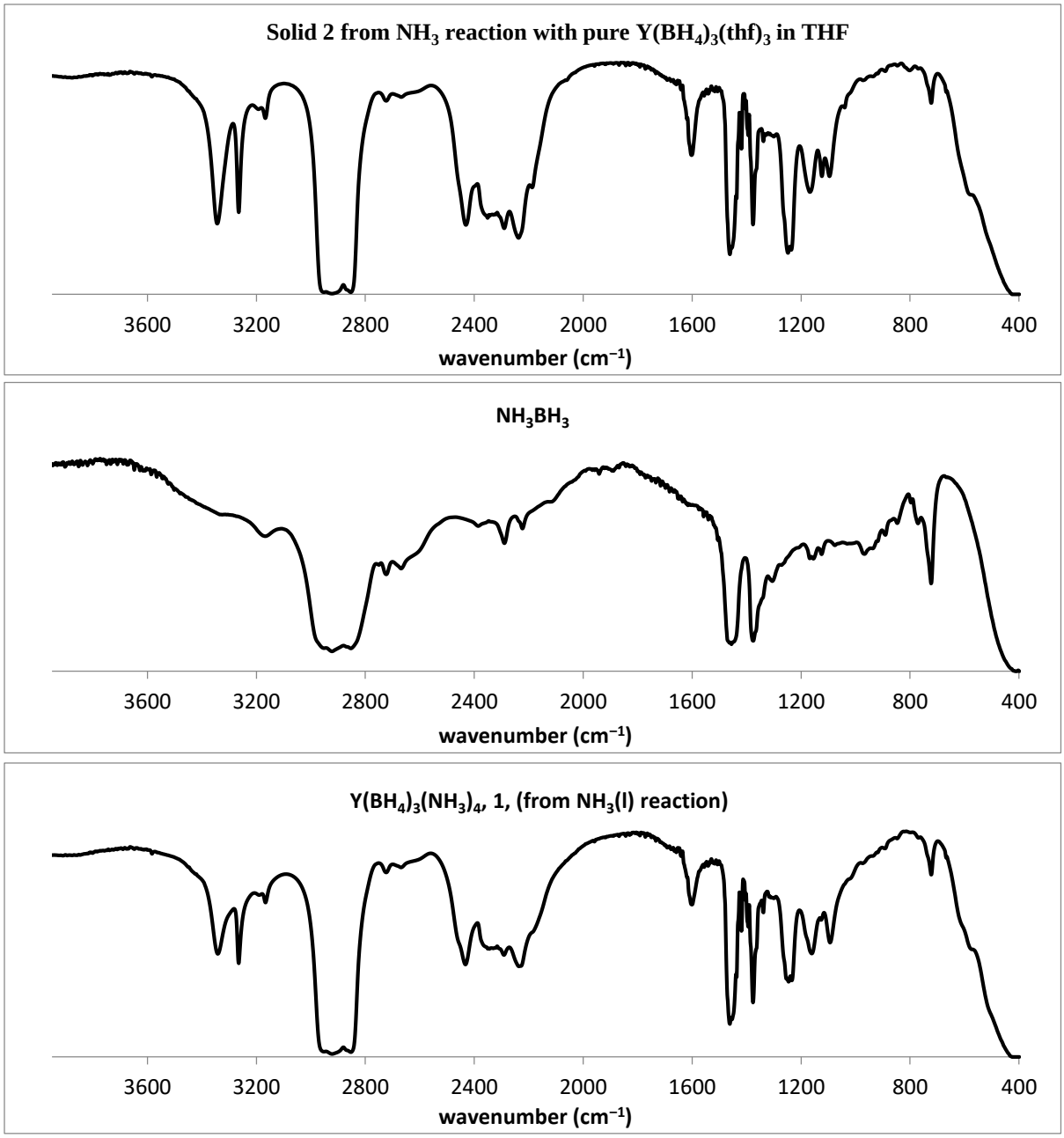

Figure A3.1. Comparison of FT-IR spectra of solid 2, ammonia-borane and pure $Y(BH_4)_3(NH_3)_4$ (**1**).

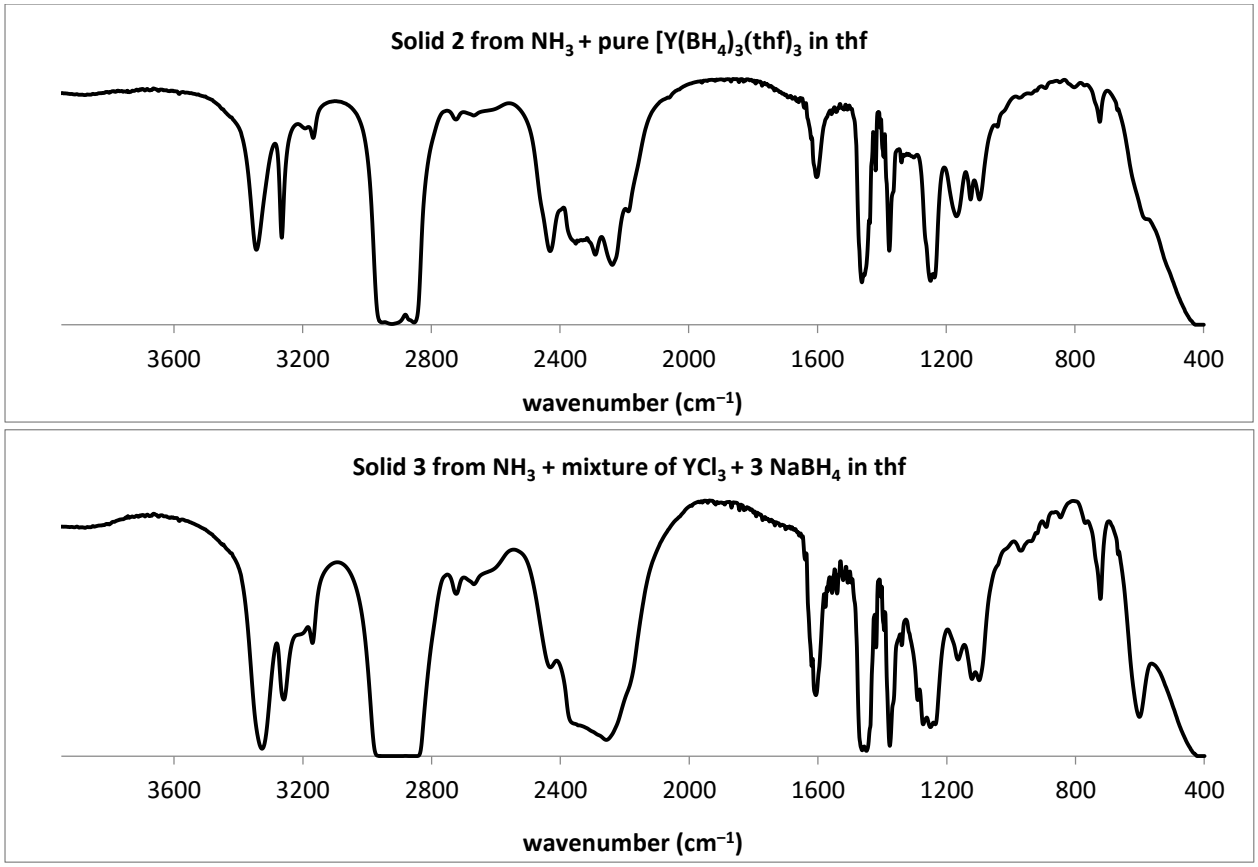

Figure A3.2. FT-IR spectra of solids **2** and **3**.

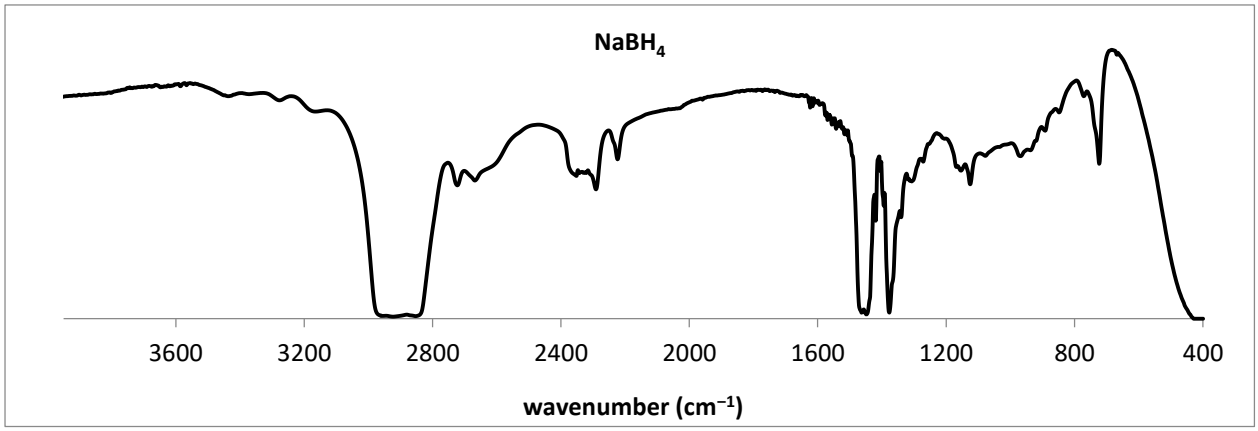

Figure A3.3. FT-IR spectra of $NaBH_4$.

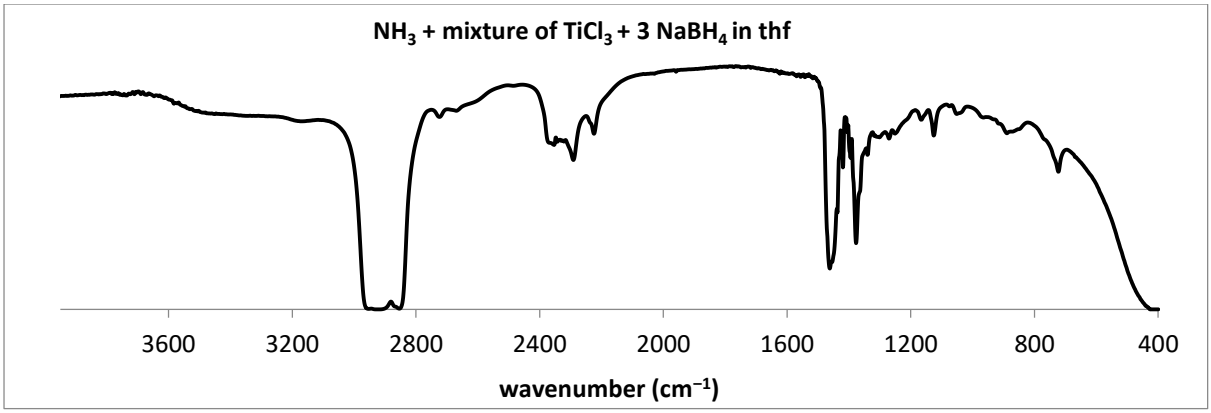

Figure A3.4. FT-IR spectrum of the solid isolated from the reaction of ammonia to the mixture of $TiCl_3$ and $NaBH_4$ in thf.

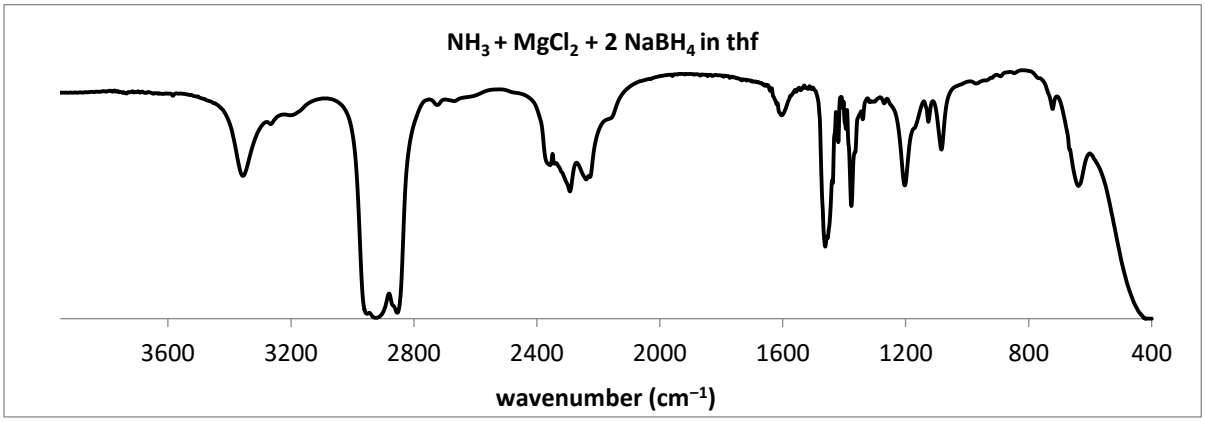

Figure A3.5. FT-IR spectrum of the solid isolated from the reaction of $MgCl_2$ and $NaBH_4$ with ammonia in thf.

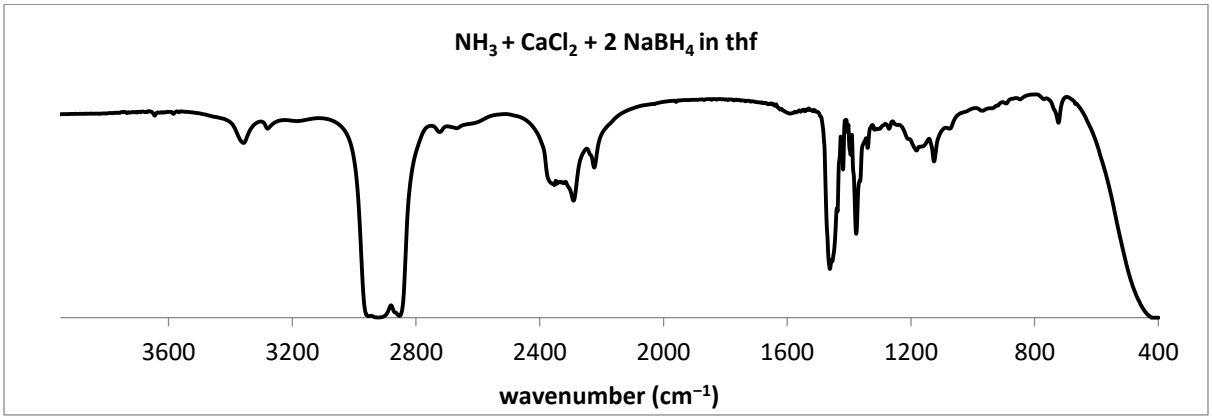

Figure A3.6. FT-IR spectrum of the solid isolated from the reaction of $CaCl_2$ and $NaBH_4$ with ammonia in thf.

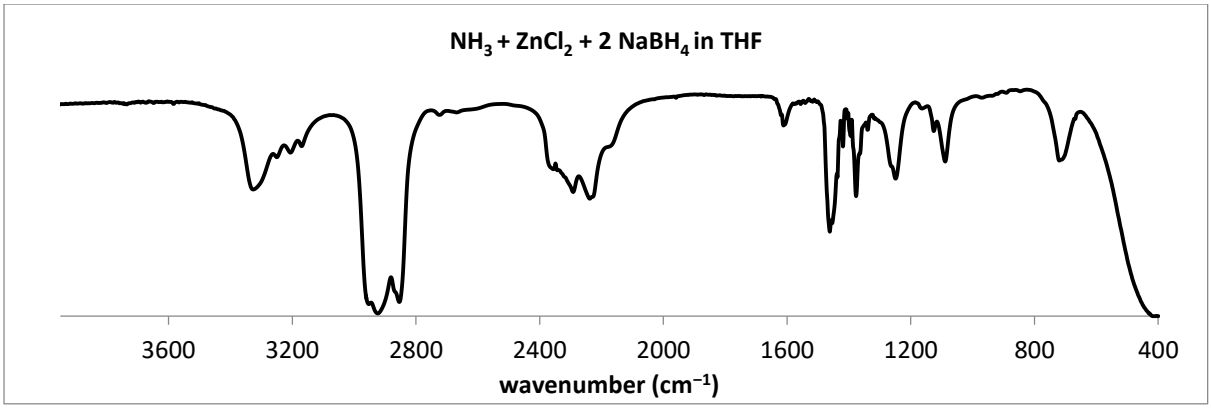

Figure A3.7. FT-IR spectrum of the solid isolated from NH_3 + $ZnCl_2$ + 2 $NaBH_4$ in thf.

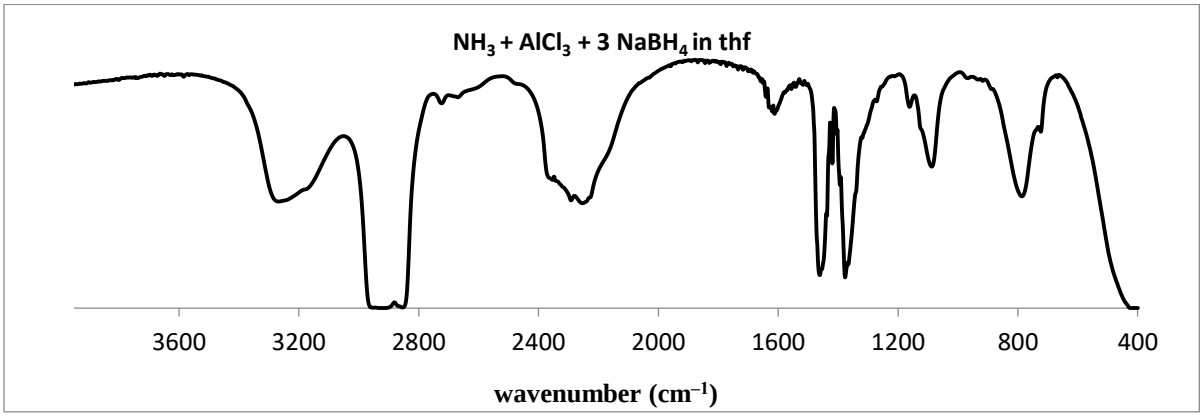

Figure A3.8. FT-IR spectrum of the solid isolated from the reaction of $AlCl_3$ and $NaBH_4$ with ammonia in thf.

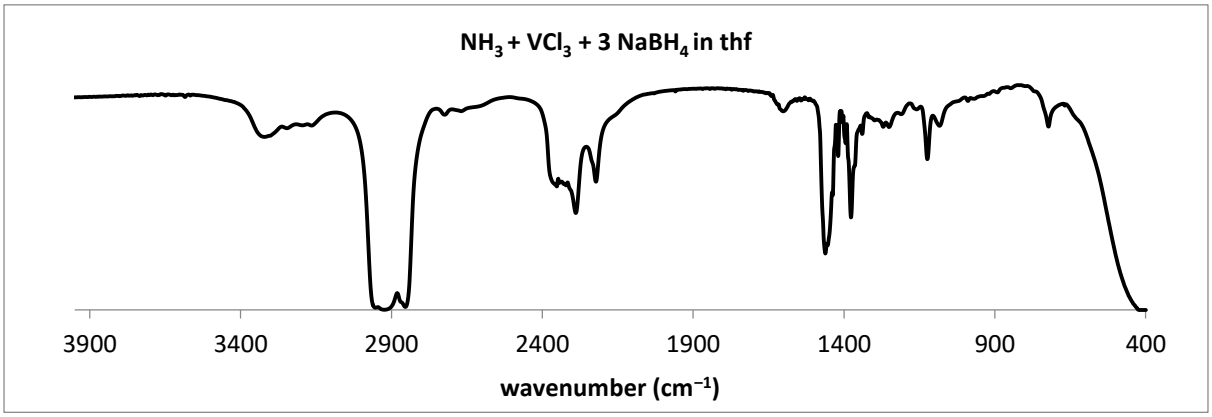

Figure A3.9. FT-IR spectrum of the solid isolated from the reaction of VCl_3 and $NaBH_4$ with ammonia in thf.

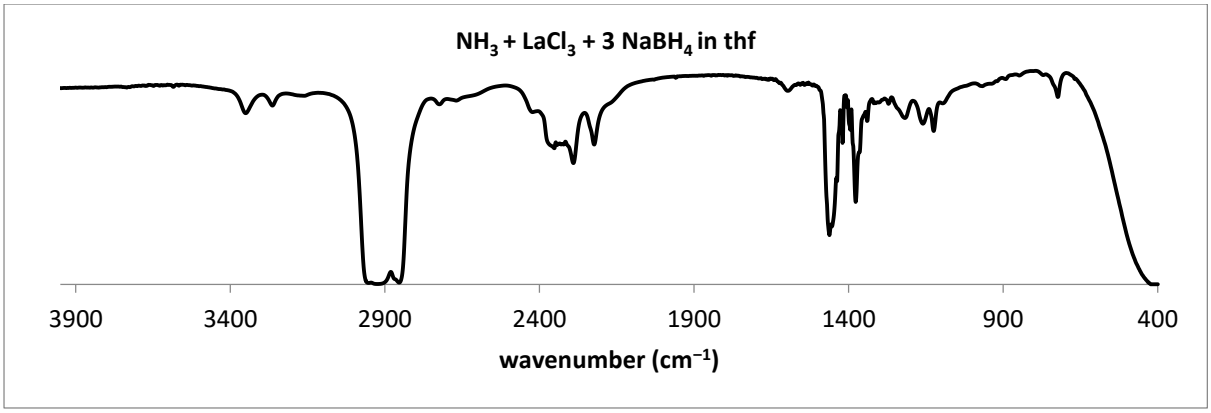

Figure A3.10. FT-IR of the solid isolated from the reaction of $LaCl_3$ and $NaBH_4$ with ammonia in thf.

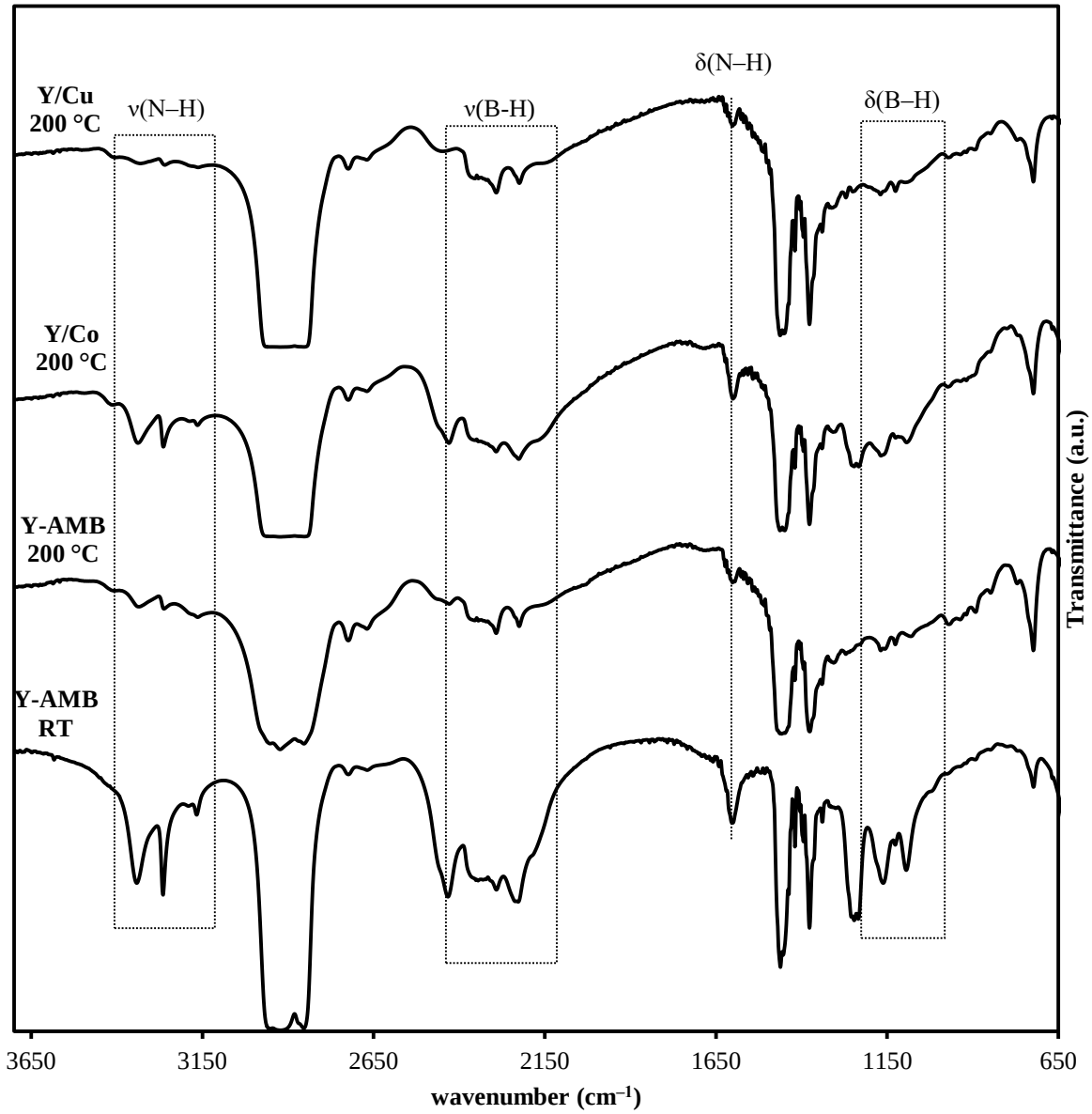

Figure A3.11. FTIR spectra of $Y(BH_4)_3(NH_3)_4$ at RT and after heating at 200°C with and without M'NP catalyst.

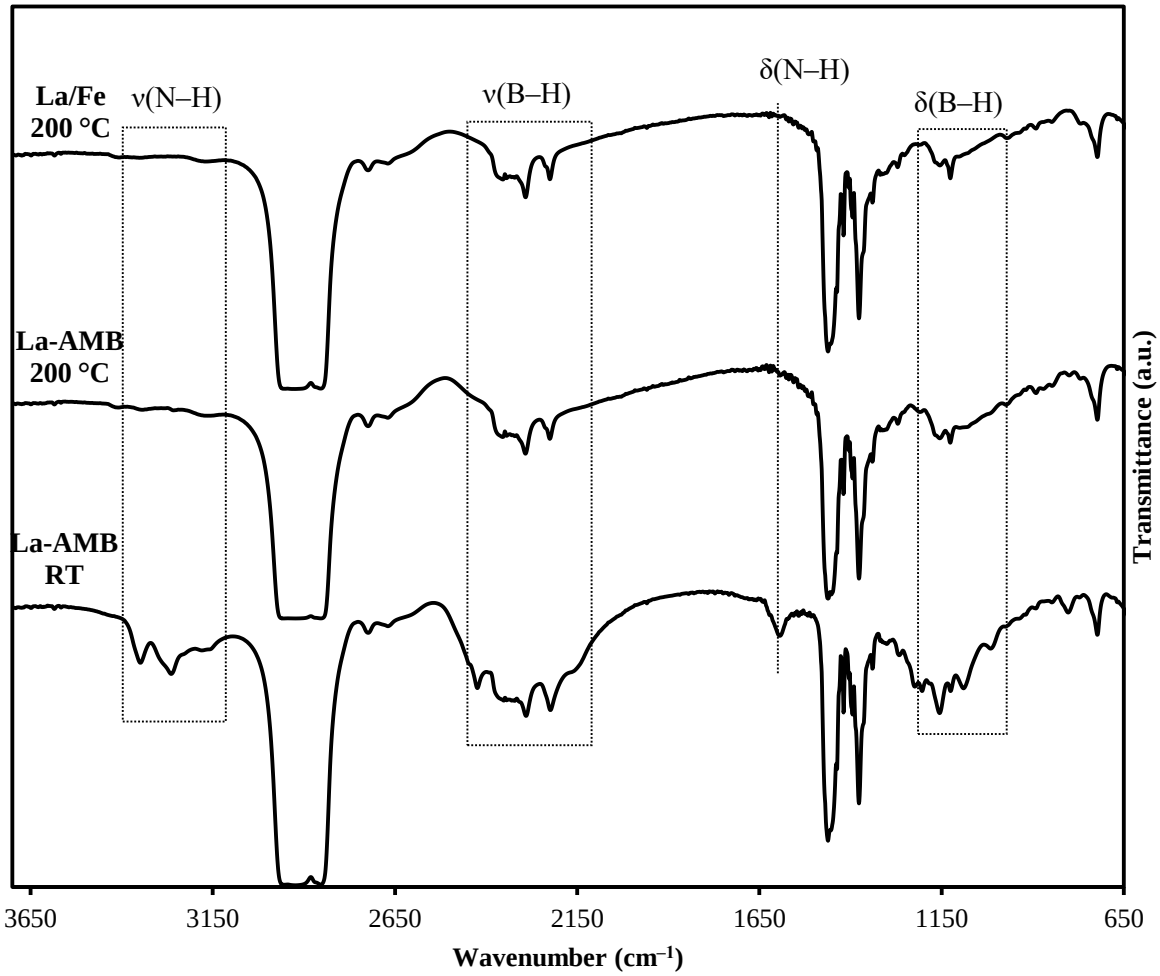

Figure A3.12. FTIR spectra of $La(BH_4)_3(NH_3)_4$ at RT and after heating at 200°C with and without FeNP catalyst.

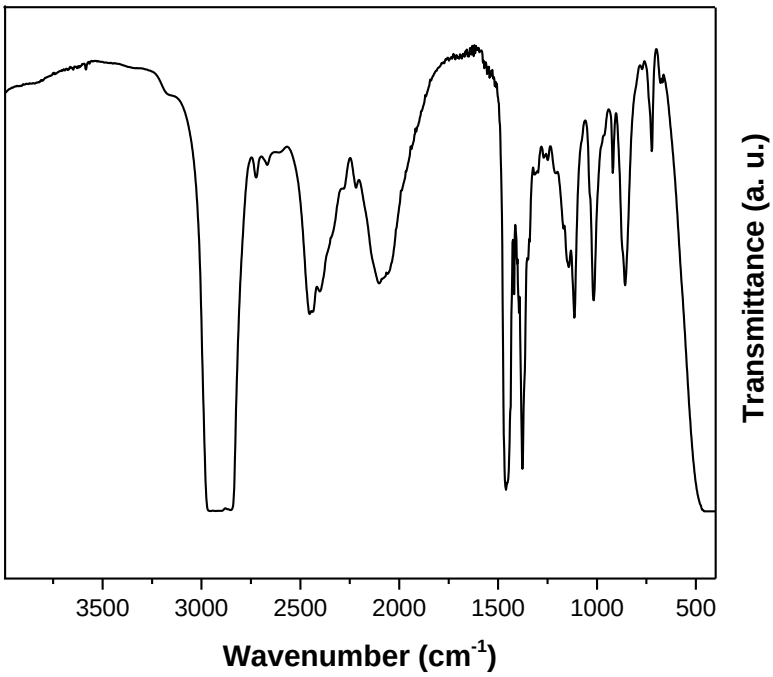

Figure A3.13. The FT-IR spectrum of $KZn(BH_4)_3 \cdot thf$ at RT.

Corelations

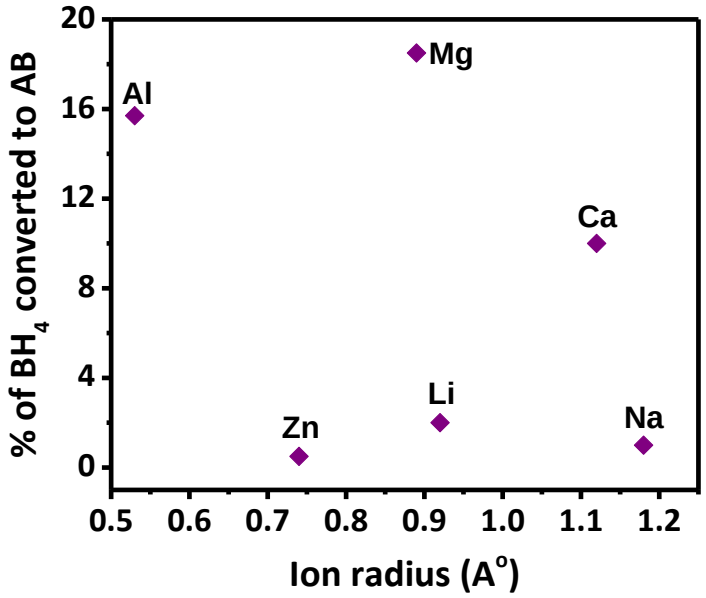

Figure A4.1. Poor correlation of ionic radius with % BH_4 converted to AB for s- and p-block elements.

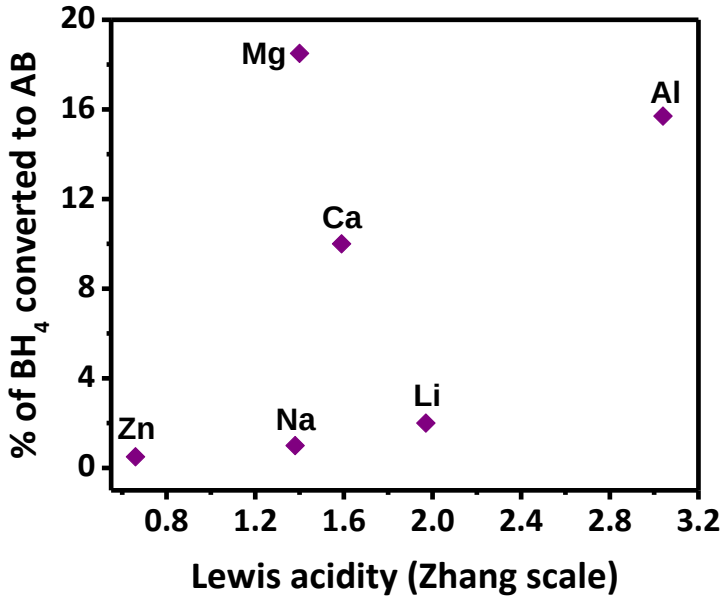

Figure A4.2. Poor correlation of Lewis acidity with % BH_4 converted to AB for s- and p-block elements.

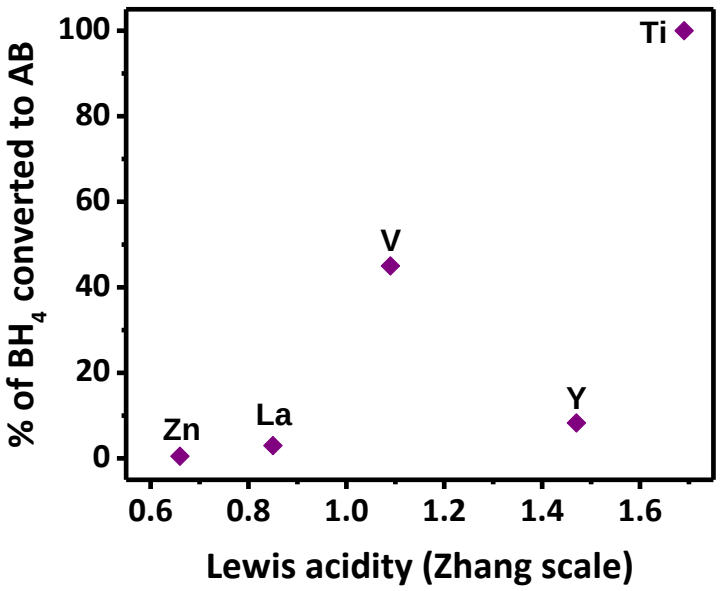

Figure A4.3. Poor correlation of Lewis acidity with % BH_4 converted to AB for d-block elements.

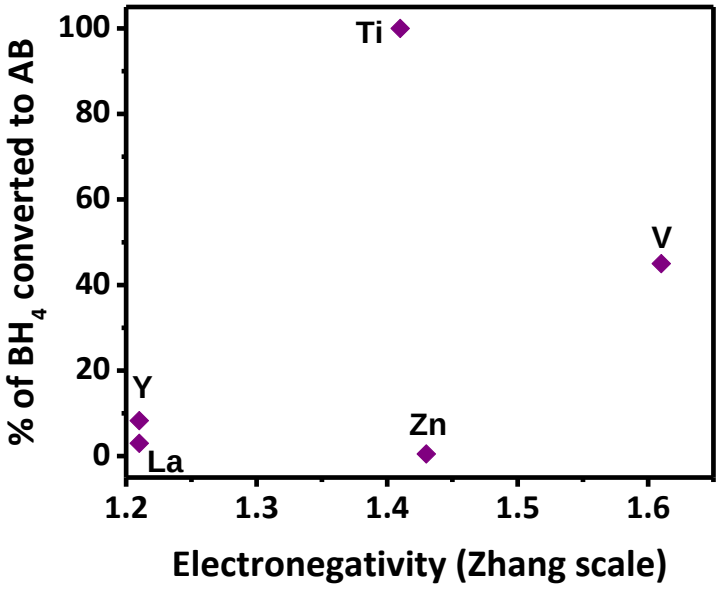

Figure A4.4. Poor correlation of ionic radius with % BH_4 converted to AB for d-block elements.

TGA-MS Results

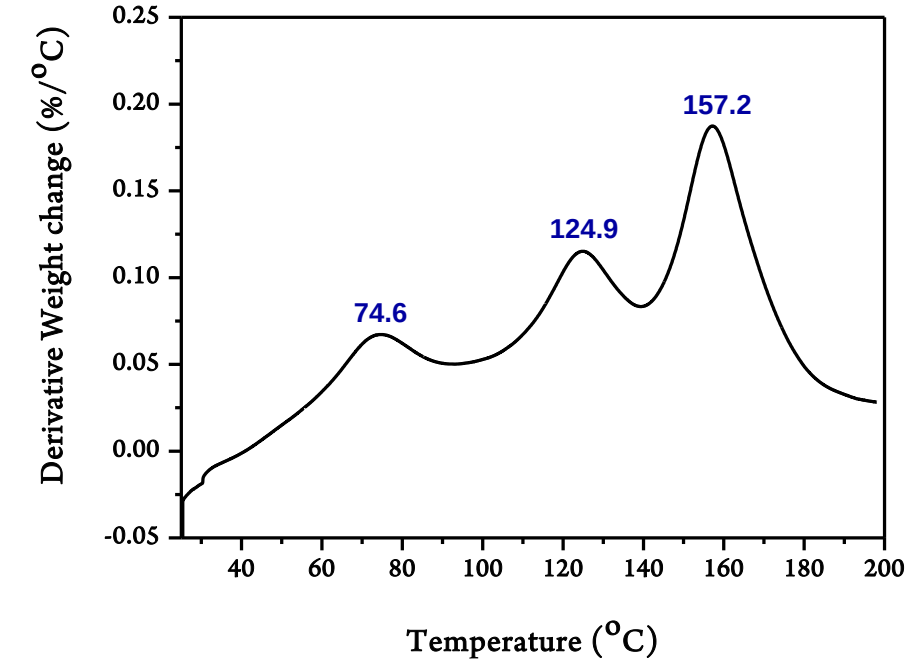

Figure A5.1. First derivative of the weight changes observed for pure $Y(BH_4)_3(NH_3)_4$ (1) during heating from RT to 200 °C (ramp= 5 °C/min) under nitrogen.

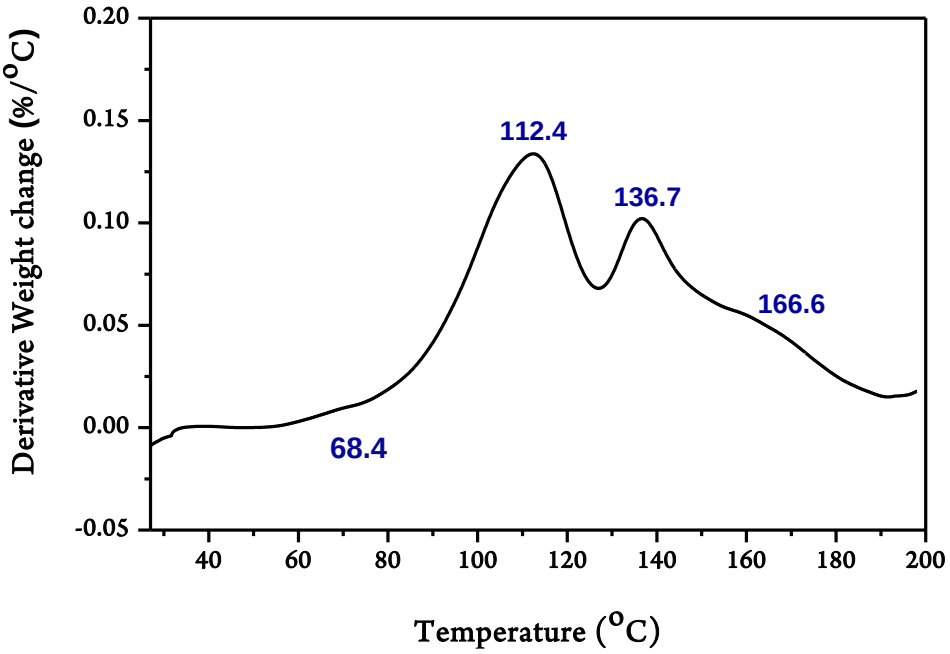

Figure A5.2. First derivative of the weight changes observed for pure $La(BH_4)_3(NH_3)_4$ (2) during heating from RT to 200 °C (ramp= 5 °C/min) under nitrogen.

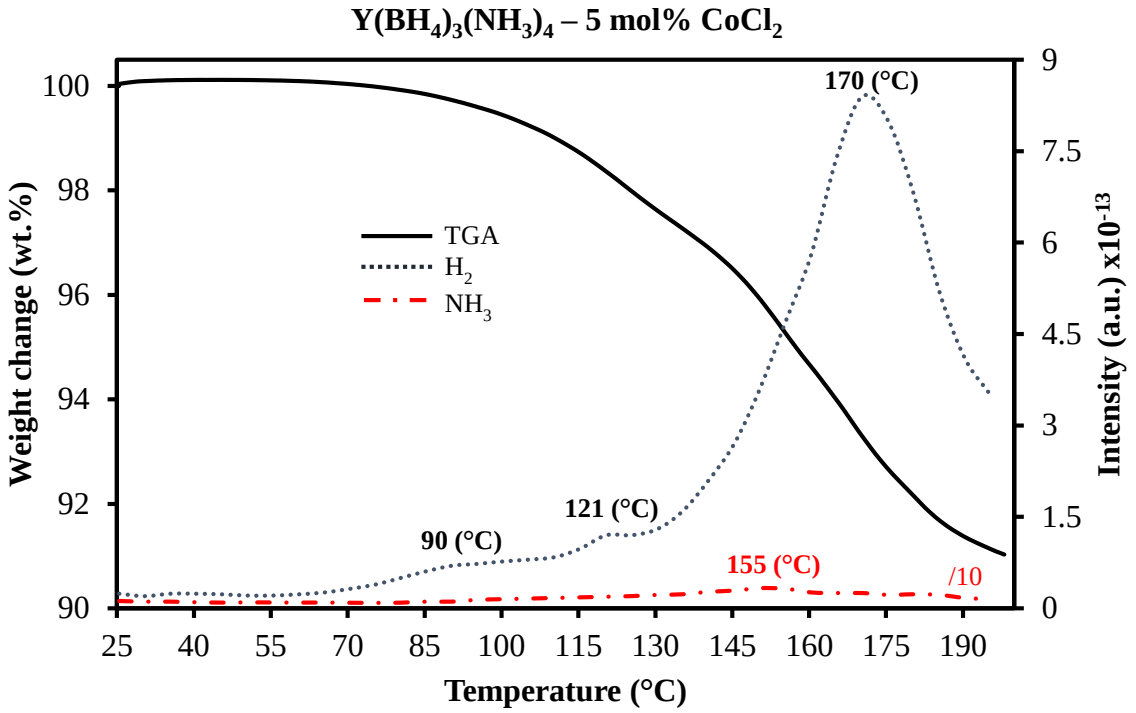

Figure A5.3. TGA-MS results for $Y(BH_4)_3(NH_3)_4$ loaded with 5 mol% $CoCl_2$ (5 °C/min ramp). Major events observed at 124.1, 153.9 and 167.9 °C.

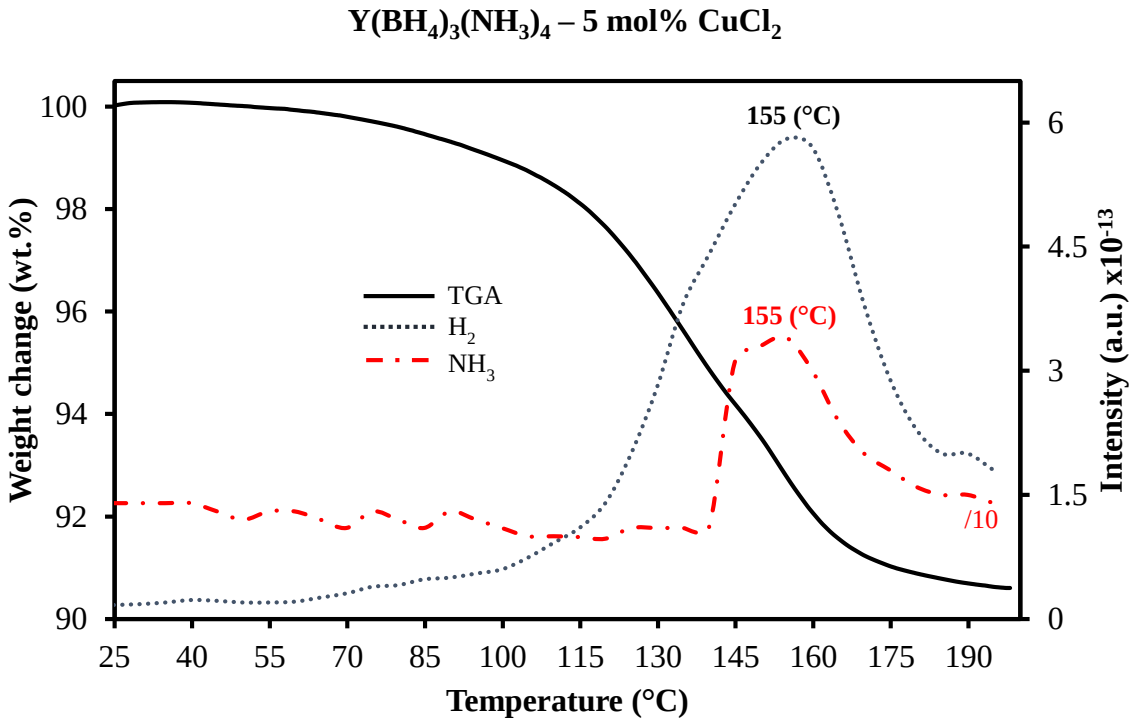

Figure A5.4. TGA-MS results for $Y(BH_4)_3(NH_3)_4$ loaded with 5 mol% $CuCl_2$ (5 °C/min ramp). Major events observed at 83.8, 94.9, 134.8 and 154.0 °C.

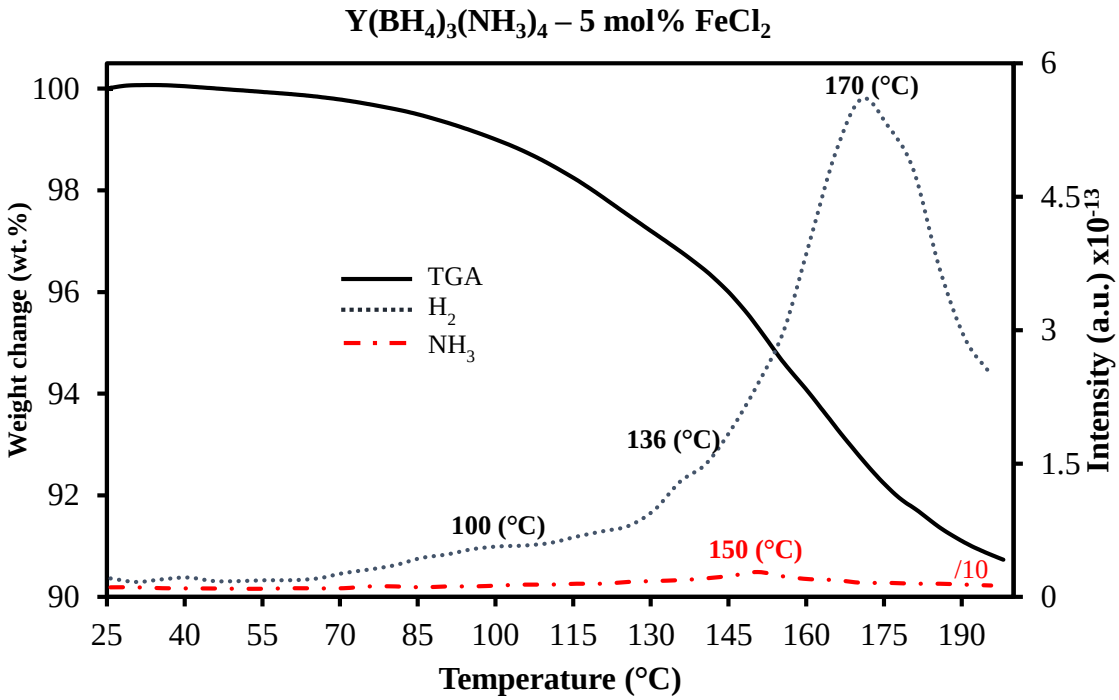

Figure A5.5. TGA-MS results for $Y(BH_4)_3(NH_3)_4$ loaded with 5 mol% $FeCl_2$ (5 °C/min ramp). Major events observed at 91.9, 120.2, 152.6, 164.2 and 184.6 °C.

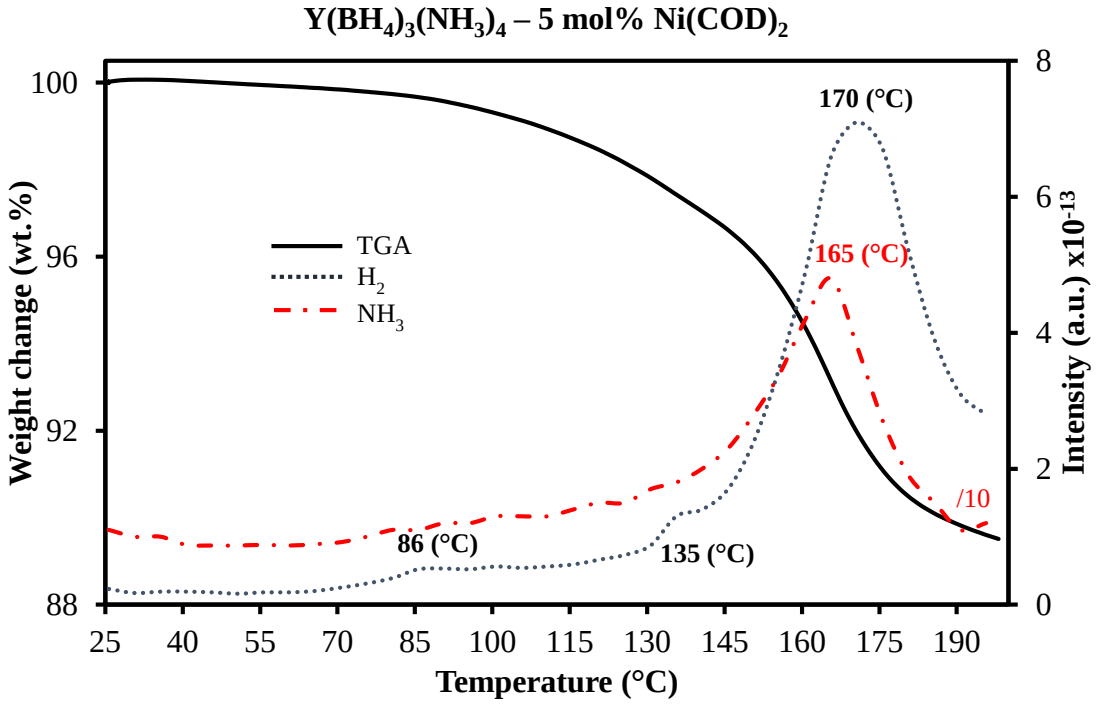

Figure A5.6. TGA-MS results for $Y(BH_4)_3(NH_3)_4$ loaded with 5 mol% $Ni(COD)_2$ (5 °C/min ramp). Major events observed at 132.3 and 165.1 °C.

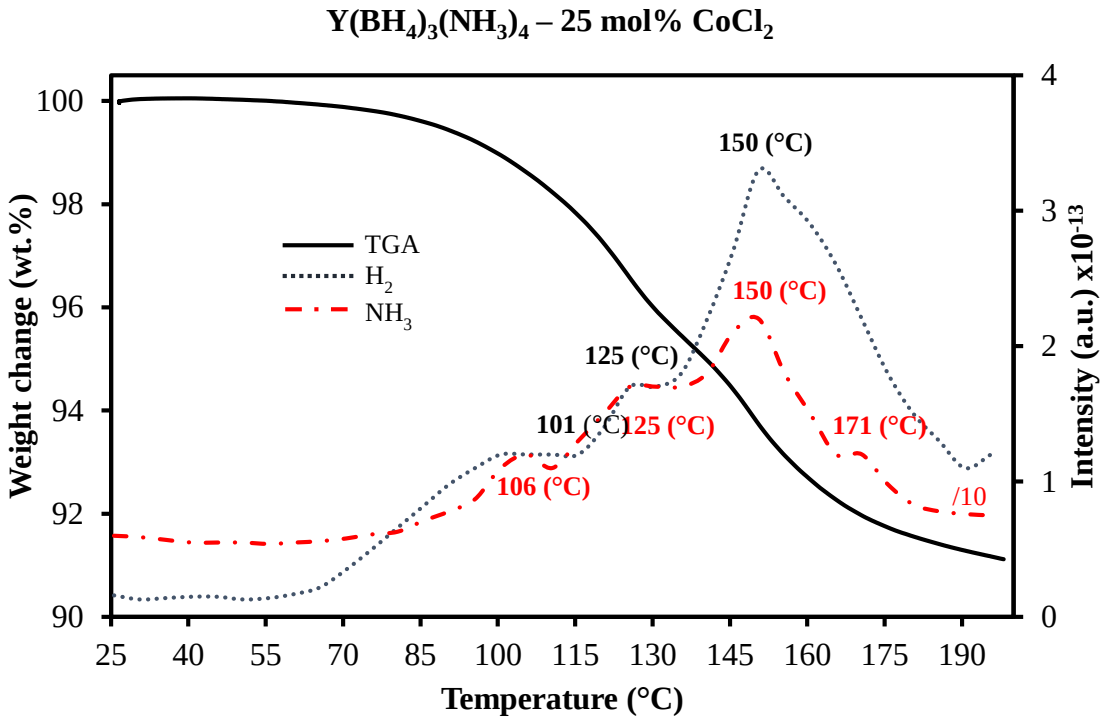

Figure A5.7. TGA-MS results for $Y(BH_4)_3(NH_3)_4$ loaded with 25 mol% $CoCl_2$ (5 °C/min ramp). Major events observed at 102.4, 124.6 and 148.6 °C.

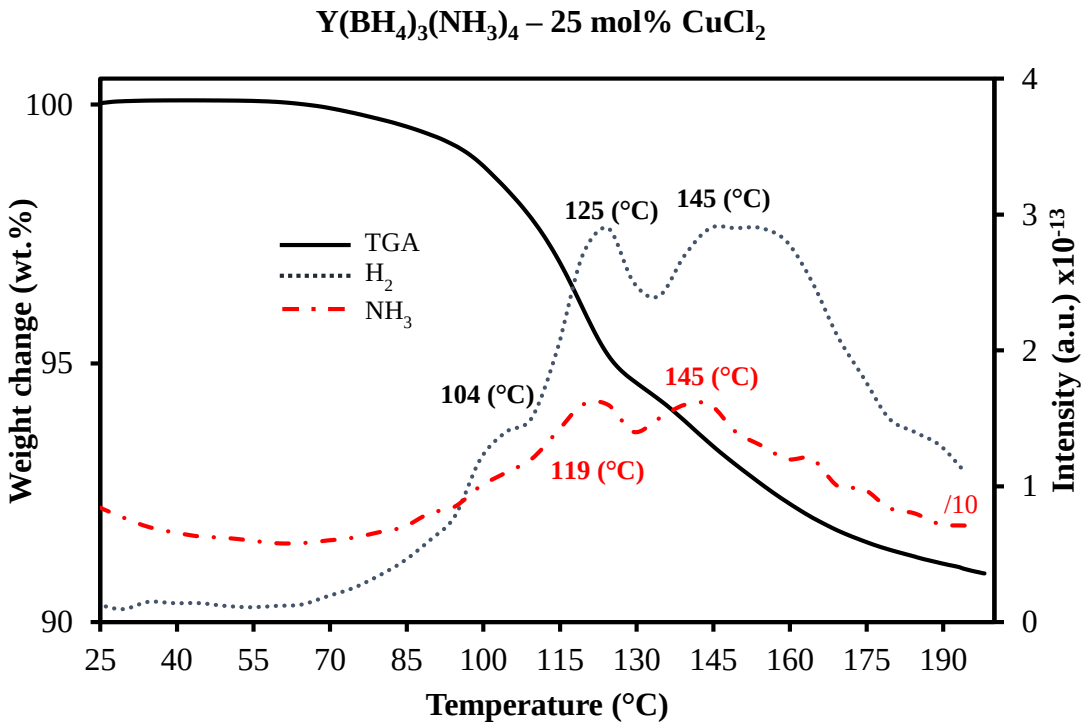

Figure A5.8. TGA-MS results for $Y(BH_4)_3(NH_3)_4$ loaded with 25 mol% $CuCl_2$ (5 °C/min ramp). Major events observed at 72.3, 100.8, 118.7 and 140.4 °C.

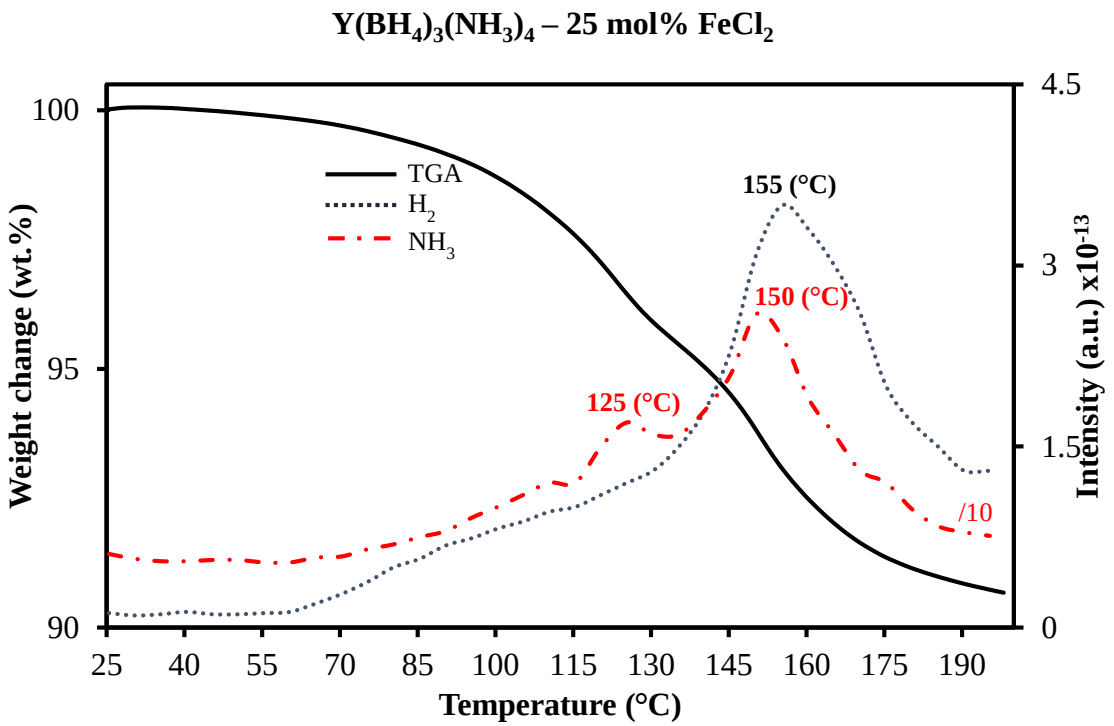

Figure A5.9. TGA-MS results for $Y(BH_4)_3(NH_3)_4$ loaded with 25 mol% $FeCl_2$ (5 °C/min ramp). Major events observed at 123.6 and 151.0 °C.

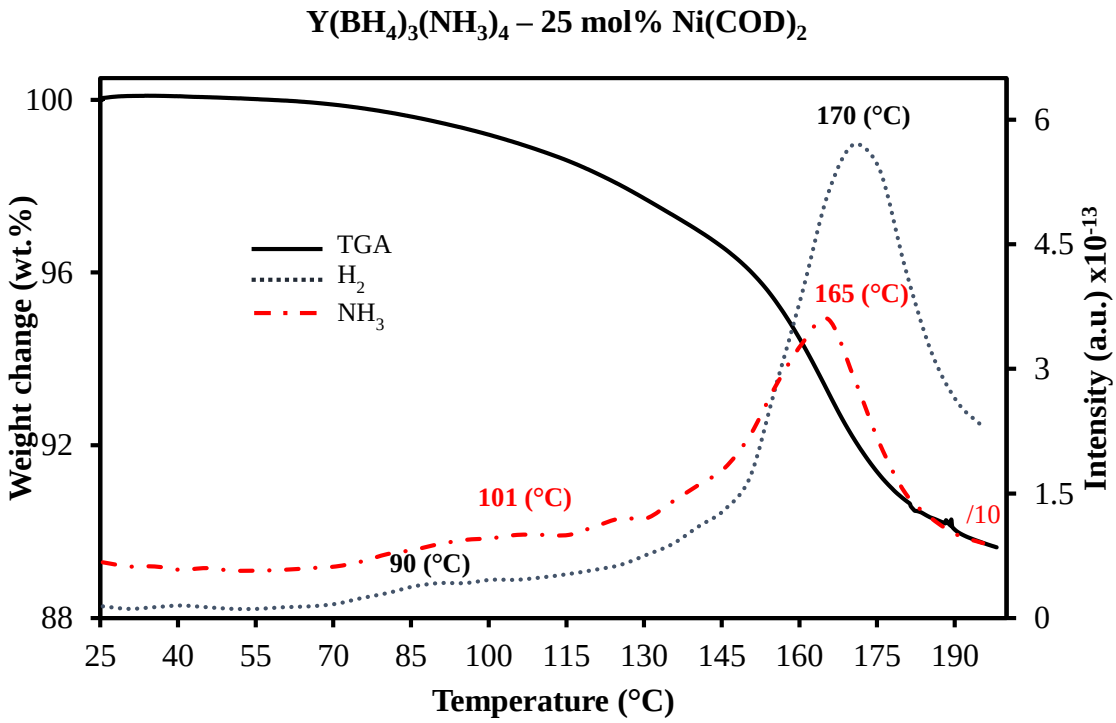

Figure A5.10. TGA-MS results for $Y(BH_4)_3(NH_3)_4$ loaded with 25 mol% $Ni(COD)_2$ (5 °C/min ramp). Major events observed at 139.1, 164.6, 140.9 and 191.2 °C.

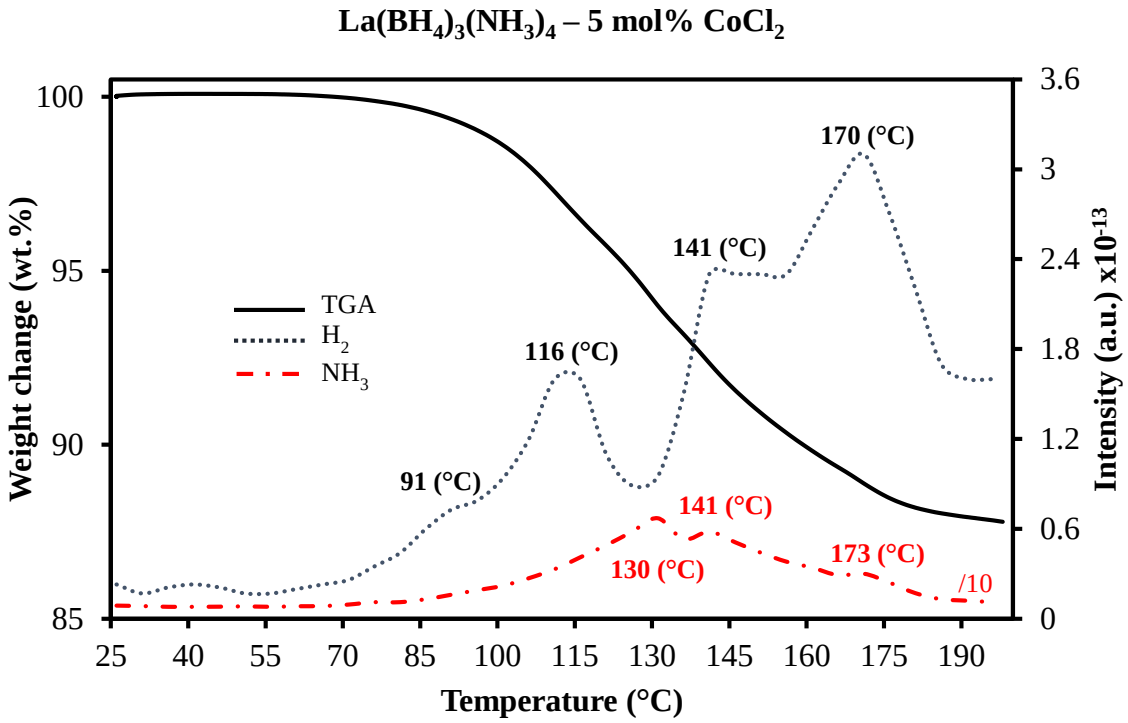

Figure A5.11. TGA-MS results for $La(BH_4)_3(NH_3)_4$ loaded with 5 mol% $CoCl_2$ (5 °C/min ramp). Major events observed at 110.7, 128.7, 140.9 and 171.1 °C.

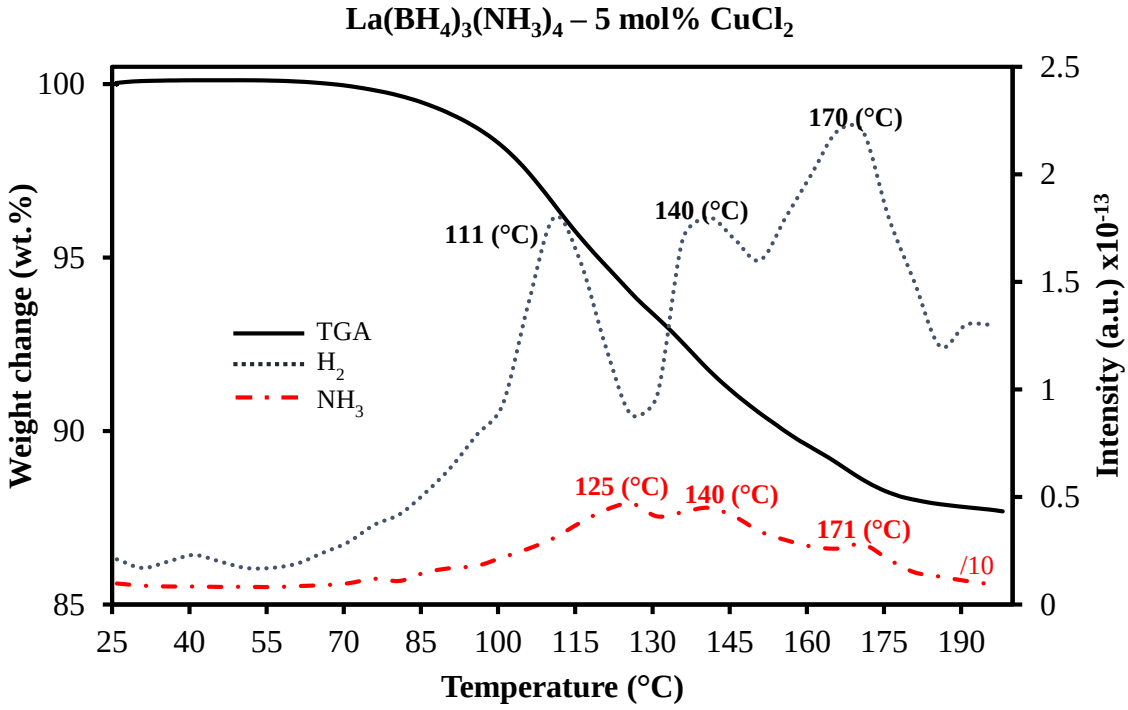

Figure A5.12. TGA-MS results for $La(BH_4)_3(NH_3)_4$ loaded with 5 mol% $CuCl_2$ (5 °C/min ramp). Major events observed at 109.7, 124.3, 137.8 and 168.9 °C.

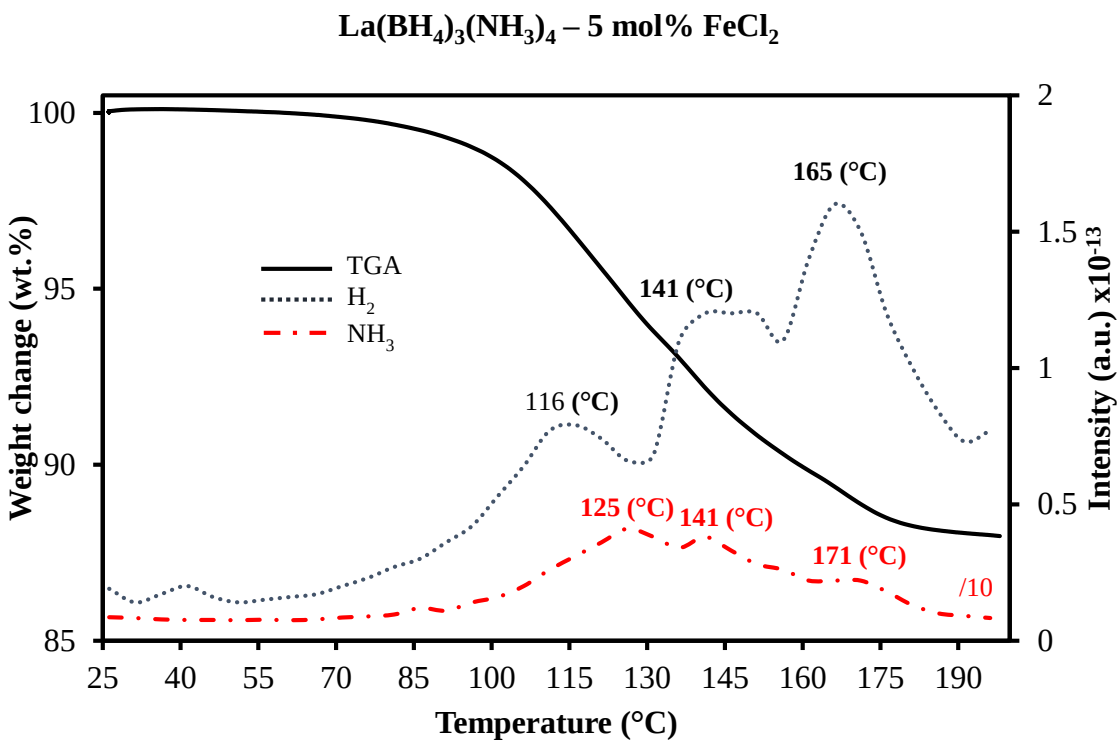

Figure A5.13. TGA-MS results for $La(BH_4)_3(NH_3)_4$ loaded with 5 mol% $FeCl_2$ (5 °C/min ramp). Major events observed at 123.1, 138.8 and 169.4 °C.

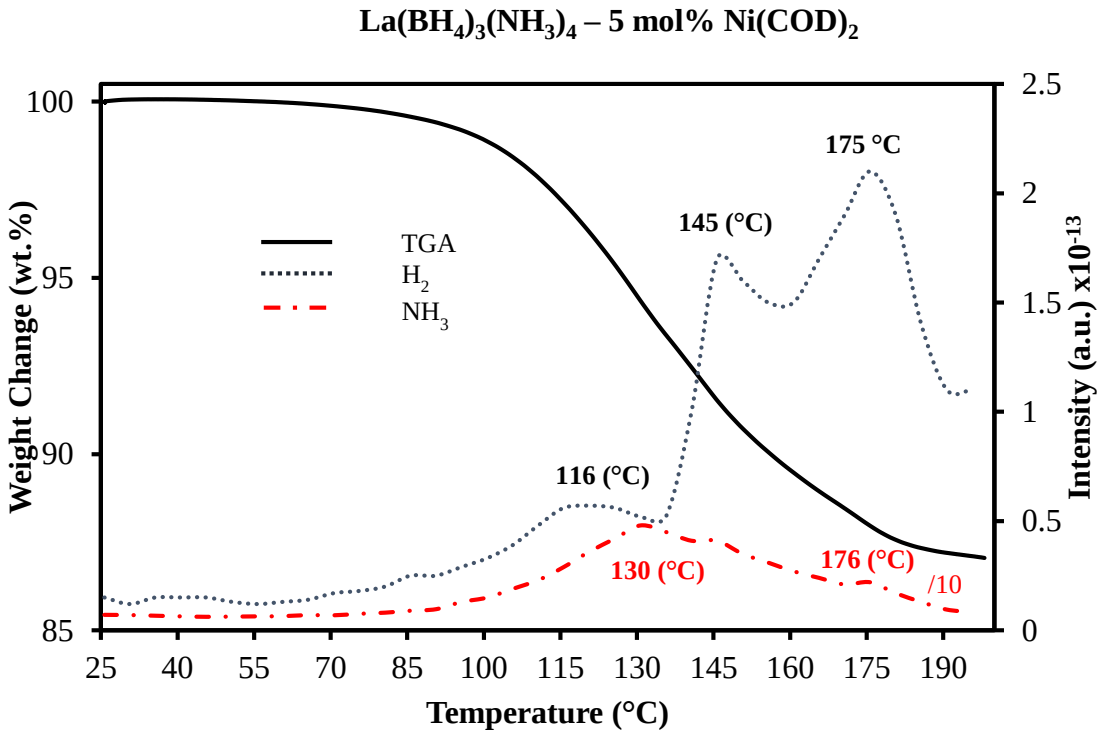

Figure A5.14. TGA-MS results for $La(BH_4)_3(NH_3)_4$ loaded with 5 mol% $Ni(COD)_2$ (5 °C/min ramp). Major events observed at 128.2, 143.7 and 174.3 °C.

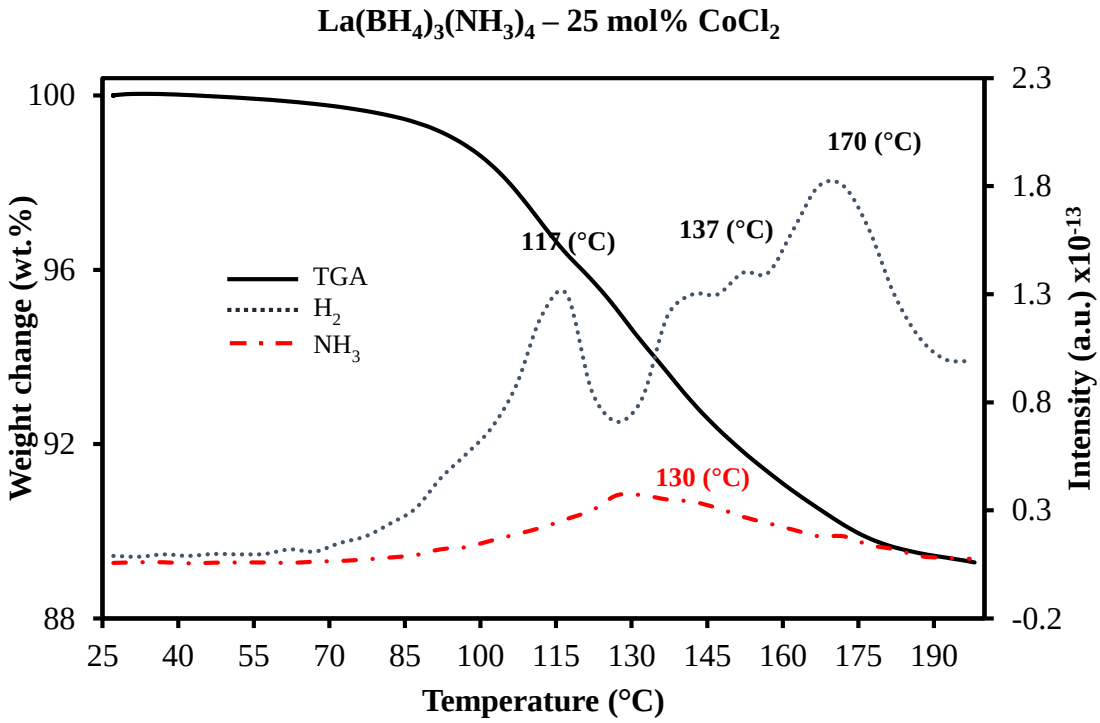

Figure A5.15. TGA-MS results for $La(BH_4)_3(NH_3)_4$ loaded with 25 mol% $CoCl_2$ (5 °C/min ramp). Major events observed at 111.2, 127.9, 139.6 and 171.8 °C.

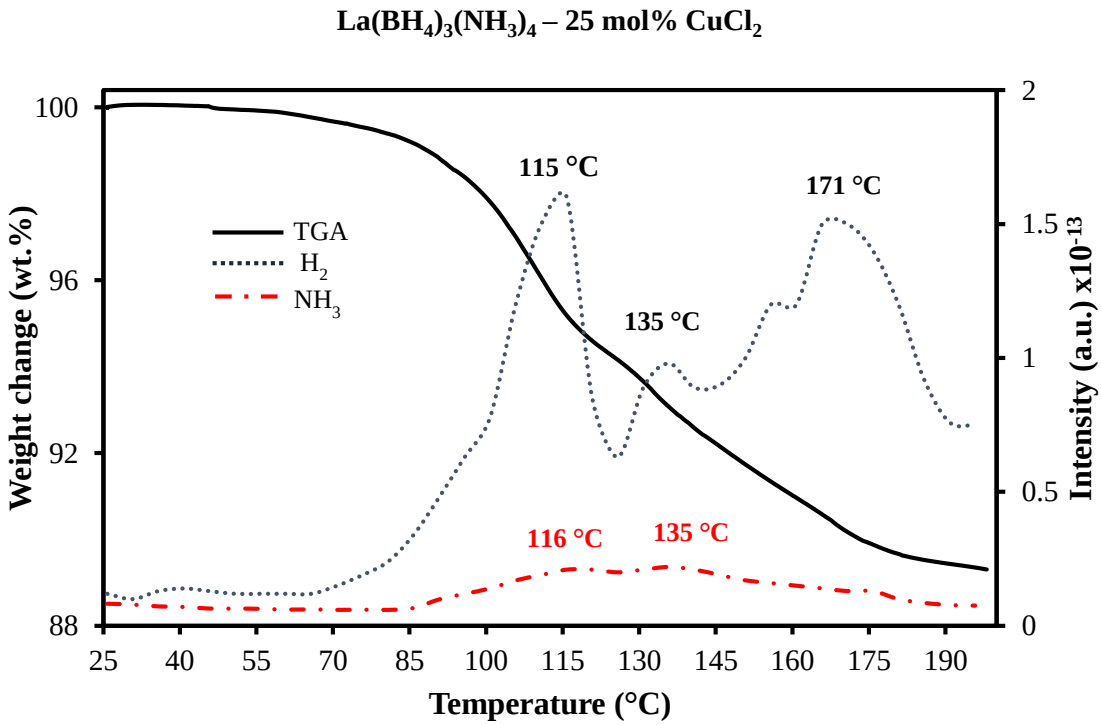

Figure A5.16. TGA-MS results for $La(BH_4)_3(NH_3)_4$ loaded with 25 mol% $CuCl_2$ (5 °C/min ramp). Major events observed at 89.6, 108.5, 132.6 and 168.4 °C**.**

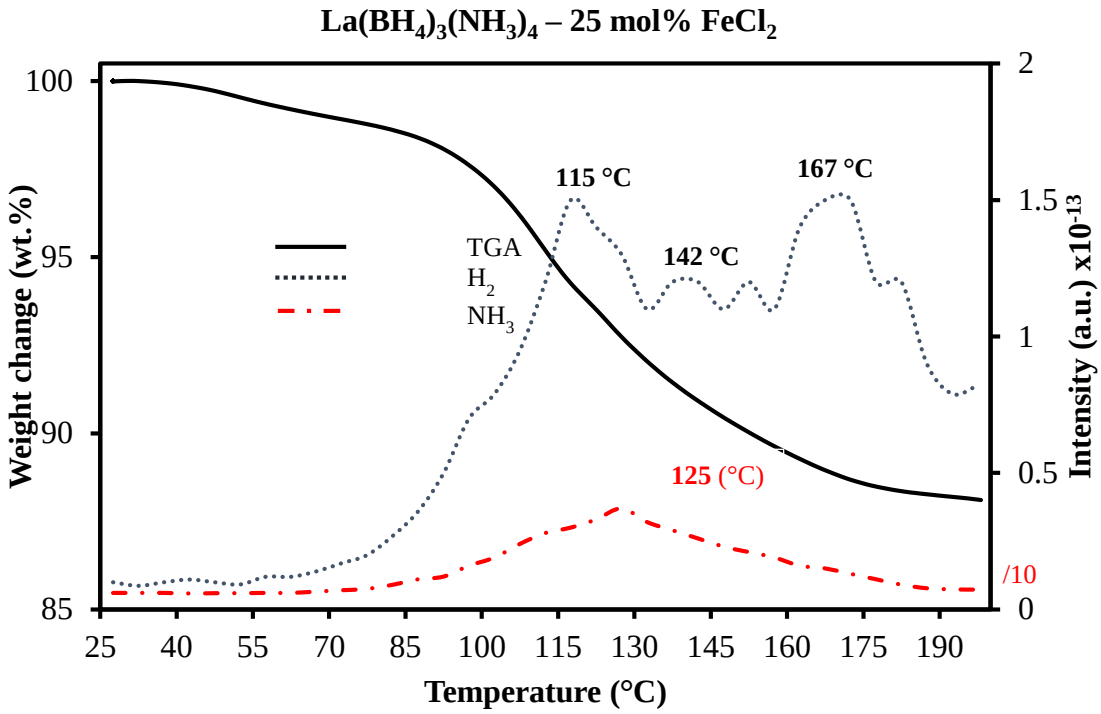

Figure A5.17. TGA-MS results for $La(BH_4)_3(NH_3)_4$ loaded with 25 mol% $FeCl_2$ (5 °C/min ramp). Major events observed at 111.3, 125.7 and 167.7 °C.

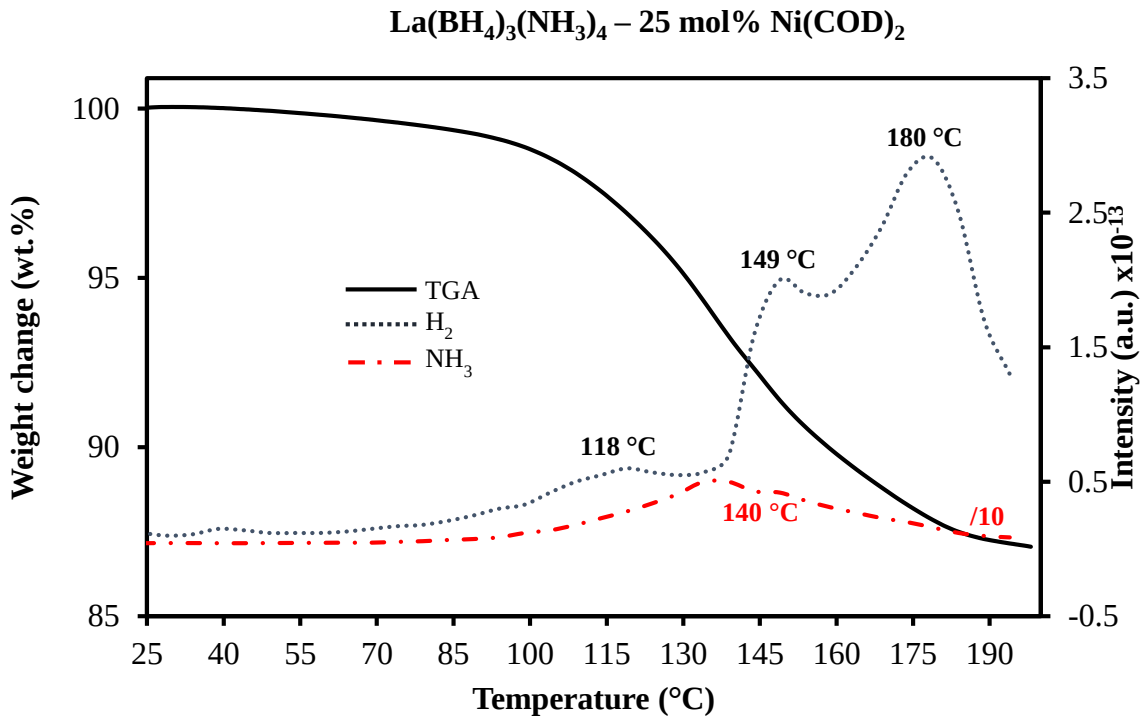

Figure A5.18. TGA-MS results for $La(BH_4)_3(NH_3)_4$ loaded with 25 mol% $Ni(COD)_2$ (5 °C/min ramp). Major events observed at 135.6, 147.4 and 177.1 °C.

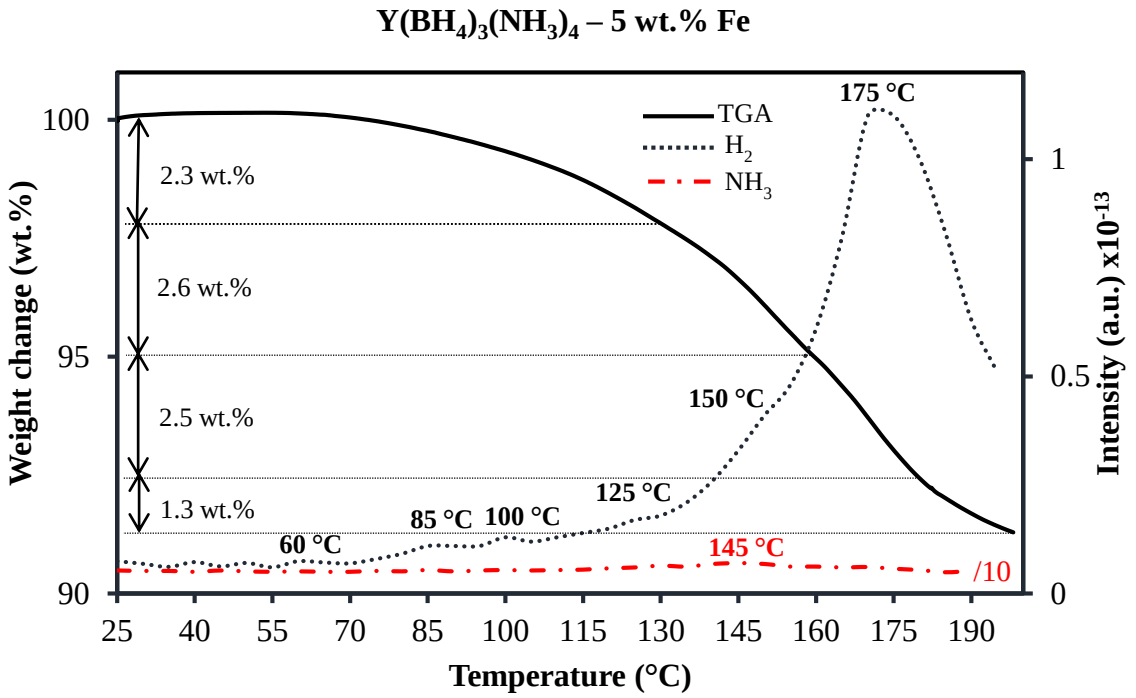

Figure A5.19. TGA-MS results for $Y(BH_4)_3(NH_3)_4$ loaded with 5 wt.% FeNPs (5 °C/min ramp). Major events observed at: 78.4, 120.1, 149.7 and 171.7 °C.

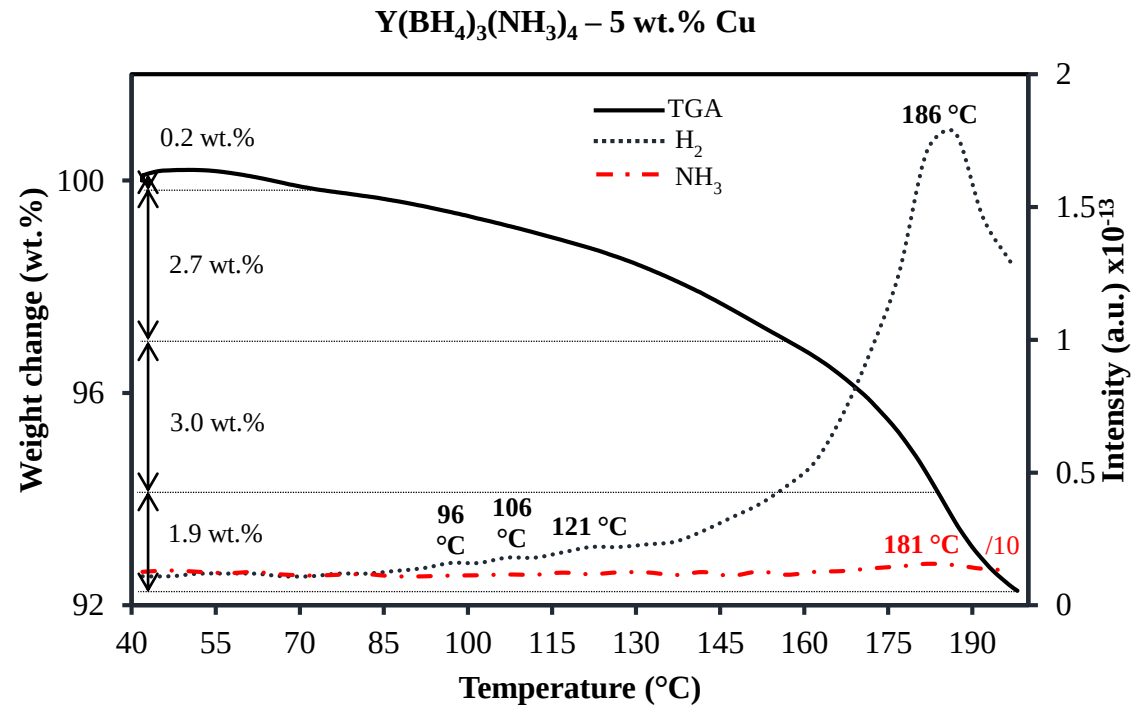

Figure A5.20. TGA-MS results for $Y(BH_4)_3(NH_3)_4$ loaded with 5 wt.% CuNPs (5 °C/min ramp). Major events observed at: 61.9, 117.7 and 178.2 °C.

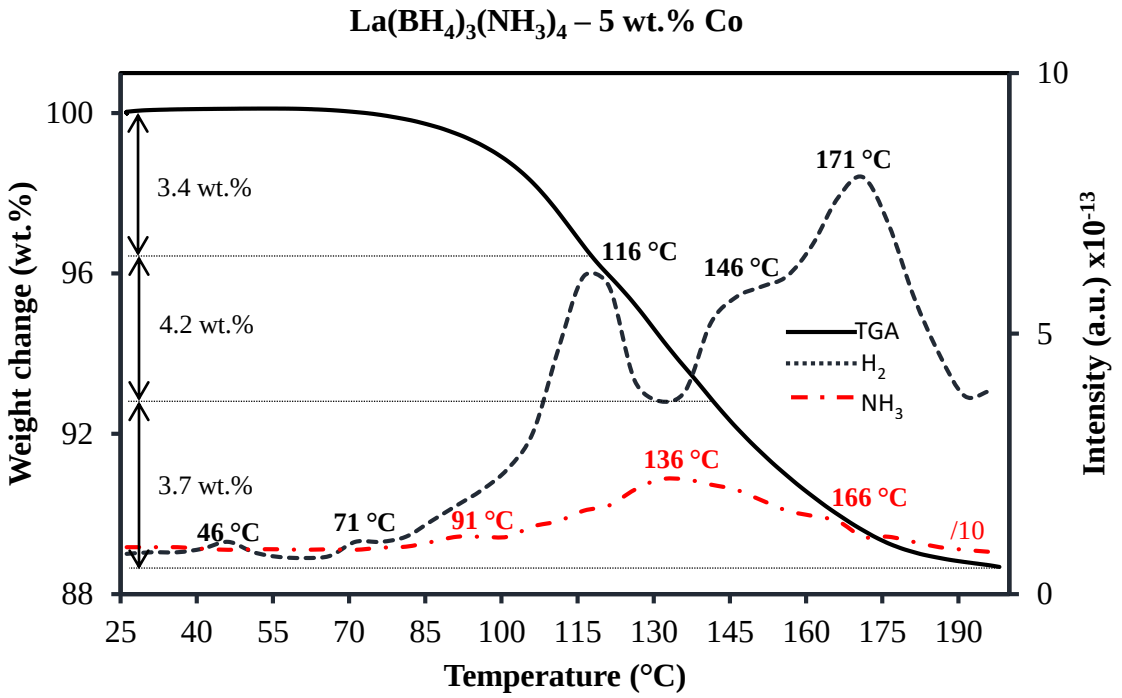

Figure A5.21. TGA-MS results for $La(BH_4)_3(NH_3)_4$ loaded with 5 wt.% CoNPs (5 °C/min ramp). Major events observed at: 113.7, 129.5, 141.8 and 171.0 °C.

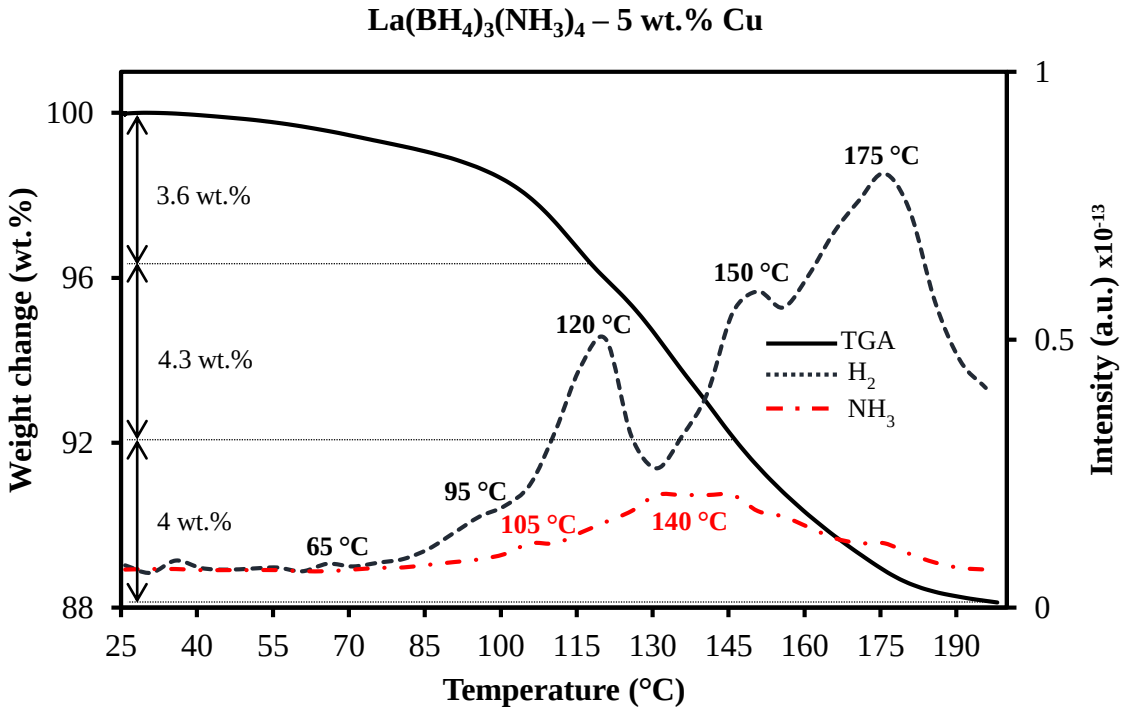

Figure A5.22. TGA-MS results for $La(BH_4)_3(NH_3)_4$ loaded with 5 wt.% CuNPs (5 °C/min ramp). Major events observed at: 114.3, 133.4, 144.3 and 174.5 °C.

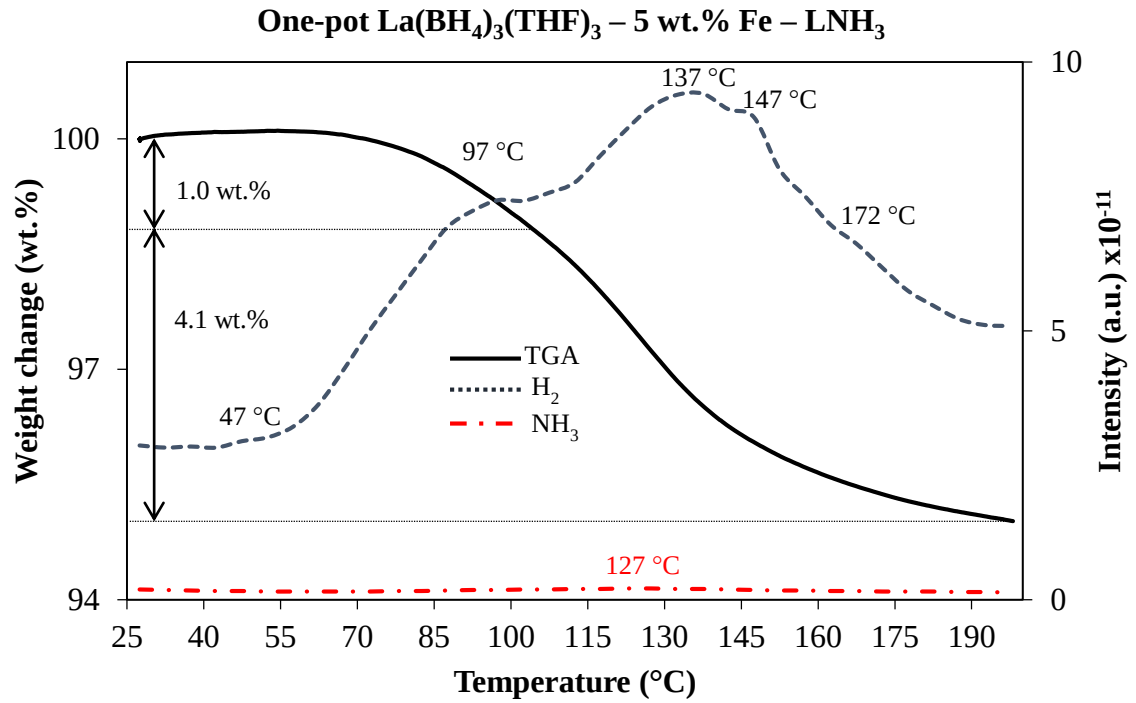

Figure A5.23. TGA-MS results for one-pot synthesis of $La(BH_4)_3(NH_3)_4$/FeNPs in liquid NH_3. Major events observed at: 90.5 and 126.4 °C.

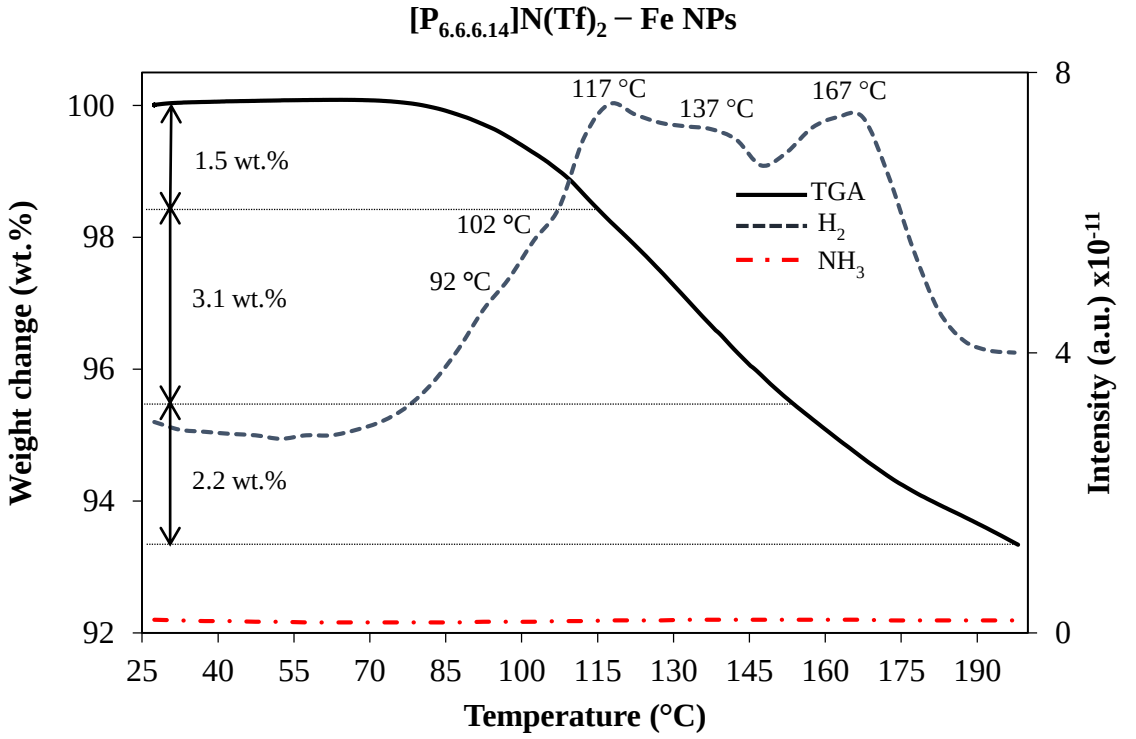

Figure A5.24. TGA-MS results for heat treatment of $[P_{6.6.6.14}]N(Tf)_2$/FeNP (5 wt.%) mixture from RT to 200 °C.

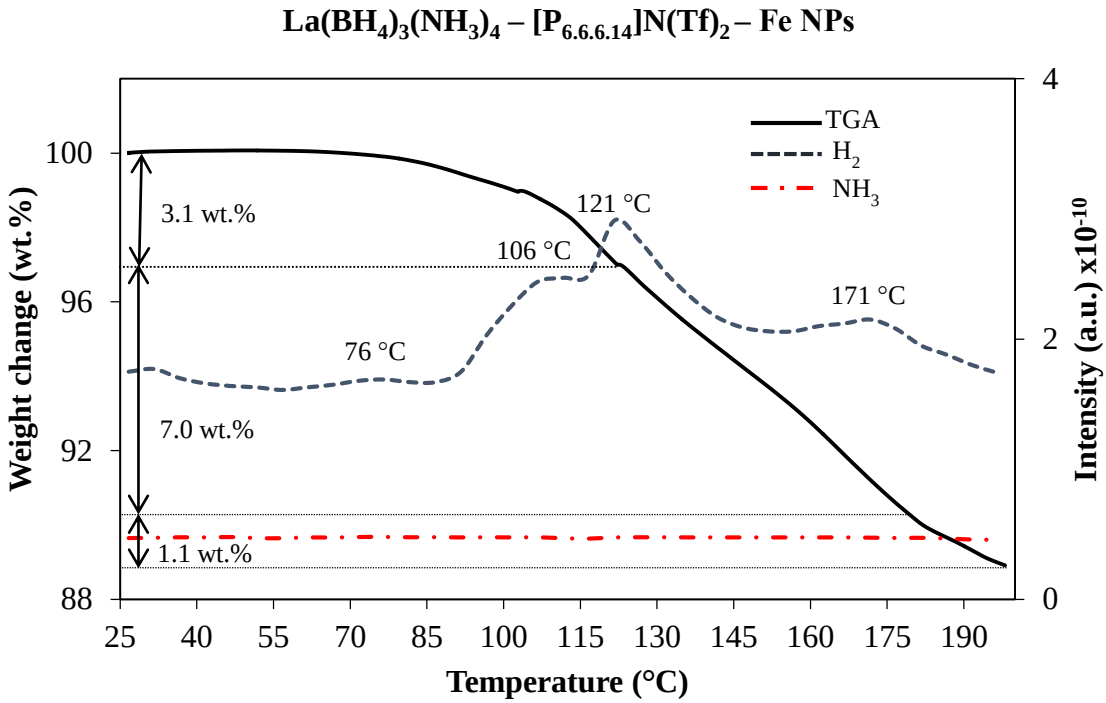

Figure A5.25. TGA-MS result of $La(BH_4)_3(NH_3)_4$/FeNPs in $[P_{6.6.6.14}]N(Tf)_2$ heated from RT to 200 °C (5 °C/min ramp). Major events observed at: 88.9, 97.9, 117.3, 128.1 °, 164.3, 177.9 and 191.1 °C.

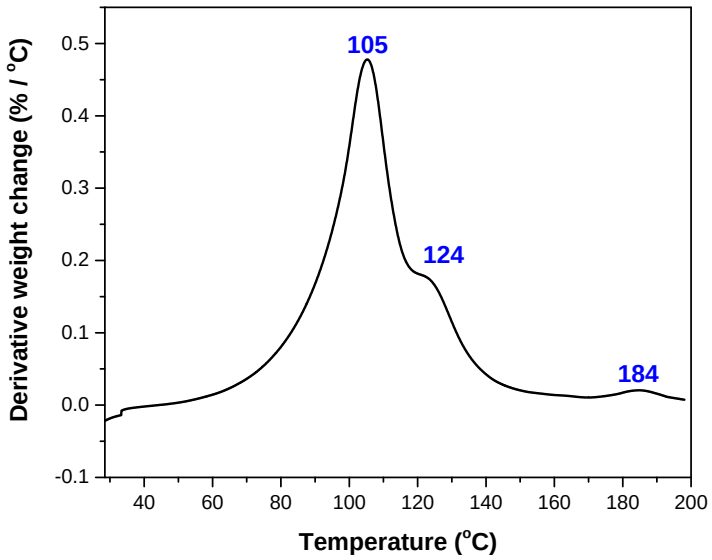

Figure A5.26. First derivative of the weight changes observed for pure $KZn(BH_4)_3(NH_3)_3$ during heating from RT to 200 °C (ramp= 5 °C/min) under nitrogen.

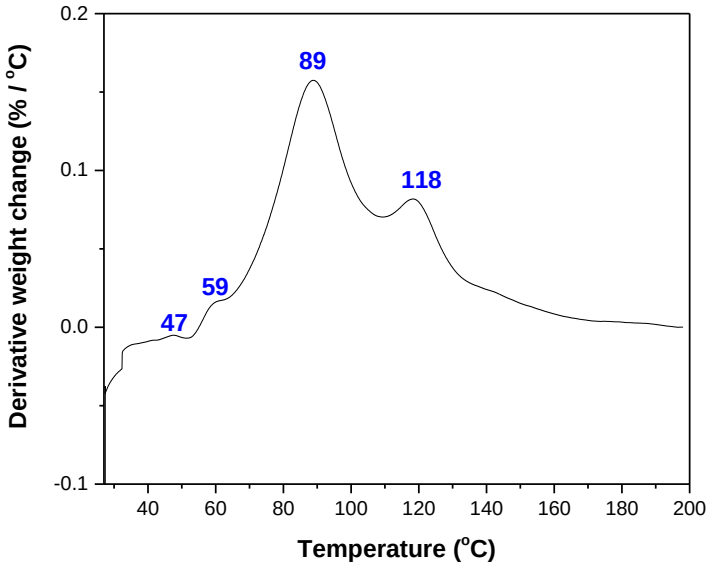

Figure A5.27. First derivative of the weight changes observed for $KZn(BH_4)_3(NH_3)_3$/FeNPs during heating from RT to 200 °C (ramp= 5 °C/min) under nitrogen.

PXRD (Powder X-Ray Diffraction) Data

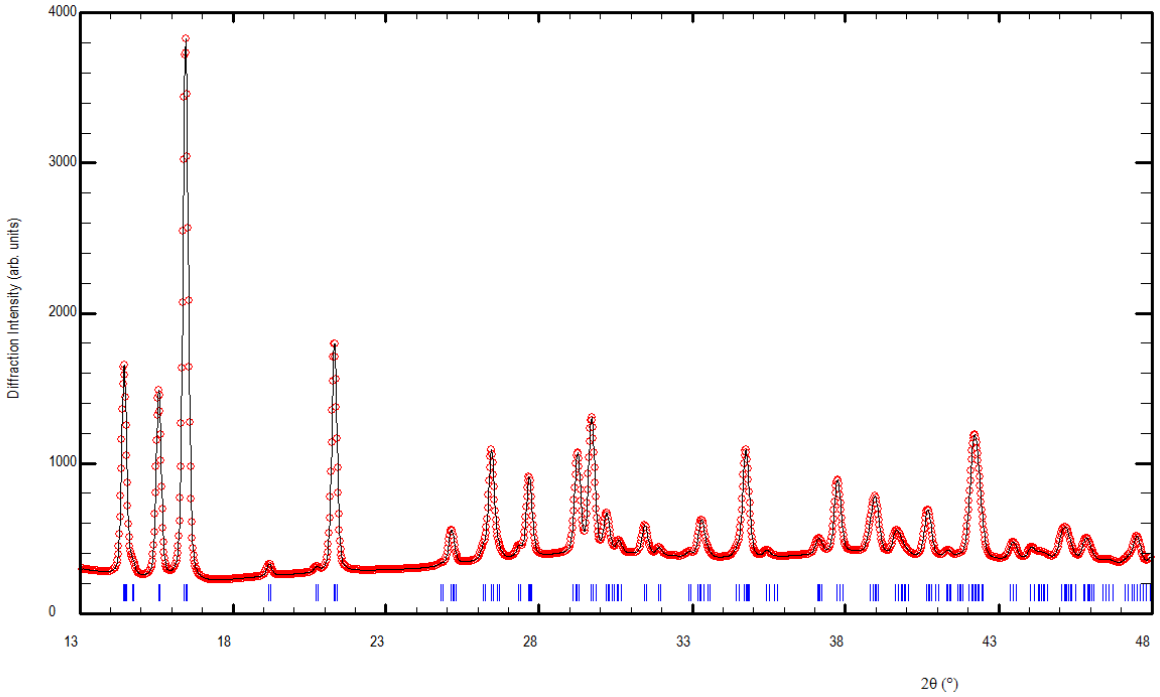

Figure A6.1. PXRD of $Y(BH_4)_3(NH_3)_4$ from the reaction of pure $Y(BH_4)_3(thf)_2$ with liquid ammonia at –50 °C. Full-pattern profile fitting of powder X-ray diffraction data recorded at 300 K. Unit cell parameters are listed in Table 1.

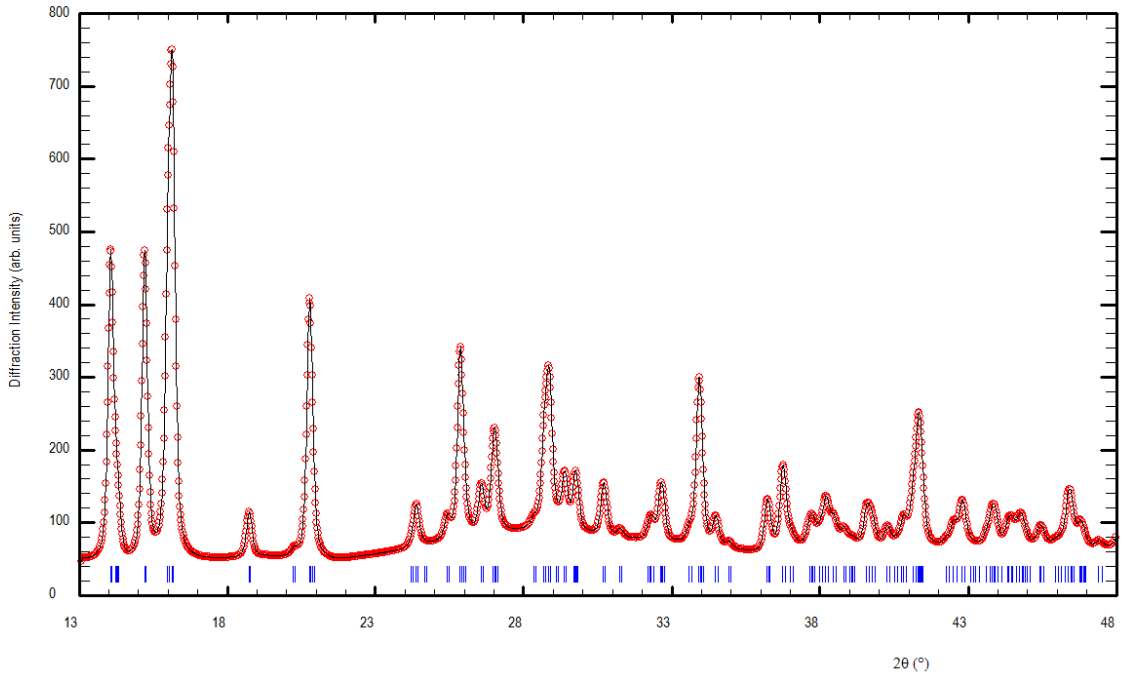

Figure A6.2. PXRD of $La(BH_4)_3(NH_3)_4$ from the reaction of pure $La(BH_4)_3(thf)_3$ with liquid ammonia at –50 °C. Full-pattern profile fitting of powder X-ray diffraction data recorded at 300K. Unit cell parameters are listed in Table 1.

Table A6.1. BYB, NYN and BYN bond angles from Jensen's $Y(BH_4)_3(NH_3)_4$ model·

Bond	Angle	Bond	Angle
N^2YN^1	87.616(1)	N^1YN^3	137.151(2)
N^2YB^3	90.045(1)	N^1YN^4	137.288(2)
N^2YN^3	79.423(1)	N^3YN^4	80.244(1)
N^2YN^4	79.392(1)	B^2YB^3	138.131(1)
N^2YB^2	89.915(1)	N^1YB^3	69.050(1)
B^1YN^3	100.339(1)	B^3YN^3	70.295(1)
B^1YN^4	100.399(1)	N^3YN^4	80.244(1)
B^1YB^2	90.183(1)	N^4YB^2	70.349(1)
B^1YN^1	92.720(1)	B^2YN^1	69.117(1)
B^1YB^3	90.097(1)	N^2YB^1	179.663(1)
N^4YB^3	150.097(1)	N^3YB^2	150.132(1)

Table A6.2. Intermolecular dihydrogen bond lengths below 2.5 Å from Jensen's $Y(BH_4)_3(NH_3)_4$ model.

From	To	Distance (Å)
$N^1_{eq}H^{13}$	$B^2_{eq}H^{11}$	2.141(2)
$N^1_{eq}H^{14}$	$B^1_{eq}H^{7}$	2.149(5)
$N^1_{eq}H^{15}$	$B_{ax}H^{2}$	2.127(9)
	$B_{ax}H^{4}$	2.131(3)
$N_{ax}H^{16}$	$B^2_{eq}H^{12}$	1.689(6)
$N_{ax}H^{17}$	$B_{ax}H^{1}$	1.862(5)
$N_{ax}H^{18}$	$B^1_{eq}H^{8}$	1.684(5)
$N^2_{eq}H^{19}$	$B^2_{eq}H^{12}$	2.225(7)
	$B^1_{eq}H^{6}$	2.393(7)
$N^2_{eq}H^{20}$	$B_{ax}H^{2}$	1.883(6)
$N^2_{eq}H^{21}$	$B^1_{eq}H^{8}$	2.214(6)
	$B^1_{eq}H^{5}$	2.393(3)
	$B^1_{eq}H^{7}$	2.279(8)
$N^3_{eq}H^{22}$	$B^1_{eq}H^{8}$	2.224(1)
	$B^1_{eq}H^{6}$	2.235(0)
	$B^2_{eq}H^{10}$	2.392(1)
$N^3_{eq}H^{23}$	$B_{ax}H^{4}$	1.882(1)
$N^3_{eq}H^{24}$	$B^2_{eq}H^{9}$	2.238(2)
	$B^2_{eq}H^{11}$	2.268(0)

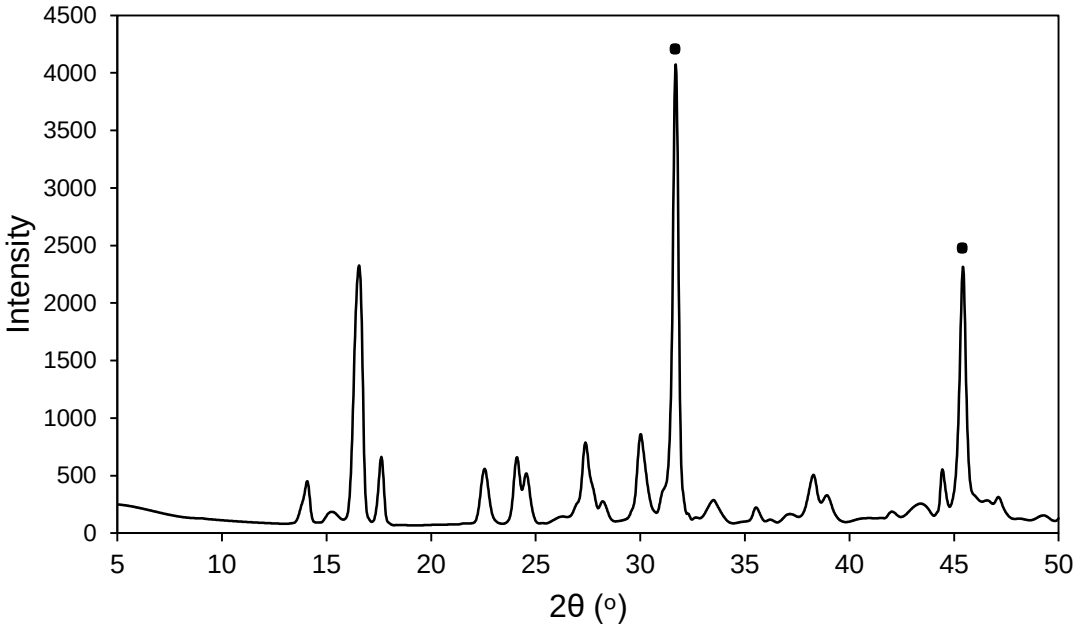

Figure A6.3. PXRD results of the solid **3** obtained from the addition of ammonia to a solution filtrate after the reaction of $ZnCl_2$ with 1.7 equiv. of $NaBH_4$ in thf at RT. The peaks assigned with the asterisk is due to the metallic PXRD sample holder.

SEM and TEM Images

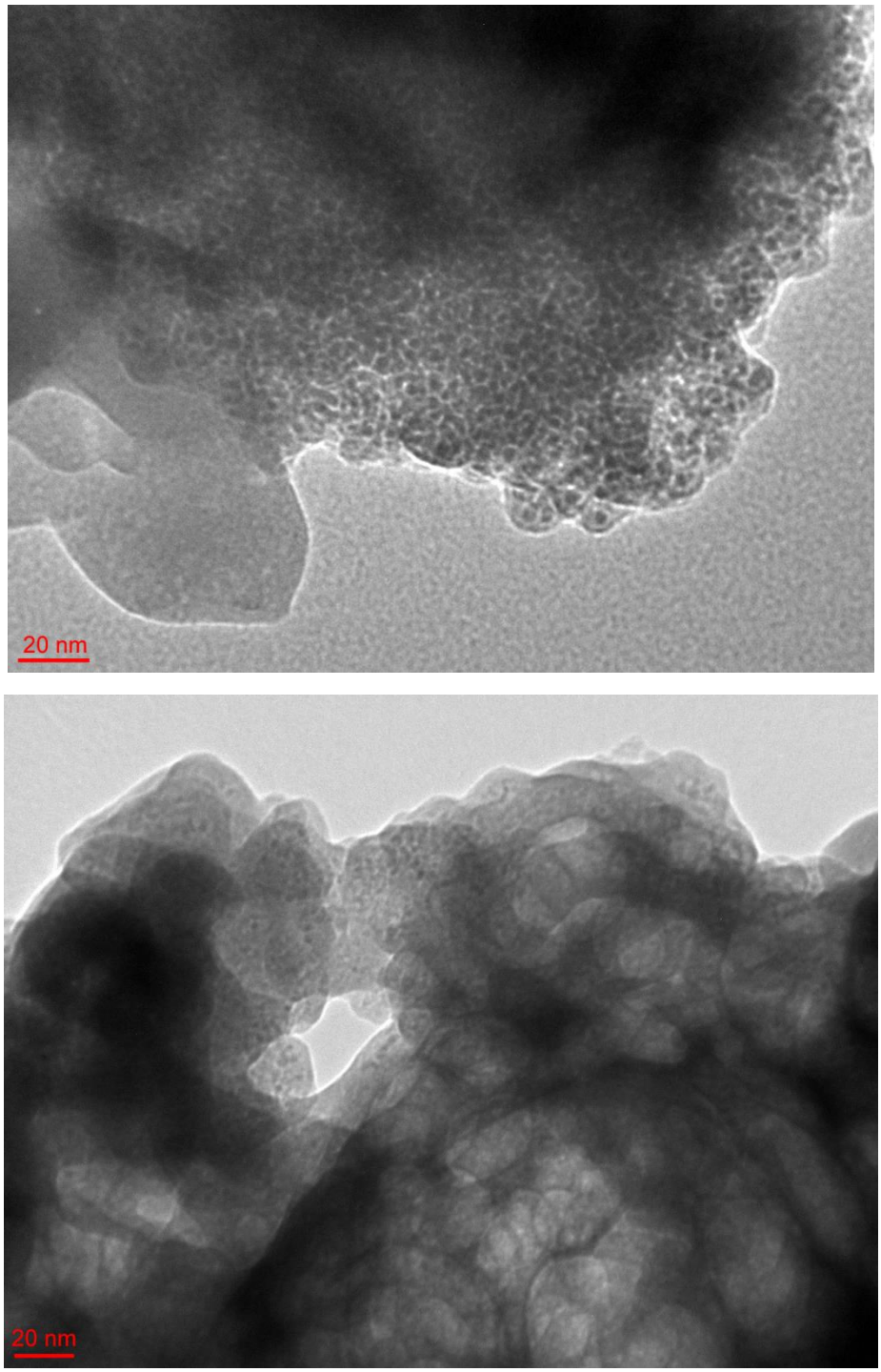

Figure A7.1. TEM images of the Co nanoparticles (5 wt.%) loaded on $Y(BH_4)_3(NH_3)_4$ (top) and $La(BH_4)_3(NH_3)_4$ (bottom). Non-homogeneity of the nanoparticle dispersion is clearly shown.